

ORNL



3 4456 0007220 3

ORNL/TM-7086
DRAFT

**OAK
RIDGE
NATIONAL
LABORATORY**



FUSION ENERGY DIVISION LIBRARY

EBT-P Preliminary Conceptual Design Report

A. L. Boch, Project Manager

FED LIBRARY DEC 18 1979

OPERATED BY
UNION CARBIDE CORPORATION
FOR THE UNITED STATES
DEPARTMENT OF ENERGY

9/14/80

Contract No. W-7405-eng-26

FUSION ENERGY DIVISION
EBT-P PRELIMINARY CONCEPTUAL DESIGN REPORT

A. L. Boch, Project Manager

| | | |
|----------------------|--------------------|------------------|
| R. G. Alsmiller, Jr. | R. B. Easter | T. J. McManamy |
| F. W. Baity, Jr. | O. C. Eldridge | J. W. Melton |
| V. C. Baker | W. M. Fletcher | R. A. Michelotti |
| J. K. Ballou | T. A. Gabriel | J. R. Moore |
| D. B. Batchelor | J. C. Glowienka | L. W. Owen |
| F. M. Bieniosek | W. R. Hamilton | G. F. Pierce |
| W. B. Bigney | H. H. Haselton | W. H. Power |
| B. L. Bishop | G. R. Haste, Jr. | R. K. Richards |
| S. K. Borowski | C. L. Hedrick, Jr. | J. A. Rome |
| R. A. Brown | E. F. Jaeger | J. Sheffield |
| D. B. Campbell | S. P. Kinsey | D. A. Spong |
| J. A. Cobble | S. A. Larson | J. D. Stout |
| R. J. Colchin | R. A. Lillie | P. A. Tabor |
| R. A. Dory | M. S. Lubell | N. A. Uckan |
| L. Dresner | J. W. McCormick | T. Uckan |
| H. O. Eason, Jr. | H. C. McCurdy | T. L. White |
| R. A. Wright | | H. T. Yeh |

Date Published: October 1979

NOTICE This document contains information of a preliminary nature. It is subject to revision or correction and therefore does not represent a final report.

Prepared by the
OAK RIDGE NATIONAL LABORATORY
Oak Ridge, Tennessee 37830
operated by
UNION CARBIDE CORPORATION
for the
DEPARTMENT OF ENERGY



3 4456 0007220 3

CONTENTS

| | |
|--|-----|
| ABSTRACT | vii |
| EXECUTIVE SUMMARY | ix |
| 1. INTRODUCTION | 1 |
| 2. PHYSICAL DESCRIPTION OF PROJECT | 3 |
| 3. PROJECT PURPOSE AND JUSTIFICATION | 5 |
| 3.1 PROJECT PURPOSE | 5 |
| 3.2 JUSTIFICATION OF NEED AND SCOPE | 5 |
| 4. PRINCIPAL SAFETY, FIRE, AND HEALTH HAZARDS | 7 |
| 4.1 SAFETY ACTIVITIES | 7 |
| 4.1.1 Division and Plant Safety Activities | 7 |
| 4.1.2 Department of Energy Safety Requirements | 7 |
| 4.1.3 Preparatory Safety Activities | 7 |
| 4.2 SAFETY PRECAUTIONS | 7 |
| 4.2.1 Industrial Safety | 7 |
| 4.2.2 Microwave Safety | 7 |
| 4.2.3 Seismic Considerations | 8 |
| 4.2.4 Fire Protection | 8 |
| 4.3 RADIOLOGICAL SAFETY | 8 |
| REFERENCES | 9 |
| 5. ENVIRONMENTAL IMPACT | 11 |
| 5.1 ENVIRONMENTAL CONSIDERATIONS | 11 |
| 5.2 ENERGY CONSERVATION | 11 |
| 6. QUALITY ASSURANCE PLANNING | 13 |
| 7. ASSESSMENT OF RESEARCH AND DEVELOPMENT INTERFACE | 17 |
| 7.1 MAGNET DEVELOPMENT | 17 |
| 7.2 MICROWAVE DEVELOPMENT | 17 |
| 7.2.1 Microwave Sources | 18 |
| 7.2.2 Microwave Distribution | 18 |
| 7.2.3 Microwave Supporting Subsystems | 18 |
| 8. PROJECT SCHEDULE | 21 |
| 9. PROPOSED METHOD OF ACCOMPLISHMENT | 25 |
| 9.1 INTRODUCTION | 25 |
| 9.2 ETM/ORO/ORNL MEMORANDUM OF AGREEMENT: EBT — PROOF-OF-PRINCIPLE PROJECT | 25 |
| 10. COST ESTIMATE | 33 |
| 11. OUTLINE SPECIFICATIONS | 35 |
| 11.1 GENERAL CODES, STANDARDS, AND SPECIFICATIONS | 35 |
| 11.1.1 Structural | 35 |
| 11.1.2 Architectural | 36 |
| 11.1.3 Civil | 36 |
| 11.1.4 Piping | 36 |
| 11.1.5 Instrumentation | 37 |
| 11.1.6 Electrical | 37 |

| | | |
|---------|--|-----|
| 11.1.7 | Plumbing, Heating, Ventilating, and Air Conditioning | 38 |
| 11.1.8 | General | 39 |
| 11.2 | BUILDING ADDITIONS AND MODIFICATIONS | 39 |
| 11.2.1 | Building Demolition and Site Preparation | 39 |
| 11.2.2 | Power Supply Enclosures | 40 |
| 11.2.3 | Cryogenic Equipment Mounts and Enclosures | 41 |
| 11.2.4 | Control Room | 42 |
| 11.2.5 | Building Electrical Service | 44 |
| 11.2.6 | Device Enclosure and Support Structure | 44 |
| 11.3 | OTHER STRUCTURES | 46 |
| 11.3.1 | Cooling Tower | 46 |
| 11.3.2 | Helium Tanks and Pad | 46 |
| 11.4 | BASIC DEVICE | 46 |
| 11.4.1 | Toroidal Vessel | 47 |
| 11.4.2 | Magnetics System | 48 |
| 11.4.3 | Microwave Heating System | 54 |
| 11.4.4 | Vacuum Pumping System | 57 |
| 11.4.5 | Utilities | 59 |
| 11.4.6 | Instrumentation and Control | 61 |
| | REFERENCES | 67 |
| | APPENDIX | 69 |
| A.1 | ENGINEERING ANALYSIS | 71 |
| A.1.1 | SHIELDING ANALYSIS | 71 |
| A.1.1.1 | Introduction | 71 |
| A.1.1.2 | Method of Calculation | 71 |
| A.1.1.3 | Results | 73 |
| A.1.2 | VACUUM VESSEL THERMAL ANALYSIS | 82 |
| A.1.3 | MAGNETIC FORCE ANALYSIS | 86 |
| A.1.4 | STRAY MAGNETIC FIELDS | 90 |
| A.1.5 | CRYOGENIC SYSTEM HEAT LOAD ESTIMATE | 90 |
| A.1.6 | MICROWAVE/CRYOPUMP ISOLATION SYSTEM CALCULATIONS | 93 |
| A.1.6.1 | Perforated Copper Plate Design | 93 |
| A.1.6.2 | Absorbent Section | 94 |
| A.1.6.3 | Microwave Power into Cryopump | 94 |
| | REFERENCES | 95 |
| A.2 | EBT-P THEORY AND OPERATION | 97 |
| A.2.1 | EBT-P THEORY AND SCALING | 97 |
| A.2.2 | EBT-P OPERATION | 98 |
| A.2.3 | SUMMARY | 99 |
| | REFERENCES | 99 |
| A.3 | RELATIVISTIC ELECTRON RINGS | 113 |
| A.3.1 | DRAG COOLING OF THE RELATIVISTIC ELECTRON ANNULUS | 113 |
| A.3.2 | ANNULUS MICROWAVE POWER SCALING | 114 |
| A.3.3 | SCALING PROJECTIONS FOR EBT-P | 115 |
| | REFERENCES | 117 |

| | | |
|-----------------------|--|-----|
| A.4 | MAGNETICS DESIGN | 119 |
| A.4.1 | MIRROR COILS | 119 |
| A.4.2 | GLOBAL FIELD ERROR CORRECTION COILS | 123 |
| A.4.3 | MIRROR COIL DESIGN CONSIDERATIONS | 130 |
| A.4.3.1 | Introduction | 130 |
| A.4.3.2 | Examples of Metastable Magnets | 132 |
| A.4.3.3 | Design Considerations for the EBT-P Magnet | 134 |
| A.4.3.4 | Summary | 139 |
| REFERENCES | | 142 |
| A.5 | MICROWAVE HEATING | 143 |
| A.5.1 | INTRODUCTION | 143 |
| A.5.2 | DEVELOPMENT OF MICROWAVE ACTIVE DEVICES | 143 |
| A.5.3 | AUXILIARY SYSTEMS | 144 |
| A.5.4 | COMPONENTS AND TRANSMISSION | 144 |
| A.5.5 | MICROWAVE-PLASMA COUPLING | 146 |
| A.6 | DIAGNOSTICS/DATA ACQUISITION | 147 |
| A.7 | FUTURE OPTIONS | 149 |
| A.7.1 | ASPECT RATIO ENHANCEMENT COILS | 149 |
| A.7.2 | ION CYCLOTRON HEATING EXPERIMENTS IN EBT-P | 153 |
| A.7.2.1 | Introduction | 153 |
| A.7.2.2 | Fast Wave | 155 |
| A.7.2.3 | The Slow Wave | 157 |
| A.7.2.4 | Antennas | 158 |
| A.7.2.5 | ICRH System Specifications | 160 |
| A.7.3 | NEUTRAL BEAMS FOR EBT | 161 |
| A.7.3.1 | Introduction | 161 |
| A.7.3.2 | Rationale | 161 |
| A.7.3.3 | Previous Work | 161 |
| A.7.3.4 | Goal of the Present Study | 161 |
| A.7.3.5 | Status | 162 |
| A.7.4 | FORCED-FLOW CRYOGENIC SYSTEM | 165 |
| REFERENCES | | 168 |
| A.8 | TEN-YEAR EBT PROGRAM — FY 1980-89 | 169 |
| A.8.1 | EBT HIERARCHY | 169 |
| A.8.2 | SCHEDULE | 171 |
| A.8.3 | THE 48 CAVITIES — EBT-PU | 171 |
| A.9 | DRAWINGS | 173 |
| LIST OF ABBREVIATIONS | | 263 |

ABSTRACT

Experiments in the ELMO Bumpy Torus (EBT-I) have demonstrated that plasma currents produced by microwave-heated electron annuli can provide macroscopically stable plasma confinement in a steady-state bumpy torus. EBT experiments have established a reference case in which the data agree sufficiently well with neoclassical transport theory to warrant a full test of transport scaling. This proof-of-principle device, EBT-P, is designed to be a steady-state, microwave-heated toroidal fusion device with plasma parameters extrapolable to near reactor-relevant regime. As such, EBT-P would provide a test of scaling, accelerate the development of the technology required for later reactor applications, provide a demonstration of the capability to analyze and control higher beta plasmas, test theoretical studies of EBT transport, and provide a focus for reactor applications design studies. As proposed, the device will be 11.2 m in diameter with 36 superconducting magnets. Microwave heating will be accomplished at 110 GHz for bulk heating and at \sim 60 GHz for profile heating. The report further describes in detail the basic device, including machine diagnostics, personnel protection requirements, and support utilities for construction at the Y-12 Plant, Building 9201-2.

EXECUTIVE SUMMARY

BACKGROUND

During 1978 the U.S. Department of Energy's (DOE's) Office of Fusion Energy (ETM) initiated an aggressive development program to broaden the base of the magnetic fusion research program by fostering the development of several of the most promising alternate fusion concepts.

Several alternate concepts were reviewed in detail by ETM during briefings held in October 1978. The Oak Ridge National Laboratory's (ORNL's) ELMO Bumpy Torus (EBT) concept was selected by ETM's Concept Review Committee as one of the alternate concepts to be pursued to a proof-of-principle level. The proof-of-principle experiment is defined as one having a hydrogen plasma with an ion temperature in the keV range and an $n\tau$ product of 10^{12} - 10^{13} cm^{-3} sec.

As part of the overall EBT program plan, ORNL was authorized to proceed with project definition design studies for EBT proof-of-principle experiments (EBT-P). This report documents that effort.

Sections 1 through 11 of this report summarize the preliminary conceptual engineering design effort for the EBT-P device. The appendix includes the scientific basis for the engineering studies, a brief discussion of EBT-P theory, a look at future experimental options, and all engineering drawings produced for this report (see Sect. A.9 for all drawing callouts).

SUMMARY OF PLASMA CONFINEMENT IN EBT

An ordinary bumpy torus with only vacuum magnetic fields is magnetohydrodynamic (MHD) unstable. However, in the EBT¹ at ORNL, this problem has been circumvented by the application of electron cyclotron heating (ECH), which, as discovered in mirror research at ORNL, creates high beta (β), hot electron annuli that modify the toroidal magnetic field in such a way as to prevent MHD instabilities. The primary motivation for EBT confinement research is the fusion reactor goal that, in this configuration, could provide high β , steady-state operation in a large aspect ratio, high accessibility reactor embodiment.

The demonstration of the stabilization of the toroidally confined plasma by the energetic electron annulus prompted additional studies of the confinement properties of the configuration. Even in the low magnetic field (6 kG) of ORNL's EBT-I device, the stable toroidal plasma attains significant density ($\bar{n}_e \sim 10^{12}$ cm^{-3}), temperature ($T_e \sim 300$ eV, $T_i \sim 100$ eV), and confinement time ($\tau_e \sim 5$ msec) with 18 GHz, ~ 50 kW of microwave power. This permits favorable comparison with a diffusive neoclassical transport model.¹ With these encouraging results as a baseline, a new experiment, EBT-Scale (EBT-S), is presently under way to provide deeper insight into the scaling of plasma parameters with higher microwave frequency (28 GHz), magnetic field (10 kG), and heating power (≤ 200 kW).

The EBT-I device has experimentally provided a proof-of-principle: the demonstration of a smooth transition from the typical MHD-unstable bumpy torus regime [when the annulus beta (β_{annulus}) is low] into a macrostable hot plasma regime extending over a significant range of operating conditions provided β_{annulus} exceeds the theoretically predicted value for stability. In the six years since EBT-I began operating, work has progressed from a demonstration of this macrostability to an increasingly detailed understanding of plasma properties. [It should be noted that there is now a second EBT, the Nagoya Bumpy Torus (NBT) in Nagoya, Japan, which is operating and obtaining results similar to those of EBT-I.²]

Stability calculations have shown that the annuli and the toroidal plasma in EBT serve to stabilize each other and that unstable coupling of the two plasmas does not occur,^{3,4} a fact verified in EBT-I at low β . Theoretically, ballooning modes in the toroidal core plasma lead to upper limits on the containable amount of core plasma (it is found that values of β_{core} cannot greatly exceed β_{annulus} .)

However, the resulting values of β_{core} are high enough to be attractive for reactor designs. Calculations based on MHD theory led to early concern about the ballooning instability of the annulus. However, MHD theory provides an inadequate description of annulus behavior, and a kinetic treatment demonstrates that ballooning modes are stabilized. Also, a number of microinstabilities that could conceivably occur in this system have been studied and are found to be stable for the expected field and plasma gradients.⁵

So far, theoretical studies have provided no significant evidence of macroscopically unstable behavior of the toroidal plasma in interesting regimes, and the EBT-I experiment has demonstrated nearly quiescent T-mode operation with very low density fluctuation levels.¹ In experiments collisionless scaling (energy confinement time τ_E increases with temperature) has been observed, and the magnitude of τ_E is consistent with neoclassical theory.⁶⁻⁹ The results of a comparison between the experimentally observed plasma parameters (ion and electron temperatures, plasma density, and confinement time) and the values and behavior predicted by neoclassical theory are very encouraging: in the T-mode the EBT-I plasma parameters seem entirely consistent with neoclassical transport predictions. The correspondence is, of course, in a limited range of parameters and has a coarse nature, as dictated by the small size of the experiment and by diagnostic limitations associated with operation at low microwave frequency, low magnetic field, and low plasma density.

THE LOGIC OF THE EBT-P DESIGN

This report summarizes the work that was undertaken on EBT-P during 1979. This device has evolved from the earlier EBT-II design,^{10,11} which was presented to ETM's Concept Review Committee. The further optimization of the design reflects advances made in the theoretical studies of the EBT plasma. Much of this work has been published,^{6-9,12} and a brief summary of the salient points is given in Sects. A.2, A.3, and A.4. One paper yet to be published is appended to Sect. A.2.⁸ The device is designed in its basic form to achieve $n\tau \geq 10^{12} \text{ cm}^{-3} \text{ sec}$ with $n \geq 10^{13} \text{ cm}^{-3}$ and $T \geq 1 \text{ keV}$. The device parameters that should give these conditions have been established by using simple EBT scaling arguments.^{10,11} For several years EBT scaling has been a fundamental element in design studies; it is based upon basic theoretical scaling laws with coefficients determined from experimental measurements from EBT-I/S. The more detailed theory compares favorably with experimental results in the T-mode of operation in EBT and confirms that the gross behavior of the toroidal core density and temperatures is dominated by the neoclassical electron transport coefficients, leading to EBT scaling of (see Sect. A.2) $n\tau \sim A^2 T_e^{3/2}$ for small collisionality ν/Ω , where collisionality is defined as $\nu/\Omega \sim n/T_e^{5/2} (BR_c a_p)$. Here a_p is the mean plasma radius, and A is the magnetic aspect ratio defined as R/R_c , where R and R_c are the major radius of the torus and the magnetic radius of curvature, respectively. For conservative estimates, the collisionality is assumed to be constant.

It is possible to modify the aspect ratio and mirror ratio with coils additional to the simple toroidal coil set; such coils are known, respectively, as aspect ratio enhancement (ARE) coils and trim coils. The effective aspect ratio with ARE coils may be written as $A_{\text{eff}} = (R/R_c) f_{\text{ARE}} \cong A f_{\text{ARE}}$. Such coils on EBT-P might lead to an enhancement factor as high as $f_{\text{ARE}} \sim 2$ (see Sect. A.7.1).

Finally, the cutoff for microwave propagation (electron plasma frequency $\omega_{pe} \leq$ electron cyclotron frequency, ω_{ce}) imposes an upper limit on density n , which scales as the square of the magnetic field; i.e., $n_{\text{max}} \sim f_{\mu}^2 \sim B_r^2$, where f_{μ} is the applied microwave frequency and B_r is the resonant magnetic field. The resonance occurs in the region between the coils, and for mirror ratio $M \sim 2$, the maximum field at the coil $B_M \sim 2B_r$.

Using the above formulae and scaling from EBT-I, one can find that EBT-P should have $f_{\mu} \geq 60 \text{ GHz}$, $B_r \geq 2 \text{ T}$, $B_M \geq 4 \text{ T}$, and $A > 8$.

A machine such as this, with the additional constraint that the plasma radius should scale up from the present device toward the radius expected for the next phase (see Sect. A.8), will have a larger major radius and larger toroidal coils. In comparison to EBT-I, which has $R_C = 1.5$ m and uses 5 MW of coil power for $B_r = 0.6$ T, EBT-P will have $R > 3$ M; consequently, with copper coils the needed power will be in excess of 50 MW. Because the steady-state operation of EBT-P is an important consideration and because further power is required for producing the rings and plasma, we follow the EBT-II logic in using superconducting coils.¹⁰ Because of the need for radiation shielding and dewar and thermal shields, this in turn modifies the magnetic geometry. Designs have been considered that have a magnetic geometry and single-particle confinement comparable with that in EBT-I. This constraint is applied to ensure that scaling from EBT-I would be valid (see Sect. A.4).

The end result of these optimizations is the proposal for a basic device with $R = 5.6$ m, 36 cavities, $A = 16$, and $a_p = 0.19$ m. The field proposed for these coils is as large as we believe possible with present superconducting coil technology, $B_M = 8$ T (see Sect. A.4). The maximum resonant frequency is $f = 110$ GHz. Programs are under way to produce prototype coils (see Sects. 7.1 and A.4) and to develop the high frequency gyrotrons for operation at 110 GHz and 60 GHz (see Sects. 7.2 and A.5). To make this program both cost- and time-effective, we propose a device that will be upgraded in stages.

Following are some upgrade options.

- (1) Although the device can operate at 110 GHz with 60-GHz profile heating, it may well start at 60 GHz, using the existing EBT-S 28-GHz gyrotrons for profile heating.
- (2) The application of ion cyclotron heating (ICH) is discussed in Sect. A.7.2.
- (3) The application of neutral beams is discussed in Sect. A.7.3.
- (4) To accommodate powerful steady-state neutral beam heating with its associated high particle flux, we propose the addition of a divertor to maintain a constant plasma density that is below microwave cutoff.
- (5) The basic machine is designed with trim coils to vary the mirror ratio, and to allow for the addition of ARE coils (see Sect. A.7.1).
- (6) Finally, the device is designed for a rebuild in a 48-coil version.

The parameters of the basic machine and the ultimate upgraded device are given in the table following this. To accelerate the program and check the efficiency of the various options, we have proposed and are implementing a more aggressive experimental program on the present EBT device (see Sect. A.8). EBT-I uses up to 60 kW of 18-GHz power plus up to 30 kW of profile heating at 10.8 GHz. EBT-S will initially use up to 200 kW at 28 GHz plus 60 kW at 18 GHz. Upgrades approved for FY 1980 include ARE coils, ICH, a diagnostic neutral beam, and design studies for a divertor. In addition, more extensive diagnostics and data acquisition systems are being applied. Proposed for FY 1981-1983 are the application of further ECH power, ICH power, a divertor, and more powerful neutral beams.

EBT-P device parameters

| | Basic device | Ultimately upgraded device |
|---------------------------------------|---|----------------------------|
| Machine | | |
| Number of coils | 36 | 48 |
| Magnetic field-on-axis (cavity, coil) | 2.5-3.0 T, 5.7 T | |
| Major radius | 5.6 m | 7.2 m |
| Coil mean radius (mirror, trim) | 35 cm, 52 cm | |
| Aspect ratio (coil) | 16:1 | 20 → 40 |
| Mirror ratio | 1.9-2.3 | |
| Hot electron annulus | | |
| n_e | $1-6 \times 10^{12} \text{ cm}^{-3}$ | |
| T_e | 500-2000 keV | |
| β_{annulus} | 10-50% | |
| Toroidal plasma | | |
| n_e | $\sim 1.6 \times 10^{13} \text{ cm}^{-3}$ (nom) | $\sim 6 \times 10^{13}$ |
| T | $\sim 2 \text{ keV}$ (nom) | ≥ 3 |
| Maximum β | 0.5% (nom) | $\geq 3\%$ |
| Mean plasma | $\sim 19 \text{ cm}$ | |
| Plasma volume | 4000 liters | ~ 5200 |
| $n\tau$ | $10^{12} \text{ sec cm}^{-3}$ | 10^{13} |
| Particle confinement | | |
| Trapped | $\sim 75\%$ | $\sim 85\%$ |
| Passing (toroidal) | $\sim 20\%$ | $\sim 55\%$ |

REFERENCES

1. R. A. Dandl et al., Oak Ridge National Laboratory Report ORNL/TM-6457, Oak Ridge, Tennessee (1978).
2. T. Shoji et al., "Plasma Confinement in Nagoya Bumpy Torus," paper A2.2 presented at the 9th European Conf. on Controlled Fusion and Plasma Physics, Oxford, England, September 17-21, 1979.
3. D. B. Nelson and C. L. Hedrick, Nucl. Fusion 19 (3), 283-392 (1979).
4. D. B. Nelson, Oak Ridge National Laboratory Report ORNL/TM-6824, Oak Ridge, Tennessee (1979).
5. D. B. Batchelor and C. L. Hedrick, Nucl. Fusion 19, 235 (1979).
6. E. F. Jaeger and C. L. Hedrick, Nucl. Fusion 19, 443 (1979).
7. E. F. Jaeger, C. L. Hedrick, and W. B. Ard, "Radial Transport in EBT with Constant Edge Neutral Beams," to be published in Phys. Rev. Lett.
8. E. F. Jaeger, C. L. Hedrick, and D. A. Spong, Oak Ridge National Laboratory Report ORNL/TM-6806, Oak Ridge, Tennessee (1979); submitted to Nucl. Fusion.
9. D. A. Spong, E. G. Harris, and C. L. Hedrick, Nucl. Fusion 19, 665 (1979).
10. R. A. Dandl et al., Oak Ridge National Laboratory Report ORNL/TM-5955, Oak Ridge, Tennessee (1978).
11. L. A. Berry, C. L. Hedrick, and N. A. Uckan, Oak Ridge National Laboratory Report ORNL/TM-6743, Oak Ridge, Tennessee (1979).
12. S. K. Borowski, N. A. Uckan, E. F. Jaeger, and T. Kammash, Oak Ridge National Laboratory Report ORNL/TM-6910, Oak Ridge, Tennessee (1979); to be published in Nucl. Fusion.

1. INTRODUCTION

During 1978 the U.S. Department of Energy's (DOE's) Office of Fusion Energy (ETM) initiated an aggressive development program to broaden the base of the magnetic fusion research program by fostering the development of several of the most promising alternate fusion concepts. An alternate concept is a plasma confinement approach that does not fall within the main-line tokamak or mirror fusion programs and that appears to show promise for a fusion reactor. It is intended that the development effort lead to testing experimentally one or more alternate concepts at the proof-of-principle level by the end of FY 1984. The proof-of-principle experiment is defined as a hydrogen plasma confinement experiment in which nearly all of the relevant dimensionless physics parameters such as collisionality, beta, etc., are near enough to the reactor plasma regime to allow a reasonable extrapolation. Typical plasma conditions for such an experiment might be an ion temperature in the keV range and an $n\tau$ product of 10^{12} - 10^{13} cm^{-3} sec.

Several alternate concepts were reviewed in detail by ETM during briefings held in October 1978. Based on evaluations by ETM's Concept Review Committee, the Oak Ridge National Laboratory's (ORNL's) ELMO Bumpy Torus (EBT) concept was accepted as one of the alternate concepts to be pursued at a proof-of-principle level. A Memorandum of Agreement (MOA), dated March 15, 1979, between ETM, DOE's Oak Ridge Operations (ORO), and ORNL was prepared as a key planning document for the initial phases of the project. This MOA, included in Sect. 9, outlines the role of key participants. As part of the overall EBT program plan, ORNL was authorized to proceed with project definition design studies for EBT proof-of-principle experiments (EBT-P). This report documents that effort.

The EBT-P device as defined in this report is proposed for construction at ORNL's Building 9201-2, located in the Y-12 Plant. EBT-P will use 36 superconducting coils to provide the required steady-state, cyclotron resonant, toroidal magnetic field of 3.9 T for electron cyclotron heating (ECH) with microwaves at 110 GHz. The peak design fields are 8.0 T in the coil, 5.7 T in the coil throat, and 3.0 T in the cavity midplane. Bulk ECH will be provided by six 110-GHz, 200-kW continuous wave (cw) gyrotrons, and profile heating will be provided by three 60-GHz, 200-kW cw gyrotrons. The torus major radius and mean coil radius are 560 cm and 35 cm, respectively, yielding a mechanical aspect ratio of approximately 16. The basic device parameters of microwave frequency and power, magnetic field, and size should allow experiments that operate in near or similar collisionless regime as observed in the present experiment, EBT-I, and thus provide a definitive test of plasma scaling. The EBT-P design also includes planning for the possible future addition of aspect ratio enhancement (ARE) coils, neutral beam and ion cyclotron heating, a divertor, and the expansion of the torus to larger diameter configurations. Planning considerations for these options are discussed in greater detail throughout the report.

Sections 1 through 11 of this report summarize the preliminary conceptual engineering design effort for the EBT-P device. The appendix includes the scientific basis for the engineering studies, a brief discussion of EBT-P theory as well as a look at future experimental options, and all engineering drawings produced for this report (see Sect. A.9 for all drawing callouts).

2. PHYSICAL DESCRIPTION OF PROJECT

This preliminary design report is based on the installation of the EBT-P experiment in Building 9201-2 in the Y-12 Plant. The device and its enclosure will be located on the second floor immediately west of the existing EBT-1/S. Drawings X2E-14270-0008 (sheets 1 and 2) show the physical layout of the equipment required for EBT-P. Plan and elevation views of the device are shown in Drawings X2E-14270-0003 and X2E-14270-0004. The physical characteristics of the device are presented in Table 2.1.

The EBT-P device is a 5.6-m major radius, 36-sector toroidal device. The toroidal vacuum vessel is composed of 36 aluminum mirror cavity sectors alternating with 36 auxiliary vacuum liner sectors. Each auxiliary vacuum liner is located concentric with the inner bore of each mirror coil vacuum dewar assembly with a 0.05-0.10-in. radial clearance and contains flexible expansion joints to accommodate

Table 2.1. EBT-P design parameters

| | | |
|---------------------------------|---|------------------------|
| Torus | | |
| Torus major radius | | 5.6 m |
| Number of sectors | | 36 |
| Minimum clear bore radius | | 19 cm |
| Torus volume | | 10.4 m ³ |
| Torus surface area | | 88.87 m ² |
| Superconducting magnet assembly | | |
| | Mirror coil | Trim coil |
| Number of coils | 36 | 36 |
| Winding mean radius | 35 cm | 52 cm |
| Winding area | 465 cm ² | 164 cm ² |
| Design current density | 6600 A/cm ² | 6700 A/cm ² |
| Maximum field at winding | 8.0 T | 2.0 T |
| Device magnetics | | |
| | Trim coil on | Trim coil off |
| Mirror ratio | 1.9 | 2.3 |
| Coil central field | 5.7 T | 5.7 T |
| Mirror central field | 3.0 T | 2.5 T |
| Mirror coil current density | 5000 A/cm ² | 6600 A/cm ² |
| Trim coil current density | 6700 A/cm ² | 0 |
| Microwave heating system | | |
| | Bulk | Profile |
| Number of gyrotrons | 6 | 3 |
| Frequency | 110 GHz | 60 GHz |
| Total power | 1.2 MW | 600 kW |
| Torus vacuum system | | |
| Primary system | 18-3000 liter/sec cryosorption pumps | |
| Ultimate pressure | 5 x 10 ⁻⁷ torr | |
| Operating pressure | ~10 ⁻⁶ torr | |
| Pumping speed per port | 1000 liter/sec | |

thermal expansion of the torus. Access ports for diagnostics, etc., are provided in the mirror cavity sectors, located between each vacuum dewar assembly.

The steady-state EBT-P plasma is contained by the magnetic field generated by the 36 mirror (toroidal field) coils, which have radially split windings (primary mirror winding and auxiliary trim winding), allowing adjustment of the device mirror ratio. Each coil consists of these two liquid-helium-cooled (pool boiling) NbTi superconducting windings enclosed in a stainless steel case. Each of these encased coils is mounted internal to a stainless steel vacuum dewar via a system of titanium tension struts that carries the magnetic load from the coils to the dewar outer ring to the device structural supports. A tungsten alloy shield located on the inner bore and sides of the vacuum dewar external to the evacuated area protects each superconducting coil from photon (bremsstrahlung) radiation. Power is supplied to the mirror windings and trim windings from their respective high current dc power supplies through helium-vapor-cooled leads arranged in series fashion. Automatic quench protection is provided for each coil.

Stabilization and heating of the plasma are provided by the injection of 1.8 MW of microwave power at frequencies of 60 and 110 GHz into the toroidal vessel. The microwave power is transmitted from the nine gyrotron power sources to the vacuum vessel via separate bulk and profile oversized waveguides having symmetrical connections to each mirror cavity. The gyrotron is a microwave power oscillator based upon the principles of the cyclotron resonance maser. No auxiliary heating is included in the base design, although provisions have been made to accommodate the eventual addition of neutral beam injectors.

Primary pumping of the toroidal vacuum vessel is accomplished through the use of eighteen 10-in. cryosorption pumps located on every other mirror cavity. A roughing system, composed of cryosorption and turbomolecular pumps, is utilized for the initial pumpdown of the toroidal vacuum vessel and coil vacuum dewars and for the regeneration of the primary cryosorption pumps. Primary pumping of the coil vacuum dewars is accomplished through the use of a 7-in. cryosorption pump on each dewar. The torus cryosorption pumps will be shielded from scattered microwave energy by a water-cooled, perforated copper plate located in each pumping port.

The experiment is housed in a three-level, concrete/lead enclosure extending from 4 ft below first floor level (9201-2) to 19 ft above second floor level. The two upper levels — the operating level and the mezzanine level — are surrounded by a 27-in.-thick concrete/lead biological radiation shield. At the operating level the torus structure is mounted to a concrete pad supported by concrete columns. Approximately 4 ft above the operating floor is the torus midplane. The mezzanine floor, directly below the operating floor, provides operating access to diagnostic and ancillary equipment. Entrance to the experiment will be through a "darkroom maze" on the mezzanine level that is designed to attenuate reflected radiation. Housed on the lower level of the enclosure are the gyrotron assemblies, the regulator and crowbar portion of the gyrotron power supplies, and the mirror coil dc power supplies.

A control room located adjacent to the shielded enclosure in the northwest low-bay area will house all instrumentation and control components and diagnostics.

Mechanical equipment associated with device operation will be located reasonably close to the device where space is available. The cold box and liquid helium storage dewar portion of the helium refrigeration equipment will be located on the north low-bay roof inside a metal enclosure, and the compressor will be located on a covered concrete pad at the west end of the building. Located outside the building will be helium gas storage tanks to accommodate the gas-equivalent content of the liquid helium system.

The gyrotron power supplies will be located in two areas adjacent to the experiment site. The high voltage switchgear will be located on an open, fenced concrete pad on the south side of Building 9201-2, and the remainder of the high voltage power supply equipment will be sheltered in a building addition at the west end of the building.

3. PROJECT PURPOSE AND JUSTIFICATION

3.1 PROJECT PURPOSE

The purpose of the EBT-P project is the design, procurement, fabrication, installation, and operation of an experimental fusion device based on the EBT concept; this device, however, will provide a higher density, higher temperature proof-of-principle extension of that concept extrapolable to the reactor plasma regime.

Experiments in the ELMO Bumpy Torus (EBT-I and EBT-S) have demonstrated that plasma currents produced by microwave-heated, hot electron annuli can provide macroscopically stable plasma confinement in a steady-state bumpy torus. The EBT experiments have established a reference case in which the data agree sufficiently well with neoclassical transport theory to make imperative a full test of the transport scaling. If the EBT approach can be extended to confine high beta toroidal plasmas, it will offer an attractive alternative to the tokamak and magnetic mirror approaches to controlled thermonuclear fusion.

Our present understanding of equilibrium, stability, and transport in EBT has suggested a sequence of experimental devices and related research activities leading progressively toward an attractive full-scale reactor. The implementation of the steps in this sequence hinges on the development of very high power cw microwave sources at millimeter wavelengths.

The EBT-P device described herein would provide a test of scaling, accelerate the development of the technology required for later reactor applications, provide a demonstration of the capability to analyze and control higher beta plasmas, test theoretical studies of EBT transport, and provide a focus for reactor application design studies.

3.2 JUSTIFICATION OF NEED AND SCOPE

A quote from the DOE "Report on the Concept Review Committee Recommendations for Proof-of-Principle Alternate Concept Programs," DOE/ET-0085, summarizes the current DOE policy and the basis for this project:

The recently announced DOE policy statement on the development of fusion energy places increased emphasis on the testing of promising alternate concepts. More specifically, this policy suggests comparisons of promising alternatives with tokamaks and mirrors in the mid 1980's. In order to make these concept comparisons, it is necessary to extend greatly the scientific data base for the alternative concepts toward the reactor regime to provide significant experimental tests. These significant tests have been designated as proof-of-principle (POP) experiments and have most of the important dimensionless parameters in or near the reactor regime. A POP experiment for an alternate concept can be considered the scientific equivalent of PLT in the tokamak program.

It has long been recognized that a bumpy torus configuration would contain single particles. The vertical drift motion, a common feature of all toroidal devices that results from the variation of the magnetic field with major radius, is combined in the bumpy torus with an azimuthal drift that is the result of the variation of the magnetic field with minor radius. Although single particles are well contained, a plasma is unstable in a simple bumpy torus. The variation of the magnetic field in minor radius, the feature resulting in single-particle confinement, is such that the energy can be reduced if the plasma expands to regions of lower magnetic field. This gives rise to magnetohydrodynamic (MHD) instabilities. The unique feature of the ELMO Bumpy Torus (EBT) is the fact that the magnetic field is modified by plasma currents such that an unstable configuration is transformed into a stable one.

Early ORNL experiments revealed that an annulus of high energy electrons was formed in a simple mirror with electron cyclotron resonance heating (ECRH). These annuli significantly modified the

vacuum magnetic field. It has been conjectured that if the same effect occurred in a bumpy torus, it would stabilize the plasma. EBT, which first operated in 1973, verified this principle. This device has now operated with ECRH using frequencies at 10.6 and 18 GHz to achieve plasmas with densities of 10^{12} and electron temperatures of 400 eV.

The parameters achieved, as well as a number of technological features of EBT, made this device attractive as a candidate for a fusion reactor. Some of these advantages include steady-state operation, modular construction, and high aspect ratio (the ratio of major to minor radius).

An *ad hoc* committee convened by ETM, with John Foster as chairman, examined the fusion effort in the U.S. Their recommendation was to broaden the research effort to include alternatives to the leading concepts. To implement that recommendation, a review of alternative concepts was held in 1978 to identify the most promising ones. A portion of the report on that review is quoted above. As a result of that review, EBT was chosen as one concept for more intensive development.

The leading concepts are the tokamak and mirror approaches. Both of these concepts are being extensively studied throughout the world. Experimental devices of both types have been constructed in many different countries. In contrast, until very recently, the U.S. was the only country with a bumpy torus program. However, there is now another bumpy torus that uses ECH in Nagoya, Japan.

The plasma parameters in EBT-P will exceed those of EBT-I/S, allowing experimental verification of the EBT scaling laws. In addition, the technology will be more advanced than that of EBT-I/S. Large volume, high field superconducting coils will be developed to provide the steady-state magnetic fields; high power, high frequency microwave sources will be developed to provide ECH.

Several different microwave frequencies will be used in EBT-P. Just as in EBT-I/S, a high frequency will be used for bulk heating, and a lower frequency — about half the higher frequency — will be used for profile heating. In EBT-P these frequencies will be 110 and 60 GHz. The capability will be provided, however, to add additional heating. This will be additional power not only at the same frequencies, but also at other frequencies (e.g., 90 GHz).

The device will be a flexible research tool capable of significant modifications. Although the initial device will have 36 coils, the effective size can readily be expanded in two ways. The first is a straightforward increase in the size of the device by increasing the number of coils to 48 with a corresponding increase in the major radius. The second is to increase the effective size through the addition of special coils, aspect ratio enhancement (ARE) coils. The coils will modify the magnetic field configuration such that effectively large aspect ratios are attained without increasing the mechanical aspect ratio.

4. PRINCIPAL SAFETY, FIRE, AND HEALTH HAZARDS

4.1 SAFETY ACTIVITIES

4.1.1 Division and Plant Safety Activities

Because the EBT-P facility will be located in Building 9201-2 at the Y-12 Plant and operated by the Fusion Energy Division (FED) of ORNL, it will be subject to the safety programs of both Y-12 and ORNL.

The Y-12 safety policy is defined as follows:

It is the policy of the Y-12 Plant to establish an effective accident prevention program and to maintain the necessary staff, service, and advisory groups to assist line supervision who are responsible for the safety of employees and equipment. Whenever our safety objective conflicts with our other objectives, safety shall be our first consideration.

This policy is implemented by the Plant Superintendent, the Central Safety Committee consisting of division and shift superintendents, three other safety committees at lower levels, a safety department, and a radiation safety department.

Within the Fusion Energy Division, a permanent Division Safety Officer provides liaison to and ensures compliance with the Y-12 safety program and oversees the Division safety activities. The FED safety program implements the Y-12 safety program with procedures specific to fusion experiments.

4.1.2 Department of Energy Safety Requirements

DOE safety requirements are stated in DOE Manual 0550, "Operational Safety Standards." All phases of the EBT-P project will be carried out in compliance with these requirements.

4.1.3 Preparatory Safety Activities

A formal Safety Analysis Report will be prepared and submitted to the Y-12 Central Safety Committee and the DOE ORO office. They must review and approve the report before operation can begin.

Prior to initial operation, a detailed check of the experiment will be performed to verify that all equipment is in good operating order, that all controls and instrumentation are operating properly, and that the field installation has been done correctly. A committee of qualified technical personnel from outside the EBT-P operating group will review the engineering design from a safety standpoint and witness the check of the experiment.

4.2 SAFETY PRECAUTIONS

4.2.1 Industrial Safety

All equipment will be fitted with safety devices and/or protective guards to prevent operator injury. Piping, pressure vessels, and electrical work will conform to applicable codes and standards. (Union Carbide Corporation General Design Criteria Y-EF-538 specifies 13 standards applicable to electrical systems.)

Any hazardous electrical areas will be interlocked with a master key located on the master control panel. Removal of this key shuts down the machine. Also, an emergency trip control that shuts down the 13.8-kV breakers leading to the power supplies will be under the control of the operating officer.

Operations involving liquefied gases will use the procedures, protective clothing, and equipment developed for handling cryogenic liquids. Hydrogen flammability hazards will be controlled by established procedures.

4.2.2 Microwave Safety

The device is designed to contain totally the injected microwave energy. The vacuum vessel metal-to-metal seals are of special design to ensure microwave containment as well as vacuum integrity. All openings for diagnostic access and vacuum pumpout will have traps to contain the microwaves at the injected frequencies.

All access doors through the biological shield around the device will be interlocked with the microwave power supplies. The interlock system will be redundant and designed such that all access doors must be locked and the keys inserted in a panel in the control room before the microwave power supplies can be energized.

4.2.3 Seismic Considerations

The new portions of the facility will be designed in accordance with the seismic design criteria for DOE facilities to prevent unacceptable hazards to persons or property.

4.2.4 Fire Protection

Building 9201-2 is equipped with automatic sprinkler systems for protection of the building and equipment. Fire alarm boxes and sprinkler annunciator alarms are connected through the Y-12 Plant fire alarm system to the fire and guard headquarters and to the plant emergency control center, which is manned at all times.

In addition to the fire alarm system, all fire doors and alarms associated with the water distribution system are monitored by the plant monitoring system, which provides in a matter of seconds information on the exact location of an alarm and on planned procedures. (The system is presently being computerized and expanded to include the fire alarm boxes and sprinkler annunciator alarms for ORNL-occupied buildings at Y-12, including Building 9201-2.)

The Y-12 Plant Emergency Squad, consisting of 13 persons, responds to all alarms with a pumper, a fully equipped emergency truck, and an ambulance. Another pumper and a CO₂ truck serve as back-up. Under mutual aid agreements personnel and equipment from ORNL, the Oak Ridge Gaseous Diffusion Plant, and the City of Oak Ridge respond to larger emergencies.

4.3 RADIOLOGICAL SAFETY

The biological shielding for EBT-P is based on a dose rate of 2.5 mrem/hr, which is within the limits required for unrestricted occupancy. The radiological hazards have been determined by approximate methods based on worst case assumptions. However, a detailed analysis and more refined input data may permit a reduction of the shielding requirements.

The main source of radiation with an ionized hydrogen plasma will be bremsstrahlung from hot electrons in the annuli striking the aluminum side walls of the cavities. Radiation from all other sources will be much lower in either energy (<100 keV) or intensity and will therefore be rapidly attenuated in any shielding adequate for the hot electron bremsstrahlung.

In the present design the southeast corner of the control room is nearer the machine than any other point in the control room; therefore, the dose rate is determined at this point, which is ~10 m from the

center of the torus. The calculations assume a point source located at the center of each cavity; however, the geometrical factor that increases the effective shielding is ignored, as are the shielding effects of the machine components and supporting structure.

In determining the heat input to the superconducting coils, a maximum of 1 MW of microwave power was assumed to dissipate in the electron annuli and be converted to bremsstrahlung in the cavity liner with a conversion efficiency of 1.85%. A similar assumption will be made here with the corresponding result that the biological shield will have a wide margin of safety. Also, the photon energy spectra of Edelsack et al.¹ are used where the maximum electron temperature is taken to be 2 MeV.

The contribution to the dose rate due to the bremsstrahlung can be reduced to <2.5 mrem/hr by a combination shield consisting of a shield around the cavities of 3.8-cm-thick tungsten alloy plus an enclosing wall composed of 12 in. of lead and 15 in. of concrete. This is calculated by numerically integrating the 2-MeV bremsstrahlung spectrum with and without the attenuation produced by the shielding.²

REFERENCES

1. E. A. Edelsack, W. E. Kreger, W. Mallet, and E. Scofield, *Health Phys.* 4, 1-15 (1960).
2. E. P. Blizard, "Nuclear Radiation Shielding," in *Nuclear Engineering Handbook*, McGraw-Hill, New York, 1958.

5. ENVIRONMENTAL IMPACT

The impact of the EBT-P facility on the environment during either the construction or operation phase will be minimal. The basic toroidal device will be located within Building 9201-2, with auxiliary structures and enclosures located exterior to the building as required. The major items to be located outside of Building 9201-2 are a power supply building addition, a transformer pad located south of 9201-2, a covered helium compressor pad, gaseous helium storage tanks, and interconnecting utility piping and conduit. Once completed, these items in themselves will pose no major threat to the environment. Normal construction safeguards for the prevention of dust, erosion, etc., will minimize problems during this phase. Consumption of resources during the operation phase will have the only apparent impact on the environment. These impacts can be isolated to power consumption, waste heat rejection, and hazardous radiation emission; none of these, when treated properly, need have an adverse impact.

5.1 ENVIRONMENTAL CONSIDERATIONS

Waste heat rejection will be accomplished by a circulating demineralized water system through a new cooling tower to be installed on an existing basin. The total waste heat from EBT-P will be approximately 19 MW while the device is in full operation. The fogging resulting from the disposal of the waste heat is not considered significant.

Although electrical power consumption will be significant, it will require no new power-generating capacity. As a result of existing loads within the building, additional transformer capacity of 30 MVA must be installed. The project will have no significant impact on the power-generating reserves in the area.

Radiation protection in the form of a concrete and lead shield immediately surrounding the device will be required. Such a shield will be designed so that the radiation levels outside the enclosure will be below the current maximum DOE radiation exposure level (see Sect. 4).

5.2 ENERGY CONSERVATION

The facilities will be designed using techniques and equipment that reflect, where feasible, a good energy-efficient design. Good engineering judgments will be used in determining potential areas of energy use reduction and recovery. Because of the experimental and intermittent nature of the device, waste heat recovery during operation on a large scale does not appear to be feasible.

6. QUALITY ASSURANCE PLANNING

All phases of the definitive design, fabrication, installation, and operation of the EBT-P project will be conducted in accordance with an approved Project Quality Assurance Plan (PQAP) in order to prevent potential significant quality problems that could impact facility safety, reliability, and costs. The PQAP will be developed and implemented during the Title I design in accordance with the requirements of DOE-ORO and ORNL's Quality Assurance (QA) Office.

A preliminary Project Quality Assurance Assessment (PQAA) has been performed for the EBT-P project as defined in this preconceptual design report (see below). This assessment is based on the work breakdown structure (WBS) shown in Fig. 6.1 and was prepared in accordance with "Quality Assurance Assessments," ORNL QA Procedure QA-L-1-103. The PQAA identifies each project element and assesses both the consequences and probability of a quality failure within that element. Items having significant failure consequences and negligible (or acceptable) failure probability are identified as noncritical items. Items having significant or unknown failure consequences and significant or unknown failure probability are identified as critical items. The PQAP will establish the policies and methods, define the responsibilities, and identify applicable DOE, UCC-ND, or subcontractor organizational elements necessary to ensure effective and timely implementation of the technical requirements needed to prevent or reduce the probability of critical item failures.

The requirements of the PQAP will be required by contract specification and purchase order, as applicable, to be passed on to all subtier contractors, fabricators, or consultants performing work on or supplying services to the EBT-P project.



OAK RIDGE NATIONAL LABORATORY
QUALITY ASSURANCE ASSESSMENT

PRELIMINARY

| |
|-------------------------|
| ASSESSMENT NO. 29-79 |
| REVISION NO. |

| | |
|--|------------------------|
| PROJECT TITLE EBT-P (4460-0702) | DATE 9/28/79 |
| DIVISION Fusion Energy | PROGRAM EBT Program |
| PARTICIPATING DIVISIONS AND OUTSIDE ORGANIZATIONS One IP from the following: Grumman Aerospace Corp., McDonnell Douglas, Inc., Westinghouse Electric Corp., EBASCO | |
| APPLICABLE QA STANDARDS FOR THIS PROJECT SPP D-2-16 ORO IMD 02XX | |

1. **PROJECT DESCRIPTION** - Engineering design, procurement, fabrication and installation of an experimental fusion device in Bldg. 9201-2. Plasma volume will be contained inside a toroidal shaped vacuum vessel composed of 36 superconducting magnet-dewar assemblies alternating with 36 aluminum cavities. Major radius of the torus will be 5.6 meters, and the assembly will be contained inside a lead-shielded enclosure immediately to the west of EBT-1. Nine gyrotrons, located outside of the device enclosure, will supply microwave power to the plasma at frequencies up to 110 GHz. A control room will be provided for control instrumentation, data acquisition, and plasma diagnostics, Est. Design and Const. Cost \$40-70 M Temp. Range Ambient to 4.2° K Press. Range 1 Atm. to 5 X 10⁻⁷ Torr

2. **PROJECT BREAKDOWN** (Breakdown of the project into major structures, systems, subsystems, and components)

| | |
|--|--------------------------|
| GROUP 1 Building Additions and Modifications | Group 6 Device Utilities |
| GROUP 2 Toroidal Vessel | Group 7 Instrumentation |
| GROUP 3 Magnetics System | |
| GROUP 4 Microwave Heating | |
| GROUP 5 Vacuum and Fueling System | |

3. **ASSESSMENT OF CONSEQUENCE AND PROBABILITY OF FAILURE**
(Indicate S if consequence is significant and S or U if the probability is significant or unknown. A blank space will indicate negligible or acceptable consequence or probability)

| | | GROUP NUMBER | | | | | | |
|--|-------------|--------------|---|---|---|---|---|---|
| | | 1 | 2 | 3 | 4 | 5 | 6 | 7 |
| Effect on Human Health and Safety or Environment will be: | Consequence | - | S | S | S | - | S | S |
| | Probability | - | - | U | - | - | - | - |
| Loss of Experimental Data or Meeting Program Objectives will be: | Consequence | - | S | S | S | - | S | - |
| | Probability | - | - | U | U | - | U | - |
| Effect on Funding and Schedule will be: | Consequence | - | - | S | S | - | - | - |
| | Probability | - | - | U | U | - | - | - |

SIGNATURES

Originator R.A. Brown Date 9-28-79 Approved by (QAC) [Signature] Date 9-28-79
 Approved by [Signature] Date 9-28-79 [Signature] Date 9/28/79
 Approved by _____ Date _____ Reviewed by (QAD) _____ Date _____

4. DESCRIPTION OF POTENTIAL QUALITY PROBLEM (For each group listed in part 2 in which the consequences of failure are significant and the probability of failure is significant or unknown, provide a brief description of the potential quality problem).

- Group 2 - Toroidal vessel problems could significantly affect the cost and schedule of this program since even a small unexpected problem could delay installation and check-out of many subsequently installed subsystems.
- Group 3 - Magnet coils and power supplies are essential to operation of the device. A failure or degradation in the performance of either would adversely affect device operation. Coils and supplies must be designed and manufactured to achieve a high degree of reliability.
- Group 4 - Microwave heating is critical to the basic experimental concept of EBT fusion devices. Individual subsystems should be sufficiently reliable to permit extended operation at the required high power levels without degradation of performance. Replacement equipment includes various items that have a long procurement lead time, which could adversely affect experimental data, cost, and schedule if one should fail.
- Group 5 - High quality vacuum system components are critical to achieving the low pressures required for system operation. Although this equipment in general is standard off-the-shelf equipment and will likely be designed with some extra capacity, a failure of one or more components could affect the timeliness and quality of experimental data.
- Group 6 - Device utilities should be designed to minimize the overall probability of device failure by the prudent use of redundant equipment with a reasonable margin of reserve capacity.
- Group 7 - Instrumentation will be extensive, in order to monitor the basic equipment operating conditions and to gain the necessary experimental data. It must be both precise and sufficiently redundant to permit safe operation despite individual instrument failures.

5. ASSESSMENT RECOMMENDATIONS

- QA Plan Required (Required when the consequence of failure is significant and the probability is either significant or unknown).
- QA Plan not Required (Indicate rationale in Part 6).
- QA Program Index Required (Required for RDT F2-2 compliance, optional otherwise).
- Impact on current Project QA Plan necessitates its revision. Revise by _____

6. RATIONALE (Justify when no project QA Plan is required).

7. This Assessment will be reviewed and up-dated, if necessary, by During Title I Design

DATE OR MILESTONE

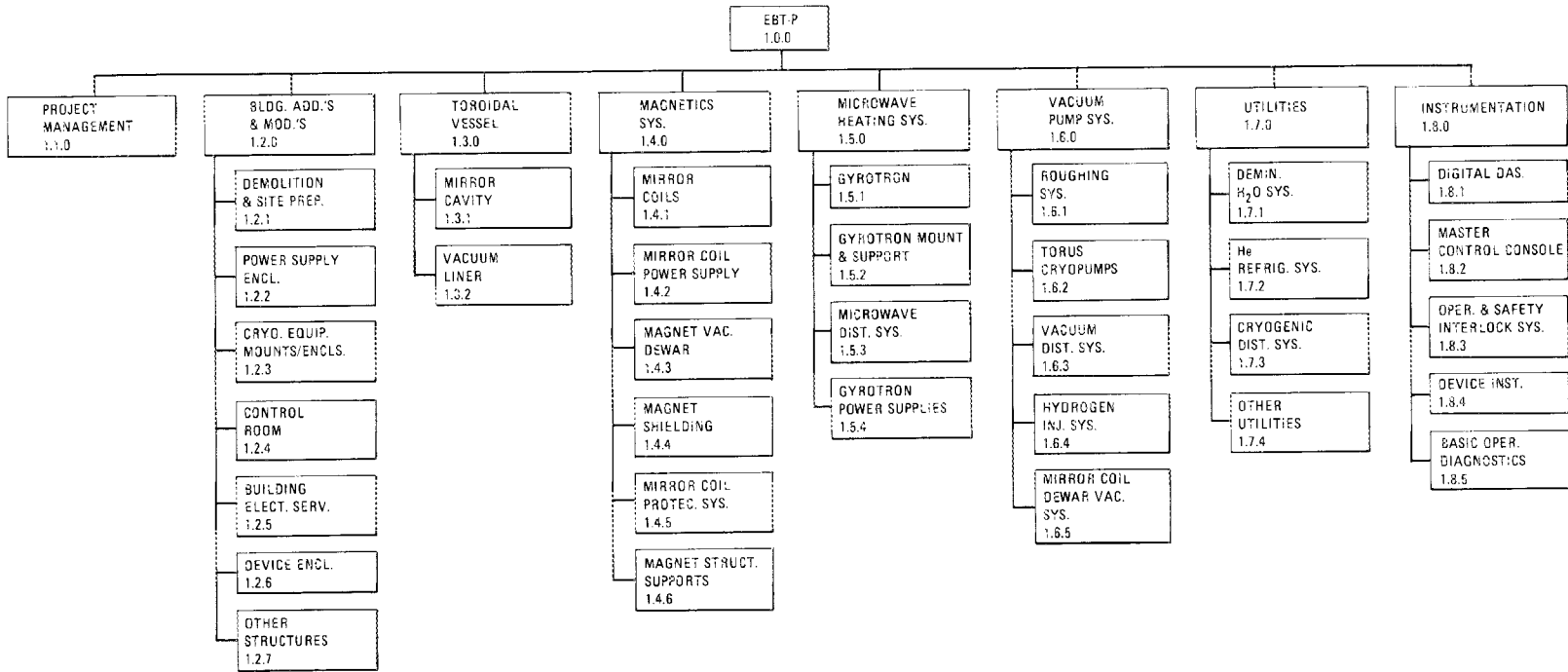


Fig. 6.1. Work breakdown structure for EBT-P.

7. ASSESSMENT OF RESEARCH AND DEVELOPMENT INTERFACE

Successful realization of EBT-P requires significant advances in some areas of technology. The ongoing EBT-S experimental program will have an essential role in extending the technology by providing important operating experience and serving as a test bed for subsystems and components; other needs will require development efforts specifically for EBT-P.

Two major subsystems, the superconducting mirror magnets and the microwave sources, have been identified as requiring intensive development efforts. Development tasks for these components have been initiated. A consistent and vigorous effort will be required to produce results on a schedule consistent with the needs for EBT-P. A third subsystem, neutral beams, will also require a substantial development effort, but such an effort has not yet started. Although neutral beams are not required for the initial EBT-P installation, a development program must be defined and initiated at an early date in order to maintain the credibility of neutral beam injection as a future option (see Sect. A.7.3).

As the design of EBT-P proceeds, it may be determined that other subsystems and components will require some level of development before enough confidence can be gained on these systems or components to include them on EBT-P; ion cyclotron heating is a notable example (see Sect. A.7.2).

7.1 MAGNET DEVELOPMENT

A development effort for the mirror magnets has been initiated at ORNL. The purposes of this development task are (1) to demonstrate design features and fabrication techniques that will produce the required field accuracy and eliminate systematic (cumulative) field errors; (2) to solve the problems of structural containment and of maintaining proper alignment in the dewar after cooldown and energizing; (3) to evaluate thermal design features and determine heat removal capability; and (4) to develop techniques, facilities, and criteria for acceptance testing of the coils manufactured for EBT-P. In short, the development effort is aimed at reducing the risk of proceeding with the final design and manufacture of a full complement of 36 magnets.

The magnet development program consists of two parallel efforts. One effort requires the design, fabrication, and testing of two instrumented test magnets of the NbTi pool-boiling concept as proposed for EBT-P. The coils will include heaters embedded in portions of the conductor for simulating heat input from gamma rays and other sources. The magnets will be tested separately and then as a pair in a two-magnet array as they would be installed on EBT-P. The other effort is intended to retain flexibility for an alternate design concept based on a Nb₃Sn superconductor and forced-flow cooling. One instrumented test magnet will be built and tested individually and then with one or both NbTi magnets, again as it would be mounted in EBT-P. Sufficient Nb₃Sn superconducting material will be procured for a second magnet if additional magnet testing is required.

The development test schedule as now proposed will provide significant test results which will be available early enough to provide useful data for the EBT-P design; they will also be available prior to ordering the superconductor for all 36 magnets (April 1981). Essentially complete test results will be available prior to the start of magnet manufacture (February 1982). Once the industrial participant who will direct the final design and manufacture of the mirror magnets for EBT-P is selected, he will need to interact with the development activity, assist in determining appropriate acceptance tests, monitor or participate in performance tests, and apply the experience thus gained to the overall EBT-P program.

7.2 MICROWAVE DEVELOPMENT

The microwave heating capability planned for EBT-P will provide substantial cw power (~1.2 MW) at a frequency of 110 GHz for bulk heating and a lower cw power (~600 kW) at a frequency of perhaps 60 GHz for profile heating.

The microwave system includes three basic elements: (1) a multiple array of microwave sources (gyrotrons); (2) a microwave distribution system for the efficient transfer of energy to the plasma; and (3) supporting electrical and electronic subsystems for monitoring, control, and safety. These basic elements require an intensive, complementary development effort that is being performed by ORNL as a continuation of the microwave heating support activities conducted for many years by the ORNL EBT program.

7.2.1 Microwave Sources

The time required to develop the microwave sources is the principal uncertainty affecting the EBT-P schedule.

Much of the technology needed is being developed under a program started in April 1976 to develop a 28-GHz, 200-kW cw gyrotron for EBT-S. This work is being done by Varian Associates, Palo Alto, California, under subcontract to ORNL. At the time the work started, available tubes were capable of no more than a few kW steady state. Accomplishments include the attainment of 105 kW for several minutes in May 1978 and the successful operation of EBT-S with 50 kW of microwave heating (cw) in September 1978. However, despite the significant progress, the experience indicates that the development of a reliable 200-kW cw tube is a difficult task.

In FY 1979 parallel programs were initiated to develop 110-GHz, 200-kW cw gyrotrons for EBT-P. Two industrial firms, Varian Associates and Hughes Aircraft Company (Torrance, California), are working under ORNL subcontracts with identical work statements. It is projected that with a continuing vigorous effort, the development can be completed by September 1982, making the gyrotron sources a near-pacing item for EBT-P. However, the development of the 110-GHz tube is expected to be technically difficult; therefore, scheduled predictions cannot be made with confidence.

A specific program to develop a lower frequency gyrotron for profile heating of EBT-P has not yet begun. The concept now being followed is to develop the more difficult 110-GHz tube and then to scale the frequency, and consequently various components of the tube, down to the lower frequency. More recently, however, proposals have been offered that would initiate a concurrent effort to develop a 60-GHz tube that could fill a need both for a microwave source for tokamak and mirror machine applications and for EBT-P profile heating. Such a program would allow EBT-P operation at a reduced performance level using 60-GHz microwaves for bulk heating and the soon-to-be-available 28-GHz gyrotrons for profile heating but would reduce the dependence of EBT-P on the timely success of the 110-GHz development effort.

7.2.2 Microwave Distribution

The microwave distribution system will require general component development as well as microwave circuit development specifically for EBT-P. Much of the experience gained in developing and operating the 28-GHz system on EBT-S will be applicable to EBT-P; however, an additional development effort will probably be required that takes into account specific characteristics of EBT-P and of the microwave sources being developed for it. A dedicated test facility appears desirable for this task and for the task described in Sect. 7.2.3 below. The results of this effort will provide guidance and verification for the EBT-P design.

7.2.3 Microwave Supporting Subsystems

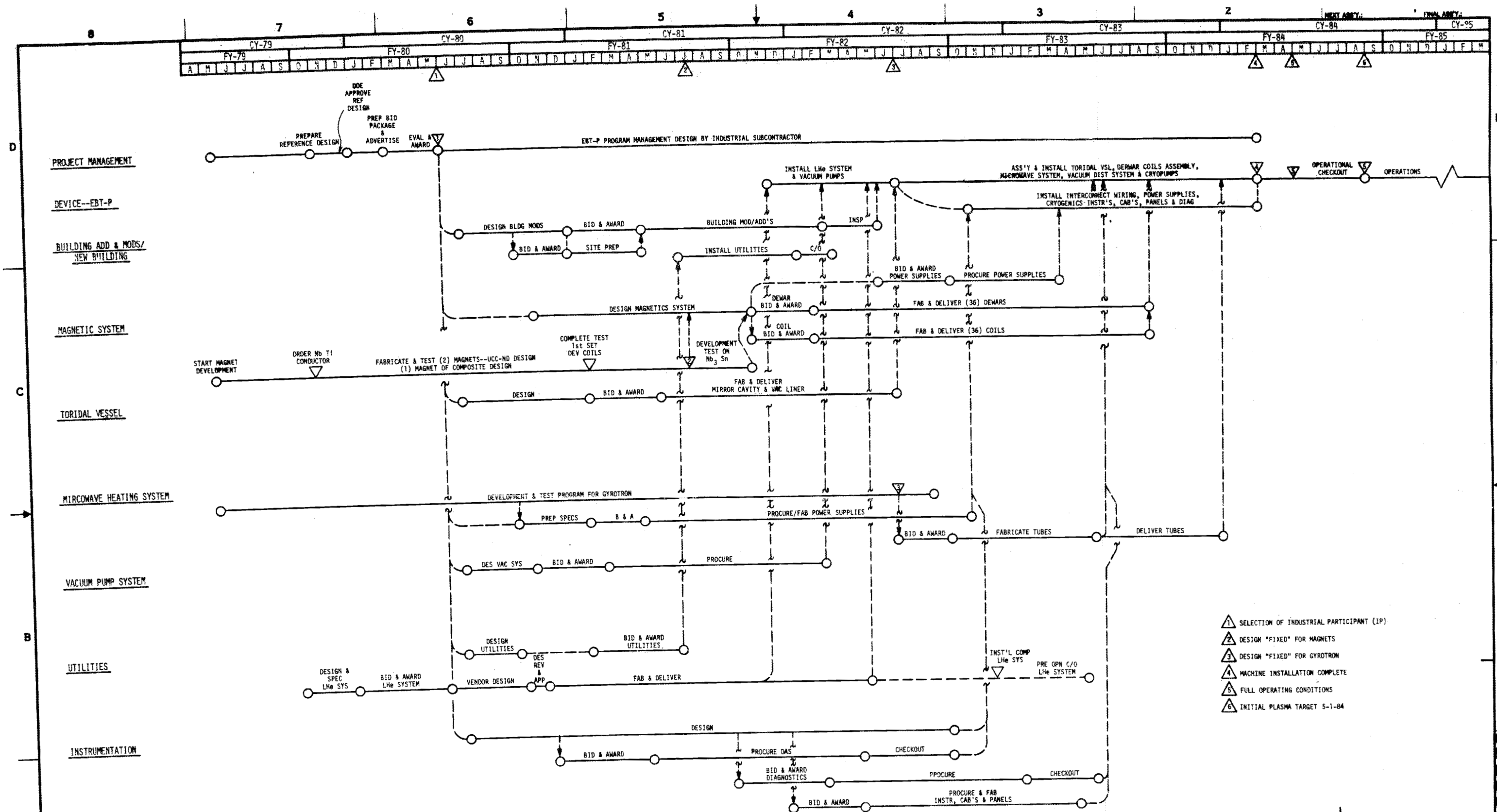
These subsystems include the dc power supplies, automatic control networks for component protection, operational and performance monitoring, controls for operating multiple microwave sources, and personnel

safety systems. Experience on EBT-S will be applicable; however, a supplementary development effort will be required to address the complex control aspects of EBT-P operation using multiple microwave sources.

8. PROJECT SCHEDULE

The preliminary project schedule for EBT-P is shown schematically in Drawing D-XRP-14270-001, which follows in this section. Major elements of the work breakdown structure are included, and timing relationships are based on several key assumptions:

- (1) The project scope will not deviate significantly from that contained in this report.
- (2) The industrial participant will be selected and put under subcontract on the date shown.
- (3) The superconducting coil prototype work at ORNL will meet schedule milestones.
- (4) The gyrotron development program schedule will be met.
- (5) Advance engineering for the liquid helium system will be initiated in early FY 1980.



NO REPRESENTATION OR WARRANTY, EXPRESSED OR IMPLIED, IS MADE AS TO THE ACCURACY, COMPLETENESS OR USEFULNESS OF THE INFORMATION OR STATEMENTS CONTAINED IN THESE DRAWINGS, OR THAT THE USE OR EMPLOYMENT OF ANY INFORMATION, APPARATUS, METHOD OR PROCESS DESCRIBED IN THESE DRAWINGS MAY INFRINGE PRIVATE RIGHTS OF OTHERS. NO LIABILITY IS ASSUMED WITH RESPECT TO THE USE OF, OR FOR DAMAGES RESULTING FROM THE USE OF, ANY INFORMATION, APPARATUS, METHOD OR PROCESS DESCRIBED IN THESE DRAWINGS. DRAWINGS MADE AVAILABLE FOR INFORMATION TO OTHERS ARE NOT TO BE USED FOR OTHER PURPOSES, AND ARE TO BE RETURNED UPON REQUEST OF THE PURCHASING CONTRACTOR.

| REV | ISSUED FOR COMMENT 9-17-79 | DESCRIPTION | BY | CHK | SECT | DEPT | DATE | REQ | DATE | ACQD | DATE | ENDA | DATE | CA | EC | EE | EM | IE | M | PD | SE | XAD | |
|-----|----------------------------|-------------|----|-----|------|------|------|-----|------|------|------|------|------|----|----|----|----|----|---|----|----|-----|--|
| | | | | | | | | | | | | | | | | | | | | | | | |

| | | | |
|--|------|---|--|
| TOLERANCES UNLESS OTHERWISE SPECIFIED FRACTIONS : XX DECIMALS : XXX DECIMALS : ANGLES : BREAK SHARP EDGES : FINISH : | | DES P. A. TABOR DRW S. MILLIS <i>SM</i> 9-19-79 CHK SECT DEPT & PLANT | UNION CARBIDE CORPORATION - NUCLEAR DIVISION <small>UNION CARBIDE CORPORATION IS A DIVISION OF UNION CARBIDE CORPORATION, A CORPORATION INCORPORATED IN THE UNITED STATES OF AMERICA. ALL RIGHTS RESERVED.</small> EBT-P PROJECT DEFINITION STUDIES PRELIMINARY SCHEDULE 9201-2 SITE 36 COIL CASE |
| UCC NO | ENDA | SCALE | NO |
| PLANT | BLDG | FL | SHT. |
| 1 | 06 | 06 | 06 |
| PLANT | BLDG | FL | SHT. |
| 1 | 06 | 06 | 06 |
| PLANT | BLDG | FL | SHT. |
| 1 | 06 | 06 | 06 |

9. PROPOSED METHOD OF ACCOMPLISHMENT

9.1 INTRODUCTION

It is proposed that this experiment be conducted by the U.S. Department of Energy (DOE) with the Union Carbide Corporation Nuclear Division (UCC-ND) as the program manager and technical advisor on the project. In turn, UCC-ND will subcontract the detailed design and fabrication of the device to a major industrial participant and other subcontractors as required.

To accomplish the design and construction of this device in an orderly manner consistent with the policies of each major participant, a Memorandum of Agreement (MOA) was negotiated between DOE's Office of Fusion Energy (ETM), their Oak Ridge Operations Office (ORO), and UCC-ND, or the Oak Ridge National Laboratory (ORNL), which details the roles and responsibilities of each participant. The MOA is quoted here and forms the basis for the design and construction responsibilities for ORNL and the industrial participant (IP). The approved schedule showing critical DOE and ORNL milestones for the project initiation phase is shown in Fig. 9.1 (referred to in the MOA as attachment B).

9.2 ETM/ORO/ORNL MEMORANDUM OF AGREEMENT: EBT - PROOF-OF-PRINCIPLE PROJECT

I. Statement of Purpose

It is the intention of the Office of Fusion Energy (ETM) of the Department of Energy (DOE) to implement the design and fabrication of an Elmo Bumpy Torus - Proof-of-Principle experiment (EBT-POP) with significant industrial participation in all phases of the project and with minimum procedural delays. It is the purpose of this Memorandum of Agreement (MOA) to document the internal agreements, plans, and responsibilities of the primary participants in initiating the EBT-POP project. Those participants are three in number: ETM, DOE's Oak Ridge Operations Office (ORO), and Union Carbide Corporation's Nuclear Division, hereinafter referred to as the Oak Ridge National Laboratory (ORNL). ETM and ORO will execute their project management responsibilities in accordance with DOE policy. This MOA shall govern until the industrial participant (IP) is selected and it is superseded by a Project Management Plan (PMP).

II. Agreements

The following agreements shall constitute the basis for proceeding with the EBT-POP project:

- A. ORNL is assigned responsibility for management of the EBT-POP project, including the project research and development and the EBT-S experiment. In addition, ORNL is assigned responsibility for technical coordination of the national EBT program, including theoretical research and off-site experimental activities. DOE will rely on ORNL in this lead role for effective execution of the EBT program.
- B. It is intended in pursuing this project that industry shall have a major role, not only in the fabrication of the EBT-POP, but also in the project definition, design, and subsequent experimental operation. The goal is the selection of a primary industrial participant (IP), whose role will lead to broad corporate responsibilities for, and identification with, the ultimate success of the EBT program.
- C. The IP will be selected from among several organizations who will be first competitively selected to conduct project definition studies and later will competitively propose to build the EBT-POP experiment, which, as eventually approved by ETM, may be a combination of design features from all of the studies.

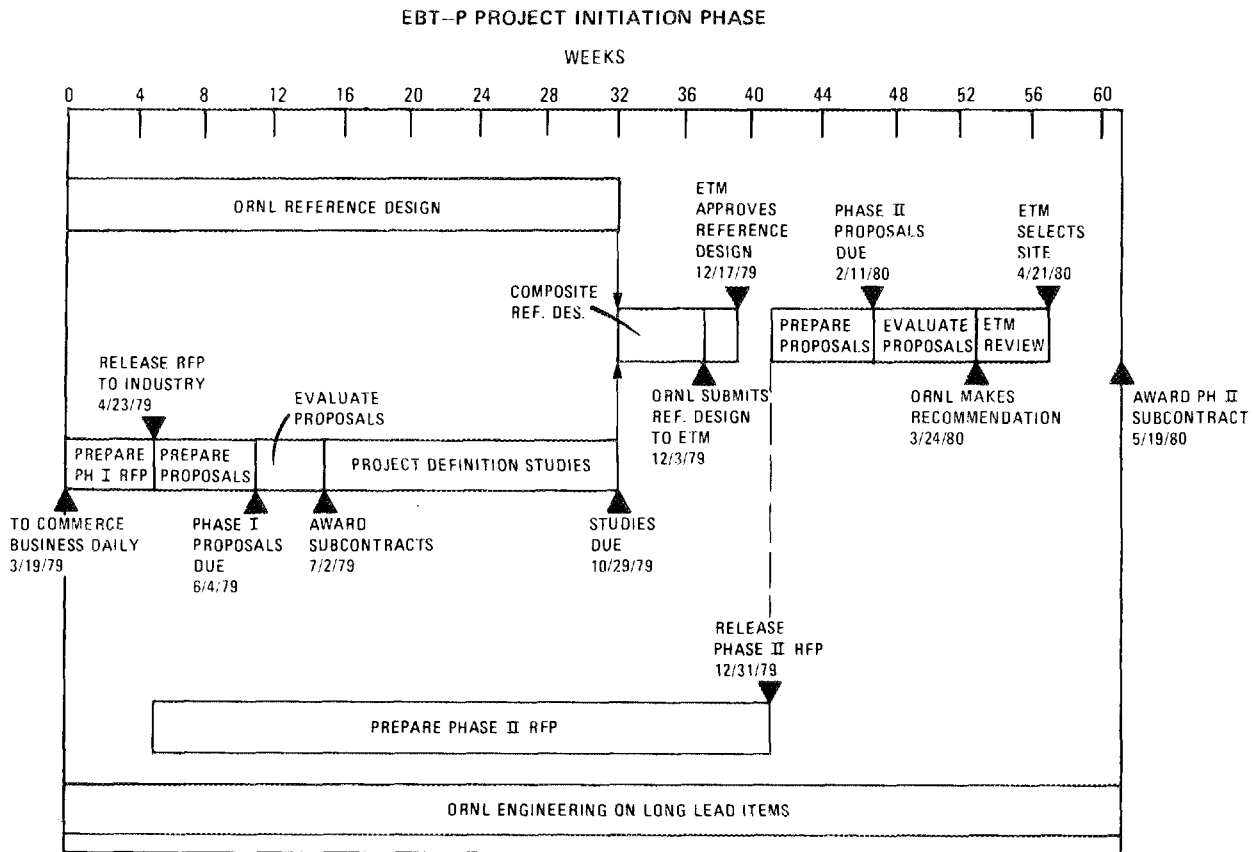


Fig. 9.1. The approved activity schedule for the EBT-P project initiation phase (referred to in the MOA as attachment B).

D. ETM and ORO will be provided the opportunity to participate with ORNL in all activities related to EBT-POP project definition and execution, including, but not limited to:

- Establishment of qualification and evaluation criteria
- Subcontractor selection as nonvoting ex officio members of the Evaluation Board
- Overview of subcontractor activities through ORNL
- Evaluation of subcontractor deliverables

ETM and ORO staff authorized to receive selection-type information in their capacity as nonvoting ex officio members will be set forth in separate correspondence.

- E. Authorized ETM and ORO staff will be provided copies by ORNL of all proposals and studies received by ORNL at the same time as these documents are available for ORNL internal evaluation and review.
- F. Long-lead research and development activities critical to the success of the EBT-POP, and generic to all anticipated designs, will be started at the earliest practical time by ORNL for later transferral to the cognizance of the industrial participant if determined by DOE, in consultation with ORNL, to be appropriate.
- G. EBT-S activities, including participation by industry, will proceed without restrictions from the EBT-POP. All necessary precautions shall be taken to assure that all EBT-POP industrial competitors have fair and equal access to information pertinent to EBT-POP studies and related efforts.
- H. Only Phase I (project definition) subcontractors will be eligible for selection as the IP in the Phase II (design, fabrication, and installation) competition. (Thus selection for Phase I shall technically constitute prequalification for Phase II.)
- I. The site for the EBT-POP will be determined by ETM.

III. Project Initiation Plan

The intended plan for initiating the EBT-POP project through Phase I project definition studies and proposals for Phase II implementation of the project is outlined in attachments A and B. For convenience in discussion and reference, the plan is broken down into a number of "steps." The important features of the plan are given in the descriptions of the steps.

Step

Activity

Phase I

- 1 RFP Preparation — ORNL will prepare the RFP for the selection of several subcontractors to conduct Phase I project definition studies. Proposed subcontract terms and conditions will be included in the RFP. These subcontractors will be deemed qualified for Phase II by their participation in Phase I. A Commerce Business Daily (CBD) announcement for Phase I will be issued as early as possible to allow the industrial community time to determine its interest.
- 2 Proposal Preparation — Proposers (including consortia, partnerships, joint ventures, etc.) will submit proposals to ORNL. The proposals will emphasize capabilities and experience that relate to the POP experiment task. Specific experience in the physics of EBT will not be required, but capabilities to contribute in a significant way to the physics design definition for EBT-POP, to the device design, fabrication and installation, and to the subsequent experimental operation will be important factors.

| <u>Step</u> | <u>Activity</u> |
|-------------|--|
| 3 | <u>Proposal Evaluation</u> – ORNL will evaluate the proposals and award, subject to ORO approval, several project definition study fixed price subcontracts. Methods will be employed to allow work to begin as soon as practicable after the selections are made. Authorized ETM and ORO staff will participate as nonvoting ex officio members in the selection process. |
| 4 | <u>Project Definition Studies</u> – The subcontractors will conduct approximate four-month technical studies to develop their ideas of the objectives, design features, performance parameters, schedule, cost and manpower requirements, R&D requirements, and <u>generic</u> site requirements and submit a full written report upon completion. The results of this work will <u>not</u> constitute that subcontractor's proposal for Phase II. |
| 5 | <u>ORNL Support and Management</u> – In parallel with steps 1-4, ORNL will maintain its program activities and technical support work for EBT-POP, including design efforts. ORNL will provide subcontractors with sufficient latitude in this Phase to develop their own independent ideas and approaches. |
| 6 | <u>Recommended Reference Design</u> – ORNL will evaluate the Phase I studies and synthesize and consolidate the best subcontractor ideas along with its own ideas into a proposed reference design, with recommended objectives, parameters, costs, schedule, etc., for the project. ETM and ORO will participate in this process as advisors. ORO will review the ORNL recommendations and transmit them to ETM with its own evaluation and comments. |
| 7 | <u>ETM Review</u> – Based on the recommended reference design, ETM will conduct a review of the project, including technical community input, to conclude the project definition phase. ETM will reassess the EBT program during this step. Continuation of the EBT-POP project will be contingent upon cost, schedule, and technical merit considerations. Assuming the project is continued, the final reference design will be that established and approved by ETM after consultation with ORO and ORNL. |

Phase II

| | |
|----|--|
| 8 | <u>RFP Preparation</u> – In parallel with the above activities, ORNL will prepare the RFP for Phase II (design, fabrication, and installation) subject to ORO approval, on a schedule that allows the RFP to be released when the final reference design is approved by ETM. The RFP will be issued only to Phase I subcontractors. |
| 9 | <u>Proposal Submission</u> – Proposals will be based on the project final reference design as approved by ETM. Proposals will be requested for the government-owned ORNL site from each proposer. In addition, proposers may submit proposals for an alternate site of their choice, other than ORNL. Submission of alternate site proposals will not be required. |
| 10 | <u>Long-Lead Engineering</u> – For those areas of the project where components or systems have pacing or long delivery schedules and which are not specific to a particular site or design approach, ORNL will begin engineering work to avoid unnecessary delay. Each of these areas will be reviewed on a case-by-case basis by ORO and approved by ETM before work on it can begin. Following the IP selection, the responsibility for those areas may be transferred to the IP for completion. |

| <u>Step</u> | <u>Activity</u> |
|-------------|---|
| 11 | <u>ORNL Evaluation and Selections</u> -- ORNL will evaluate all Phase II proposals and select the best proposal for an ORNL site and the best proposal for an alternate site. Authorized ETM and ORO staff will also participate as nonvoting ex officio members in this process. ORNL will submit all Phase II proposals and its evaluation and selections to ORO, who will forward these, with comments, to ETM for its consideration and site determination. |
| 12 | <u>ETM Site Selection</u> -- Authorized ETM staff, with ORO support, will review all Phase II proposals and the ORNL selections. Limiting itself to the two ORNL site/IP selections, ETM will determine the site which it considers to be in the best overall interest of the EBT program and the fusion program generally. |
| 13 | <u>Negotiation with IP</u> -- Following the ETM site selection, ORNL will negotiate with its selected IP, to establish a basis for beginning project design work as soon as practicable. The initial CFFF subcontract will be for design, fabrication, and installation only. The IP will have the opportunity to participate meaningfully in the operation of the experiment, the precise nature and extent of that involvement to be determined by ETM and to be negotiated later. ETM will consider the site selected and other factors in reaching its determination. |

IV. Cost and Schedule

The project initiation schedule indicated in attachments A and B is intended as a target schedule that each of the signatory organizations will exert its best efforts to meet. The schedule is considered optimistic but achievable.

DOE has initially budgeted \$44M as the Major Device Fabrication (MDF) cost target for the design and fabrication of EBT-POP. The current schedule calls for the effective contract between ORNL and its IP to begin by mid FY 1980 and plasma experiments to begin by the end of FY 1983. All parties accept these as targets and will use their best technical and management efforts to develop and implement a proof-of-principle project within these goals.

V. Responsibilities and Commitments (Summary)

The primary intended responsibilities of ORNL, ORO, and ETM in the project initiation phase have been identified in the discussion of the plan above and will not be repeated in detail here. In summary they are as follows:

ORNL

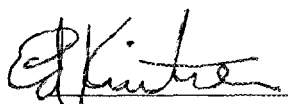
ORNL will coordinate the overall EBT program and will be responsible for the management of EBT-POP and EBT-S such that fusion program objectives and constraints are met. ORNL will conduct the procurement process to enable the expeditious selection of, and award of an ORNL subcontract to, the IP.

ORO

ORO will provide the formal administrative reviews and approvals for the procurement decisions and will participate in the technical and management decisions in anticipation of field office project management responsibilities in accordance with DOE policy. Following project approval, ORO will take the lead in developing a comprehensive PMP.

ETM

ETM will provide overall programmatic guidance, project overview and definition, and funding for EBT-POP and other components of the EBT program. Authorized ETM staff will have the opportunity to participate in related ORNL EBT-POP activities. The establishment of the final reference design and the site selection decision will be made by ETM.



E. E. Kintner
ETM

3/21/79

Date



H. Postma
ORNL

3/27/79

Date



J. A. Lenhard
ORO

3-27-79

Date

ATTACHMENT A

EBT-POP Memorandum of Agreement

| | |
|--|----------|
| • ORNL begins reference design | 3-1-79 |
| • Commerce Business Daily announcement released | 3-19-79 |
| • Release Phase I RFP | 4-23-79 |
| • ORNL initiates Phase II RFP preparation | 4-23-79 |
| • Phase I proposals due | 6-4-79 |
| • Award Phase I subcontracts | 7-2-79 |
| • Phase I Project definition studies completed | 10-29-79 |
| • ORNL completes reference design ^a | 12-3-79 |
| • ETM establishes final reference design and approves project continuation | 12-17-79 |
| • ORNL releases Phase II RFP ^b | 12-31-79 |
| • Phase II proposals due | 2-11-80 |
| • ORNL completes Phase II selections | 3-24-80 |
| • ETM ratifies one ORNL selection based upon ETM site selection | 4-21-80 |
| • UCC-ND authorizes IP to start work | 5-19-80 |

^aDesign may continue at ORNL for long-lead items.

^bThis date assumes no substantial change from ORNL reference submittal.

10. COST ESTIMATE

A cost estimate for the EBT-P project has been prepared and is being included under separate cover. The estimate reflects the construction of a device, as described in this document, at the ORNL Y-12 facility subject to the conditions specified in the ETM/ORO/ORNL MOA.

11. OUTLINE SPECIFICATIONS

Outline specifications are grouped by section according to the general character of the work involved in various sections and subsections. These sections include

- (1) building additions and modifications,
- (2) toroidal vessel,
- (3) magnetics system,
- (4) microwave heating system,
- (5) vacuum pumping system,
- (6) utilities, and
- (7) instrumentation.

11.1 GENERAL CODES, STANDARDS, AND SPECIFICATIONS

The design of EBT-P will be in accordance with the latest editions of all applicable codes, standards, regulations, and other pertinent documents of all local, state, and national government agencies having jurisdiction and of commonly accepted trade organizations.

The codes and standards used in the preparation of this report are listed below.

11.1.1 Structural

American Concrete Institute

- Building Code Requirements for Reinforced Concrete
- Ultimate Strength Design Handbook, Vol. I
- Ultimate Strength Design of Reinforced Concrete Columns

American Institute of Steel Construction

- Steel Construction Manual

American Iron and Steel Institute

- Specification for the Design of Cold Formed Steel Structural Members

American National Standards Institute

- American National Standard Building Code Requirements for Minimum Design Loads in Buildings and Other Structures

American Society for Testing and Materials

- ASTM A615, Specification for Deformed and Plain Billet-Steel Bars for Concrete Reinforcement
- ASTM A36, Structural Steel

American Society of Civil Engineers

- ASCE Paper No. 3269, Wind Forces on Structures

International Conference of Building Officials

- Uniform Building Code

Masonry Institute

- Masonry Design Manual

National Concrete Masonry Association

- TR75B, Specifications for Design and Construction of Loadbearing Concrete Masonry

Portland Cement Association

- Analysis and Design of Small Reinforced Concrete Buildings for Earthquake Forces

Prestressed Concrete Institute

Design Handbook for Precast and Prestressed Concrete Structures

Steel Joist Institute

Standard Specifications

Steel Structures Painting Council

Steel Structures Painting Manual, Vol. I: Good Painting Practice; Vol. II: Systems and Specifications

11.1.2 ArchitecturalFactory Mutual

Handbook of Industrial Loss Prevention

National Fire Protection Association (NFPA)

No. 101, Code for Life Safety from Fire in Buildings and Structures

11.1.3 CivilAmerican Association of State Highway and Transportation Officials (AASHTO)

AASHTO M 36, Zinc Coated (Galvanized) Corrugated Iron or Steel Culverts and Underpass

AASHTO M 190, Bituminous Coated Corrugated Metal Pipe and Pipe Arches

American Petroleum Institute (API)

STD 650-73, Welded Steel Tanks for Oil Storage

American Water Works Association (AWWA)

AWWA C 151-76, Standard for Ductile Iron Pipe Centrifugally Cast in Metal Molds or Sand-lined Molds for Water and Other Liquids

AWWA C 800-71, Standard for Gate Valves 3 inches through 48 inches for Water and Other Liquids

AWWA C 800-64, Standard for Installation of Cast Iron Water Mains

National Fire Protection Association (NFPA)

NFPA 13-76, Standard for the Installation of Water Sprinklers

NFPA 20-76, Standard for the Installation of Centrifugal Fire Pumps

NFPA 24-73, Standard for Outside Protection

11.1.4 PipingAmerican National Standards Institute (ANSI)

B16.5, Steel Pipe Flanges and Flanged Fittings

B36.10, Wrought-Steel and Wrought-Iron Pipe

B36.19, Stainless Steel Pipe

American Petroleum Institute (API)

Standard 620

Standard 650

Standard 527, Seat Tightness of Safety Relief Valves with Metal to Metal Seats

American Society for Testing and Materials (ASTM)

A53, Specification for Welded and Seamless Steel Pipe

A105, Specification for Forged or Rolled Steel Pipe Flanges, Forged Fittings, and Valves and Parts for High-Temperature Service

A312, Specification for Seamless and Welded Austenitic Stainless Steel Pipe

American Society of Mechanical Engineers (ASME)

Boiler and Pressure Vessel Code, Section VIII, Division 1, "Pressure Vessels"

Boiler and Pressure Vessel Code, Section IX, "Welding Qualifications"

American Water Works Association (AWWA)

C 203, Coal-Tar Enamel Protective Coatings for Steel Water Pipe

C 500, Gate Valves for Ordinary Water Works Service

C 106, Cast-Iron Pipe Centrifugally Cast in Metal Molds, for Water or Other Liquids

American Welding Society (AWS)

D7.0, Standard Specifications for Field Welding of Steel Water Pipe Joints

D10.4, Welding of Austenitic Chromium-Nickel Steel Piping and Tubing

A5.4, Specification for Corrosion-Resisting Chromium and Chromium-Nickel Steel Covered Welding Electrodes

Compressed Gas Association (CGA)

P-1, Safe Handling of Compressed Gases in Containers

Compressed Gas Handbook

Hydraulic Institute (HI)

Standards, Centrifugal Pump Section

Manufacturers Standardization Society of the Valve and Fittings Industry (MSS)

SP-42, 150 lb Corrosion Resistant Cast Flanged Valves

SP-61, Hydrostatic Testing of Steel Valves

SP-25, Standard Marking System for Valves, Fittings, Flanges, and Unions

Portland Cement Association (PCA)

Design and Control of Concrete Mixtures

The Pipe Fabrication Institute (PFI)

ES4, Standard Practice, Shop Hydrostatic Testing of Fabricated Piping

ES5, Standard Practice, Cleaning Fabricated Piping

ES11, Recommended Practice for Permanently Affixing Identification Symbols to Fabricated Piping

Tubular Exchanger Manufacturers Association (TEMA)

Standards

11.1.5 InstrumentationInstrumentation Society of America (ISA)

ISA - S5.1 1973, Standard Instrumentation Symbols and Identification (ANSI Y32.20)

11.1.6 ElectricalAmerican National Standards Institute (ANSI)

ANSI C34.2 - 1968 (B1973), Practices and Requirements for Semiconductor Rectifiers

ANSI 83.9 - 1972, Racks, Panels, and Associated Equipment

Insulated Power Cable Engineers Association (IPCEA)

IPCEA S-19-81, Rubber Insulated Wire and Cable

IPCEA S-61-402, Thermoplastic Wires Cable

IPCEA S-54-401, American Standard Requirements for Metallic and Associated Coverings for Insulated Cables

Joint Industrial Council (JIC)

EPB-1-1967, Electrical Standards

National Electrical Manufacturers Association (NEMA)

NEMA TR-11, Power Transformers

NEMA SG3, Power Operated Circuit Breakers

NEMA AB1, Molded Case Circuit Breakers

National Fire Protection Association (NFPA)

NFPA No. 70-1978, National Electrical Code

NFPA No. 72D, Proprietary Protective Signaling Systems

11.1.7 Plumbing, Heating, Ventilating, and Air ConditioningAir-Conditioning and Refrigeration Institute (ARI)

ARI STD 210, Unitary Air-Conditioning Equipment

ARI STD 410, Forced Circulation Air-Cooling and Air-Heating Coils

ARI STD 430, Central Station Air-Handling Units

Air Diffusion Council (ADC)

ADC Test Code 1062R2, Diffusers

Air Moving and Conditioning Association, Inc. (AMCA)

AMCA STD No. 210, Test Code for Air Moving Devices

American Society of Heating, Refrigerating and Air Conditioning Engineers, Inc. (ASHRAE)

Standard 36B-63, Fundamentals, Systems, Applications, Equipment Air Distribution

American Society of Mechanical Engineers (ASME)

ASME PTC11-1946, Test Code for Fans

ASME PTC23-1958, Atmospheric Water Cooling Equipment Test Code

American Society of Plumbing Engineers (ASPE)

Standard National Plumbing Codes

American Water Works Association (AWWA)

AWWA C203-66, Pipe Coverings Underground

Associated Air Balance Council (AABC)Air and Water System Balance – National Standards For Field Measurements and Instrumentation,
Total System BalanceCast Iron Soil Pipe Institute (CISPI)CISPI STD HS-67, 301 - 69I and HSN - 68I, Pipe, Fittings, Coupling and Rubber Gaskets to Seal
Joints in Hub and Spigot Cast Iron Soil Pipe and FittingsCooling Tower Institute (CTI)

CTI Bulletin ATP - 105, Acceptance Test Procedure for Industrial Water-Cooling Towers

National Environmental Balancing Bureau (NEBB)

System Testing and Balancing Procedures for Testing - Balancing Adjusting of Environmental Systems

National Fire Protection Association (NFPA)

NFPA No. 90A, Standard for the Installation of Air Conditioning and Ventilating Systems

NFPA No. 91, Standard for the Installation of Blower and Exhaust Systems

Plumbing and Drainage Institute (PDI)

Standard PDI-WH 201, Water Hammer Arrester

Sheet Metal and Air Conditioning Contractors National Association (SMACNA)

SMACNA Standard Air Duct, Fire Dampers

11.1.8 GeneralCode of Federal Regulations (CFR)

10 CFR 20, Standard for Protection Against Radiation

U.S. Department of Energy (DOE)

ERDA Manual, Chapter 0550, Occupational Safety Standards

ERDA Manual, Chapter 0552, Fire Protection

ERDA Manual, Appendix 6301, General Design Criteria

ERDA Manual, Appendix 6101, Management of Construction Projects

11.2 BUILDING ADDITIONS AND MODIFICATIONS

This section presents facility requirements for demolition, structural and architectural systems, piping systems, electrical systems, fire protection, and heating, ventilating, and air conditioning systems.

11.2.1 Building Demolition and Site Preparation

Demolition for the EBT-P device enclosure will include complete removal of the first and second floors of Building 9201-2 within the rough area bounded by column lines 3, 7, f, and k. This will necessitate relocating the 1-MW power supply vault for EBT-S and resupporting the west end of the EBT-S equipment platform.

The required second floor demolition will be as outlined on Drawing S2E-8945A-SK4. Only the principal high-bay building columns will remain within the outlined area. The masonry wall along column line k between column lines 4 and 6 will be site cleared to the underside of the low-bay roof in order to make room for the new enclosure shield wall. A second penetration through that wall will be provided between columns 6 and 7 above the low-bay roof level for the environmental control supply duct to the device enclosure.

The extent of the first floor demolition will be as outlined on Drawing S2E-8945A-SK6. The "track" structure will be removed down to the footings. Immediately below the existing first floor there is a plenum chamber off the northwest building air tunnel; this will also be removed.

A dust screen will be provided around the entire area for the duration of the demolition work.

On the low-bay roof in the area bounded by column lines 5, 6, k, and d, an existing 4- by 4-ft roof hatch will be expanded to a 10- by 10-ft opening for the HVAC supply and return ducts for the control room and the return duct from the device enclosure (see Drawing S2E-8945A-SK10).

11.2.2 Power Supply Enclosures

The total volume of power supplies and related equipment required to run EBT-P is considerable, necessitating a building addition to Building 9201-2. Two additions will be necessary. The components having the promise of least reliability will be placed in a building on the west wall of 9201-2 complete with uniraill cranes, a service area, and utilities. The balance of the equipment will be on a fenced concrete pad behind the railroad tracks south of 9201-2.

Demolition and site preparation

Demolition for the new power supply building addition on the west end of Building 9201-2 will include site clearance of the remains of Building 9732-2. The existing fan for the cyclotron area will be relocated and its concrete support pad removed. The existing windows on the west end of Building 9201-2 will be removed and filled in with brick. The existing storm sewer running between Buildings 9105 and 9201-2 will be encased in concrete in the area to be occupied by the new compressor building addition. The line and an intermediate catch basin will be relocated to accommodate the new power supply building addition. The existing area sidewalks will be removed and rerouted as necessary for the new addition (see Drawing S2E-8945B-SK1).

Structural and architectural

The new power supply building addition (see Drawing S2E-8945A-SK2) will be 137 ft long by 42 ft wide by 39 ft high. The structure will be an insulated, preengineered steel frame enclosure with a 20-ton capacity bridge crane that will be operational over the entire width and length of the enclosed area. The floor system will be a reinforced concrete slab on grade.

Access will be provided via 3- by 7-ft personnel doors in the north and south end walls in addition to a 10-ft-wide by 12-ft-high overhead roll-up door for equipment access in the south wall.

Equipment maintenance will be done in the service bay area provided at the south end of the enclosure.

A new power supply equipment pad will be provided on existing grade at the southwest corner of Building 9201-2 (see Drawings S2E-8945A-SK1 and -SK3). The pad will be 21 ft wide by 175 ft long in the east-west direction. The entire pad perimeter will be rimmed with a 7-ft-high security fence. The central portion of the pad, which will hold the inductrols, will be diked to contain oil spills and water in the event of a fire. The area will drain through a manually operated gate valve to the creek immediately to the south of Building 9201-2.

Access to the equipment will be through 6-ft-wide double swinging gates in the east and west end perimeter fences and a 4-ft pedestrian gate in the north side fence. For maintenance, equipment will be installed and removed with a mobile crane.

Piping

Section 11.4.5 includes a complete discussion of piped services.

Heating, ventilating, and air conditioning

Ventilation will be provided to prevent the temperature in the enclosure from exceeding 110°F during the summer. The new ventilation system will consist of supply ductwork, return/exhaust ductwork, a supply fan, a return/exhaust fan, dampers, and a pneumatic control system. During the winter, dampers

will be modulated to vary the amount of return and outside air to provide a supply air temperature that will maintain space conditions at 40°F (minimum). Steam unit heaters will be installed to provide heat during the periods when the power supplies are inoperative. The HVAC system layout is as shown on Drawings H2E-34111-SK01, -SK02, and -SK03.

Electrical

The contents of the building addition and concrete pad are illustrated in Drawing E2E-14270-0002. Basically the pad contains the primary input, fused disconnect switches, vacuum circuit breakers, and induction voltage regulators for the high voltage microwave power supplies located in the new building addition. The pad also contains three small substations for 2.4-kV and 480-V power. The 480-V circuit breaker distribution panel is located in the north end of the building addition.

Fire protection

Automatic sprinkler systems will be installed to protect the new transformers, power supplies, regulators, and other equipment provided for EBT-P.

Two new deluge sprinkler systems will be installed, one to protect the equipment on the equipment pad and the new 30-MVA transformer on the south side of Building 9201-2 and one to protect the equipment in the power supply building addition. The systems will be hydraulically designed to provide a minimum water flow density of 0.25 gpm/ft² to the oil-filled equipment. A new valve house erected near the equipment pad will house both deluge valves. Water supply to the valve house will be extended from a nearby 10-in. main.

The sprinkler system will be provided with water flow and supervisory alarms that will upon activation transmit a coded signal to the Y-12 Fire Department and other emergency organizations.

The fire protection system will be designed and installed in accordance with NFPA standards for automatic sprinkler, alarm, and detection systems.

11.2.3 Cryogenic Equipment Mounts and Enclosures

The enclosures necessary to house the device cryogenic system components include the helium compressor enclosure and the refrigeration equipment enclosure. These enclosures provide protection from the weather for the cryogenic system components.

Structural and architectural

The cold box building addition for the helium refrigeration system will be located on the low-bay roof 1A between column lines 3, 5, k, and m (see Drawing S2E-8945A-SK10). The structure will be an insulated 22-ft-high steel-framed enclosure with corrugated metal roofing and siding.

The two cold boxes inside the enclosure will be supported on a special steel structural framing system. A maintenance platform will be provided around both vessels approximately 12 ft above the existing roof elevation. Access will be provided through one 6-ft-wide by 8-ft-high set of double swinging doors.

Structural steel framing will also be provided for the new helium dewar on the low-bay roof immediately to the east of, and adjacent to, the cold box building addition.

The helium compressor building addition (see Drawing S2E-8945A-SK8) will be 26 ft 6 in. high by 40 ft wide by 44 ft long. The steel-framed structure will be located just west of the existing northwest fan room on Building 9201-2 between column lines k and n. Two new compressors will be mounted inside on

independent, structurally isolated foundation pads in the reinforced concrete slab on-grade floor system. Maintenance and removal of the compressor components will be facilitated by a 3-ton-capacity, underhung bridge crane suspended from the roof framing system. A sheet metal wall will be provided along the west face only, leaving the north and south faces open to provide continued unimpeded air flow to the fan room.

Piping

Section 11.4.5 includes a complete discussion of piped services.

Electrical

The principal cryogenic equipment requiring electrical input will be the helium compressors, located outside Building 9201-2 adjacent to the northwest corner. These units will require ~2500 kVA at 2.4 kV. This power will be supplied from a 13.8/2.4-kV power transformer dedicated solely for this purpose and located on the new power supply pad south of Building 9201-2 (see Drawing E2E-14270-0003). The power cables will be run in conduit outside along the west wall of the new power supply building addition (see Drawing E2E-14270-0004).

The other cryogenic-related components requiring electrical input will be a cold box and associated cooling fans, to be located on the roof of Building 9201-2 above the experiment. The total power required will be ~50 kVA at 480 V, 3 ϕ . This power will be routed in conduit from a 480-V circuit breaker panel located at the north end of the new power supply building addition (see Drawing E2E-14270-0004).

Fire protection

The compressor building housing the two helium compressors will be protected by a wet pipe sprinkler system. An antifreeze loop will be extended from an existing wet pipe system in 9201-2 to the compressor building. The system will be designed for ordinary hazard occupancy according to the NFPA No. 13 pipe schedule.

The sprinkler system will be provided with water flow and supervisory alarms that will upon activation transmit a coded signal over the plant fire alarm system to the Y-12 Fire Department and other emergency organizations.

The fire protection system will be designed and installed in accordance with NFPA standards for automatic sprinkler, alarm, and detection systems.

11.2.4 Control Room

This section describes the construction of the control room immediately north of the device enclosure. Included in this section is a description of the basic structural and architectural requirements, the heating, ventilating, and air conditioning systems, the electrical requirements, and the fire protection systems.

Structural and architectural

The control room for EBT-P will be located on the second floor of Building 9201-2 in the low-bay area bounded by column lines 2-1/2, 5-1/2, k, and m (see Drawing S2E-8945A-SK9). The room will be enclosed with 1-hr-fire-rated metal stud and sheetrock walls. Access will be provided by 3-ft-wide by 7-ft-high personnel doors in the northeast, northwest, and southwest corners. An interior mezzanine

will be provided with a 100-psf-capacity sheet metal floor 9 ft above the main control room floor. Two sets of stairs will be provided for personnel access to the mezzanine. A 1/2-ton-capacity hoist and monorail will be provided for equipment access. The underside of the mezzanine structural framing will be finished with metal furring strips and sheetrock, as will the existing walls and columns below the mezzanine.

Cable tray and conduit access to the experiment will be provided through a radiation-shielded maze on the mezzanine between column lines 5 and 5-1/2. This maze will also accommodate the HVAC return duct from the experiment enclosure. The underside of the second floor slab will be reinforced with structural steel in order to support the lead-shielded maze.

Heating, ventilating, and air conditioning

The control room will be conditioned to maintain an inside design temperature of $78^{\circ}\text{F} \pm 2^{\circ}\text{F}$ and a relative humidity level of $50\% \pm 10\%$ by a new factory built-up modular unit located on the northwest low-bay roof. The built-up modular unit will consist of a return and air intake section with fan, filter section (95% ASHRAE STD 57-76), chilled water section, steam heating section, and supply fan section. Controls will be pneumatic. Insulated supply and return ductwork will be extended from the HVAC unit to serve the mezzanine and first floor of the computer room. The HVAC unit will have the capability of using outside air for cooling when conditions permit. A new chiller to be located on the first floor in the northwest fan room will be utilized to provide chilled water for the control room supply unit and the device enclosure supply unit. The HVAC system layout is as shown on Drawing H2E-34111-SK3.

Electrical

The EBT-P control room will require ~100 kVA for control cabinets and 30 kVA for lighting. This power will be supplied as 480-V, 3- ϕ power in conduit from the 480-V circuit breaker panel located at the north end of the new power supply building addition (see Drawing E2E-14270-0004). These conduits will terminate in cabinets containing 480/120-V transformers and distribution circuit breakers located in the control room. Power to individual control cabinets will be carried by overhead cable trays.

Fire protection

The control room will be provided with a preaction sprinkler system. A new preaction valve will be installed on an existing sprinkler water supply manifold located near the enclosure. Pneumatic/heat-activated devices will be installed to activate the preaction valve. The system will be designed for ordinary hazard occupancy, and piping will be sized according to the NFPA No. 13 pipe schedule. A smoke detection system will also be installed. The sprinkler system will be provided with water flow and supervisory alarms that will upon activation transmit a coded signal to the Y-12 Fire Department and other emergency organizations.

The fire protection system will be designed and installed in accordance with NFPA standards for automatic sprinkler, alarm, and detection systems.

11.2.5 Building Electrical Service

Primary electrical power for the EBT-P project will be provided through a new substation installed south of Building 9201-2. The new substation will consist of

- (1) a 30-MVA, 161/13.8-kV power transformer;
- (2) a 161-kV transformer disconnect switch with mounting pedestals, remotely controlled motorized operator, and magnetizing current interrupting devices;
- (3) transformer primary and secondary lightning arresters;
- (4) a metal-clad indoor 13.8-kV switchgear;
- (5) a 15-kV metal-clad bus duct to connect the power transformer secondary to the new switchgear;
- (6) metering, protective relaying, control, monitoring, and auxiliary power facilities for the substation.

The new switchgear will be located on the second floor of Building 9201-2 directly above the existing switchgear room. The 13.8-kV feeders from the new switchgear to the EBT-P power supplies and utilities will consist of 15-kV shielded cable enclosed in rigid steel conduit. A bus tie circuit providing a backup power source to EBT-P will be installed from the new switchgear to the existing 13.8-kV bus.

The new power transformer will be protected with a pneumatic rate-of-rise water deluge sprinkler system. Alarm devices will be connected to the existing Y-12 Plant Gamewell system and also into the Y-12 Plant emergency monitoring system.

To protect adjacent structures from oil fires, a concrete wall will be provided around the transformer.

Concrete foundations will be provided for the transformer, firewall, and 161-kV lightning arrester and disconnect switch support structures. A dry well filled with crushed rock will be provided under the new power transformer to contain and cool spilled oil.

A metal fabric security fence with a pedestrian gate will be provided around the substation.

This 13.8-kV power will supply all of the high voltage microwave power supplies for the experiment. Also required are 2500 kVA of 2.4-kV power (for the helium compressors) and 3000 kVA of 480-V power for various magnet supplies, cooling fans, vacuum pumps, and air conditioning (see Drawing E2E-14270-0001). Control room 120-V power will be derived from a 480/120-V transformer located in the control room. A separate 2500 kVA, 13.8/2.4-kV transformer and switchgear and two 1500-kVA, 13.8/480-V transformers and switchgear will be installed on the east end of the new power supply pad to meet power needs at these voltages. All 480-V circuit breakers will be located on the north end of the power supply building addition in order to minimize the total length of 480-V conduit, which is considerable (see Drawing E2E-14270-0002).

The estimated electrical power demand loads for EBT-P, including future options, are summarized in Table 11.0 (see p. 68).

11.2.6 Device Enclosure and Support Structure

The device enclosure must provide adequate x-ray radiation shielding as required to reduce the exposure to acceptable levels both outside the enclosure and in the basement area (where auxiliary equipment is located) and working space for the various device-related operations. The enclosure must also serve as a structural support for the device.

Structural and architectural

The device enclosure and support structure will be located in the high-bay area of Building 9201-2 between column lines 3, 7, f, and k. (See Drawings S2E-8945A-SK4, -SK5, -SK6, and -SK7.) The three-story, 58-ft-ID reinforced concrete dodecagon will be supported by two concrete ring foundations carried to rock at the existing basement level. The first floor inside the 27-in.-thick concrete/lead enclosure walls will be a 9-in.-thick reinforced concrete slab on grade at elevation 925 ft, 4 ft below the main building ground floor. Fork lift and pedestrian access will be provided by a concrete ramp at the northwest corner of the facility. Equipment access will also be available by way of the main high-bay bridge crane and a service pit located on the west side of the enclosure. Class-A-rated overhead roll-up-type fire doors will be provided at both the ramp and pit entrances to the enclosure. Access to the upper levels of the structure will be by way of a 10-ton-capacity electric elevator. The elevator shaft and a utility chase at the back of it will be shielded with 15 in. of concrete and 12 in. of lead to prevent radiation leakage from the device at the upper shielded levels.

The mezzanine, at elevation 939 ft, will be the main operating level. Access will be provided by stairs from both the first and second floors of the main building through a shielded maze at the southwest corner of the facility. The main enclosure walls at this level will be shielded with 15 in. of reinforced concrete and 12 in. of prefabricated lead panels. The floor will be shielded with a 15-in.-thick reinforced concrete floor slab supporting 12 in. of lead bricks and a 3-in.-thick unreinforced concrete floor topping. The elevator shaft and utility chase will be shielded up to the underside of the second floor at elevation 949 ft.

At the second floor level, the concrete and lead shield walls will continue up to elevation 968 ft. At that elevation a removable structural steel roof framing system will be installed and shielded with 14-in.-thick modular lead panels. Major equipment access/egress at this level will be through the roof via the existing second floor bridge crane. The second floor framing system will consist of structural steel and grating to a radius of 13 ft 4 in. around the centerline of the elevator shaft, which is 11 ft 4 in. square. The remainder of the floor will be an 8-in.-thick structural slab.

On the outside of the device enclosure at both building floor elevations, the gap between the limits of the building demolition and the ring walls will be covered with removable structural steel framing and floor plate.

Piping

Section 11.4.5 includes a complete discussion of piped services.

Heating, ventilating, and air conditioning

The device enclosure will be conditioned to maintain an inside design temperature of $75^{\circ}\text{F} \pm 2^{\circ}\text{F}$ by utilizing a new built-up modular unit located on the northwest low-bay roof. A positive pressure of 0.05-in. w.g. with respect to surrounding areas will be maintained in the enclosure by the supply system. The built-up modular unit will consist of a return and outside air section with fan, filter section (95% ASHRAE STD 57-76), cooling coil section, and supply fan section. Controls will be pneumatic. Insulated supply and return ductwork will be extended to the device enclosure from the HVAC unit, which will have the capability of using outside air for cooling when conditions permit. The HVAC system layout is as shown on Drawings H2E-34111-SK01, -SK02, and -SK03.

Electrical

The principal equipment related to device enclosure and support requiring significant electrical input will be a chiller for the air conditioning system. This will be located in the basement of Building 9201-2 and will require ~110 kVA at 480 V, 3 Ø. This will be supplied in conduit from the 480-V circuit breaker panel located at the north end of the new power supply building addition (see Drawing E2E-14270-0004).

Fire protection

A preaction sprinkler system will be provided for the various levels inside the device enclosure. The new preaction valve serving the control room and installed on an existing sprinkler water supply manifold will also service the system for the equipment and experiment areas inside the enclosure. Pneumatic/heat-activated devices will be installed in the enclosures to activate the preaction valve. The system will be designed for ordinary hazard occupancy, and piping will be sized according to the NFPA No. 13 pipe schedule. The sprinkler system will be provided with water flow and supervisory alarms that will upon activation transmit a coded signal to the Y-12 Fire Department and other emergency organizations.

The fire protection system will be designed and installed in accordance with NFPA standards for automatic sprinkler, alarm, and detection systems.

11.3 OTHER STRUCTURES

Other structures associated with the EBT-P facility include the cooling tower and concrete pads for the helium storage tanks.

11.3.1 Cooling Tower

Primary cooling of the EBT-P facility will be accomplished by a new 19-MW cooling tower, a three-cell tower to be built on an existing seven-cell basin. The use of the existing basin will be economical and will provide room for the expansion of the cooling system if the facility expands.

The cooling tower will be of redwood and will be a counterflow type. Required electrical service and fire protection are already available at the existing basin.

11.3.2 Helium Tanks and Pad

A 24-in.-thick by 15-ft-wide by 85-ft-long reinforced concrete support slab will be provided for the high pressure helium storage tanks located approximately 100 ft southwest of Building 9201-2 (see Drawing X2E-14270-0008). In addition, five 24-ft-high steel tube pipe supports will be provided for the helium supply line from the tanks to Building 9201-2.

11.4 BASIC DEVICE

The basic EBT-P device is composed of the following subsystems:

- (1) toroidal vessel,
- (2) magnetics system,
- (3) microwave heating system,

- (4) vacuum pumping system,
- (5) device utilities, and
- (6) instrumentation system.

These systems are discussed in the following sections.

11.4.1 Toroidal Vessel

The EBT-P toroidal vacuum vessel, designed as a separate component independent of the mirror coil dewar structure, will contain the high energy plasma. It will allow an ultrahigh vacuum to be maintained using viton elastomer seals with interference fits at all flanges. The torus is composed of 36 each of the mirror and vacuum liner cavities. Both vessel components are fabricated from high strength aluminum alloys. The vessel major radius is 5.6 m. Drawings X2E-14270-0011, Sheets 1 and 2, describe in detail the vacuum vessel.

It is anticipated that separating the vacuum liner cavity from the mirror coil dewar structure will reduce fabrication costs. The proposed design of the torus incorporates a 0.050-0.100-in. clearance between the coil cavity liner and the mirror coil dewar. This clearance allows for added adjustment capabilities between the mirror coil and the vessel as well as for assembly purposes. Also, this gap should allow machining tolerance requirements to be reduced.

The 36-sector vessel is assembled by bolting the joining flanges between each vacuum liner cavity and mirror cavity. Prior to assembling the torus, the coil cavity liner halves must be installed inside the coil bore and welded.

Because of the number of sectors and the large major radius, the location of each joining toroidal flange is critical in preventing excessive stresses during operation. Vessel flanges should be located within ± 0.002 in. of design position. Although these tolerances are not unreasonable for the size of the torus components, final flange machining of the coil cavities will be done after the liner halves have been welded to ensure proper alignment. To allow for thermal expansion resulting from the high temperatures the liner will see during operation, the 0.125-in.-thick cavity side wall sections will be designed to flex. In order to further define deflections and stress levels, a finite element model of the vacuum vessel that considers pressure loads and thermal expansion should be completed.

The vessel support apparatus is located at the flanges between the vacuum liner cavity and the mirror cavity and is mounted to the mirror coil I-beam members. This approach will allow adjustments to be made at the torus support points in both circumferential and vertical directions.

A support system and diagnostic access ports are provided in each mirror cavity. No instrumentation ports are provided in the coil cavity liner because of space limitations resulting from gamma ray shielding and the mirror coil structure.

Table 11.1 lists a breakdown of the general vessel characteristics.

Table 11.1. Toroidal vacuum vessel specifications

| | |
|--------------------------------------|--|
| Torus volume | 368.4 ft ³ (10.44 m ³) |
| Internal surface area | 756.64 ft ² (88.87 m ²) |
| Deionized cooling water requirements | |
| Mirror cavity | 240 gpm (15.14 liter/sec) |
| Coil cavity | 1116 gpm (70.41 liter/sec) |
| Major radius | 18.37 ft (5.6 m) |

11.4.2 Magnetics System

The magnetics system function consists of *generating a toroidal magnetic field to contain the steady-state plasma* and includes the mirror coil dewar system and associated power supply system.

Mirror coils

The first stage of EBT-P will have a major radius of 5.6 m and 36 mirror magnets. Each mirror magnet will consist of two concentric solenoids, one wound inside the other. This arrangement will allow the mirror ratio to vary in the range 1.96-2.30. The size, shape, mirror ratio, maximum field, and maximum current density were set in a series of tradeoffs between plasma physics requirements and reasonable goals for a moderate-risk magnet system. The magnet parameters are listed in Table 11.2, and Drawings X2E-14270-0005, X2E-14270-0006, X2E-14270-0007, and E2E-14270-0003 refer to the magnet system.

The rationale for the choice of a NbTi pool-boiling system is discussed in Sect. A.4.3. The conductor and conductor insulation scheme, the rationale for the winding scheme, bobbin design, steps in winding the coil, and the protection system are discussed below.

As pointed out in Sect. A.4.3, the copper-to-superconductor ratio should be kept low and the operating current should be kept low with respect to the critical current. The conductor size and the operating and critical currents are given in Table 11.2. The conductor will be monolithic or built up of a superconducting element and a copper element.

The turn-to-turn insulation is a 50% covering of the conductor surface with a barber pole wrap of 0.5-mm-thick Nomex lacing tape. The voltage per turn in the inner coil during a system dump is ~ 0.3 V; the maximum voltage between adjacent turns is then ~ 30 V. Hence, the minimum distance between turns can easily insulate this voltage.

The insulation from the windings to the bobbin is discussed later in this section.

The winding scheme for the mirror coils must be chosen carefully to keep the field errors low. These errors are introduced by crossovers, by layer-to-layer transitions in the magnet, and by leads. The largest potential error is the result of the large separation of the leads as they leave the winding. The choice of the winding scheme strongly influences the lead placement. Two common winding types are layer winding and pancake winding. An inappropriate layer winding scheme would feed the conductor on to the bobbin through a hole in a side plate and then wind each layer and bring the other lead off the outside diameter. The bad feature of this scheme is that there is an uncompensated current lead the length of the coil build. It is possible to design a layer winding that eliminates this problem, but it requires conductor joints at one end of the magnet. One can also make a design of a pancake winding with uncompensated leads on each end of the coil. Pancake-wound coils for this application have another disadvantage. If the conductor is graded, there must be two joints in each pancake to make the change of grade and two more joints to connect the pancakes electrically. All joints take considerable time to make, thus increasing the overall winding cost. But as in the layer-wound case, proper designs of pancake-wound coils are also possible, e.g., the mirror magnets for EBT-S.

A hybrid winding scheme has been chosen for the EBT-P coils. Basically, this design consists of a layer-wound coil with a pie (one-half of a pancake) wound on one end to bring the conductor next to the bobbin to the outside diameter as a lead. There will be an even number of layers and the same number of turns in the pie so that the two leads end up on the outside diameter on the same end of the coil. The leads can then be brought out close together for good field error compensation. The lead spacing will be set by helium breakdown voltages during a possible dump.

In the inner coil there will be two grades of conductor. A conductor with a 3:1 Cu:SC ratio will be used in the high field areas. A conductor with the same dimensions and less superconductor will be

Table 11.2. Magnet parameters

| | Inner coil | Outer coil |
|--|------------------|------------------|
| Winding dimensions | | |
| Inner radius (cm) | 27.0 | 49.5 |
| Outer radius (cm) | 42.5 | 54.5 |
| Axial length (cm) | 30.0 | 30.0 |
| Number of turns per coil | 2000 | 700 |
| Current density in winding (A/m ²) | | |
| Mirror ratio (MR) = 2.3 | 6600 | 0 |
| MR = 1.96 | 5000 | 6700 |
| Operating current (A) | | |
| MR = 2.3 | 1535 | 0 |
| MR = 1.96 | 1163 | 1568 |
| Peak operating field (T) | 8 | 2 |
| Winding type ^a | Hybrid | Hybrid |
| Cooling type | Pool boiling | Pool boiling |
| Conductor size ^b (mm) | 2.9 x 5.0 | 2.9 x 5.0 |
| Number of grades | 2 | 1 |
| Insulation turn to turn | | |
| | 50% covered | 50% covered |
| | Barber pole wrap | Barber pole wrap |
| | 0.5-mm thick | 0.5-mm thick |
| Minimum copper:superconductor ^c | 3 | To be determined |
| Critical current (all grades) (A) | 2800 | 2800 |
| Stored energy (MJ) (total all magnets) | | |
| MR = 2.3 | 109 | |
| MR = 1.96 | 152 | |

^aA hybrid winding is a particular combination of pancake and layer winding; see text for explanation.

^bBecause of dimensional tolerance and strength requirements, a cable or a braid will not be used.

^cThe copper:superconductor ratio will change from one grade of conductor to another. The final ratio will be determined by the conductor manufacturer after the other conductor parameters are met.

used in the low field regions to help reduce costs. The hybrid scheme requires only one joint between the two conductor grades. The actual number of joints in the magnet depends on a number of things, such as the maximum length of conductor that can be manufactured, but in any case there should be many fewer joints than in a pancake-wound coil.

The outer coil is not wound directly onto the inner coil's turns because structural banding is needed on the inner magnet to keep the turns nearest the bobbin pressed against the bobbin insulation when the coil is fully energized. It is not practical to wind the outer coil on the banding of the inner coil. Therefore, the outer coil will have its own bobbin with space left between the outer bobbin and the outside diameter of the inner coil to serve as a small helium plenum and lead space.

The alignment of the inner and outer coils is important because the field error has to be small when one or both coils are used. The proper alignment of the coil axis is the best way to ensure this. At first thought it seems reasonable to put each coil on its own bobbin and then attach the two bobbins, but this is difficult when one also designs for the out-of-plane fault loads. The bobbin can be made self-aligning by welding onto a cylinder circular end plates large enough to accommodate both coils. The cylinder will then be used as the bobbin for the inner coil after it is machined to the proper dimensions. The bobbin for the outer coil is made in two C-shaped parts. Afterward the holes for the bolts and alignment pins are drilled and countersunk before the inner coil is wound. Then the sections are disassembled, and the inner coil is wound. Once the insulation for the inner coil is put in place, the inner coil is wound, and the leads are brought to the outside diameter of the bobbin, the outer coil bobbin will then be put into place and held by the aligning pins while it is bolted to the side plates. Covers will be put over the pins and bolts, and the plate seal will be welded to the bobbin side plates. The bobbin insulation for the outer coil will be put in place, and the outer coil will be wound. The leads will be put in position and the outer cover plates bolted on and seal welded.

The insulation between the bobbin and the windings will be slotted G-10 sheets covered with a solid sheet to electrically insulate the winding cavity from the bobbin. The helium circulation next to the bobbin is designed to keep the x-ray heat deposited in the bobbin and to keep heat conducted from the structure through the support struts away from the magnet turns. During steady-state operation, the helium in the windings will then cool only the superconductor heated by the x-rays. Helium circulation between the two bobbins is provided by slots machined on the ends of the outer coil's bobbin. There will be enough slots to vent the helium in the inner coil during a quench without an excessive pressure buildup.

The motivation for the winding scheme and a general description of it were given earlier; below is a description of the winding sequence. After the bobbin insulation is installed for the inner coil, enough high field conductor for the entire high field, layer-wound portion of the coil will be wound (uninsulated) on one end of the bobbin. Then the pie (one-half of a pancake) section of the coil will be wound on the other end. The lead will be bent into an insulated slot in the bobbin, and the banding needed for the pie will be wound on. As the conductor is wound, with the proper winding tension being maintained, a 50% barber pole wrap of Nomex tape is applied. The high field conductor will then be unwound from the bobbin and transferred to another spool. The 1 mm of insulation between the pie and the layer-wound section will be put in place. This insulation is a sandwich of two slotted sections on each side of a solid piece of G-10. While it is being layer wound, the high field conductor will be held in tension and insulated in the same way as the conductor for the pie. The number of turns per layer will be monitored, and when the proper number has been wound on (in this design 49 turns), a polycarbonate wedge will be placed between the last turn and its neighbor to hold the last turn tightly against the insulation on the end plate. The winding cavity width is determined by adding 1.5 mm to the maximum width of a layer, given the acceptable tolerances of the conductor and the insulation dimension. After the wedge is inserted, the transition to the next layer is made and that layer is wound. After the proper number of layers has been wound, the joint to the low field conductor is made on the end of the coil away from the pie. The low field conductor will then be wound the same way as the high field conductor. The problem of getting the lead out of the layer-wound section has not been resolved yet; however, one solution is to wind one or two fewer turns in the pie than layers in the layer-wound section so that the bottom of the conductor in the loose layer is higher than the banding on the pie. The lead from the layer-wound part can then be bent into a special insulation block that fits over the pie and through the 1 mm of insulation between the two sections. The leads are insulated and brought out as close together as possible in a radial slot in the bobbin. After the two outer bobbin sections

are installed, the outer coil is wound the same way as the inner coil with the exception of the conductor grade change. The pie will be wound on the other end of the bobbin from the pie for the inner coil.

The purpose of protection is to ensure the integrity of the magnet in case of quench and other fault events. For the operating current and conductor cross section/composition, the energy stored in the magnet needs to be removed in a fairly short time (~ 10 sec). During this amount of time, it is not possible to absorb the stored energy (4.3 MJ/magnet) internally because the normal zone propagates slowly (~ 2 m/sec). To dump the energy externally, switching is required.

The number of switches required depends on the acceptable level of transient voltage to ground. For the pool-boiling magnet proposed, a 600-V limitation is needed. This implies that each inner coil has its own dump resistor and that each pair of outer coils has a dump resistor.

Details of the protection circuit are shown in Drawing E2E-14270-0003. Characteristics of the protection circuit are shown in Table 11.3. There will be two of these circuits, one for the inner coils (36 sections) and one for the outer coils (18 sections). During normal operation all inner (outer) coils are connected in series to minimize the field error. The power supplies may produce a few amperes of current in the dump resistor during normal operation. The error field produced is small because dump resistors are placed several meters away from the magnet.

Table 11.3. Protection characteristics

| | Inner coils | Outer coils |
|--|-------------|-------------|
| Inductances | | |
| Self (H) | 92.1 | 26.8 |
| Mutual (H) | | 31.1 |
| Dump resistor/section (Ω) | 0.375 | 0.36 |
| Number of coils per section | 1 | 2 |
| Peak voltage (V) | | |
| MR = 2.3 | 576 | 200 |
| MR = 1.96 | 436 | 564 |
| Percent of stored energy dumped in the resistors | | |
| MR = 2.3 | 85.6% | 14.4% |
| MR = 1.96 | 63.2% | 36.8% |

The same scheme may be used for 48-coil systems because the protection characteristic is determined by energy stored in the coil.

The number of switches used would be significantly reduced if a higher operating current (~ 5 kA) were used. The main problem with that seems to be field error associated with leads.

A scheme similar to the present one has been proposed for ISABELLE ring magnets.^{1,2}

Voltage differences across each magnet (Drawing I2E-14270-A009) are monitored by voltage taps and differential amplifiers. Because coils are identical and carry the same current during normal operation, the voltage drop across each coil should be the same. The voltage between neighboring coils is compared by a second stage of differential amplifiers. Deviation from zero indicates quench or shorts.

If V_1 has quenched, it will show up in both channel V_1-V_2 and channel $V_{36}-V_1$. Hence, the particular magnet that has problems can be located.

A similar scheme has been proposed for short detection in TFTR toroidal field magnets.³

Mirror coil power supply

All of the superconducting mirror coils and mirror trim coils will be powered by special-purpose, solid-state, high current dc power supplies. Each supply will have provisions for remote programming, remote sensing, automatic crossover, over-current cutoff, and reverse voltage protection. All of the mirror coils will be connected in series and powered by one 200-V, 2-kA dc supply; all of the mirror trim coils will be connected in series and powered by one 150-V, 2-kA dc supply. A schematic representation of this is shown in Drawing E2E-14270-0003. The relatively high voltages of these supplies are required in order to charge up the high inductance coils in a reasonable amount of time (30 min). These power supplies will be located on the first floor of Building 9201-2 directly under the experiment (see Drawing E2E-14270-0005). They will be connected to the mirror coils with rigid copper bus. AC power will be supplied in conduit, routed from the 480-V circuit breaker panel in the power supply building addition (see Drawing E2E-14270-0004).

Magnet vacuum dewar

The magnet vacuum dewar assembly provides an insulating vacuum for the superconducting mirror coil and satellite dewar. The cylindrical outer portion of the coil dewar also serves as a magnetic-load-transferring member. Drawings X2E-14270-0005, -0006, and -0007 show details of the dewar structure.

The external case of the coil dewar is fabricated from a 1-in.-thick stainless steel plate. Super-insulating material will be installed with a liquid-nitrogen-cooled liner prior to the installation of the coil case. The inner bore of the coil dewar is fabricated from 3/8-in.-thick stainless steel.

Welded around the mirror coil case is the major portion of the dewar case. Access inside the dewar for final assembly and maintenance is available through a flanged section. Vapor-cooled conductor leads are brought through the dewar case at a top center location. The liquid helium is fed from the satellite dewar to the mirror coil case at the top center location also. The satellite dewar is supported by the coil dewar case.

The dewar case is designed to carry maximum out-of-plane loads of 260,000 lb (1.1565×10^6 N) to two stainless steel I-beam supports at the base of the coil dewar. The centering force load members and the coil case gravity load member are connected to the coil dewar structure. These members that transmit magnetic loads from the coil case to the major load-bearing structures have threaded adjustment devices attached to the coil dewar case.

The mirror coil structural support members are designed to transfer magnet-centering loads and possible out-of-plane loads. The structural members connecting the coil case to the dewar case also provide for a means of coil position adjustment (relative to the dewar) in any combination of axial or radial directions.

There are a total of 11 support struts connecting the coil case to the dewar case. In case of a coil quench, four pairs of struts are needed to carry the out-of-plane loads, a maximum of 260,000 lbs (1.156×10^6 N). One strut is designed to carry a maximum centering load of 110,000 lb (4.893×10^5 N). A possible negative centering load of 4000 lb (1.779×10^4 N) and the gravity loads of the coil are carried by two other struts. All major load-carrying struts are tension loaded. Only the gravity load member is loaded in compression. The struts are designed to use a high strength titanium alloy for fabrication. All struts are attached to both the coil case and the dewar case by ball joint connections. The coil adjustments are made by turning threaded members mounted in the dewar case.

The superconducting mirror coils are maintained at 4.2K in a bath of liquid helium; the magnet is suspended in a vacuum of 10^{-6} torr for thermal insulation. The supports transmit all loads on the magnet from the coil case at 4.2K to the vacuum dewar, which is at 300K. Between the temperature extremes

of 300K and 4.2K, there is a cold wall that is cooled to 80K by liquid nitrogen. This intermediate temperature surface is thermally attached to each support member. Thus, the cold wall reduces the conductive heat leak through the supports as well as reducing the radiation heat transfer to the coil. Layers of aluminized mylar superinsulation further reduce radiation heat leak by creating isothermal layers with low emissivity. The satellite dewar will be similarly constructed.

The structural supports can be thermally optimized to reduce heat leak by taking advantage of the thermally dependent mechanical properties of titanium alloys. One alloy considered, Ti-5 Al-2.5 Sn, is 16% stronger at 4.2K than it is at 80K and is 60% stronger at 80K than it is at 300K. The cross-section area of the support can decrease by the same percentage as the strength increases, thus reducing the area available for conductive heat transfer.

The vacuum in the dewar will be initially provided by a commercial cryopump while the coil is warm. After the coil has cooled down, the case can be valved off and the cold surfaces will act as a huge cryopump with many times the effective pumping speed of the commercial pump. A molecular sieve will be attached to either the coil case or the cold wall to further increase pumping speed and capacity.

Magnet shielding

Each superconducting mirror coil dewar requires a gamma-ray-shielding device for winding insulator protection as well as for limiting thermal loads on the helium cryogenic system. Primary radiation emission is expected to result from electron collisions with the vacuum liner at the torus throat. Bremsstrahlung emissions resulting from these electrons impacting the throat are attenuated by the shielding material installed around the mirror coil dewar (on the inner bore).

Both depleted uranium and tungsten were considered as a possible shielding material. These materials were most attractive because of the effective shielding thickness required for each. (By minimizing shielding thickness, a more desirable mirror field is attained.) Because of possible difficulties with a depleted uranium shield (see Sect. A.1.1. of the Appendix), a high tungsten alloy powder is incorporated in this design.

The tungsten shielding components are water cooled to reduce vacuum liner operating temperatures and to minimize heat loads on the mirror coil dewar. As seen in the thermal model of the vacuum vessel, approximately 4100-kW power input to the dewar nitrogen system from the shielding results from gamma ray conversion.

The shielding components are designed to be formed with cooling tube passages and bolted together. Each complete unit is attached to the coil dewar. Drawing X2E-14270-0006 shows the tungsten shield units.

Based on the radiation analysis, we predict that approximately 252 W of power will be absorbed by the mirror coils (7 W/coil).

Mirror coil protection system

In the event that energy must be rapidly removed from the mirror and/or mirror trim coils, specialized circuitry will be required. The basic idea involves electrically isolating each coil with switches and then allowing each coil to discharge into a resistive element. By first isolating the coils, we avoid the problem of ground fault voltages adding to prohibitive levels. The electrical details for implementing this plan are shown schematically in Drawing E2E-14270-0003. During steady-state operation, current flows through the SCR's and the mirror coils. The dc contactor is open, and the dump resistor is effectively shorted out by the superconducting coil. When the decision to dump is made, all dc contactors will be closed; then all SCR's will be commutated open, leaving all mirror coils free to

discharge into their respective dump resistors. The use of the contactors will preclude any potential problems with commutating all SCR's simultaneously.

The SCR-forced commutation circuitry includes a capacitor bank to force the SCR current to zero, a power supply to maintain the capacitor bank, and a saturable reactor to prolong the current zero crossing. In the detailed design use will be made of circuits similar to those designed for experiments at Los Alamos Scientific Laboratory (except in that case vacuum circuit breakers were used). In this instance, solid-state switches are preferable to vacuum circuit breakers because the interrupting voltage is only 600 V and space is a factor.

The switches and dump resistor will be packaged as a unit for each coil and suspended from the ceiling of the experiment enclosure (see Drawing X2E-14270-0004). Connections to the coils will be made with rigid copper bus. Internal connections and some of the interconnections between switch/dump resistor units will be braided copper cable.

Magnet structural supports

The magnetic loads are transferred from the dewar case to the floor structure by three beam members. Two stainless steel I-beams welded to the dewar case transfer out-of-plane loads and gravity loads. A box beam located on the outside of the torus carries both ARE coil and mirror coil centering loads. Drawings X2E-14270-0005, 0006, and 0007 show the details of the magnet structural supports.

11.4.3 Microwave Heating System

The microwave heating system provides energy to heat and stabilize the plasma and is composed of the following subsystems:

- (1) the gyrotrons,
- (2) the gyrotron mounting tanks and support equipment,
- (3) bulk and profile power distribution systems, and
- (4) power supplies.

A detailed description of each of these subsystems is given below.

Gyrotron

Cyclotron resonance devices are considered the most promising type of microwave tube for development to the power and frequency levels required by EBT-P; a complete description of the current development effort is given in Sect. A.5 in the Appendix.

An exact physical description of the EBT-P gyrotrons is not possible at this time primarily because of the uncertainty in the output coupler design. However, work performed under a Varian Associates subcontract indicates that the tubes required for EBT-P should have about the same microwave power conversion efficiency as the tubes now being used on EBT-S and will therefore require the same amount of water cooling. The EBT-P gyrotron's cathode design should also be very similar to that used on the 28-GHz EBT-S tube and will, therefore, require the same type of oil bath for high voltage insulation and cooling. An output window design is currently being developed for the 28-GHz gyrotron that uses a fluorinated hydrocarbon as a forced-convection coolant, and the higher frequency gyrotrons will probably use an output window that is almost identical. The size of the EBT-P gyrotrons is, however, not known; therefore, a liberal amount of head space has been left in the containment structure to accommodate very long tube designs.

Gyrotron mount and support

The EBT-P gyrotrons will be mounted on the lid of an oil tank containing transformer oil so that the high voltage cathode can be both cooled and isolated electrically. A small centrifugal pump will be used to circulate cooling oil through the gyrotron gun, and the system will be completely contained in the tank to prevent any possibility of oil leakage. Each of the nine tanks will be movable so that the gyrotrons can be installed and replaced through the access hatch on the west side of the containment building. Estimates of the heat load in the oil tank have been made and indicate that free convection cooling of the tank's surface will be sufficient to maintain the oil temperature at an acceptable level.

One possible configuration of the gyrotron and its mounting tank is shown in Drawing X2E-14270-0009.

Nine fully instrumented water manifolds will be installed in the torus enclosure basement and will provide cooling water for each gyrotron and one section of the microwave distribution system. Read-outs of both water flow rate and temperature difference will be available in the control room so that each tube's status can be continuously monitored.

This system will allow the operation of all nine tubes simultaneously for plasma physics experiments or one tube at a time for the tube and distribution system development work.

The fluorocarbon coolant circulation system currently in use on EBT-S is considered prototypical of those required for EBT-P. Again, nine separate systems will be used to facilitate the operation of individual tubes.

Microwave power distribution system

Conventional microwave systems use a dominant-mode waveguide in which power propagation is possible in only one mode. The EBT-P gyrotrons, however, will be coupled to the torus with a power distribution system that utilizes a waveguide many wavelengths in diameter. This is because the required diameters of dominant-mode systems at 60 and 110 GHz would be much too small to handle the proposed power levels and because the transmission losses of dominant-mode systems are, in general, much too high for practical power transmission networks.

Power is coupled from the EBT-S gyrotron to the torus through a system that consists of several straight sections of waveguide and a toroidal distribution manifold that couples power to the plasma through a series of straight waveguide links. A similar system will be used on EBT-P because the feasibility of this approach has now been experimentally verified. In addition, the EBT-S device will be readily available to aid in component development.

The microwave power distribution network for EBT-P, shown schematically in Drawing X2D-14270-0002, will be constructed from the following five subsystems:

- (1) horizontal and vertical waveguide sections fabricated from copper tubing that will connect the tubes to the distribution manifolds,
- (2) a coupling and power-sensing device that will connect the horizontal waveguide run from the gyrotrons to the vertical section of waveguide that couples power to each of the distribution manifolds,
- (3) mode filters that will be used at strategic points in the system to dissipate microwave power that has undergone conversion from the low loss circular electric modes to some other mode type that could become trapped in the system,
- (4) two toroidal distribution manifolds (one for bulk and the other for profile heating power) to be used to distribute the power from each gyrotron to an integral number of torus cavities, and
- (5) individual waveguide links to connect every torus cavity to each of the two distribution manifolds.

The detailed design of each of the subsystems listed above will be based on criteria generated by both the gyrotron development subcontracts and the component research conducted on the EBT-S facility.

Precision-drawn copper tubing is commercially available and will be used to fabricate the horizontal and vertical waveguide sections. Mode conversion at waveguide joints will be minimized by using alignment rings between mating flanges so that the total axial misalignment is less than a few thousandths of an inch.

The waveguide-coupling device used to connect the horizontal and vertical waveguide runs, as well as to provide a mechanism for sampling both forward and reflected power, will be based either on the design currently being used on EBT-S or on a more efficient version that is developed using the existing machine as an experimental test vehicle.

Mode filters are devices that provide much higher loss to noncircular electric modes. Steel pipes have been used successfully on EBT-S and will also be used on EBT-P.

Both the toroidal distribution manifolds and the 72 waveguide links that connect them to each of the 36 torus cavities are sized so that the average power density in each manifold and link is the same as in the gyrotron output waveguides. The bulk heating power manifold is divided into six segments with flat copper plates so that each of the high frequency gyrotrons is electrically isolated from the others; the profile heating manifold is divided into three segments for the same reason. Each manifold will also be equipped with a scattering wedge at the input waveguide feed point and power-balancing irises at each of the waveguide cavity link connections.

The waveguides will be initially purged with dry nitrogen gas to remove all traces of water vapor, and a very small overpressure will be maintained in the guides at all times. Each of the nine waveguide runs will be isolated from the high vacuum distribution manifold by Varian-supplied FC-75 cooled windows identical to those used on the gyrotrons.

Either free convection or water cooling will be used to cool the entire distribution system, but a decision on which type to use cannot be made until the mode distribution at the gyrotron output flange is known. A probable mode distribution assumption has been made, however, and the resulting power losses were determined to be easily compatible with water cooling; the conceptual design of the distribution system includes the components necessary to accomplish this.

Gyrotron power supplies

High voltage dc power supplies will be used to power the nine gyrotron microwave tubes to be used for bulk and profile heating on EBT-P. Each supply will be variable and regulated and will consist of a beam supply having a nominal rating of 100 kV at 10 A and a gun anode supply nominally rated at 40 kV at 0.2 A.

The design and configuration of these power supplies will be based on the prototype power supply developed for EBT-S. A one-line schematic of the gyrotron power supplies is included in Drawing E2E-14270-0001.

Nearly all major components of these high voltage power supplies will be accommodated by a new building addition adjacent to the west wall of Building 9201-2 and by a new power supply pad south of Building 9201-2. These building additions and the power supply component layout are shown on Drawing E2E-14270-0002. Details of the building itself are elaborated upon in Sect. 11.2.2.

Also required for gyrotron operation will be low voltage, high current gyrotron magnet power supplies. These magnets will be superconducting and will require approximately 10 V at 2400 A. These supplies and the regulations for the 40-kV gun anode power supplies should be in close proximity to the microwave tubes. They will be located on the first floor in Building 9201-2 directly under the experiment. The physical layout for these supplies and the tubes is depicted in Drawing E2E-14270-0005.

Power for these supplies will be run in conduit from the power supply building addition as shown in Drawing E2E-14270-0004.

11.4.4 Vacuum Pumping System

The torus vacuum system initially evacuates the torus, removes impurities released by surface outgassing during operation, and provides sufficient hydrogen pumping speed for pressure control. A separate system is provided for coil magnet dewar evacuation prior to cooldown.

The torus is constructed of unbaked aluminum and assembled using Viton O-rings. The following are the assumed system parameters used for calculating pumping requirements:

| | |
|------------------------------|---|
| Surface area | 100 m ² |
| Volume | 10.6 m ³ |
| Outgassing rate ^a | 1.5 x 10 ⁻⁸ torr-liter/sec/cm ² |
| O-ring gas throughput | 4 x 10 ⁻⁴ torr-liter/sec |
| Base pressure | 5 x 10 ⁻⁷ torr |

^aAssumed outgassing rate after 24 hr.

Roughing system

The roughing system is designed with a cryogenic primary system to perform the following functions: (1) initially evacuate torus from 1 atm to 10⁻⁴ torr and (2) regenerate cryosorption pumps while device is operating.

The proposed system is shown schematically in Drawing X2D-14270-0001. The principal components are

- (1) one 50-cfm mechanical pump,
- (2) two Varian Megasorb Modules, and
- (3) one 1500-liter/sec turbomolecular pump.

On one mirror cavity a microwave isolation plate and a 10-in. gate valve are installed on a lower port. A 10-in. pipe connects this to a 6-in. gate valve below floor level and the turbomolecular pump. Also mounted below floor level are the two Megasorb Modules (which are connected to the 10-in. pipe) and the 50-cfm mechanical pump.

Approximately 1 hr is required to pump from 1 atm to 10⁻⁴ torr.

Below 10⁻⁴ torr the pressure is determined by the outgassing rate, which is a function of time and the pumping speed.

Crossover to the cryosorption pumps can occur as high as 0.5 torr. Going down to 10⁻⁴-10⁻⁵ torr, however, avoids preloading the pumping surfaces. In addition, the turbopump allows pressure on the order of 10⁻⁵ torr to be maintained with the primary vacuum system down for maintenance.

Torus cryopumps

Commercially available cryosorption pumps were selected for the primary vacuum system in a machine without steady-state or high power neutral beams. Eighteen CTI CRYO-TORR 10 pumps appear capable of achieving the desired base pressure of 5 x 10⁻⁷ torr with the assumed outgassing load and the microwave isolation system described below.

Cryopump microwave isolation. Microwave power needs to be kept out of the vacuum system for the following reasons:

- (1) to prevent arcing and damage to components,
- (2) to increase the power absorbed by the plasma, and
- (3) to keep cryogenic systems from exceeding the refrigeration capacity or evolving previously pumped gases.

A perforated copper plate followed by a pipe coated with a microwave-absorbent material is proposed. As detailed in Drawing X2E-14270-0011, the proposed plate is 1/16 in. thick with 45-mil-diam holes set in a triangular pitch with a spacing of 55 mil center to center. Using Chen's theory⁴ the attenuation at 110 GHz for normal incidence is 34 dB. The absorbent coated section prevents the region behind the plate from being a high-Q cavity for leakage radiation. It is estimated that <1 W of microwave radiation would enter the cryopump. Testing should be performed, however, to determine the isolation system and vacuum pump performance under anticipated conditions.

Cooling the plate for heat loads on the order of 2 W/cm² appears feasible with tubes brazed or soldered to the rear surface.

The net molecular gas flow transmission probability for particles incident on the 11.5-in.-diam port to the cryopump was estimated to be 0.195. This results in a net pumping speed of 1000 liter/sec per pump for air, 1600 liter/sec for water vapor, and 1975 liter/sec for H₂.

Magnetic effects. The cryosorption pumps use a closed-cycle refrigerator with a small motor and permanent magnet. The refrigeration unit is 53 in. from the centerline, where the stray field is 100 G or less. Magnetic shielding, if required, appears feasible. The resulting error fields ($\Delta B/B$) on the plasma centerline in the radial direction are estimated to be on the order of 10⁻⁷.

Cryopump H₂ capacity. The hydrogen capacity of the CRYO-TORR 10 pump is 6 standard liters. The net H₂ pumping speed is 1975 liter/sec. Under an up-to-air accident with all 18 pumps holding 6 standard liter, the net volume fraction of H₂ in the torus would be 1%, which is well below the 4-6% explosive mixture. Sixteen hours of pumping at 5 x 10⁻⁶ torr would produce a 2-5% mixture of H₂ in the pump unit itself with the gate valve closed at 1 atm.

Continuous torus pumping is possible by dividing the pumps into three groups of six and using two groups at any given time with the other group down for eight hours for regeneration. Any given pump would operate for 16 hours followed by an 8-hour regeneration period.

Vacuum distribution system

There is no separate high vacuum distribution system. The torus itself provides a very high conductance from a cavity that is not pumped to a neighboring cavity that is pumped.

Hydrogen injection system

Assuming all pumps have a net H₂ pumping speed of 1975 liter/sec, the H₂ throughput would range from 0.35 torr-liter/sec at 10⁻⁵ torr to 0.035 torr-liter/sec at 10⁻⁶ torr. Pressure can be controlled by one VEECO PV-10 piezoelectric valve and APC-110 automatic pressure controller. Maximum throughput for this system is 1 torr-liter/sec at 1-atm pressure differential. The valve response time is <2 msec full open to full close.

Mirror coil dewar vacuum system

As shown in Drawing X2D-14270-0001, a separate vacuum system is provided for the magnet dewars. A 0-cfm pump is used to rough down to 0.2 torr through a 4-in.-ID manifold. Individual CTI CRYO-TORR 7

pumps on each dewar are then used to evacuate the dewars to 10^{-5} torr prior to cooldown. The same system is also used in evacuating and flushing the helium lines.

11.4.5 Utilities

Utilities described in this section include those systems with the function of furnishing water, cryogens, air, gases, and electrical service to the device.

Demineralized water system

The primary cooling of the device and auxiliary equipment will be by a demineralized water system. The demineralized water loop will consist of the components identified on Drawing P2D-57700-0001.

The primary loop of the water system will consist of (1) a three-cell, 19-MW cooling tower; (2) seven low pressure, 2250-gpm pumps (six plus a spare); and (3) a 19-MW demineralized water/tower water heat exchanger. The cooling tower will be erected on an existing cooling tower basin located south of the southwest corner of Building 9201-2. The seven pumps for circulation of the tower water will be located in the existing pump house, Building 9404-3.

The secondary loop of the water system consists of all of the demineralized water components. These components are the recirculation pumps; the sidestream demineralizer; the 19-MW, 4500-gpm heat exchanger; and the heat loads of the EBT-P device and the auxiliary equipment.

The nine gyrotrons will require approximately 625 gpm each of water for a total of 5625 gpm. A total of 1300 gpm of water will be needed to cool the helium compressors in the helium liquefaction/refrigeration system. The microwave distribution manifolding will require 125 gpm of cooling water. The torus vacuum liners will need 1400 gpm of demineralized cooling water. The photon shields, mirror cavities, and microwave screens on the torus collectively will require 320 gpm of water. The electrical power supplies and other equipment will need 250 gpm of cooling water. The control room and device enclosure air conditioner chiller will require 400 gpm of cooling water. The addition of ARE coils would require 2250 gpm of cooling water. The addition of neutral beam injectors would require 250 gpm of demineralized cooling water. These cooling loads total approximately 12,000 gpm of demineralized cooling water.

The required flow of cooling water requires a 24-in.-diam main supply and return pipe from the pumps to the facility. The various branches are sized in Drawing P2D-57700-0001 based on each component's cooling requirements.

Cryogenic supply systems

A helium liquefaction/refrigeration system and a liquid nitrogen system will be purchased and installed to supply the cryogens required by the superconducting magnet coils, the torus cryopumps, and other devices.

The helium liquefaction/refrigeration system will have a nominal capacity of 600 liter/hr of liquid helium production and 3700 W of refrigeration, both at 4.2K. The major components are one or more cold boxes, a helium compressor for each cold box, a 5000-gal liquid helium storage dewar, and five 25,000-gal ambient temperature, high pressure, gaseous helium storage tanks. The cold box(es) and storage dewar will be located on the low-bay roof to minimize the length of cryogenic helium transfer piping (see Drawing P2E-95306-0001). The compressors will be located west of Building 9201-2 in the helium compressor building addition (see Drawing X2E-14270-0008, sheet 2). The high pressure (15 atm) storage

tanks will be located as shown on Drawing X2E-14270-0008, sheet 1) and will be connected to the compressors via a 4-in.-diam pipe. The helium liquefaction/refrigeration system will be connected to the Y-12 Plant gaseous helium system, which will provide the initial helium fill and all makeup gas required.

The liquid nitrogen system will have a nominal capacity of 4000 liter/hr. The major components are two liquid nitrogen tank trucks that will be filled as necessary at the Y-12 Plant air separation facility. The nitrogen off-loading station will be at the northwest corner of Building 9201-2 as shown on Drawing X2E-14270-0008.

Cryogenic distribution system

The cryogenic distribution system provides the EBT-P facility with liquid helium (LHe) and liquid nitrogen (LN₂) for superconducting magnets. Cryogens are required by the mirror coils around the toroidal cavity and by the gyrotron coils located below the mirror coil ring. The system has been designed for expansion without major equipment modification. The refrigeration system has enough capacity to supply the 1.2×10^6 liter/sec of cryocondensation pumping that would be required for pulsed neutral beam injection.

A schematic is included on Drawing P2D-57681-0001, which illustrates the components and basic operation of the distribution system. All of the LHe and cold gaseous helium (GHe) transfer lines, valves, and bayonet connections are vacuum-jacketed, superinsulated LN₂-shielded components. All of the LN₂ transfer lines and components are vacuum jacketed and superinsulated. The cold nitrogen vent lines will be vacuum insulated within the facility area to prevent icing or condensation and will meet critical dimensional constraints. Outside the facility area these lines can use larger foam insulation.

The warm GHe lines that vent the mirror coil and gyrotron coil vapor-cooled leads will be uninsulated and have a temperature-controlled heater to heat the vent gas above the dew point during cooldown and operation.

LHe lines connect the storage dewar to the gyrotron supply header and to the satellite dewar supply header; the satellite dewars supply 1-atm liquid to the mirror coils. Cold GHe lines carry gas from the gyrotron return header and from the satellite dewar return header back to the cold box. These lines can also be vented to the compressor suction through a heater during cooldown. LN₂ is also supplied to each satellite dewar, providing cold wall cooling for the satellite and magnet dewars. N₂ vent gas will be vented outside the building.

The liquid in the satellite dewars provides coolant for the vapor-cooled leads; the liquid level will be controlled by a level control valve. To ensure proper cooling for the vapor-cooled leads, a blower will be used to maintain 0.5-atm suction on the warm gas lead return line. Each lead will have a remotely actuated flow control valve so that proper cooling can be ensured on each of the 216 (108 pairs) vapor-cooled leads.

Valves and bayonets have been provided to allow for maintenance work on a valve or a coil without requiring warmup and subsequent cooldown of the entire facility. Valves for maintenance and repair will be manually operated. All control valves that are necessary to equalize He or N₂ flows throughout the system will be remotely actuated. Cooldown of the facility using the refrigerator described in the preceding section should take approximately six days, assuming that the cooldown is not limited by thermal stress conditions created by thick cross sections.

Miscellaneous utilities

The miscellaneous utilities for EBT-P will include instrument air, steam, and helium gas.

The steam piping will be installed from the reducing station at the northwest corner of Building 9201-2 to the air-handling units on the low-bay roof at columns 4-1/2 and k. Steam piping will also be installed from the reducing station to the west building addition. The pipes will supply 350 lb/hr of steam at 25 psig for heating the west building addition and 100 lb/hr of steam at 25 psig for heating the control room and device enclosure.

Instrument air piped from the Y-12 Plant system will be used as necessary for instrumentation and valve operation.

Helium gas piped from the Y-12 Plant system will be used for the initial fill of the helium liquefaction/refrigeration system, helium system makeup gas, and device component purges after repairs.

11.4.6 Instrumentation and Control

General

The control and monitoring of EBT-P will be accomplished by a combination of analog and digital systems with the startup and operation of each subsystem supervised from a master control console (MCC). This section of the report describes the instrumentation and control systems required for machine startup and operation. The only diagnostics considered are those required for machine operation.

Instrumentation for basic machine operation will be divided and described as follows: vacuum system, cryogenic system, magnet system, auxiliary systems, microwave system, interlock system, data acquisition, the MCC, grounding and shielding, personnel safety, and machine diagnostics.

The instrumentation requirements are summarized in Table 11.4, and the control room layout is shown in Drawing I2E-14270-A006.

Vacuum system

The EBT-P vacuum shall be established and maintained by a system of mechanical, turbomolecular, and cryosorption pumps. The vacuum system instrumentation and controls shall include all the transducers and circuits to monitor and control the torus and magnet system vacuum levels. The instrumentation shall include Pirani gauges, ion gauges, residual gas analyzers, and vendor-furnished instrumentation required for the monitoring, control, and regeneration of the cryosorption pumps. The operation of the vacuum system shall be controlled by a programmable logic controller, and all operations shall be performed at the vacuum system location on the MCC.

The Pirani gauges shall monitor and control the system pumpdown. This gauge has been utilized on the Large Coil Program (LCP) and was chosen for wide-rangeability and compatibility with magnetic fields. The only area questionable with this gauge is microwave effects. If this develops into a problem, thermocouple gauges shall be used. The Pirani gauges shall provide the control points for the required pump operations. The gauge controllers shall have set points that can be set over the range of the instrument and shall provide contact closure inputs to a programmable logic controller (PLC). The PLC shall provide an operator-assisted-type operation to ensure safe and logical operation from the MCC. The Pirani gauge set points shall be input to the PLC through isolated input cards and the remote vacuum valves controlled through isolated output cards. The display and controls for the vacuum system on the MCC will give the operator control and system status information at all times. In addition to digital meters furnished with the Pirani gauge controllers, an analog output shall be input to a

Table 11.4. Proposed EBT-P instrumentation

| System | Parameter | Sensor | Quantity | Location |
|---------------|-----------------------------|--------------------------|---------------------|-----------------------------|
| Vacuum | Low vacuum | Pirani gauge | 82 | Torus Piping Dewars |
| | High vacuum | Ion gauge | 76 | Torus Piping Dewars |
| Cryogenic | LN ₂ flow | Orifice | 1 | LN ₂ piping |
| | LN ₂ temperature | Type E thermocouple | 50 | LN ₂ piping |
| | LHe temperature | Type E thermocouple | 50 | LHe piping |
| | | Carbon glass thermometer | 36 | LHe magnet piping |
| | | Silicon thermometer | | |
| LHe level | Superconducting probe | 37 | Dewars | |
| Magnet | Differential voltage | Voltage taps | 180 | Coils Vapor-cooled leads |
| | | Temperature | Type E thermocouple | 216 |
| | | Carbon glass thermometer | 144 | Coils |
| | | PRT | 72 | Coils |
| | Strain | Strain gauge | 144 | Structure |
| | Pressure | Strain gauge | | |
| | | Pressure transducer | 36 | Dewars |
| Cooling water | Flow | Flow switches | TBD | Piping |
| | | Flow meters | TBD | Piping |
| | Temperature | Differential temperature | | |
| | | Transducers | TBD | Piping |
| | | Thermocouples | TBD | Piping |

digital computer and be available for patching onto a strip chart recorder. There are a total of 82 Pirani gauges, as shown on Drawing I2E-14270-A008.

The system operating vacuum shall be monitored and controlled by a series of ion gauges and ion gauge controllers. Ion gauges shall be provided on each torus cavity for diagnostics, on each magnet dewar to monitor and indicate insulating vacuum, and in the piping system for indication and control. The dewar ion gauges shall also act as an input to the superconducting coil control and protection circuitry. The ion gauge controller outputs shall be input to a computer and be available for patching to a strip chart recorder. In addition, any ion gauges required for control shall act as an input to the PLC. The present design calls for the use of a CVC Bendix ion gauge, chosen because of ease in providing magnetic shielding and because of experience on the present EBT device.

In addition to the magnetic shielding, a microwave shield will be provided on each of the torus ion gauges. The effects of this shield on response time will be evaluated during detailed design. A piezoelectric valve shall be provided on one torus cavity for hydrogen injection. The piezoelectric valve throttling is controlled by a dc power supply setting, and the time the valve is open shall be controlled by preset pulses.

There shall be two residual gas analyzers (RGA) provided for evaluating the operation of the EBT-P vacuum system. The RGA shall be of the quadrupole type with a cathode ray tube (CRT) display; in addition, the output of the units shall be input to a digital computer to provide an ongoing record.

Cryogenic system

The cryogenic system for EBT-P shall furnish the liquid helium and liquid nitrogen required for the operation of the device. The cryogenic instrumentation is shown in Drawing I2E-14270-A007. The liquid nitrogen, to be supplied from an exterior trailer system, shall be monitored by a series of Type E thermocouples, a flow meter, or a load cell at the supply. The thermocouples shall be mounted in separate sections of the transfer lines and switched to common read-outs. The supply of liquid nitrogen shall be monitored at all times with an alarm for low liquid nitrogen supply.

The liquid helium system shall be composed of all components supplying or requiring liquid helium. The temperatures shall be monitored by silicon thermometers, carbon glass thermometers, and platinum resistance thermometers. The liquid helium levels shall be monitored and controlled by superconducting level probes, and pressures are to be monitored by cryogenically rated strain gauge transducers. As presently envisaged, all liquid helium transfer shall be controlled by remote-operated valves with the valve operators mounted at room temperature. The liquid helium shall be supplied by a closed-loop liquefier/refrigerator controlled by instrumentation supplied by the vendor. An existing large refrigerator is controlled by a vendor-supplied PLC and three mode controllers designed for direct digital control. The size and complexity of the proposed system indicate that digital computer control will be required. The cryogenic system shall be controlled by a PLC, and required operator functions shall be from the MCC.

Magnet system

There shall be a total of 72 pool-boiling superconducting coils on the EBT-P device. These coils are supplied in 36 dewars with a mirror coil and a trim coil provided in each dewar. The instrumentation for the magnet system shall be divided into two sections: coil monitoring and coil protection. The coil monitoring instrumentation is shown in Drawing I2E-14270-A009. A satellite liquid helium dewar shall be supplied at each coil location. The liquid level of this dewar shall be continuously monitored, indicated, and alarmed by a superconducting level probe. In addition, the rate of liquid helium usage shall be calculated and stored to indicate any potential problems with the coils. This level shall have a dual set point and shall act as an input to the coil dump circuitry. The dewar pressure shall be continuously monitored by strain gauge pressure transducers, burst disks, and pressure relief valves that protect the dewar. The temperature sensors furnished with the coils shall be kept to a minimum because of the difficulty of installing instruments on the coils. As a minimum, Type E thermocouples shall be installed on the coil support structure to observe cooldown, and carbon glass thermometers shall be installed to monitor operational temperatures. These sensors were chosen for wide-range ability and magnetic field compatibility. The cooldown thermocouples shall be switched to a common indicator, and the thermometers shall be conditioned and input to a digital computer. There shall be strain gauges installed to observe the structure during cooldown and initial operation. These gauges will not be required during operation. The vapor-cooled leads shall be purchased with a thermocouple and carbon glass thermometer. The thermocouple shall monitor the gaseous temperatures, and the carbon glass thermometers shall be mounted at liquid helium temperatures. These transducers shall be continuously monitored and alarmed. The thermocouple shall have a dual set point and act as an input to the dump circuitry. The required heat sinking of leads, cabling of connector selections, and signal isolation

shall follow procedures developed for the LCP. The 36 mirror coils shall be supplied from one power supply and the 36 trim coils from another. The power supplies shall be procured with the required control options to control the power supply from the MCC. The expected control modes shall be a rampup and rampdown for the current with operator-selected rates. The magnet control computer shall continuously monitor the voltage taps and temperature transducers on the coils and leads and, in the event of a discrepancy between coils, initiate a current level hold. If the coils equalize, the current will automatically start ramping again toward the final current set point; however, if the coils remain unbalanced, the operator will have the option of continuing to charge or to deenergize the coils. This shall be performed from the MCC, and the operator shall be able to display all coil signals on a CRT. The coil protection circuitry is shown in Drawings I2E-14270-A005 and -A009. The coil quench detection shall be based on signals from voltage taps installed across each coil and subtracted from the voltage tap signals from two adjacent coils. These signals shall be conditioned with isolation and differential amplifiers to a level of -10 to +10 V. These high level signals shall act as inputs to hard-wired quench detectors, which shall have a high level and low level comparator. A quench signal is produced when the input exceeds the high level set point or when the input exceeds the low level set point and remains above it for a length of time presettable from 1-99 sec. The output from the quench detector shall act as an input to the coil dump signal. Sensors providing input signals to the dump circuitry measure dewar level, vapor-cooled lead temperature, dewar vacuum, and ground fault detector output. The coil dump or protection circuit shall be a dedicated PLC or, if required during design, a hard-wired system. All magnet signals shall be scanned and stored by the magnet system computer, but no portion of the coil protection circuitry shall be scanned or sampled. When a coil dump signal is generated, all coils shall dump at the same time. Each coil has a normally open switch across its terminals and a normally closed switch in series with the positive coil lead. The dump signal first closes all the normally open switches and then opens the normally closed switches, causing the coils to discharge through the parallel dump resistors across each coil. The present design assumes that any dump signal discharges all coils, both mirror and trim.

Auxiliary systems

The auxiliary systems' instrumentation shall be composed of all the transducers required to monitor plant services supplied to the EBT-P. All cooling water lines shall be monitored by flow switches and, if applicable, flow meters. In critical areas of the system, thermocouples and differential temperature transducers shall be installed. The instrument air system shall be controlled by air sets and filter regulators, and all valving dependent on instrument air shall be designed for safe operation in the event of loss of instrument air. The auxiliary systems shall be controlled by and provide input to the system interlock PLC's.

Microwave systems

Each microwave power input subsystem consists basically of the following: gyrotron oscillator, power supplies, mounts, microwave distribution (waveguide), utility services (fluids and electrical power), personnel protection, instrumentation for monitoring and control, and installation hardware (cables, conduit, cabinets, etc.).

The microwave power system requires several fluid inputs for cooling: demineralized water, oil, nitrogen, and helium. Instrumentation (see Drawing I2E-14270-SK01) to monitor fluid flow rates, temperatures, pressures, and power dissipation will be installed, operated, and monitored with PLC's. The PLC's will interface with the control console a PDP-11/60 computer centrally located in the control room

for each gyrotron and related support system. The manual controls with direct reading instruments will be installed in instrument cabinets located at the north side of the control room. Each of the nine gyrotrons will require approximately three instrument cabinets for a total of 27. The microwave power system, in addition to fluid inputs, requires power inputs that require more sophisticated controls and monitoring. The PDP-11/60 computer will be used to monitor and control all inputs to each gyrotron from its power supplies. It will accept status information from the PLC, from field instruments, from the individual power supplies, and from the control console as directed by the console operator. An eight-channel analog recorder will be provided for each gyrotron for long-term data collection.

The PDP-11/60 shall be programmed with special tailored algorithms to bring the gyrotrons from an off condition to a full on condition. The program will provide for single, sequential, or collective gyrotron operation while monitoring all critical parameters for fault conditions. In addition, the computer control system will provide operator interface for manual control, alarms, emergency shutdown, status information on demand, printouts of out-of-tolerance conditions, and CRT display of each gyrotron operating parameter (voltage, current, power, etc.) (see Drawing I2E-14270-SK01).

Personnel protection from microwave emissions will be provided by sensors located in the EBT-P test area and in the control room. Alarms will be located in these areas to warn operating personnel (see Drawing I2E-14270-SK02).

Interlocks

The EBT-P devices shall be interlocked to provide for safe, sequential, and orderly operation. The inputs to the interlock system shall be contact closures, limit switches, instrument set points, push buttons, flow switch outputs, and other process variables required. For a system as complex as EBT-P, traditional relay logic is not practical. The size and complexity of the system necessitate the use of PLC's to control the system. The PLC is a solid-state, programmable device designed to operate in an industrial environment and to perform control functions formerly performed by relays. The most obvious advantage of the PLC in a complex system is that it is programmable and is thus able to be incorporated into large systems with relative ease. The PLC basically consists of four parts: processor, input/output, power supply, and programmer. These are furnished as a package with all required interface and interconnecting cables. The only user wiring required is field wiring to the input/output cards. The PLC programming consists of a series of user oriented commands to duplicate relay implementation of a ladder diagram. The present design plan is based on utilizing optically isolated input/output cards with a common mode voltage rating of 1500 V for 10 msec. These cards are optically isolated from the controller for noise elimination. The PLC's shall be programmed for control from the MCC. The first consideration in the system interlock scheme shall be personnel safety, and the expected interlock scheme consists of personnel safety interlocks on the auxiliary systems, vacuum system, cryogenic system, magnet system, and microwave system. The required programming shall be performed to allow supervised overrides for testing and trouble-shooting. All systems and subsystems affecting the operation of the interlocks shall be designed for fail-safe operation.

Data acquisition

The EBT-P shall be provided a computer-based digital data acquisition system. The system, shown in Drawing I2E-14270-A010, consists of two 16-bit microcomputers controlling various EBT-P subsystems and communicating with a 16-bit minicomputer that shall record and store data, control peripherals, provide supervisory control to the liquifier/refrigerator, and communicate with the MCC. In addition, a medium-sized 16-bit minicomputer shall be supplied for monitor and control of the microwave system. This decision was made because of the complexity of the microwave system and the unknown factors in tube

conditioning and control. The vacuum system, facility variables, and cryogenic system are instrumented with relatively slow-speed transducers, but the congregate number of signals to be monitored and displayed is large. From an operational standpoint it is practical to provide a method of displaying all of these signals at one location. In EBT-P this location shall be either the data acquisition cabinets or the MCC. In addition, a means of storing data to provide time histories of selected variables shall be required, especially during facility startup. The slow-speed signals shall be scanned by a slow-speed scanner supplied with an automatic thermocouple reference junction. The output of the scanner shall be input to a DEC-11/23 microcomputer. The memory requirements for the DEC-11/23 shall be determined during detailed design, but the present concept calls for providing 64 K of solid-state memory and a VT-100 video terminal. A data link shall be provided to an 11/60 minicomputer for long-term storage and data output.

The magnet system shall have a DEC-11/23 to monitor the coils and to provide control of the power supplies. The decision was made to dedicate a microcomputer to the superconducting coils because of the number of variables and the sampling speed required during a coil quench. This system shall also utilize a DEC-11/23 with 64 K of solid-state memory, but a high-speed scanner shall also be provided in addition to a slow-speed scanner for variables such as temperature and level. The sampled signals shall not affect the coil protection circuitry. This PDP-11/03 shall also communicate with the central PDP-11/60.

The central PDP-11/60 shall have 128-K solid-state memory, a printer/plotter, a moving head disk, a video terminal, and DMA interface to the 11/23's. This computer shall serve three primary functions: to store data from the LSI-11/23's, to provide total system supervision, and to provide operator-requested outputs to the MCC. The main operator access to all facility data shall be through the PDP-11/60. In addition to these functions, the control algorithms for the liquefier/refrigerator controller shall be generated in the 11/60.

The cost and complexity of the microwave tubes affected the decision to dedicate a PDP-11/60 to the monitoring and control of these tubes. At the present there is no set method of conditioning and starting up these tubes digitally, but it would be desirable in terms of time and technical considerations to do so. The microwave 11/60 shall be configured like the main facility 11/60. The actual software requirements for the data acquisition system have not been worked out, but an operating system shall be furnished with multitask and multiterminal capabilities and an extended Fortran IV compiler.

In addition to the digital system, there shall be a patching system and analog recorders provided to allow the operators to make real-time records. The variables to be connected to the patching system shall be selected during the detailed design phase.

Master control console

A master control console (MCC) shall be furnished as a centralized facility control location. The MCC shall be divided according to the various systems to be controlled. The panel shall be designed with a semigraphic representation of each subsystem. There shall be a set of lighted flat pack push buttons and LED lamps for control and status indication. The operation of all system PLC's shall be from the MCC. In addition, CRT display shall be provided to allow the operator to call up and display data from the PDP-11/60. Also, all critical variables displayed 100% of the time shall be read at the MCC on digital panel meters. The present design calls for inclusion of a system annunciator at the MCC.

Grounding and shielding

The EBT-P grounding and shielding design shall closely follow the techniques utilized on ISX-B. The first consideration shall be personnel safety and the second the elimination or reduction of electromagnetic interference. The basic concept requires the design of a low-impedance ground bus to which all control room cabinets and control room ends of the signal cables are connected. This ground bus is extended into the cable trays, and all low level signal cables are run in these trays. The cables to be utilized shall be shielded coaxial or twisted shielded pairs. The termination of cable shields shall be evaluated for each sensor during the detailed design phase and installed, where possible, in the best fashion to guarantee data quality.

Personnel safety

A system of interlocks shall be provided to prevent personnel from entering any hazardous area during an experiment. A series of Kirk key-type interlocks will regulate the operation of all hazardous subsystems. These shall be the first set of permissives to be satisfied for the PLC's, and unless they are satisfied, the systems will not be operable. The microwave monitors provided for personnel safety are discussed earlier.

Machine diagnostics

The diagnostics to be furnished shall consist of only those diagnostics required for machine operation. These shall include an ion gauge in each cavity (covered in the description of the vacuum system), a single-channel interferometer, a pair of multichannel laser interferometers, a diamagnetic loop, a toroidal current coil, and four field correction coils. The diagnostics shall be input to a PDP-11/34 computer through a CAMAC crate; in addition, each diagnostic shall be furnished with a strip chart recorder.

REFERENCES

1. W. B. Sampson, *Proc. Magnet Technology*, MT-6, p. 460 (1977).
2. K. E. Robbins, W. B. Sampson, and M. G. Thomas, *IEEE Trans. Nucl. Sci.*, NS-24, 3, p. 1318 (1977).
3. C. Neumeier and M. Wertheim (EBASCO/Grumman Aerospace), private communication, 1979.
4. C. C. Chen, *IEEE Trans. Microwave Theory Tech.*, Vol. MTT-21, 1 (1973).

Table 11.0. Required electrical power for EBT-P

| | Ratings | kVA |
|---|---------------------|---------|
| Microwave power supplies | | |
| Beam power | 100 kV, 10 A x 10 | 10,000 |
| Gun anode | 40 kV, 0.2 A x 10 | 80 |
| Gyrotron magnet (SC) | 10 V, 2400 A x 10 | 240 |
| Mirror coil power supplies (SC) | 200 V, 2000 A | 400 |
| Mirror trim coil power supplies (SC) | 150 V, 2000 A | 300 |
| Global field error correction power supplies | 65 V, 500 A x 4 | 130 |
| Utilities | | |
| Helium refrigerator | 2500 | } 3,000 |
| Vacuum pumps | 50 | |
| Control room power | 100 | |
| Lighting | 70 | |
| Air conditioning | 125 | |
| Power supply cooling fans | 105 | |
| Miscellaneous power | 50 | |
| Subtotal | | 14,150 |
| <u>Future options</u> | | |
| Neutral beams | | |
| Accel power | 20 kV, 12.5 A x 4 | 1,000 |
| Decel power | 5 kV, 1 A x 4 | 20 |
| Source table | | |
| Arc supply | 150 V, 400 A x 4 | } 250 |
| Filament supply | 12 V, 200 A x 4 | |
| Beam magnet | 6 V, 75 A x 4 | |
| ARE coil power (available from existing motor-generator sets) | 23.4 V, 6408 A x 96 | 14,400 |
| Three additional microwave power supplies | | 3,100 |
| Additional utilities | | 1,000 |
| Subtotal | | 18,770 |
| Total | | 33,920 |

APPENDIX

A.1 ENGINEERING ANALYSIS

A.1.1 SHIELDING ANALYSIS

A.1.1.1 Introduction

Because of the expected large loss of electrons on the magnetic coil assemblies and other components of the proposed EBT-P plasma device, the induced gamma field from bremsstrahlung will be very intense. These gammas will yield increased heating loads on the superconducting cryogenic coils as well as producing a significant biological hazard. In this section the results from a series of one-dimensional (1-D) calculations in which the gamma heating loads were determined are presented for several coil shield configurations. Also given are 1-D results that indicate the level of biological dose for varying thicknesses of either lead or concrete that have been proposed for the primary shielding. The calculational methods are described in Sect. A.1.1.2, and in Sect. A.1.1.3 the calculated results are presented and discussed.

A.1.1.2 Method of Calculation

Calculational methods

The transport of electrons, positrons, and gammas through the magnet assembly was carried out using the EGS-PEGS code system.¹ This Monte Carlo code package takes into account all physical processes that are important in the energy range of interest, i.e., ≤ 10 MeV. These processes include Compton scattering, pair production, photoelectric effect, Moller scattering, Bhabha scattering, electron-positron annihilation, bremsstrahlung, and, through the use of the continuous slowing-down approximation, the energy loss of the charged particles.

The EGS-PEGS code system could have been used for the entire set of calculations except for the large statistical uncertainties associated with the calculated results at large shielded distances from the radiation source. To circumvent this problem, the EGS-PEGS code system was used to generate only photon spectra. These spectra were then input to the 1-D discrete ordinates transport code ANISN.² This code has been used extensively for 1-D shielding calculations and is very applicable to deep penetration problems.

With the photon spectra from EGS-PEGS, the ANISN calculations were carried out using an S_8 angular quadrature and a 21-photon energy group cross-section set containing a P_3 Legendre approximation of the transfer cross sections. These cross sections, which cover the energy range 0.01-14 MeV, were stripped from the DLC-31³ few-group 37-neutron/21-gamma group microscopic cross-section library using the AXMIX code.⁴ This code was also utilized to obtain the macroscopic cross sections by folding the microscopic data with the theoretical atom densities of aluminum, tungsten, ^{238}U , and copper, and lead and with the elemental atom densities of the concrete used in the Tower Shielding Facility.⁵

The photon-heating kerma factors for aluminum, ^{238}U , and copper were obtained from the Evaluate Photon Interaction Library⁶ and were processed into the DLC-31 photon energy group structure using the SMUG module in the AMPX code system.⁷ The photon flux-to-dose conversion factors were taken from the DLC-31 library.

Geometry

The 1-D geometries employed in EGS-PEGS and ANISN and in both the coil-heating and biological dose calculations consisted of a series of infinitely long concentric cylinders as shown in Fig. A.1.1. In the heating calculations [Fig. A.1.1(a)], electrons were assumed to be isotropically incident on the front face of the 1-cm-thick aluminum liner for the transport utilizing the EGS-PEGS code system.

ORNL-DWG 79-3123 FED

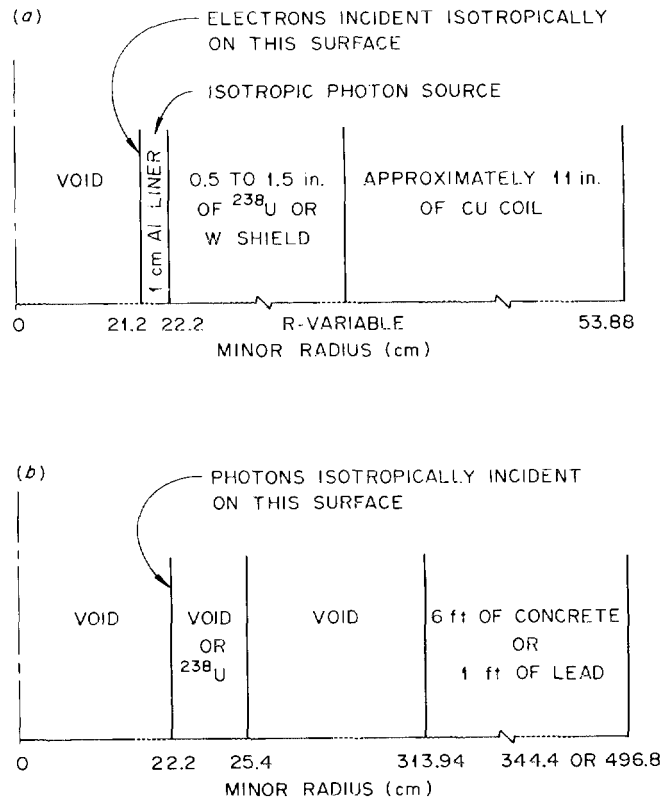


Fig. A.1.1. One-dimensional geometric models:
 (a) geometric model for coil-heating calculations;
 (b) geometric model for biological dose calculations.

Although the bremsstrahlung gammas produced by the electrons were somewhat smeared radially throughout the aluminum, the photon source was placed at a radius of 21.3 cm for the ANISN calculations. The angular distribution associated with these gammas is isotropic because the electron source was assumed to be isotropic. However, some calculations were performed for normally incident gammas to determine angular sensitivity. Coil shield thicknesses of 0.5, 1.0, and 1.5 in. were considered for both the ^{238}U and tungsten shields.

The biological dose calculations were performed using the geometry illustrated in Fig. A.1.1(b). In these calculations the biological dose rates for up to 1 ft of lead and 6 ft of concrete were obtained with and without 1.25 in. of ^{238}U coil shielding. The bremsstrahlung spectra used in the heating calculations were again used for these calculations. These photon sources were assumed to be isotropically incident on the inner face of the ^{238}U (or voided) region.

Electron loss distribution

The rate at which electrons are lost from the plasma was assumed to be proportional to a Maxwellian distribution weighted by $E^{-3/2}$, i.e.,

$$\text{Loss} = A \times \exp(-E/kT)/E,$$

where E is the electron energy and T represents the plasma temperature. This distribution was normalized to a maximum power loss of 1 MW, yielding a normalization constant of $A = 6.242 \times 10^{18}/kT$.

Because very low energy electrons do not contribute significantly to either the photon heating or the biological dose, only electrons with energies >0.239 MeV were considered. For kT values of 1.0, 1.5, and 2.0 MeV, the number of electrons lost from the system per second with energies >0.239 MeV is 5.99×10^{18} , 5.37×10^{18} , and 4.80×10^{18} , respectively. These numbers were obtained by integrating the loss distribution of electrons with energies of up to 10 MeV. For a kT of 2.0 MeV, the integration was also carried out up to 20 MeV, which produced a loss rate of 4.81×10^{18} electrons/sec.

The cumulative bremsstrahlung spectra for the various kT values were obtained from the following expression:

$$h(E_\gamma) = \frac{\int_{0.239}^{10 \text{ MeV}} g(E_\gamma, E_e) \exp(-E_e/kT)/E_e dE_e}{\int_{0.239}^{10 \text{ MeV}} \exp(-E_e/kT)/E_e dE_e},$$

where $g(E_\gamma, E_e)$ represents the bremsstrahlung spectrum produced from electrons of energy E_e . In a similar fashion the heating and dose rates can be obtained. As stated above, for $kT = 2.0$ MeV (hereafter referred to as 2.0* MeV), the integral was also extended to 20 MeV, assuming the bremsstrahlung spectra from electrons with energies greater than 10 MeV were the same as those produced by 10-MeV electrons.

A.1.1.3 Results

Energy deposition in superconducting coils

The bremsstrahlung spectra obtained from the EGS-PEGS calculations are given in Table A.1.1 for a large range of electron energies. The photon energy group structure used in this study is also given in Table A.1.1. This group structure corresponds to the 21-photon energy group structure in the DLC-31 cross-section library.

Table A.1.1. Bremsstrahlung spectra for photons above 0.01 MeV (photons/electron)

| Photon upper energy (MeV) | Electron energy (MeV) | | | | | | |
|----------------------------------|-------------------------|------------|------------|------------|------------|------------|------------|
| | 0.489(1.0) ^a | 0.989(1.5) | 1.489(2.0) | 1.989(2.5) | 2.489(3.0) | 2.989(3.5) | 3.489(4.0) |
| 14 | 0 | 0 | 0 | 0 | 0 | 0 | 0 |
| 10 | ↑ | ↑ | ↑ | ↑ | ↑ | ↑ | ↑ |
| 8 | ↑ | ↑ | ↑ | ↑ | ↑ | ↑ | ↑ |
| 7 | ↑ | ↑ | ↑ | ↑ | ↑ | ↑ | ↑ |
| 6 | ↑ | ↑ | ↑ | ↑ | ↑ | ↑ | ↑ |
| 5 | ↑ | ↑ | ↑ | ↑ | ↑ | ↑ | 0 |
| 4 | ↑ | ↑ | ↑ | ↓ | ↓ | ↓ | 1.11-4 |
| 3 | ↑ | ↑ | ↓ | ↓ | 0 | 0 | 5.56-4 |
| 2.5 | ↑ | ↓ | ↓ | 0 | 1.11-4 | 8.89-4 | 2.33-3 |
| 2.0 | ↑ | ↓ | 0 | 5.56-4 | 1.67-3 | 3.22-3 | 4.22-3 |
| 1.5 | ↑ | 0 | 8.89-4 | 2.56-3 | 5.67-3 | 9.78-3 | 1.31-2 |
| 1.0 | ↓ | 2.22-4 | 1.89-3 | 5.89-3 | 8.89-3 | 1.49-2 | 1.67-2 |
| 0.7 | 0 | 2.44-3 | 5.89-3 | 1.06-2 | 1.58-2 | 2.23-2 | 2.67-2 |
| 0.45 | 1.20-3 ^b | 4.00-3 | 7.33-3 | 1.34-2 | 2.08-2 | 2.74-2 | 2.88-2 |
| 0.3 | 4.80-3 | 1.27-2 | 2.14-2 | 3.33-2 | 4.37-2 | 5.38-2 | 7.12-2 |
| 0.15 | 2.00-3 | 7.89-3 | 1.50-2 | 2.12-2 | 2.88-2 | 3.86-2 | 4.51-2 |
| 0.1 | 4.00-3 | 9.33-3 | 1.77-2 | 2.38-2 | 3.12-2 | 3.79-2 | 4.61-2 |
| 0.07 | 6.80-3 | 1.27-2 | 2.46-2 | 2.86-2 | 4.10-2 | 4.98-2 | 5.83-2 |
| 0.045 | 6.00-3 | 1.19-2 | 2.30-2 | 3.03-2 | 4.00-2 | 4.97-2 | 6.06-2 |
| 0.03 | 6.40-3 | 1.38-2 | 2.36-2 | 3.32-2 | 3.99-2 | 5.29-2 | 5.97-2 |
| 0.02 | 8.00-3 | 2.51-2 | 3.70-2 | 5.43-2 | 6.86-2 | 8.18-2 | 9.01-2 |
| Total γ 's/e ⁻ | 3.92-2 | 1.00-1 | 1.78-1 | 2.58-1 | 3.46-1 | 4.43-1 | 5.24-1 |

| | 3.989(4.0) | 4.489(5.0) | 4.989(5.5) | 5.489(6.0) | 5.989(6.5) | 6.989(7.0) | 6.989(7.5) |
|------|------------|------------|------------|------------|------------|------------|------------|
| 14 | 0 | 0 | 0 | 0 | 0 | 0 | 0 |
| 10 | ↑ | ↑ | ↑ | ↑ | ↑ | 0 | 0 |
| 8 | ↑ | ↑ | ↑ | ↑ | ↓ | 0 | 0 |
| 7 | ↑ | ↑ | ↓ | ↓ | 0 | 1.11-4 | 4.00-4 |
| 6 | ↓ | ↓ | 0 | 0 | 2.22-4 | 1.11-3 | 1.60-3 |
| 5 | 0 | 0 | 4.44-4 | 1.67-3 | 2.00-3 | 3.33-3 | 6.00-3 |
| 4 | 1.00-3 | 2.44-3 | 2.89-3 | 5.33-3 | 8.22-3 | 9.44-3 | 1.28-2 |
| 3 | 2.22-3 | 3.22-3 | 4.22-3 | 5.33-3 | 6.78-3 | 8.78-3 | 9.00-3 |
| 2.5 | 4.11-3 | 4.78-3 | 6.44-3 | 1.02-2 | 1.08-2 | 1.42-2 | 1.46-2 |
| 2.0 | 7.00-3 | 1.06-2 | 1.49-2 | 1.56-2 | 1.91-2 | 2.14-2 | 2.62-2 |
| 1.5 | 1.51-2 | 2.04-2 | 2.50-2 | 2.81-2 | 3.43-2 | 4.17-2 | 5.22-2 |
| 1.0 | 2.09-2 | 2.53-2 | 3.08-2 | 3.18-2 | 4.18-2 | 4.36-2 | 5.08-2 |
| 0.7 | 3.26-2 | 3.73-2 | 4.39-2 | 5.47-2 | 5.53-2 | 6.71-2 | 8.30-2 |
| 0.45 | 3.80-2 | 4.40-2 | 4.99-2 | 5.62-2 | 5.88-2 | 7.18-2 | 7.78-2 |
| 0.3 | 7.91-2 | 9.02-2 | 1.02-1 | 1.13-1 | 1.30-1 | 1.45-1 | 1.64-1 |
| 0.15 | 5.38-2 | 6.26-2 | 6.78-2 | 7.87-2 | 7.97-2 | 9.46-2 | 1.02-1 |
| 0.1 | 5.34-2 | 5.77-2 | 6.54-2 | 6.89-2 | 7.90-2 | 8.74-2 | 9.12-2 |

Table A.1.1 (continued)

| Photon upper energy (MeV) | Electron energy (MeV) | | | | | | |
|----------------------------------|-----------------------|------------|------------|------------|-------------|------------|------------|
| | 3.989(4.0) | 4.489(5.0) | 4.989(5.5) | 5.489(6.0) | 5.989(6.5) | 6.989(7.0) | 6.989(7.5) |
| 0.07 | 6.64-2 | 7.59-2 | 8.32-2 | 9.74-2 | 1.00-1 | 1.12-1 | 1.31-1 |
| 0.045 | 6.21-2 | 7.56-2 | 8.22-2 | 8.46-2 | 9.61-2 | 1.07-1 | 1.21-1 |
| 0.03 | 6.77-2 | 6.94-2 | 8.51-2 | 8.83-2 | 9.93-2 | 1.09-1 | 1.27-1 |
| 0.02 | 1.09-1 | 1.21-1 | 1.30-1 | 1.45-1 | 1.59-1 | 1.71-1 | 2.07-1 |
| Total γ 's/e ⁻ | 6.12-1 | 7.00-1 | 7.94-1 | 8.85-1 | 9.80-1 | 1.109 | 1.329 |
| | 7.489(8.0) | 7.989(8.5) | 8.489(9.0) | 8.989(9.5) | 9.489(10.0) | | |
| 14 | 0 | 0 | 0 | 0 | 0 | | |
| 10 | 0 | 0 | 0 | 4.00-4 | 6.00-4 | | |
| 8 | 1.11-4 | 4.00-4 | 1.20-3 | 1.20-3 | 2.00-3 | | |
| 7 | 1.11-3 | 1.20-3 | 1.80-3 | 4.20-3 | 3.80-3 | | |
| 6 | 3.00-3 | 4.40-3 | 5.60-3 | 5.60-3 | 7.60-3 | | |
| 5 | 5.78-3 | 7.40-3 | 8.60-3 | 1.04-2 | 1.32-2 | | |
| 4 | 1.10-2 | 1.74-2 | 1.70-2 | 2.08-2 | 2.68-2 | | |
| 3 | 1.16-2 | 1.38-2 | 1.82-2 | 1.80-2 | 2.12-2 | | |
| 2.5 | 1.59-2 | 2.14-2 | 2.68-2 | 2.54-2 | 3.22-2 | | |
| 2.0 | 2.92-2 | 3.52-2 | 4.02-2 | 4.06-2 | 5.10-2 | | |
| 1.5 | 5.24-2 | 5.46-2 | 6.86-2 | 8.42-2 | 8.74-2 | | |
| 1.0 | 5.53-2 | 5.98-2 | 7.74-2 | 9.00-2 | 9.90-2 | | |
| 0.7 | 8.44-2 | 1.02-1 | 1.10-1 | 1.25-1 | 1.43-1 | | |
| 0.45 | 9.40-2 | 1.01-1 | 1.17-1 | 1.24-1 | 1.45-1 | | |
| 0.3 | 1.84-1 | 2.06-1 | 2.50-1 | 2.55-1 | 2.88-1 | | |
| 0.15 | 1.21-1 | 1.33-1 | 1.51-1 | 1.74-1 | 1.96-1 | | |
| 0.1 | 1.16-1 | 1.26-1 | 1.39-1 | 1.61-1 | 1.84-1 | | |
| 0.07 | 1.46-1 | 1.53-1 | 1.85-1 | 2.12-1 | 2.22-1 | | |
| 0.045 | 1.39-1 | 1.54-1 | 1.79-1 | 2.05-1 | 2.24-1 | | |
| 0.03 | 1.41-1 | 1.62-1 | 1.95-1 | 2.13-1 | 2.17-1 | | |
| 0.02 | 2.29-1 | 2.68-1 | 2.91-1 | 3.16-1 | 3.51-1 | | |
| Total γ 's/e ⁻ | 1.440 | 1.621 | 1.882 | 2.086 | 2.315 | | |

^aNumbers in parentheses denote total electron energy.

^bRead as 1.20×10^{-3} .

The importance of electron energy to the total photon energy deposition rate in the superconducting coils is illustrated in Fig. A.1.2 for several ²³⁸U shield thicknesses. These results are normalized per incident electron per second and were obtained by performing separate ANISN calculations for each of the spectra in Table A.1.1. The increased energy deposition rate with increasing electron energy is the result of both the increased number of photons and the increased photon energies associated with the higher energy electrons.

To obtain the actual total energy deposition rate, the data in Fig. A.1.2 must be weighted with the electron loss distribution. Energy deposition rates obtained with the loss distribution given in Sect. A.1.1.2 are presented in Fig. A.1.3 for electron temperatures of 1.0, 1.5, 2.0, and 2.0* MeV as a

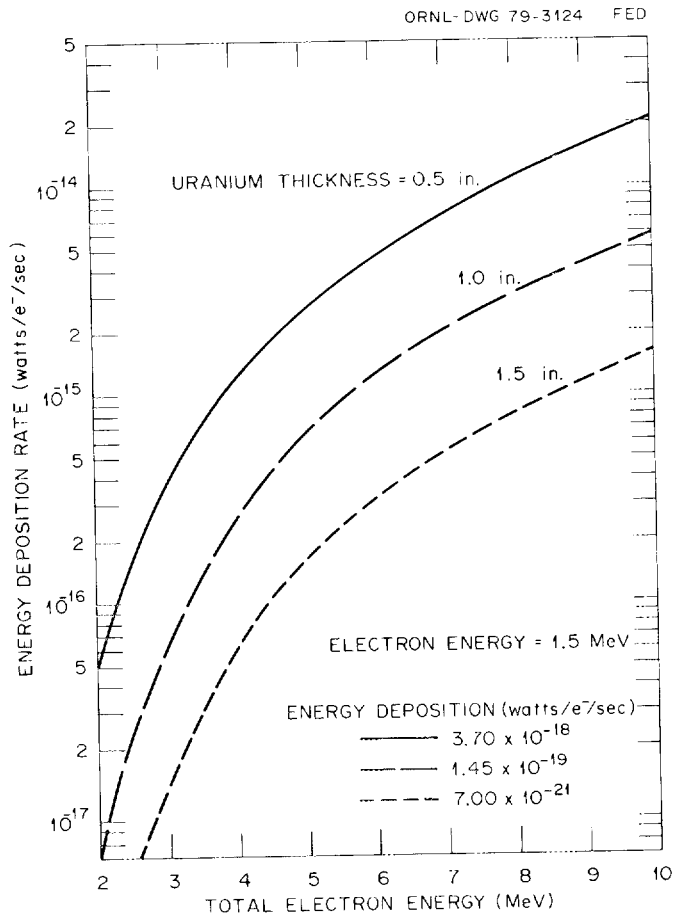


Fig. A.1.2. Normalized bremsstrahlung energy deposition rate in copper coils vs electron energy for uranium shield thicknesses of 0.5, 1.0, and 1.5 in.

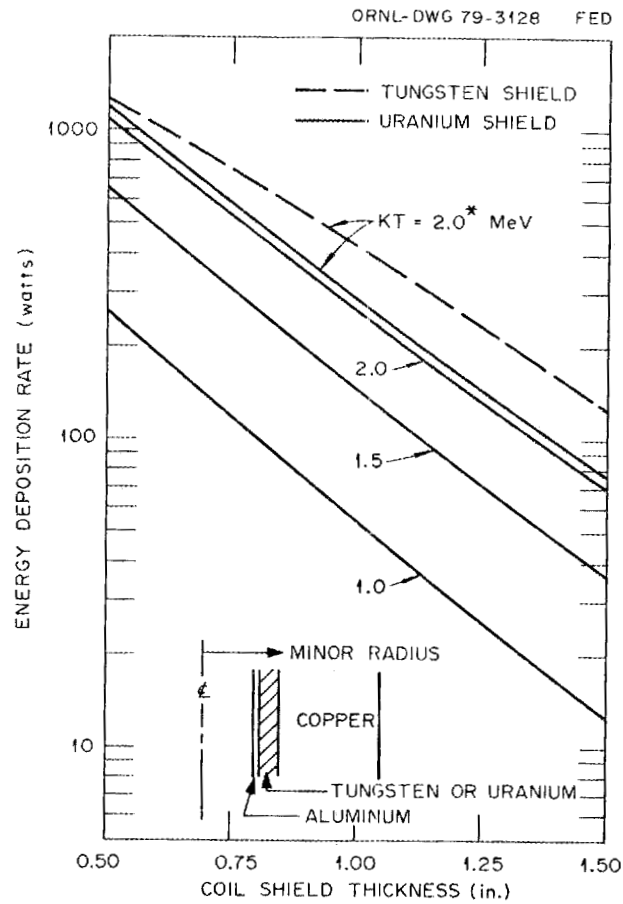


Fig. A.1.3. Total energy deposition rate in copper coils vs coil shield thickness for several electron temperatures.

function of coil shield thickness. As explained in Sect. A.1.1.2, 2.0^* MeV represents extending the integration to 20 MeV. These results have been normalized to a 1-MW electron power loss. The energy deposition rate for the tungsten shield was calculated only for the $kT = 2.0^*$ -MeV electron temperature because this temperature yields the greatest heating.

The total energy deposition rates in the aluminum liner, ^{238}U shield, and copper coil for these same electron temperatures and three ^{238}U shield thicknesses are given in Table A.1.2. These results have also been normalized to a 1 MW-electron power loss. The energy deposition rates represent only the heating due to bremsstrahlung. The remainder of the heating associated with the incident electrons amounts to $\sim 98\%$ of the total power loss. This portion of the power loss is deposited almost entirely in the aluminum liner because only some of the higher energy electrons are able to penetrate into the ^{238}U shield.

Table A.1.2. Energy deposition rate in coil materials (W)

| Material | ^{238}U thickness (in.) | Electron temperature (MeV) | | | |
|------------------|----------------------------------|----------------------------|--------|--------|---------|
| | | 1.0 | 1.5 | 2.0 | 2.0^* |
| Al ^a | 0.5 | 2530 | 3,260 | 3,840 | 3,930 |
| | 1.0 | 2520 | 3,250 | 3,840 | 3,930 |
| | 1.5 | 2520 | 3,250 | 3,830 | 3,920 |
| ^{238}U | 0.5 | 6590 | 9,670 | 12,400 | 12,800 |
| | 1.0 | 6830 | 10,200 | 13,200 | 13,700 |
| | 1.5 | 6830 | 10,300 | 13,400 | 13,900 |
| Cu | 0.5 | 260 | 644 | 1,080 | 1,170 |
| | 1.0 | 54 | 148 | 260 | 285 |
| | 1.5 | 13 | 38 | 68 | 75 |

^aEnergy deposition rate in aluminum is due to photons only. The total energy deposition rate in aluminum can be obtained simply by subtracting the combined energy deposition rate in ^{238}U and copper from the total power loss of 1 MW.

The energy deposition rate density profiles across the copper coils for an electron temperature of 2.0^* MeV are given in Fig. A.1.4. To obtain the absolute power density for a 1-MW electron power loss, these results must be multiplied by 4.81×10^{18} electrons/sec and divided by $2\pi R_{\text{major}}$, where R_{major} is the major radius of the torus. For a major radius of 5.67 m, the maximum power density with the 1-in.-thick ^{238}U shield is 0.135 mW/cm^3 .

Some of the above calculations were carried out for a maximum possible condition, i.e., normal incident photons. The results increased only by ~ 2 .

Biological dose rates

The calculated biological dose rates as a function of lead and concrete shield thickness are presented in Figs. A.1.5 and A.1.6, respectively. These results were obtained with and without 1.25 in. of ^{238}U coil shielding for the electron temperatures of interest. The isotropic photon sources used in these calculations were the same as those used in the heating calculations and again correspond to a 1-MW electron power loss. For a kT value of 2.0^* MeV in the absence of any ^{238}U coil shielding, 12.5 in. of lead or 6.3 ft of concrete is required to reduce the biological dose rate to 2.5 mrem/hr , the maximum occupational radiation level currently accepted. However, because no reduction of the photon spectra was assumed to occur due to shielding by the components of the machine, these results should represent the maximum required shielding to obtain a 2.5 mrem/hr radiation level.

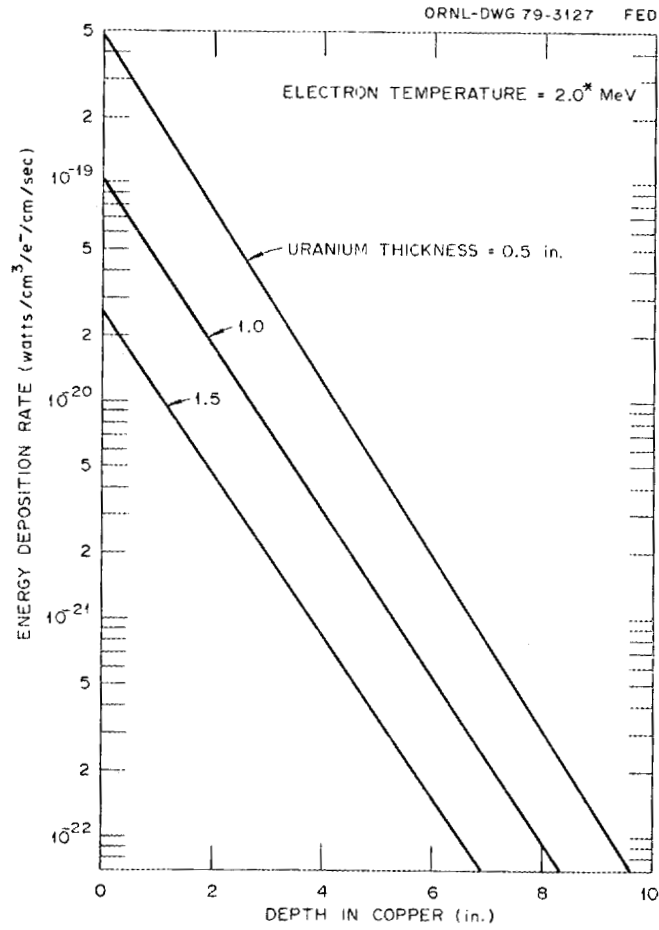


Fig. A.1.4. Normalized energy deposition rate density profiles in copper coils for uranium shield thicknesses of 0.5, 1.0, and 1.5 in.

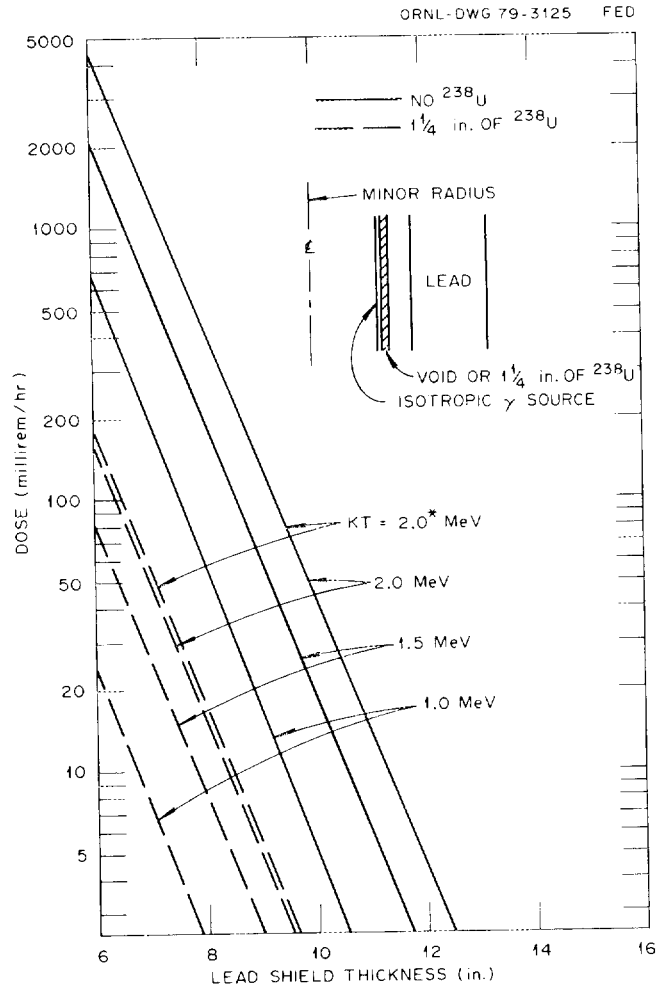


Fig. A.1.5. Biological dose rate vs lead shield thickness with and without 1 1/4 in. of ^{238}U coil shield for several electron temperatures.

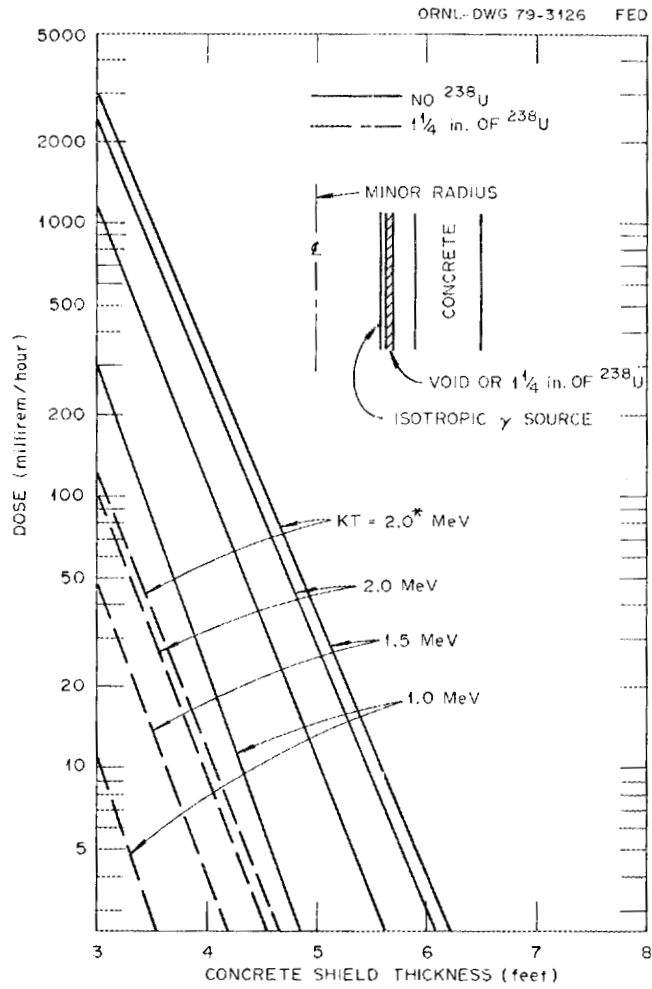


Fig. A.1.6. Biological dose rate vs concrete shield thickness with and without 1 1/4 in. of ^{238}U coil shield for several electron temperatures.

A.1.2 VACUUM VESSEL THERMAL ANALYSIS

The EBT-P torus cooling requirements were established with a conservative point of view. The vessel power input was established at 2.0 MW. Because at this time no EBT power deposition data to the vessel exist and because there is a possibility that input power will be increased in the future, a 3.0-MW plasma input power level was assumed for coolant flow calculations.

Deionized water flow rates were initially established using the following equation:

$$\dot{Q}_{\text{vessel}} = \dot{m} C_p \Delta T_{\text{H}_2\text{O}},$$

where

\dot{Q}_{vessel} = energy transfer rate,

\dot{m} = mass flow rate,

C_p = mean specific heat, and

ΔT = temperature differential of coolant assumed to be 15°F (8.3°C).

To establish the distribution of the coolant, the following assumptions were made.

- (1) The electron annulus energy loss occurs in the throat.
- (2) The plasma energy loss rates are inversely proportional to the cross-sectional area of the vessel.

Table A.1.3 shows the coolant flow distribution and the assumed energy deposition rates used for flow rate calculations.

Table A.1.3. Toroidal vessel coolant requirements and assumed energy deposition rates for EBT-P

| Toroidal vessel component name | Coolant flow per component (gpm) | Total coolant flow for toroidal vessel (gpm) | Assumed total energy deposition (MW) |
|--------------------------------|----------------------------------|--|--------------------------------------|
| Mirror cavity liner | 6.7 | 241 | 0.5 |
| Coil cavity | | | |
| Coil cavity throat | 12.4 | 446 | 0.982 |
| Coil cavity balance | 18.6 | 670 | 1.5 |
| Total (coil cavity) | 31.0 | 1116 | 2.482 |

A thermal analysis of the coil cavity using a 2-D version of HEATING5 code was performed. Also included in the model were the shielding material and the liquid-nitrogen-cooled mirror coil dewar wall. The model provided an evaluation for the deionized cooling water distribution and temperature profiles of the vessel walls to be used in the stress analysis of the vacuum liner cavity. Heating effects resulting from gamma ray attenuation were also modeled. The coil cavity was given major consideration because the majority of the plasma energy is anticipated to be distributed along the coil cavity walls and because of the complexity of the coil cavity geometry. Figures A.1.7, A.1.8, and A.1.9 show the results for the thermal analysis.

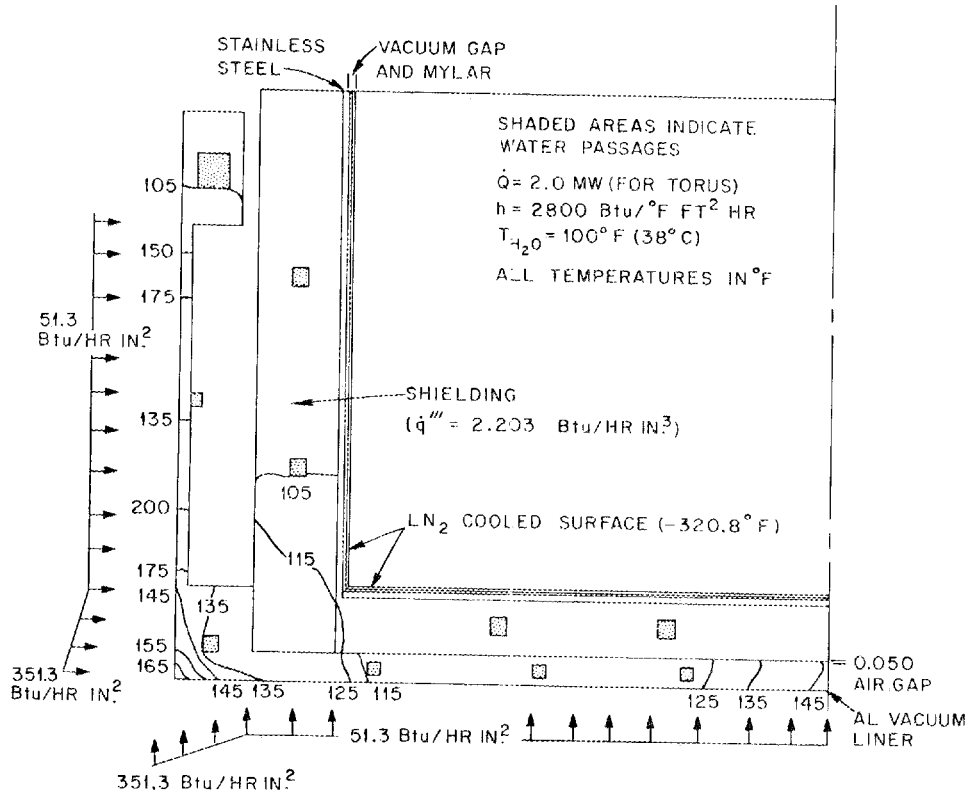


Fig. A.1.7. Vacuum liner temperature profile for 2.0-MW power.

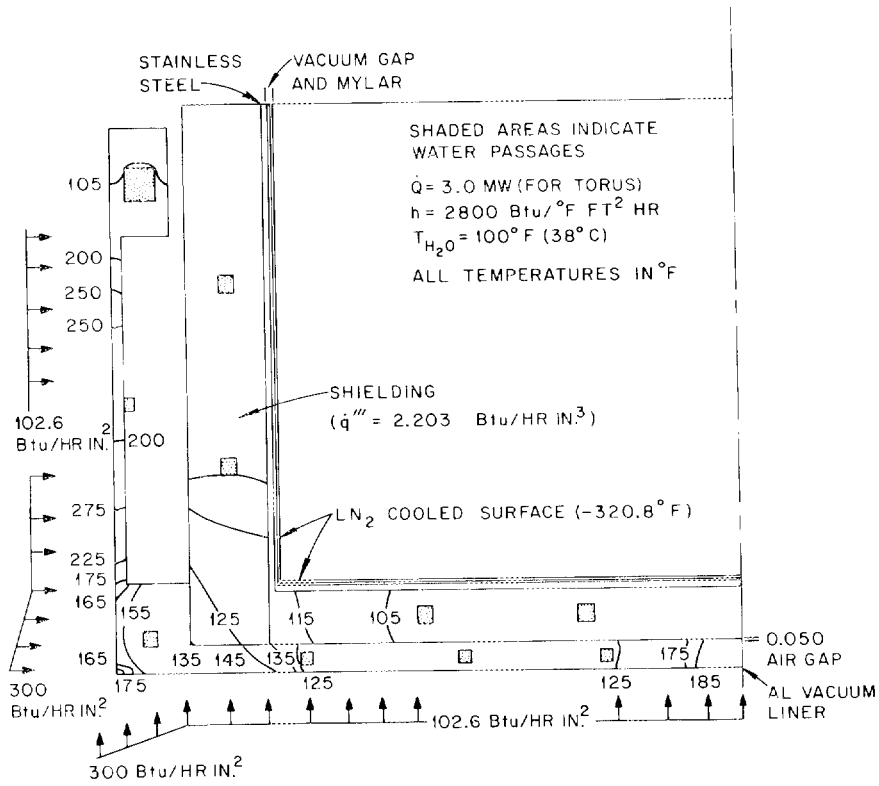


Fig. A.1.8. Vacuum liner temperature profile for 3.0-MW power.

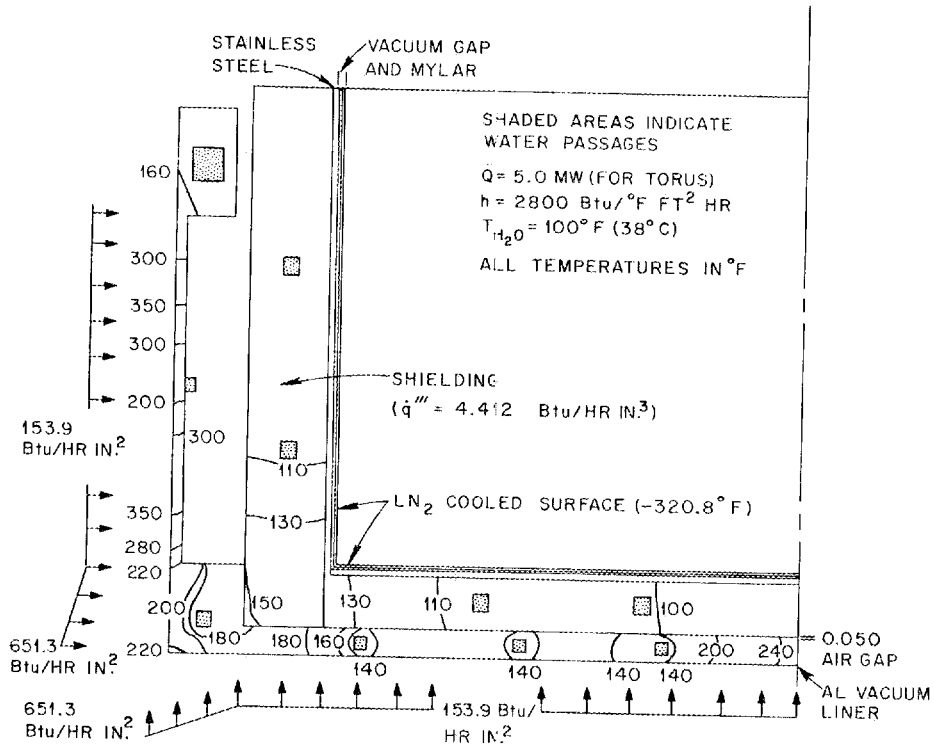


Fig. A.1.9. Vacuum liner temperature profile for 5.0-MW power.

A.1.3 MAGNETIC FORCE ANALYSIS

The magnetic loads imposed on an EBT-P mirror-trim coil pair by the other mirror and trim coils and by the ARE coils have been calculated using the BARC13 magnetic field computer program. Under normal operating conditions without ARE coils, the centering force on a mirror-trim coil pair is 53,000 lb. With the ARE coils operating, the additional centering force would be $\pm 57,000$ lb; therefore, the range of centering force on the coil pair is from 110,000 lb toward the center of the torus to 4000 lb away from the center. The lateral or sideways load on the mirror-trim coil pair due to imbalances in currents in the mirror and trim coils can be as great as 255,000 lb if half the mirror and trim coils is de-energized. The lateral load due to deenergized ARE coils can be as great as 155,000 lb.

Figure A.1.10 shows the geometry assumed for the calculations. In some calculations the mirror-trim coil pair has been treated as a single coil, but in other cases the mirror and trim coils have been treated separately. Table A.1.4 shows the contribution to the centering and lateral forces in a coil due to each of the other coils, and Table A.1.5 summarizes the net forces for several cases. Figures A.1.11 and A.1.12 show how the radial and lateral loads are distributed around the perimeter of a mirror-trim coil pair.

Table A.1.4. Forces in mirror-trim coil 1 due to other mirror-trim coils and ARE coils^a

| Coil (see Fig. A.1.10 for designations) | Centering force (positive toward torus center) | Lateral force (along coil axis) |
|---|--|------------------------------------|
| 1 | 0 | 0 |
| 2 or 36 | 89.3 | +1026 |
| 3 or 35 | 17.6 | ± 100 |
| 4 or 34 | 5.76 | ± 21.6 |
| 5 or 33 | 2.53 | ± 6.97 |
| 6 or 32 | 1.32 | ± 2.84 |
| 7 or 31 | 0.77 | ± 1.34 |
| 8 or 30 | 0.49 | ± 0.71 |
| 9 or 29 | 0.33 | ± 0.40 |
| 10 or 28 | 0.24 | ± 0.24 |
| 11 or 27 | 0.18 | ± 0.15 |
| 12 or 26 | 0.14 | ± 0.10 |
| 13 or 25 | 0.11 | ± 0.06 |
| 14 or 24 | 0.09 | ± 0.04 |
| 15 or 23 | 0.08 | ± 0.03 |
| 16 or 22 | 0.07 | ± 0.02 |
| 17 or 21 | 0.06 | ± 0.01 |
| 18 or 20 | 0.06 | ± 0.01 |
| 19 | 0.06 | 0 |
| 1 or 72 | 104.5 | 342.6 |
| 2 or 71 | 4.37 | 76.16 |
| 3 or 70 | 10.88 | 211.4 |
| 4 or 69 | 2.04 | 14.37 |
| 5 or 68 | 0.63 | 30.22 |
| 6 or 67 | 1.13 | 3.98 |
| 7 or 66 | 0.52 | 6.95 |
| 8 or 65 | 0.60 | 1.45 |
| 9 or 64 | 0.39 | 2.26 |
| 10 or 63 | 0.34 | 0.63 |
| Remaining ARE coils combined | 6.80 | 5.20 |

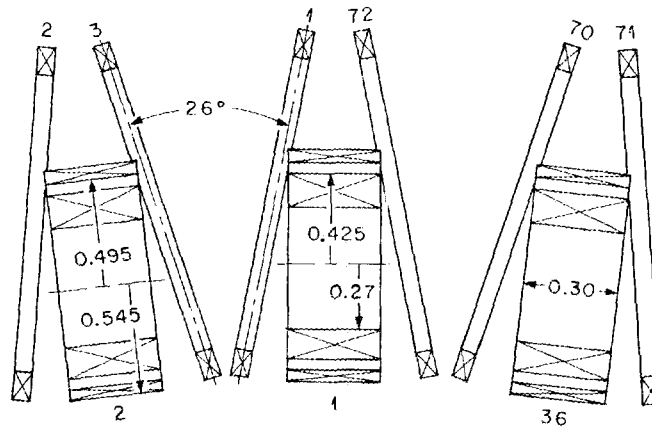
^aForces in kilonewtons; $I_{\text{MIRROR}} = 2.325 \times 10^6$ A, $I_{\text{TRIM}} = 1.005 \times 10^6$; and $I_{\text{ARE}} = 0.216 \times 10^6$. See Table A.1.5 for total forces.

Table A.1.5. Total forces on mirror and trim coils

| | Maximum centering force (kilonewtons) | Maximum lateral force (kilonewtons) |
|---|--|--|
| Case 1 ($I_{MIRROR} = 2.356 \times 10^6$ A, $I_{TRIM} = 1.005 \times 10^6$, $I_{ARE} = 0$) | | |
| Mirror coil | 144.4 | 642 |
| Trim coil | 88.3 | 492 |
| Combined | 232.7 (53,000 lb) | 1134 (255,000 lb) |
| | | } with half of mirror-trim coils deenergized |
| Case 2 ($I_{MIRROR} = 2.356 \times 10^6$ A, $I_{TRIM} = 1.005 \times 10^6$, $I_{ARE} = 0.216 \times 10^6$) | | |
| Mirror and trim coils combined | 486 (110,000 lb) | 1826 (410,000 lb) with half of mirror-trim and ARE coils deenergized |
| Case 3 ($I_{MIRROR} = 2.356 \times 10^6$ A, $I_{TRIM} = 1.005 \times 10^6$, $I_{ARE} = 0.216 \times 10^6$) | | |
| Mirror and trim coils combined | -21 (-4,000 lb) | 1826 (410,000 lb) with half of mirror-trim and ARE coils deenergized |

ORNL-DWG 79-3124 FED

ARE COIL DESIGNATIONS



MIRROR-TRIM COIL DESIGNATIONS

DIMENSIONS IN METERS

MAJOR RADIUS=5.6

Fig. A.1.10. EBT-P geometry.

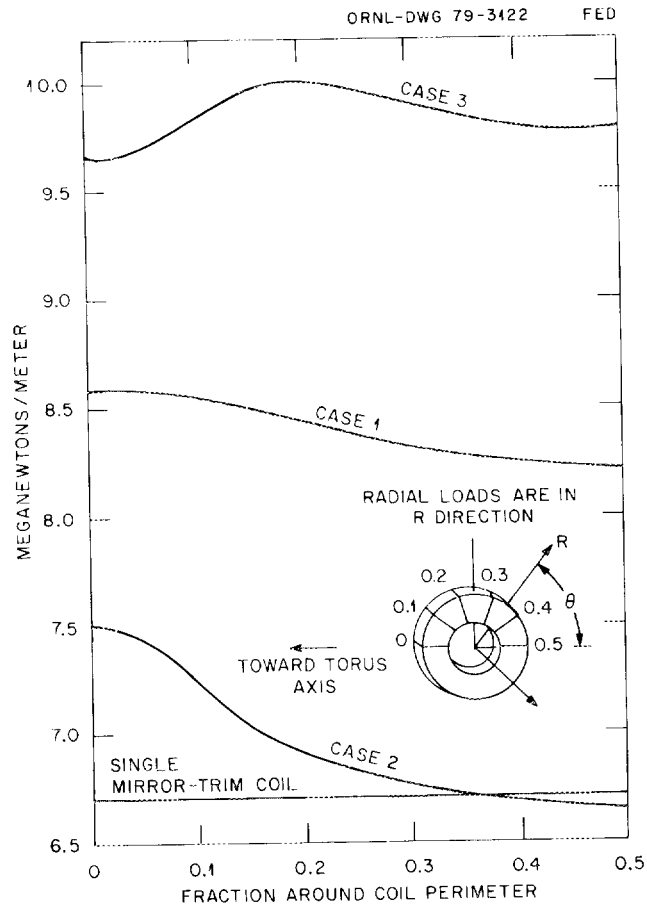


Fig. A.1.11. Radial load distribution around mirror-trim coils.

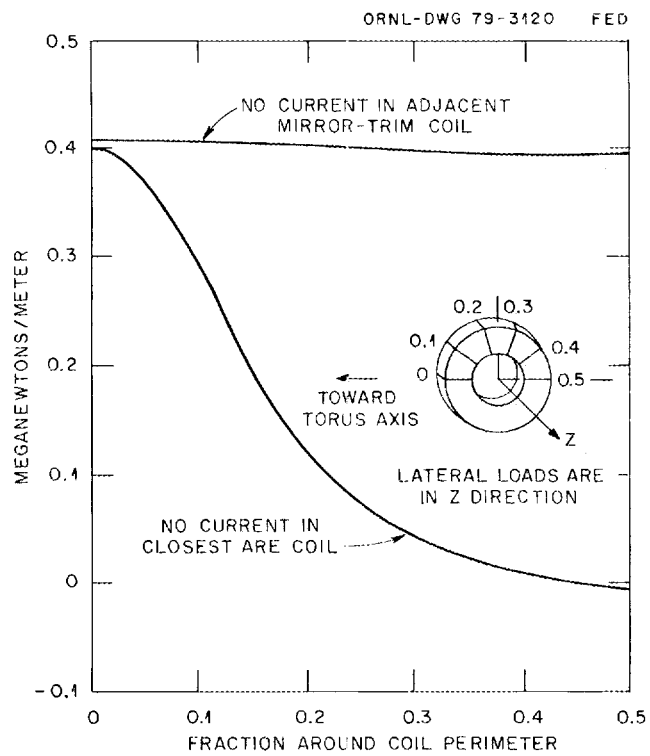


Fig. A.1.12. Lateral load distribution around mirror-trim coils due to loss of current in nearby coils.

A.1.4 STRAY MAGNETIC FIELDS

Figure A.1.13 summarizes the torus geometry. Figures A.1.14, A.1.15, and A.1.16 summarize the magnitudes of the stray magnetic fields in various regions around EBT-P. The values shown in the figures are total field magnitudes. The fields have been calculated for the case where each mirror coil carries a total of 4.06×10^6 A. The computer program BARC13 was used to calculate the magnetic fields. For the purposes of these calculations, each mirror-trim coil pair was considered as a single coil.

A.1.5 CRYOGENIC SYSTEM HEAT LOAD ESTIMATE

The following estimates are based on expansion to a 48-sector torus.

| | |
|---|--------------|
| Refrigeration loads | |
| Mirror coil heat load | |
| Internal dissipation plus gamma heating | 7.0 W/coil |
| Thermal radiation | 0.05 W/coil |
| Gravity support | 0.34 W/coil |
| Out-of-plane support | 10.0 W/coil |
| Centering supports | 5.5 W/coil |
| Total | 22.9 W/coil |
| Total for 48 coils | 1100 W |
| Gyrotron focusing solenoid heat leak | 3.0 W/coil |
| Total for 12 coils | 36 W |
| Satellite and storage dewars (1% per day) | 6 W |
| Transfer line losses | |
| Valves | 800 W |
| Bayonets | 440 W |
| Line | 48 W |
| Total line loss | 1300 W |
| Subtotal refrigeration load | 2440 W |
| Add 50% contingency ^a | 1220 W |
| TOTAL refrigeration load @4.2K | 3660 W |
| Liquefaction loads | |
| Mirror coil leads (2.8 liter/hr/kA x 2 kA x 48 coils) | 540 liter/hr |
| Gyrotron focusing solenoid leads (2.8 liter/hr/kA x | |
| 0.2 kA x 12 coils) | 7 liter/hr |
| Subtotal liquefaction load | 547 liter/hr |
| Add 0% contingency ^b | 0 |
| TOTAL liquefaction load | 547 liter/hr |

^aBased on past experience with cryogenic systems plus contingency for cooldown line and valving, burst disks and relief valves, and the eventual addition of cryopumping for neutral beam heating.

^bConservative numbers used for current in leads.

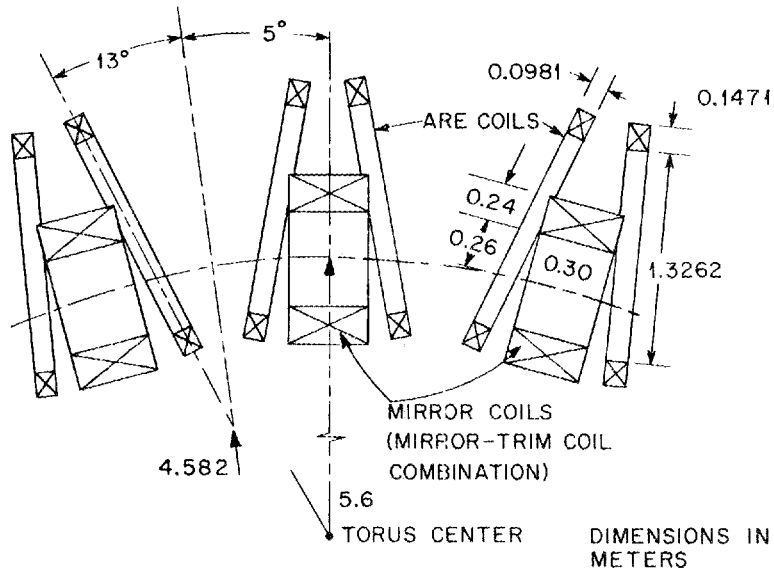


Fig. A.1.13. Torus geometry.

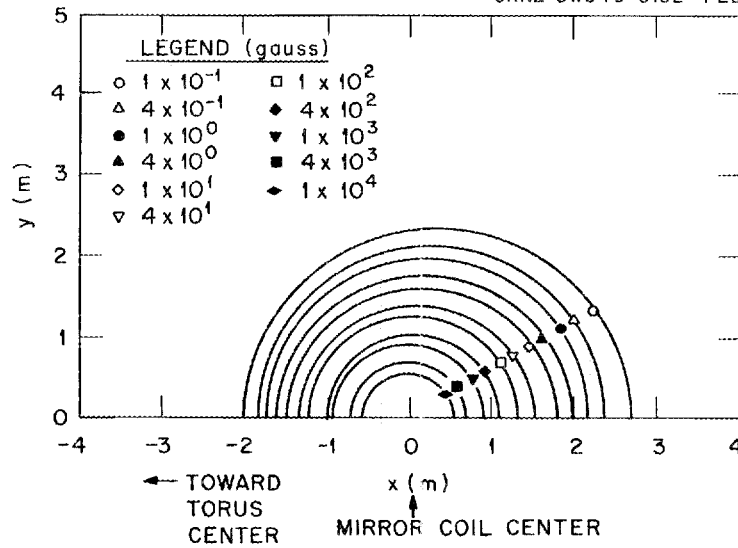


Fig. A.1.14. Elevation view of total field contours in plane midway between mirror coils. Mirror coil current = 4.06×10^6 A for both sections.

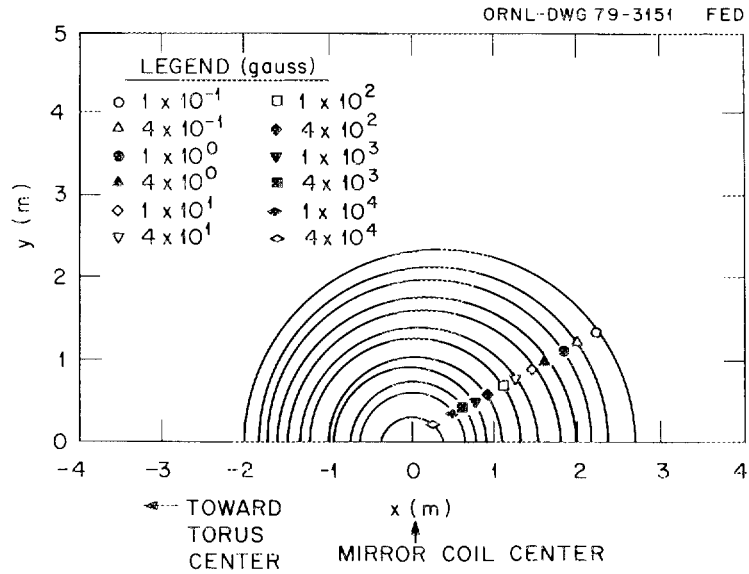


Fig. A.1.15. Elevation view of total field contours in mirror coil midplane.

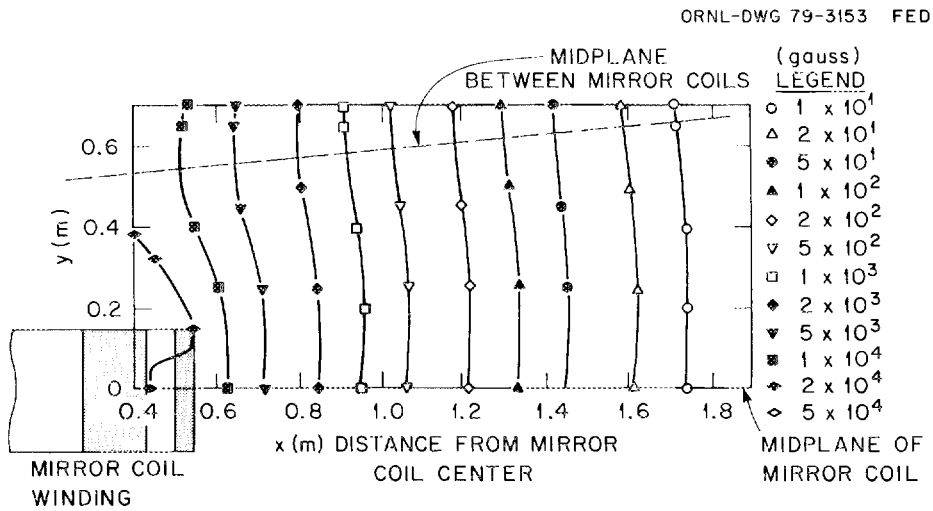


Fig. A.1.16. Plan view of total magnetic field contours.

A.1.6 MICROWAVE/CRYOPUMP ISOLATION SYSTEM CALCULATIONS

A.1.6.1 Perforated Copper Plate DesignMicrowave attenuation

The perforated copper plate design shown in Drawing X2E-14270-0001 is proposed for use at 110 GHz. Its parameters are given below:

| <u>Material</u> | <u>Copper</u> |
|--------------------------------------|---------------|
| Thickness (l) | 0.0625 in. |
| Hole diameter (2a) | 0.045 in. |
| Hole spacing on triangular pitch (d) | 0.055 in. |

Using Chen's theory the attenuation for normal incidence is given by⁸ leakage (dB) = 20 log |T|.

Here

$$T = \frac{1}{1 - j[A + B \tanh(\beta l)]} = \frac{1}{1 - j[A + B \coth(\beta l)]},$$

where

$$A = 12 \left[\frac{4}{3} \left(\frac{\lambda}{d} \right)^2 - 1 \right]^{1/2} \left[\frac{J_1' \left(\frac{4\pi a}{\sqrt{3} d} \right)}{1 - \left(\frac{4\pi a}{1.841\sqrt{3}d} \right)^2} \right]^2 - \frac{12}{\left[\frac{4}{3} \left(\frac{\lambda}{d} \right)^2 - 1 \right]^{1/2}} \left[\frac{J_1 \left(\frac{4\pi a}{\sqrt{3} d} \right)}{\frac{4\pi a}{\sqrt{3} d}} \right]^2,$$

$$B = 0.33 \left(\frac{d}{a} \right)^2 \left[\left(\frac{0.293\lambda}{a} \right)^2 - 1 \right]^{1/2}, \text{ and}$$

$$\beta = \frac{2\pi}{\lambda} \left[\left(\frac{0.293\lambda}{a} \right)^2 - 1 \right]^{1/2}$$

for $a > 0.28d$ and $d < 0.57\lambda$. For the given dimensions the attenuation is 34 dB at 110 GHz and 50 dB at 60 GHz.

Vacuum conductance

The porosity P for a triangular array of holes is given by

$$P = \frac{2\pi a^2}{\sqrt{3} d^2},$$

where

a = 22.5 mil (hole radius),

d = 55 mil (triangular pitch hole spacing), and

P = 0.6071.

For $\epsilon/2a = 1.39$, the Clausing factor K' is equal to 0.4359. The net conductance of the plate normalized to a circular aperture of the plate sizes is then $C^* = K'P = 0.2646$.

A.1.6.2 Absorbent Section

In the proposed design a 10-in. section of straight pipe coated with a microwave-absorbent material is added behind the plate. This prevents the region behind the plate including the pump from being a high-Q resonator. The exact type of coating will have to be determined from testing at 110 GHz.

Effect on conductance

For the above section with a 6.5-in.-thick, 11.5-in.-ID gate valve in series, overall normalized conductance is given by

$$\frac{1}{F} = \frac{1}{F_1} + \frac{1}{F_2} - 1,$$

where

$$F_1 = 0.2646 \text{ for the plate,}$$

$$F_2 = 0.4252 \text{ (Clausing's factor for } L/D = 1.43\text{).}$$

The net normalized conductance to the pump is thus $F = 0.195$.

Microwave absorption

Because of the complex geometry, the actual absorption should be found experimentally. A rough conservative estimate was made by treating the microwave radiation leaving the plate as isotropic thermal radiation, finding the view factor for transmission, and assuming that everything striking the walls is absorbed. This gives an additional 6.8 dB of attenuation for a total of 40.8 dB.

A.1.6.3 Microwave Power into Cryopump

Testing is required to determine the effect of low microwave power input on a cryopump's pumping ability. The most conservative assumption is probably that all power incident is absorbed on the coldest section. It was assumed that the incident power should be less than 1 W, which is below the 1.5-2 W refrigeration capacity of the CRYO-TORR 10 pump at the coldest stage.

The next question is the manner in which power input to the torus divides between the plasma and the apertures. A formal theory for this is not available. For the purpose of this report, a crude model was taken. It was assumed that power leakage out of an aperture was given by

$$P_{\text{out}} = \frac{P_{\text{in}} T_a A_a}{T_c A_c},$$

where

A_a = aperture area,

T_a = aperture average microwave power transmission coefficient,

A_c = area of plasma cutoff surface,

T_c = cutoff surface average microwave power transmission coefficient,

P_{out} = power out of aperture, and

P_{in} = power into mirror cavity.

It was further assumed that $T_c = 0.5$ (crudely assuming 0.5 extraordinary wave power transmitted and 0.5 ordinary reflected from the surface).

For comparison in EBT-I a 3-in. hole had a measured $P_{out}/P_{in} = 4.8\%$, and the above model with $T_a = 1$ gives $P_{out}/P_{in} = 3.8\%$.

For EBT-P we assume that the cutoff surface is a 16-in.-long right cylinder with a 10-in. radius. The power incident on the cryopump with six 200-kW tubes is then

$$P_{out} = \frac{6 \times 200 \times 10^3 \times 10^{-4} \cdot 0.8}{36 \times 1/2} \frac{\pi(11.5 \text{ in.})^2/4}{2\pi(10)(16)} = 0.57 \text{ W}.$$

At 60 GHz, P_{out} is an order of magnitude down.

It would be highly desirable to test the proposed pump and microwave isolation system to determine the overall system response to microwave power.

REFERENCES

1. R. L. Ford and W. R. Nelson, Stanford Linear Accelerator Center Report SLAC-210, Palo Alto, California (1978).
2. W. W. Engle, Jr., Oak Ridge Gaseous Diffusion Plant Report ORGDP-K-1693, Oak Ridge, Tennessee (1967).
3. D. E. Bartine, J. R. Knight, J. V. Pace, III, and R. W. Roussin, Oak Ridge National Laboratory Report ORNL/TM-4840, Oak Ridge, Tennessee (1977).
4. G. C. Haynes, Oak Ridge National Laboratory Report ORNL/TM-5295, Oak Ridge, Tennessee (1976).
5. R. W. Roussin and F. A. R. Schmidt, Nucl. Eng. Des. 15, 319 (1971).
6. "Evaluated Photon Interaction Library ENDF/B File 23 Format," RSIC Data Library Collection DLC-7, informal notes.
7. N. M. Greene, J. L. Lucius, L. M. Petrie, W. E. Ford, III, J. E. White, and R. Q. Wright, Oak Ridge National Laboratory Report ORNL/TM-3706, Oak Ridge, Tennessee (1976).
8. C. C. Chen, IEEE Trans. Microwave Theory Tech., Vol. MTT-21, 1 (1973).

A.2. EBT-P THEORY AND OPERATION

A.2.1 EBT-P THEORY AND SCALING

For several years EBT scaling has been a fundamental ingredient in design studies of future EBT devices.^{1,2} This scaling of the toroidal core plasma is based upon basic theoretical scaling laws with the coefficients determined from experimental measurements from EBT-I/S. A major component of this scaling is $n\tau \sim A^2 T_e^{3/2}$, which follows from neoclassical transport considerations. Recent 1-D transport calculations, which agree reasonably well with experiments, confirm this scaling and strengthen the evidence that the T-mode of operation in EBT is governed by neoclassical behavior.

The most recent calculations³ differ from earlier ones⁴ in that they use purely neoclassical transport. In earlier calculations⁴ it was necessary to introduce an artificial stabilization factor to prevent thermal runaway for low electron collisionality. However, changing the boundary conditions for the neutral hydrogen made it possible to eliminate the artificial stabilization factor.³ The newer boundary conditions correspond more nearly to the experimental observation of the behavior of neutral hydrogen in EBT than did the earlier treatment (which is more appropriate for a pulsed device such as a tokamak).

Because of the role played by the ambipolar electric field in EBT, the calculation of collisionless electron behavior with a self-consistent electric field is nontrivial. The key element has been to use a resonant form for the neoclassical ion transport coefficients and nonresonant electron transport coefficients. In the calculations of Ref. 3 analytical approximations for the ion transport coefficients in the plateau regime and the standard nonresonant approximation for electrons were used. Calculations using alternate forms for the resonant ion transport coefficients indicate that the results are nearly invariant because of adjustments of the ambipolar electric field. The gross behavior of the toroidal core plasma density and temperatures is dominated by the electron transport coefficients, leading to $n\tau \sim A^2 T_e^{3/2}$.

The purely neoclassical transport calculations should be compared only to experimental results obtained during T-mode operation in EBT. In the C-mode of operation (characterized by high electron collisionality and/or neutral hydrogen density), the plasma is noisy (unstable) and nonclassical losses dominate the transport processes.

Entry from the C-mode into the macrostable T-mode of operation in EBT requires that the hot electron rings have sufficient beta to produce a distinct local minimum in B.⁵ A crude estimate of the minimum ring beta required to stabilize the toroidal core plasma is

$$\beta_{\text{crit}} = \frac{1}{4} \frac{N^2}{R^2} (M - 1) W a_p ,$$

where

- N = number of sectors,
- R = major radius,
- M = mirror ratio,
- W = ring width, and
- a_p = plasma radius in the midplane.

Notice that by reducing the mirror ratio, the critical beta required is reduced (because the radial gradient in the vacuum B to be overcome by the hot electron ring is reduced). Thus by reducing the mirror ratio, the critical beta required for entry into the T-mode and hence the microwave power required for the rings can be reduced. On the other hand, the neoclassical transport rates for the toroidal core plasma decrease with increasing mirror ratio and ring beta. Thus, the power required to achieve a given set of plasma parameters decreases with increasing mirror ratio and ring beta while the power to sustain the rings is increased. The optimum core plasma performance for fixed microwave power is thus a function of mirror ratio. Because the detailed interaction of the core and ring plasma is a subject of ongoing research, it is not presently possible to predict an exact optimum for the mirror ratio. Accordingly, the inclusion of trim coils that permit variable mirror ratio is advisable because they allow empirical determination of the optimum.

A.2.2 EBT-P OPERATION

The purpose of operating EBT-P is to measure those properties that will allow a definitive evaluation of the bumpy torus concept. These properties include those of the plasma and of the machine and of their mutual interactions.

In principle, the primary interest is in measuring those plasma properties having the greatest impact on EBT scaling — density, temperature, and confinement time. In practice, however, many more plasma parameters are measured because of the great impact they have on scaling. These measurements are made with instruments that are, in general, remote from the experimentalist's location.

One of the unique features of EBT devices is the steady-state nature. The significance of the steady-state operation is that a given set of operating conditions can be maintained for an extended period. In practice this means that the operating conditions are held constant long enough to acquire the data required to characterize that set of conditions and then the set of conditions is changed. The time needed to acquire this data depends on the particular diagnostic devices. Some diagnostics, such as the microwave interferometer measurement of density, give results very quickly. Among the slowest are those requiring pulse-counting techniques, such as neutral charge exchange or x-ray measurements. In EBT-I these measurements have required as long as 30 min for a single data point. However, because of the higher temperatures and densities expected, this time will be much shorter in EBT-P, allowing a more rapid change of operating conditions. There is, however, one operating parameter that cannot be rapidly varied. The magnetic field, which is produced by superconducting coils, has a characteristically long time constant. It is estimated that about one-half hour will be required to charge the coils. Thus, changing the current through those coils will require a significant fraction of the charging time.

In addition to the equilibrium properties, which will be measured in the manner described above, it will be necessary to make time-dependent measurements in order to determine the time needed to reach a new equilibrium as conditions are changed. The time scales involved range from very short to very long, depending on the processes. Among the shortest time scales are those corresponding to a step change in the heating power whereas the longest times are those for establishing the wall conditions. The former, fixed by the flight times of the particles, may be as short as microseconds; the latter may range up to hours or even days.

The challenge involved in running EBT will be to establish operating procedures that will provide an optimized environment for making the measurements previously discussed while also maintaining the flexibility to change the machine configuration. Such flexibility is essential if the single device, EBT-P, is to be used to investigate a range of confinement and heating concepts.

A.2.3 Summary

The above section indicates briefly EBT theory and operating experience as applied to the design of EBT-P. The detailed work supporting this is covered in a large number of publications and is too lengthy to include in this document. A summary of theory as it stood in 1978 was included in the EBT-II proposal, ORNL/TM-5955.¹ During 1978 and 1979 further work has been undertaken that has been published in various publications.^{5,6,7,8,9} One paper that is soon to be published as ORNL/TM-6806,⁴ but is not yet generally available, is on radial transport calculations and a comparison with the experiment. This TM is re-printed here in its entirety, following the references for this section, to ensure timely availability.

REFERENCES

1. R. A. Dandl et al., Oak Ridge National Laboratory Report ORNL/TM-5955, Oak Ridge, Tennessee (1978).
2. L. A. Berry, C. L. Hedrick, and N. A. Uckan, Oak Ridge National Laboratory Report ORNL/TM-6743, Oak Ridge, Tennessee (1979).
3. E. F. Jaeger, C. L. Hedrick, and W. B. Ard, "Radial Transport in EBT with Constant Edge Neutral Flux," to be published in Phys. Rev. Lett.
4. E. F. Jaeger, C. L. Hedrick, and D. A. Spong, Oak Ridge National Laboratory Report ORNL/TM-6806, Oak Ridge, Tennessee (1979); submitted to Nucl. Fusion.
5. D. B. Nelson and C. L. Hedrick, Nucl. Fusion 19(3), 283-292 (1979).
6. D. B. Batchelor and C. L. Hedrick, Nucl. Fusion 19, 235 (1979).
7. D. A. Spong, E. G. Harris, and C. L. Hedrick, Nucl. Fusion 19, 665 (1979).
8. E. F. Jaeger and C. L. Hedrick, Jr., Nucl. Fusion 19, 443 (1979).
9. D. B. Nelson, Oak Ridge National Laboratory Report ORNL/TM-6824, Oak Ridge, Tennessee (1979).

RADIAL TRANSPORT IN THE ELMO BUMPY TORUS IN COLLISIONLESS ELECTRON REGIMES*

E. F. Jaeger, C. L. Hedrick, and D. A. Spong
Oak Ridge National Laboratory

ABSTRACT

One important area of disagreement between radial transport theory and the ELMO Bumpy Torus (EBT) experiment has been the degree of collisionality of the toroidal plasma electrons. Experiment shows relatively warm electrons ($kT_e \sim 300-600$ eV) and collisionless scaling, that is, energy confinement increasing with temperature. But results of early one-dimensional (1-D), neoclassical transport models with radially inward pointing electric fields are limited to relatively cool electrons ($kT_e \sim 100-200$ eV) and collisional scaling. In this paper these early results are extended to include lowest order effects of ion diffusion in regions where poloidal drift frequencies are small. The effects of direct, or nondiffusive, losses in such regions are neglected along with the effects of finite radial electric fields on electron transport coefficients and of self-consistent poloidal electric fields on ion transport coefficients. Results show that solutions in the collisionless electron regime do exist. Furthermore, when the effects of finite electron ring beta on magnetic fields near the plasma edge are included, these solutions occur at power levels consistent with experiment.

[Reprint of ORNL/TM-6806 (to be published);
also submitted to Nuclear Fusion]

*Research sponsored by the Office of Fusion Energy, U.S. Department of Energy under contract W-7405-eng-26 with the Union Carbide Corporation.

1. INTRODUCTION

When neoclassical transport rates are calculated in the large electric field limit of Kovrizhnykh [1] and applied in a one-dimensional (1-D), radial transport calculation [2,3] for the ELMO Bumpy Torus (EBT) [4], thermally stable, steady-state solutions with radially inward pointing ambipolar electric fields are found, as observed in experiments [4]. However, electron temperatures, as well as the magnitude of radial electric fields in these solutions [2], are consistently lower than those observed experimentally [4]. Increasing the microwave power leads to warmer electrons; but in these cases, negative electric field solutions vanish, giving way to positive electric fields that do not agree with experimental observations.

In this paper we extend the calculations of Ref. [2] to include lowest order effects of ion diffusion for finite radial electric fields in regions of phase space where poloidal drift frequencies are small [3,5,6,7]. Direct, or nondiffusive, losses [8] in these regions are neglected on the grounds that they occur far out on the tail of the distribution function and are thus of little consequence [8]. Although the effects of modest (as opposed to large) radial electric fields on electron transport coefficients and of self-consistent poloidal electric fields on ion transport coefficients appear to be important, for the sake of simplicity they are not included in this initial investigation. Rather, we consider increases in the radially inward pointing electric field resulting from conservation of charge and enhanced ion diffusion in regions of small poloidal drift frequency. Thus, our results show negative electric field solutions over a much broader range of electron temperatures than those of Ref. [2], particularly in the collisionless electron regime of experiments [4]. However, because the effects of modest radial electric fields on electron transport coefficients and of self-consistent poloidal electric fields on ion transport coefficients have not yet been considered, the results given here will not accurately model real EBT plasmas. Instead, this work should be regarded as an additional step toward a complete neoclassical treatment of EBT plasmas.

In Section 2 we discuss the differing diffusion models for ions and electrons. For electrons the assumption is that there are very few slowly orbiting particles for negative electric fields and that the flux is given approximately by the strong electric field result of Kovrizhnykh [1]. The ion flux, on the other hand, is assumed to be dominated by slowly orbiting particles for negative electric fields. As first shown numerically in Ref. [3], this leads to transport rates that are approximately independent of collisionality in the moderate collisionality regime. The first analytic treatment of this "plateau" regime for EBT has been given by Hazeltine [6]; the treatment of ions in Section 2 is essentially the same as that in Ref. [6] with modifications regarding the bounce-averaged particle orbits and the choice of the ad hoc poloidal electric field. In Section 3 we discuss solutions of the radial transport problem with a self-consistent radial electric field and transport coefficients as given in Section 2.

2. DIFFUSION MODEL

Consider the steady-state, bounce-averaged drift kinetic equation [2]

$$v_{Dr} \left. \frac{\partial f}{\partial r} \right|_{\epsilon, \mu} + \frac{v_{D\theta}}{r} \left. \frac{\partial f}{\partial \theta} \right|_{\epsilon, \mu} = C(f) \quad (1)$$

where the spatial gradients are taken with the energy ϵ and the magnetic moment μ held fixed. For large aspect ratios ($R_T/R_C \gg 1$), the components of the bounce-averaged drift velocity v_{Dr} and $v_{D\theta}$ in the radial and poloidal directions, respectively, can be expanded as

$$v_{Dr} = v_y \sin \theta + \dots$$

$$v_{D\theta} = r\Omega + v_y \cos \theta + \dots$$
(2)

where v_y denotes the vertical drift velocity due to toroidal curvature and Ω denotes the poloidal drift frequency due to magnetic gradients and curvature and to the ambipolar electric field. Typical thermal values for these drifts are

$$\Omega_0 = \frac{kT}{eBR_C r}$$

$$v_{y0} = \frac{kT}{eBR_T}$$

where kT is the thermal energy, e is the electron charge, B is the magnetic field, $R_C^{-1} = -\nabla_r B/B$ is the inverse magnetic radius of curvature, and R_T is the major radius of the torus.

Following Hazeltine [6], Eq. (1) can be linearized by expanding in the inverse aspect ratio $\delta = r/R_T = v_{y0}/(\Omega_0 R_C)$. Noting that $v_{Dr} \sim O(\delta)$ and that $v_{D\theta} \sim O(1)$ and writing $f = f_0(r) + f_1(r, \theta)$, where $f_1 \sim O(\delta)$, we find that $f_0 = f_M$, where f_M is a Maxwellian distribution

$$f_M = \frac{n}{\pi^{3/2} (2kT/m)^{3/2}} \exp \left[\frac{-(\epsilon - e\phi)}{kT} \right]$$
(3)

and that the perturbed distribution function f_1 satisfies the linear equation

$$\Omega \frac{\partial f_1}{\partial \theta} - C(f_1) = -v_y \frac{\partial f_M}{\partial r} \sin \theta$$
(4)

In Eq. (3) m is the mass, n is the density, and ϕ is the electric potential. Particle and energy fluxes are now expressed as integrals of the solution to Eq. (4):

$$r_r = \int \frac{d\theta}{2\pi} \int d^3\vec{v} f_1 v_{Dr} = -D_n \frac{\partial n}{\partial r} - D_T \frac{\partial T}{\partial r} + \mu_n n E_r$$

$$Q_r = \int \frac{d\theta}{2\pi} \int d^3\vec{v} f_1 v_{Dr} \frac{1}{2} m v^2 = -K_n \frac{\partial n}{\partial r} - K_T \frac{\partial T}{\partial r} + \mu_T n E_r$$
(5)

where E_r is the radial electric field. The volume element in velocity space is $d^3\vec{v} = -\pi(2kT/m)^{3/2} \sqrt{W} dW d\zeta$, where $W = (1/2mv^2)/kT$ is the normalized energy and $\zeta = v_{\parallel}/v$ is the cosine of the pitch angle.

For a particle- and energy-conserving BGK collision operator [7], Eqs (4) and (5) yield Kovrizhnykh's result [1] in the large electric field, large Ω limit:

$$D_n = \frac{v_{y0}^2}{6} \frac{v}{v^2 + \Omega^2} \quad K_n = \frac{7}{2} kT D_n$$

$$D_T = \frac{2n}{T} D_n \quad K_T = \frac{101}{2} kn D_n$$
(6)

where $\mu_n = (e/kT)D_n$ and $\mu_T = (e/kT)K_n$. In the radial transport calculations of Ref. [2], Eq. (6) is applied to both ions and electrons.

In the collisionless limit, Eq. (4) yields

$$\lim_{C(f_1) \rightarrow 0} f_1 = \frac{-1}{\Omega} \int d\theta v_y \frac{\partial f_M}{\partial r} \sin \theta \quad (7)$$

which is singular when $\Omega = 0$. This means that particles which experience a small average net poloidal drift motion (small Ω) contribute greatly to the perturbed distribution function f_1 and, hence, to transport losses. We call these particles "resonant."

The resonance in Eq. (7) is, depending on the degree of collisionality, limited or broadened by one of two mechanisms [6]. With a model collision operator $C(f_1) \sim \nu \partial^2 f_1 / \partial \omega^2$, where $\omega = \Omega / \Omega_0$, the collision term in Eq. (4) becomes important for $\omega \lesssim \omega_{\text{eff},c}$, where $\omega_{\text{eff},c} \sim (\nu / \Omega_0)^{1/3}$. In this case the resonance is broadened by collisions. If collisions do not scatter particles out of the small Ω region first, these particles can experience large drift orbits and, hence, large step sizes for diffusion under the influence of the vertical toroidal curvature drift v_y . Because of the radial variation in Ω , the drift surfaces are not purely vertical but rather are crescent shaped in cross section. These crescent-shaped orbits become important for $\omega \lesssim \omega_{\text{eff},b}$, where [5]

$$\omega_{\text{eff},b} = \frac{\Omega_{\text{eff},b}}{\Omega_0} \sim \delta^{1/2} \sqrt{\frac{R_c}{r_D} \frac{v_y}{v_{y0}} W_0} \quad (8)$$

is the normalized drift frequency around such an orbit. Here $W_0 = \Omega_E / \Omega_0 \sim 0(e\phi/kT)$, $\Omega_E = E_r / (Br)$, and $r_D = 1 / 2\Omega_E (\partial \Omega / \partial r)$, where r_D is the scale length for radial variation in the poloidal drift frequency. In this case the resonance is broadened by the enhanced radial excursion occurring during a crescent orbit. Comparing $\omega_{\text{eff},b}$ in Eq. (8) with $\omega_{\text{eff},c} \sim (\nu / \Omega_0)^{1/3}$, we find that resonance broadening by crescents dominates resonance broadening by collisions when $\omega_{\text{eff},c} \ll \omega_{\text{eff},b}$ or when $\nu / \Omega_0 \ll \delta^{3/2}$ [for $W_0 \sim v_y / v_{y0} \sim R_c / r_D \sim 0(1)$].

In the region $\delta^{3/2} < \nu / \Omega_0 < 1$, collisions effectively scatter particles out of the small Ω region before crescent-shaped orbits are completed. The step size is then reduced by the ratio of the effective collision time to the period of a crescent orbit. Assuming a simple Krook collision operator $C(f_1) = -\nu f_1$, Eq. (4) gives

$$f_1 = -v_y \frac{\partial f_M}{\partial r} \left[-\cos \theta \left(\frac{\Omega}{v^2 + \Omega^2} \right) + \sin \theta \left(\frac{\nu}{v^2 + \Omega^2} \right) \right] = -v_y \frac{\partial f_M}{\partial r} \left[-\cos \theta \operatorname{Re} \left(\frac{1}{\Omega - i\nu} \right) + \sin \theta \operatorname{Im} \left(\frac{1}{\Omega - i\nu} \right) \right] \quad (9)$$

Substituting into Eq. (4) verifies that Eq. (9) is indeed a solution. However, as already noted, this solution is singular in the collisionless limit when $\Omega = 0$. We can still integrate Eq. (9) over velocity space to obtain transport rates when $\Omega = \Omega(v)$ by using the Plemelj relation [5,6]

$$\lim_{\nu \rightarrow 0} \frac{1}{\Omega - i\nu} = P \left(\frac{1}{\Omega} \right) + \pi i \delta(\Omega) \quad (10)$$

Substituting Eq. (10) into Eq. (9) gives

$$\lim_{\substack{v/\Omega \rightarrow 0 \\ \Omega \rightarrow 0}} f_1 = -v_y \frac{\partial f_M}{\partial r} \left[-\cos \theta P \left(\frac{1}{\Omega} \right) + \pi \sin \theta \delta(\Omega) \right] \quad (11)$$

where P represents the Cauchy principal value integral. As noted by Hazeltine [6], Eq. (11) is independent of collisionality; thus, one might expect the BGK collision model to be more adequate for this regime than for the low collisionality crescent regime. Substituting Eq. (11) into Eq. (5) now gives, in the small Ω , collisionless limit,

$$\begin{aligned} D_n &= \frac{\pi}{2n} \int d^3\vec{v} f_M v_y^2 \delta(\Omega) \\ D_T &= \frac{n}{T} \frac{\pi}{2n} \int d^3\vec{v} f_M v_y^2 \delta(\Omega) \left(W - \frac{3}{2} \right) \\ K_T &= kn \frac{\pi}{2n} \int d^3\vec{v} f_M v_y^2 \delta(\Omega) \left(W - \frac{3}{2} \right) W \\ K_n &= \frac{3}{2} kT \left(D_n + \frac{2T}{3n} D_T \right) \end{aligned} \quad (12)$$

Evaluating the integrals in Eq. (12) requires a model for the bounce-averaged particle orbits in EBT. For $\zeta^2 \leq 1/2$, we use the approximate result of Hedrick [5]:

$$\begin{aligned} \frac{\Omega}{\Omega_0} &\sim W_0 - W(1 - a\zeta^2) \\ \frac{v_y}{v_{y0}} &\sim \frac{v_{yE}}{v_{y0}} - W \left(1 + \frac{1}{2} \zeta^2 \right) \end{aligned} \quad (13)$$

where $a = 2.1$ and $v_{yE} = E_\theta / (B \sin \theta)$. The radial component of electric field E_r is determined self-consistently in the transport solution from quasi-charge neutrality $\Gamma_{er} \sim \Gamma_{ir}$. Likewise, the poloidal component E_θ should be computed self-consistently from the additional condition $n_e(r, \theta) \sim n_i(r, \theta)$. For simplicity, however, we choose an ad hoc value for E_θ such that $v_{yE}/v_{y0} = W_0$ [5]. This makes the displacement of the equipotential surfaces in the midplane the same as that of the contours of constant B [5], as approximately observed experimentally, and causes the $\vec{E} \times \vec{B}$ and vB drifts in Eq. (13) to be coincident at $\zeta = 0$. Hazeltine [6] chooses $E_\theta = 0$, hence finding larger transport rates than those given here. Only a self-consistent calculation of E_θ can clarify which, if either, of these approximations is valid. At present, E_θ must be regarded as a free parameter.

Using Eq. (13) with $v_{yE}/v_{y0} = W_0$ for the bounce-averaged drift orbits, Eq. (12) yields, for the plateau regime $\delta^{3/2} < v/\Omega_0 < 1$,

$$\begin{aligned} D_n &= \frac{3\pi}{8\sqrt{a}} \left(1 + \frac{1}{2a} \right)^2 \Omega_0 R_c^2 \delta^2 e^{-W_0} \\ D_T &= \frac{n}{T} D_n (1 + W_0) \end{aligned}$$

$$K_n = kTD_n \left(\frac{5}{2} + W_0 \right)$$

$$K_T = knD_n \left(5 + \frac{7}{2} W_0 + W_0^2 \right) \quad (14)$$

where μ_n and μ_T are given by the relations following Eq. (6). The result in Eq. (14) is independent of v and scales as δ^2 . Kovrizhnykh [7] obtained a similar result in 1970 for weakly ionized plasmas with small E_r and arbitrary E_θ .

In the crescent regime ($v/\Omega_0 \ll \delta^{3/2}$), the dominant transport losses come from a small region of velocity space near where $\Omega = 0$. Because of the structure which may develop in the distribution function near such regions, it is important to include the differential nature of the collision operator [6,9]. Also, the ordering which leads to Eq. (4) [i.e., $v_y/\Omega \sim 0(\delta)$] does not apply [6] because $v_y/\Omega_{\text{eff},b} \sim 0(\delta^{1/2})$. Derivations of neoclassical transport coefficients in the crescent regime are currently in progress [9].

At this point we differentiate between electron and ion transport in EBT. It has been noted experimentally [10] that the ambipolar electric field points radially inward in the bulk of the toroidal plasma. Thus, ions with thermal energies on the order of the electric potential energy can experience a cancellation of electric and magnetic drifts in the poloidal direction while electrons of comparable energy cannot. The resulting resonant (or small Ω) region for electrons occupies a much smaller fraction of velocity space and occurs at higher energies than it does for ions. We take advantage of this difference to simplify the transport model and assume that electron transport is dominated by particles with large Ω and nearly circular orbits. For convenience, we use the large electric field assumption of Kovrizhnykh [1] where $\Omega \sim \Omega_E \gg \Omega_0$ and hence retain for electrons the transport rates given by Eq. (6) and used in Ref. [2]. Although this assumption is clearly not accurate for electrons, it has been widely used [2,11] in the absence of more accurate nonresonant transport coefficients. In the case of ions, on the other hand, we make the opposite assumption, that transport is dominated by resonant particles with small Ω , and thus we use the resonant transport rates given in Eq. (14). In the present radial transport calculations for the toroidal core plasma in EBT, ion temperatures vary between 40 and 80 eV and thus lead to collision frequencies $0.3 < v/\Omega_0 < 1$. These correspond to the plateau regime of Eq. (14) rather than the crescent regime. Nevertheless, transport rates in the crescent regime may still be useful for ions in the region of the hot electron rings where magnetic field gradients are enhanced by the diamagnetic plasma current in the ring.

To compare resonant and nonresonant transport rates, we plot, in Fig. 1, the radial particle flux Γ_r from Eq. (5) vs ambipolar potential well depth ϕ_0 . Ad hoc parabolic profiles are assumed for n , T_e , T_i , and ϕ where $E = -\nabla\phi = 2r\phi_0/a^2$. Solid and dashed lines represent ion and electron fluxes Γ_{ir} and Γ_{er} , respectively, calculated at $r/a = 1/2$. Assumed densities and temperatures in Fig. 1(a) are $n \sim 2 \times 10^{12} \text{ cm}^{-3}$, $kT_i \sim 55 \text{ eV}$, and $kT_e \sim 150 \text{ eV}$ at $r = 0$ with $(v/\Omega_0)_e \sim 2.76$. These values correspond approximately to the collisional electron regime in Ref. [2], where transport solutions with negative electric fields are found.

Quasi-charge neutrality is achieved at potentials for which $\Gamma_{er} \sim \Gamma_{ir}$. In Fig. 1(a), this occurs for negative electric fields ($\phi_0 < 0$) when either Kovrizhnykh's coefficients in Eq. (6) or the resonant transport coefficients in Eq. (14) are used for the ions. However, the fluxes and potential well depth are enhanced when Eq. (14) is used.

In Fig. 1(b), the electron temperature on axis is increased to $kT_e \sim 300 \text{ eV}$, corresponding to $(v/\Omega_0)_e \sim 0.52$. This corresponds approximately to the collisionless electron regime in Ref. [2], where no negative field solutions are found. In this case, Fig. 1(b) shows that no negative field solutions

are possible when Kovrizhnykh's transport rates are used for the ions. However, solutions with $\Gamma_{er} \sim \Gamma_{ir}$ still persist with $\phi_0 < 0$ for ion fluxes calculated from Eq. (14). Figure 1 illustrates the basic premise on which the transport calculations in this paper are based. That is, enhanced ion transport due to cancellation of poloidal drifts can enhance the radially inward pointing electric field in the toroidal core plasma in EBT. This, in turn, extends the region in which negative electric field solutions exist to include the collisionless regime for electron transport, as observed in the experiment [4].

3. SOLUTION OF THE RADIAL TRANSPORT PROBLEM

In this section, we extend the radial transport calculations of Ref. [2] to include effects of enhanced ion diffusion as discussed in Section 2. The transport equations can be derived [2] as a series of moments of Eq. (1). Including the radial component of Ampere's law averaged over poloidal angle, we have [2]

$$\begin{aligned} \frac{\partial n}{\partial t} &= n_0 \langle \sigma v \rangle_i n - \frac{1}{r} \frac{\partial}{\partial r} (r \Gamma_r) \\ \frac{\partial}{\partial t} \left(\frac{3}{2} n k T_i \right) &= Q_{ei} - \frac{1}{r} \frac{\partial}{\partial r} (r Q_{ir}) - n_0 \langle \sigma v \rangle_{cx} \frac{3}{2} n k (T_i - T_0) + e \Gamma_{ir} E_r + n_0 \langle \sigma v \rangle_i \frac{3}{2} n k T_0 \\ \frac{\partial}{\partial t} \left(\frac{3}{2} n k T_e \right) &= 2 m_e n \langle D_\mu \rangle - \frac{1}{r} \frac{\partial}{\partial r} (r Q_{er}) - Q_{ei} - n_0 \langle \sigma v \rangle_i n E_I - e \Gamma_{er} E_r \\ \frac{\epsilon_1}{e} \frac{\partial E_r}{\partial t} &= \Gamma_{er} - \Gamma_{ir} = (D_{ni} - D_{ne}) \frac{\partial n}{\partial r} + D_{Ti} \frac{\partial T_i}{\partial r} - D_{Te} \frac{\partial T_e}{\partial r} - n (\mu_{ni} - \mu_{ne}) E_r \end{aligned} \quad (15)$$

where r is the radial coordinate measured in a mirror midplane, t is time, $n \equiv n_e \sim n_i$, $\Gamma_r \equiv \Gamma_{er} \sim \Gamma_{ir}$, k is Boltzmann's constant, E_I is the ionization energy of atomic hydrogen, ϵ_1 is the perpendicular plasma dielectric, and Q_{ei} is the energy exchange rate between electrons and ions. Ionization and charge exchange rates are $n_0 \langle \sigma v \rangle_i$ and $n_0 \langle \sigma v \rangle_{cx}$, respectively. Resonant electrons absorb microwave power at the rate [12] $2 m_e n \langle D_\mu \rangle$. We assume that neutral density n_0 and temperature T_0 adjust instantly to changes in plasma parameters, allowing a conventional solution of a stationary kinetic equation for the neutral velocity distribution [13].

For two different neutral boundary conditions, Fig. 2 shows time-dependent solutions to Eq. (15) with the plateau transport rates of Eq. (14) applied to ions and Kovrizhnykh's transport rates [Eq. (6)] applied to electrons. The case shown is for 24 mirror sectors with plasma radius $a = 10$ cm, major radius $R_T = 150$ cm, bounce-averaged magnetic field on axis $B_0 = 6.4$ kG, and total microwave power absorbed in the toroidal plasma $P_\mu = 6.0$ kW, with a time-independent, spatially uniform power deposition profile. The energy of cold neutrals is $E_0 = 0.5$ eV. At the edge, $r = a$, plasma density and temperature are fixed at $n = 3 \times 10^{10}$ cm $^{-3}$, $T_e = T_i = 13.5$ eV, and the magnetic field gradient corresponds to an electron ring beta $\beta_a = 37\%$ [see Eq. (21), Ref. [2]]. Plotted in Fig. 2 are radial profiles of plasma density n , ambipolar potential ϕ , and ion and electron temperature kT_i and kT_e , respectively, at time intervals of 4 msec as the time-dependent calculation proceeds from the initial parabolic profiles at $t = 0$ sec. Here, the negative electric field (potential well) is maintained as the electrons penetrate deeply into the collisionless regime. This confirms our hypothesis from Fig. 1 that enhanced ion losses do, in fact, allow negative electric fields in the presence of collisionless electrons.

In Fig. 2(a) the flux of cold neutrals at the plasma edge is assumed to be determined by the toroidal plasma through instantaneous reflux of plasma particles at the wall. In this approximation the total number of plasma particles remains constant in time. In the collisionless electron regime, energy containment time increases with electron temperature, and for a constant total number of particles, there is a net positive feedback, causing electron temperature to become arbitrarily large. Steady-state solutions do not exist.

In Fig. 2(b) the flux of cold neutrals at the plasma edge is assumed constant independent of toroidal plasma parameters. Such a boundary condition is appropriate if reflux from the wall occurs on a time scale that is slow compared to the energy containment time. As the temperature and lifetime increase, so does the total number of particles, thus reducing the power deposited per particle. This provides a negative feedback mechanism that limits the thermal excursion and yields thermally stable results in the regime of the experiment, i.e., collisionless electrons with negative electric fields [14].

Experiments [4] indicate that a time on the order of tens of minutes is required for the plasma to reach equilibrium with the wall. This, along with the fact that neutral pressure is held fixed during experiments, suggests that the boundary condition used in Fig. 2(b) is the one appropriate for comparison with experiment.

The stability result in Fig. 2(b) is not dependent on the assumption of a time-independent, spatially uniform microwave heating profile. Similar results have been obtained with heating profiles proportional to density in both space and time. Also, similar stable, steady-state solutions have been obtained for high density, high power plasmas as required in proof-of-principle experiments.

Next we consider scaling of the numerical results with microwave power and edge neutral pressure. In Fig. 3 the steady-state product of electron temperature T_e and energy confinement time τ_E is plotted vs electron collisionality $(\nu/\Omega_0)_e$ at $r = 0$. Open circles represent stable, steady-state solutions to Eq. (15) with constant edge neutral flux as in Fig. 2(b). Ion transport rates from the plateau result of Eq. (14) and electron transport rates from the large electric field result of Eq. (6) are assumed. Results shown are obtained by varying the absorbed microwave power between 6 and 10 kW and the edge neutral pressure between 3×10^{-7} and 1.8×10^{-6} Torr. In all cases in Fig. 3 the shape of the potential is such as to produce a negative or radially inward pointing electric field. In the figure, thermally stable, steady-state solutions occur with $T_e \tau_E \propto (\nu/\Omega_0)_e^{-1}$ or $\tau_E \propto T_e^{3/2}$, which is characteristic of the collisionless electron regime in EBT. A similar result is shown in Fig. 34 of Ref. [4] for the EBT experiment. Comparison between theory and experiment shows very nearly the same range of electron collisionality $(\nu/\Omega_0)_e$ and nearly the same absolute magnitude of the product $T_e \tau_E$. Also, in the collisionless electron regime of Fig. 3, density, temperature, potential, and lifetime all increase with decreasing neutral pressure [14], as observed experimentally [4].

4. CONCLUSION

Radial transport calculations reported here extend results of earlier models [2] to include resonant diffusion of ions in regions where poloidal drift frequencies are small [3,5,6,7]. The effect of resonant ion transport is to broaden the region in which negative electric field solutions are possible and to make the collisionless electron regime $\tau_E \propto T_e^{3/2}$ of the experiment accessible, for the first time, to 1-D radial transport calculations. Transport solutions in this collisionless electron regime are thermally stable when the edge neutral pressure is fixed as in experiments. These calculations represent an additional step in a complete neoclassical description of radial transport in EBT. A more accurate description must include the effects of finite radial electric fields ($\Omega_E \sim \Omega_0$) on electron transport coefficients and the effects of self-consistent poloidal electric fields (E_θ) on ion transport coefficients.

ACKNOWLEDGMENTS

The authors thank W. B. Ard, G. R. Haste, R. A. Dandl, N. H. Lazar, G. E. Guest, K. T. Tsang, J. D. Callen, S. P. Hirshman, N. A. Krall, and J. B. McBride for helpful discussions and suggestions. This research was sponsored by the Office of Fusion Energy, U.S. Department of Energy under contract W-7405-eng-26 with the Union Carbide Corporation.

REFERENCES

- [1] KOVRIZHNYKH, L. M., Sov. Phys.-JETP 29 (1969) 475.
- [2] JAEGER, E. F., HEDRICK, C. L., Nucl. Fusion 19 (1979) 443.
- [3] JAEGER, E. F., SPONG, D. A., HEDRICK, C. L., Phys. Rev. Lett. 40 (1978) 866.
- [4] EBT Experimental Group, Oak Ridge National Laboratory Report ORNL/TM-6457 (1978) (submitted to Nucl. Fusion).
- [5] HEDRICK, C. L., SPONG, D. A., JAEGER, E. F., "Banana Transport in EBT," paper presented at the Annual Controlled Fusion Theory Conference, Gatlinburg, Tennessee, April 1978; HEDRICK, C. L., SPONG, D. A., OWEN, L. W., Bull. Am. Phys. Soc. 23 (1978) 876, Abstracts 8P1, 2, 3.
- [6] HAZELTINE, R. D., KRALL, N. A., Science Applications Inc. Report SAI-78-855-LJ/LAPS 44 (1978); HAZELTINE, R. D., KRALL, N. A., KLEIN, H. H., CATTO, P. J., Science Applications Inc. Report SAI02379-664LJ/LAPS49 (1979) (Submitted to Nucl. Fusion).
- [7] KOVRIZHNYKH, L. M., International Center for Plasma Physics Reports IC/70/86, IC/70/123, and IC/70/124 (September 1970); Atomic Energy Commission Reports AEC-tr-7274, AEC-tr-7284.
- [8] CALLEN, J. D., HEDRICK, C. L., "Direct Particle Losses in the ELMO Bumpy Torus," paper presented at the Annual Controlled Fusion Theory Conference, Gatlinburg, Tennessee, April 1978.
- [9] TSANG, K. T., CALLEN, J. D., HEDRICK, C. L., HIRSHMANN, S. P., SPONG, D. A., "Crescent Shape Orbit Diffusion in EBT" and CATTO, P. J., ROSENBLUTH, M. N., TSANG, K. T., "A Transport Estimate of EBT in the Banana Regime," papers presented at the Annual Controlled Fusion Theory Conference, Mount Pocono, Pennsylvania, April 1979.
- [10] COLESTOCK, P. L., CONNOR, K. A., HICHOK, R. L., DANDL, R. A., Phys. Rev. Lett. 40 (1978) 1717.
- [11] HEDRICK, C. L., JAEGER, E. F., SPONG, D. A., GUEST, G. E., KRALL, N. A., McBRIDE, J. B., STUART, G. W., Nucl. Fusion 17 (1977) 1237; McBRIDE, J. B., SULTON, A. L., Nucl. Fusion 18 (1978) 285.
- [12] ELDRIDGE, O., Phys. Fluids 15 (1972) 676.
- [13] BURRELL, K. H., J. Comp. Phys. 27 (1978) 88.
- [14] JAEGER, E. F., HEDRICK, C. L., ARD, W. B., "Radial Transport in the ELMO Bumpy Torus with Constant Edge Neutral Flux" (to be published in Phys. Rev. Lett.).

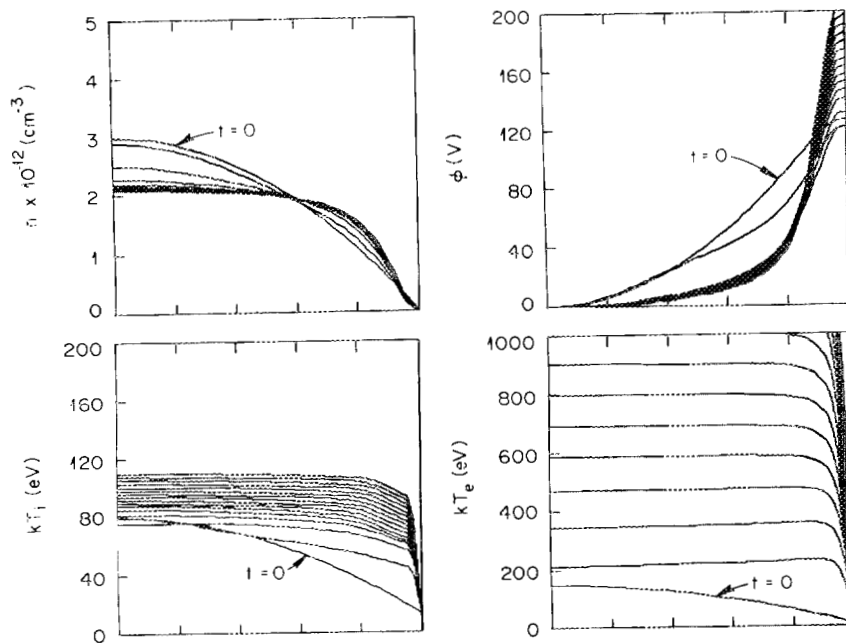
FIGURE CAPTIONS

FIG. 1. Electron (dashed) and ion (solid) particle flux Γ vs potential well depth ϕ_0 for resonant and nonresonant diffusion coefficients. Electron temperatures are in the (a) collisional and (b) collisionless regimes.

FIG. 2. Plasma profiles at time intervals $\Delta t = 4$ msec for two neutral boundary conditions: (a) constant total number of plasma particles; (b) constant flux of cold neutrals at the plasma edge.

FIG. 3. Confinement scaling with collisionality. The points represent thermally stable, steady-state solutions to Eq. (15) for resonant ion diffusion broadened by collisions [(Eq. (14))].

(a) CONSTANT TOTAL NUMBER OF PLASMA PARTICLES



(b) CONSTANT FLUX OF COLD NEUTRALS AT PLASMA EDGE

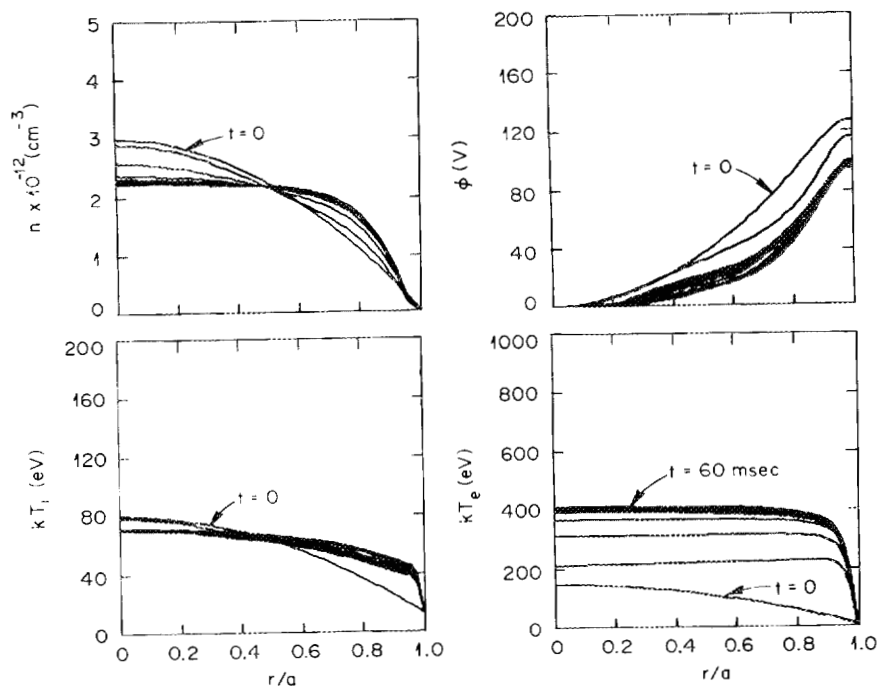


Fig. 2.

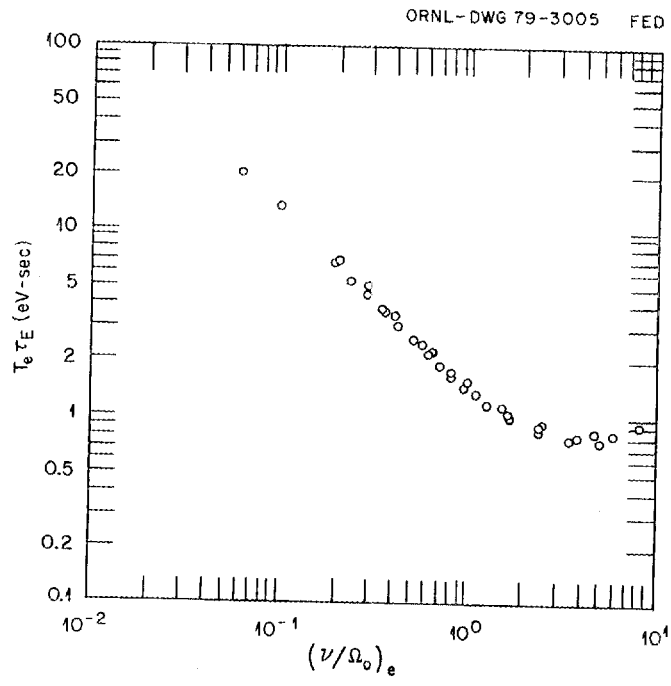


Fig. 3.

A.3 RELATIVISTIC ELECTRON RINGS

An essential feature of EBT is the presence of a relativistic electron annulus in each of the toroidal mirror sectors. These high beta annuli are formed and sustained by microwave heating and are of sufficient density and temperature for diamagnetic currents to produce the necessary minimum in the magnetic field required for the MHD stability of the toroidal core plasma. The stability of the electron ring itself requires the presence of an appreciable cold electron density component, $n_{\text{cold}}/n_{\text{hot}} > 1$.¹

Because electron rings play an important role in the confinement characteristics and performance of EBT, the tradeoff between the quality of the confinement afforded by the rings and the power required to sustain them represents an important physics question for EBT-P.

A.3.1 DRAG COOLING OF THE RELATIVISTIC ELECTRON ANNULUS

Recent studies of the ring power balance² in EBT-I have indicated that the energy transfer between the relativistic annulus electrons and the core electrons via Coulomb collisions (drag cooling) is the dominant loss mechanism. Experimental measurements of the annulus decay time³ are within a factor of ~ 2 of the theoretical drag time, indicating the importance of this loss mechanism in future EBT devices.

A lower limit of the microwave power required to sustain the annulus against drag cooling can be obtained from the binary collision model of Kamnash and Galbraith,^{4,5} which describes the slowing down of relativistic electrons in a Maxwellian plasma. The rate of energy loss for relativistic test electrons of energy E in a plasma is given by the following equation in cgs units:

$$\frac{dE}{dt} \approx \frac{4\pi n_{ep} e^4}{m_e c} \frac{\gamma^2}{\sqrt{\gamma^2 - 1}} \ln \left(\frac{T_{iw_{pe}}}{kT_{ep}} \right), \quad (\text{A.3.1})$$

where m_e is the electron rest mass and $\gamma = 1/\sqrt{1 - v^2/c^2}$ is the relativistic mass ratio. The argument of the logarithmic term differs from the usual Coulomb logarithm ($\ln \Lambda$) and can be obtained by using the quantum-mechanical minimum impact parameter for electrons incident on electrons.⁶ The parameters n_{ep} and T_{ep} represent the density and temperature of the toroidal core electrons, and ω_{pe} is the core electron plasma frequency. In mks units with T in keV, Eq. (A.3.1) can be written as

$$\frac{dE}{dt} \left(\frac{\text{W}}{\text{electron}} \right) \approx 4 \times 10^{-32} \frac{\gamma^2}{\sqrt{\gamma^2 - 1}} n_{ep}. \quad (\text{A.3.2})$$

Here the value of the natural logarithmic term has been fixed at 32.5, which is characteristic of anticipated EBT-P parameters. If there is a total of $n_A V_A N$ relativistic electrons, the microwave power level required to compensate for drag losses is given by

$$P_{\text{drag}}(\text{W}) \approx \left(4 \times 10^{-32} \frac{\gamma^2}{\sqrt{\gamma^2 - 1}} n_A n_{ep} \right) V_A N. \quad (\text{A.3.3})$$

The dependence of the drag losses on both the core and annulus densities and the ring plasma volume and the importance of the relativistic term $\gamma^2/\sqrt{\gamma^2 - 1}$ are apparent. A comprehensive experimental examination of the annulus stability boundaries is planned for EBT-S and will help to establish the acceptable range for the ratio of cold-to-hot plasma density required for ring stabilization. By defining a ring stability ratio as

$$f_R \equiv \frac{n_{\text{cold}}}{n_{\text{hot}}} \approx \frac{n_{\text{ep}}}{n_A},$$

one can write the following compact expression for the drag power loss:

$$P_{\text{drag}}(\text{W}) = \left(4 \times 10^{-32} f_R \frac{\gamma^2}{\sqrt{\gamma^2 - 1}} n_A^2 \right) V_A N. \quad (\text{A.3.4})$$

Projected values of f_R for Phases I and II are in the range of 5-10.¹

A.3.2 ANNULUS MICROWAVE POWER SCALING

Because the core-stabilizing electron annulus must be continuously driven by the microwave sources during steady-state operation, the question of power drain from the annulus is extremely important in scaling the microwave power requirements. In its most basic form the annulus power balance is given by

$$P_{\mu A} = P_{\text{synch}} + P_{\text{brems}} + P_{\text{scatt}} + P_{\text{drag}}, \quad (\text{A.3.5})$$

where P_{synch} and P_{brems} represent power lost by synchrotron and bremsstrahlung radiation, P_{scatt} is the scattering loss due to annulus electron-electron Coulomb collisions, P_{drag} represents the power lost from the relativistic electrons due to drag on the toroidal core electrons, and $P_{\mu A}$ is the microwave power required to sustain the annulus. In terms of plasma and machine parameters, Eq. (A.3.5) can be expressed in mks units as follows:

$$P_{\mu A}(\text{W}) = \underbrace{\left[6.2 \times 10^{-17} B_A^2 n_A T_A \left(1 + \frac{T_A}{204} \right) \right]}_{P_{\text{synch}}} + \underbrace{\left[5.35 \times 10^{-37} n_A^2 T_A^{1/2} \right]}_{P_{\text{brems}}} + \underbrace{\left[2.2 \times 10^{-32} \frac{n_A^2 \ln \lambda_{ee}}{T_A^{1/2}} \right]}_{P_{\text{scatt}}} + \underbrace{\left[4.0 \times 10^{-32} \frac{\gamma^2}{\sqrt{\gamma^2 - 1}} n_A n_{\text{ep}} \right]}_{P_{\text{drag}}} V_A N, \quad (\text{A.3.6})$$

where T_A is the keV, B_A is the magnetic field strength in the vicinity of the annulus, $\ln \lambda_{ee} = 24 - \ln(\sqrt{10^{-6} n_A / 10^3 T_A})$, $\gamma = 1 + T_A/511$, and $V_A N$ is the total annulus volume (where N is the total number of mirror sectors).

Confidence in the predicted value of $P_{\mu A}$ depends, however, on an accurate measurement of the total annulus volume $V_A N$, which at present is still a vague quantity. Based on experimental measurements^{7,8} and theoretical estimates, it appears that a range exists for the annulus thickness δ_A , which varies between a minimum of the relativistic electron gyrodiameter and a maximum value of $\sim 3-4$ cm as measured on ELMO.⁹ A general expression for the annulus volume per sector is given by

$$V_A \approx 2\pi a_p \cdot \delta_A \cdot L_A = 2.15 \times 10^{-2} \frac{\sqrt{\gamma^2 - 1}}{B_A} f_E \cdot a_p \cdot L_A, \quad (\text{A.3.7})$$

where f_E is a thickness enhancement factor, which allows for annuli thicknesses larger than the diameter of a relativistic electron orbit. For EBT-I, $f_E \approx 3.0$, giving an annulus thickness $\delta_A \approx 2.5$ cm. A three-gyrodiameter annulus thickness also appears to provide good agreement with ELMO annulus measurements.

A.3.3 SCALING PROJECTIONS FOR EBT-P

Reasonably good agreement between the experimental and theoretical estimates of $P_{\mu A}$ for EBT-I provides a level of confidence in the predicted annulus power requirements for EBT-P. Such an assessment is necessary for EBT-P and future machines. In the near term, it can provide valuable sizing information pertaining to the fraction of the system power necessary to drive the microwave sources. Such information will benefit the ongoing development program for millimeter wavelength, cw microwave sources by ensuring tube procurement at sufficiently high power levels. On the longer time scales envisioned for a reactor (EBTR), the continuous microwave power required to sustain the annulus during steady-state operation may become the determining factor for overall reactor efficiency. This is to be expected because following ignition, the bulk heating (either ECH or neutral beams) will be terminated and the plasma temperature maintained by alpha particle heating and collisional energy gains from the annulus.

Anticipating enhanced drag cooling in EBT-P, scaling curves have been devised for both the Phase I and Phase II operating modes. These curves enable us to determine the microwave power required to sustain the rings at a given annular beta for increasing levels of core plasma density. Figures A.3.1 and A.3.2 are based on the annulus power balance given by Eq. (A.3.6) and assume the following parameters: $n_A = 0.2 n_{ep} = 2 \times 10^{18} \text{ m}^{-3}$, $N = 36$ (Phase I), $n_A = 0.1 n_{ep} = 5 \times 10^{18} \text{ m}^{-3}$, $N = 48$ (Phase II), and $B_A = 1.97 \text{ T}$ for $f_{\mu} = 55 \text{ GHz}$.

Figure A.3.1 illustrates the scaling projections for Phase I operation with the various loss mechanisms appropriately identified. For each figure two sets of total loss curves are shown for comparison, one utilizing the binary collision model for drag cooling^{4,5} and the other using the classical expression for collisional losses.⁶ Bremsstrahlung radiation is smaller than the least of the above losses by better than two orders of magnitude and is therefore neglected.

The total loss rate is found to have a minimum that is bounded by collisional drag and synchrotron radiation losses. Drag dominates over a significant portion of the energy range and is large for small velocities, decreasing as $\sim 1/v$ until v is comparable to c . At these high energies the binary collision model shows a strong dependence on the relativistic term $\gamma^2/\sqrt{\gamma^2 - 1}$, which scales like γ for very relativistic electrons. In comparison, classical drag loss reaches a minimum when the kinetic energy of the electron is of the order of its rest mass. It then increases logarithmically.

Accelerated ring cooling occurs at high energies due to synchrotron radiation.¹⁰ This mechanism can produce losses comparable to drag, provided the magnetic fields are large and annulus temperatures are $\geq 1 \text{ MeV}$. For a fixed input power level, this additional deterioration in the annulus energy confinement time can further limit the maximum core density, which can be maintained without causing excessive cooling and possible disruptions of the annulus.

Also shown in Fig. A.3.1 is the correlation between values of annular beta and the various modes of operation observed in the EBT device. The region to the left of the cross-hatched portion of the curve corresponds to the cold, noisy C-mode of operation observed when insufficient microwave power is supplied to produce substantial annular beta. At $\beta_A \geq \beta_{\text{crit}}^A$ ($\approx 5\text{-}10\%$ in EBT-I), there is a transition from this C-mode to the quiet, macrostable T-mode, which possesses an appreciable core plasma. By delineating the unfavorable modes of operation from the desired T-mode, Fig. A.3.1 can be used to predict the microwave power level required for credible regions of annulus parameter space and a desired set of core parameters.

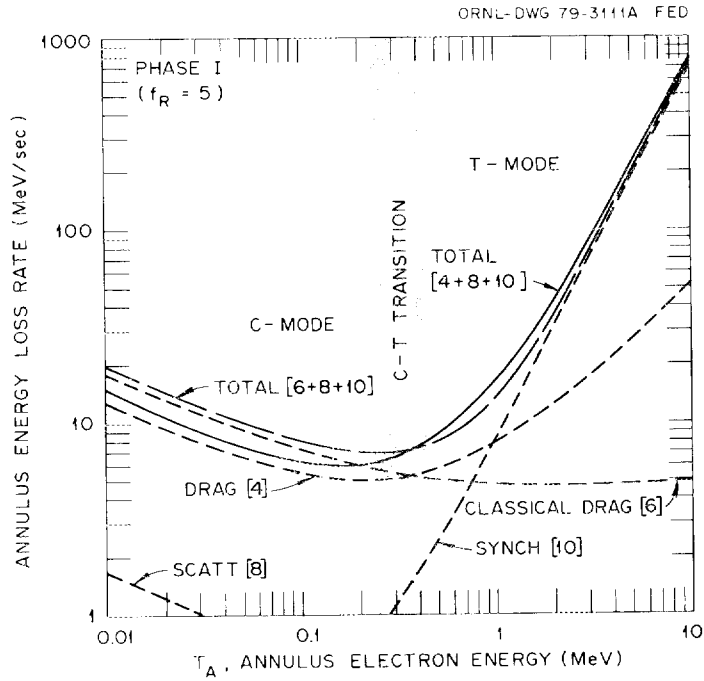


Fig. A.3.1. Annulus energy loss rate vs T_A for EBT-P.

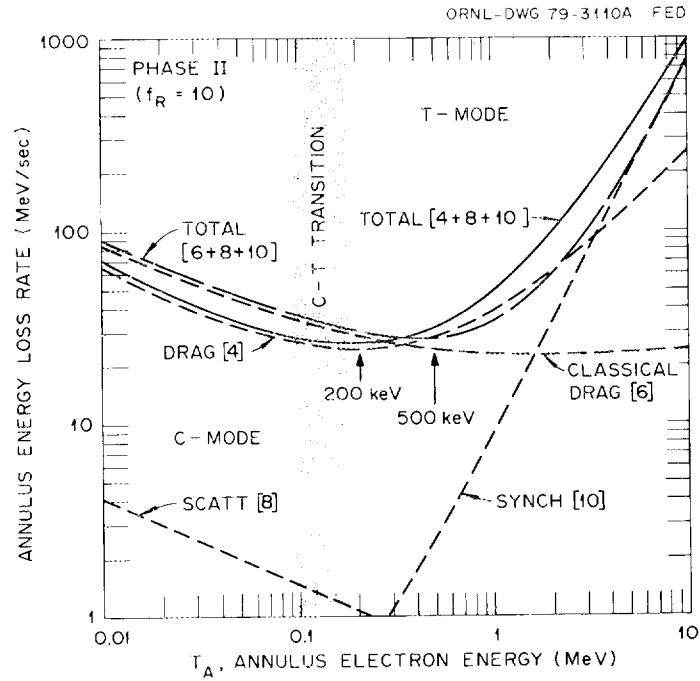


Fig. A.3.2. Annulus energy loss rate vs T_A for EBT-P.

In the transition from Phase I to Phase II operation, improved core performance and machine characteristics are expected to lead to further growth in the annulus power requirements. This increase is the result of the linear dependence of the drag losses on the core density and the larger number of sectors. A comparison of Figs. A.3.1 and A.3.2 also indicates that the variation between the total loss and drag cooling curves becomes less pronounced in going to Phase II. This is expected, however, because at high core densities, drag losses completely dominate the annulus power balance over the energy range of interest and the two curves begin to coalesce.

The results shown in Figs. A.3.1 and A.3.2 indicate that a range of annular beta values between 15-30% is achievable for projected EBT-P core plasma parameters. Using Eq. (A.3.7) for the annulus volume per sector, the required microwave power levels are in the range of ~ 300 -650 kW for the specified Phase I parameters and ~ 1.6 -2.2 MW for the Phase II parameter range. The sensitivity of these results to the uncertainties and limitations of the models used here is presently under investigation.

REFERENCES

1. R. R. Dominguez and H. L. Berk, *Phys. Fluids* 21, 827 (1978); D. B. Nelson and C. L. Hedrick, *Nucl. Fusion* 19, 283 (1979).
2. S. K. Borowski, N. A. Uckan, E. F. Jaeger, and T. Kammash, Oak Ridge National Laboratory Report ORNL/TM-6910, Oak Ridge, Tennessee (1979).
3. R. A. Dandl et al., Oak Ridge National Laboratory Report ORNL/TM-6457, Oak Ridge, Tennessee (1978).
4. T. Kammash and D. L. Galbraith, *Nucl. Fusion* 13, 464 (1973).
5. T. Kammash, *Fusion Reactor Physics - Principles and Technology*, p. 131, Ann Arbor Science Publishers, Ann Arbor, 1975.
6. J. D. Jackson, *Classical Electrodynamics*, 2nd ed., p. 618, John Wiley and Sons, Inc., New York, 1975.
7. R. A. Dandl et al., Oak Ridge National Laboratory Report ORNL/TM-6457, Oak Ridge, Tennessee (1978); R. A. Dandl et al., Oak Ridge National Laboratory Report ORNL/TM-4941, Oak Ridge, Tennessee (1975).
8. R. A. Dandl et al., Oak Ridge National Laboratory Report ORNL/TM-3694, Oak Ridge, Tennessee (1971).
9. W. B. Ard et al., Oak Ridge National Laboratory Report ORNL/TM-4510, Oak Ridge, Tennessee (1967).
10. D. J. Rose and M. Clark, Jr., *Plasmas and Controlled Fusion*, p. 251, The M.I.T. Press, Massachusetts Institute of Technology, Cambridge, 1961.

A.4. MAGNETICS DESIGN

This section includes a detailed discussion of the theory supporting the design of the mirror coils, the global field error correction coils, and design considerations for superconducting coils.

A.4.1 MIRROR COILS

A major goal of the EBT-P experiment is to study confinement and scaling in reactor-like plasmas. Proof-of-principle (POP) requires that EBT-P attain an order of magnitude or more increase in density, temperature, and confinement time over EBT-S. This goal can be realized only if the magnetics system is designed for the required plasma size and magnetic field strength B . Specifically, in the microwave-heated EBT plasma, density scales as B^2 ; therefore, an order of magnitude increase in density requires a factor of 3-4 increase in B . In order that direct particle losses not exceed those in EBT-S, the vacuum field single-particle confinement properties of EBT-P should compare favorably with EBT-S. Charge exchange losses scale as a^{-1} (a is the plasma minor radius), so the plasma radius in the coil throat should be greater than or equal to the radius in EBT-S. In addition, because neoclassical diffusive losses scale as A^{-2} (A is the aspect ratio), a significant aspect ratio scaling test requires that A for EBT-P be larger than that for EBT-S. Clearly, POP requires an EBT-P magnetics design that is a significant scale-up from EBT-S.

The first question to be addressed concerns the use of copper or superconducting mirror coils. An order of magnitude increase in B can be obtained with a "photographic enlargement" of EBT-S by a factor of $\sqrt{10}$, giving a 24-sector device with a major radius of 4.74 m and a resonant magnetic field of 3.16 T. Single-particle confinement and aspect ratio are the same as for EBT-S. However, the power dissipated in the magnets P_c is proportional to the volume (or B^3) for fixed current density, giving $P_c = 10^{3/2} \times 10 \text{ MW} = 316 \text{ MW}$. This steady-state power requirement could be reduced somewhat by making the coils larger and decreasing the current density, but only at the expense of degrading single-particle confinement. On the other hand, the coil radius and therefore the volume could be made smaller by increasing the number of coils (or aspect ratio) to maintain particle confinement. Either alternative requires 200-300 MW of steady-state power, leading to the conclusion that POP is difficult without superconducting coils.

The design of the next step in the EBT device sequence began with the EBT-II conceptual design study,¹ which was intended as a preproposal design guide. A device having 48 superconducting coils, a major radius of 5.2 m, a resonant magnetic field of 4.2 T, and $A = 20$ resulted from that study. Without ARE coils, the confinement of high energy passing particles was poorer than that in EBT-S. In addition, any significant increase in the thickness of the dewar or x-ray shield necessitated by engineering design considerations would have seriously degraded even further the confinement of transitional and passing particles. These issues have led us to focus in the present design on devices with somewhat larger mirror coils and fewer sectors. The increased coil radius makes the design less sensitive to changes in the dewar and shield thickness and reduces charge exchange losses by permitting a larger plasma radius. To keep the cost down, the number of sectors in the basic machine is reduced to 36. The engineering design permits the flexibility of upgrading to 48 sectors and adding ARE coils to give better performance. The confinement of transitional and passing particles in the basic 36-sector EBT-P is distinctly superior to that in the EBT-II design.

Particle drift orbit calculations show that single-particle confinement in EBT is sensitive to the mirror ratio M of the device. As M is increased, single-particle confinement improves, but the midplane (and resonant) magnetic field decreases for fixed current density in the mirror coils. Figure A.4.1 shows the maximum attainable magnetic field on axis in the midplane as a function of mirror ratio for NbTi superconducting magnets. An upper limit of 8 T at the windings permits a maximum field on axis in

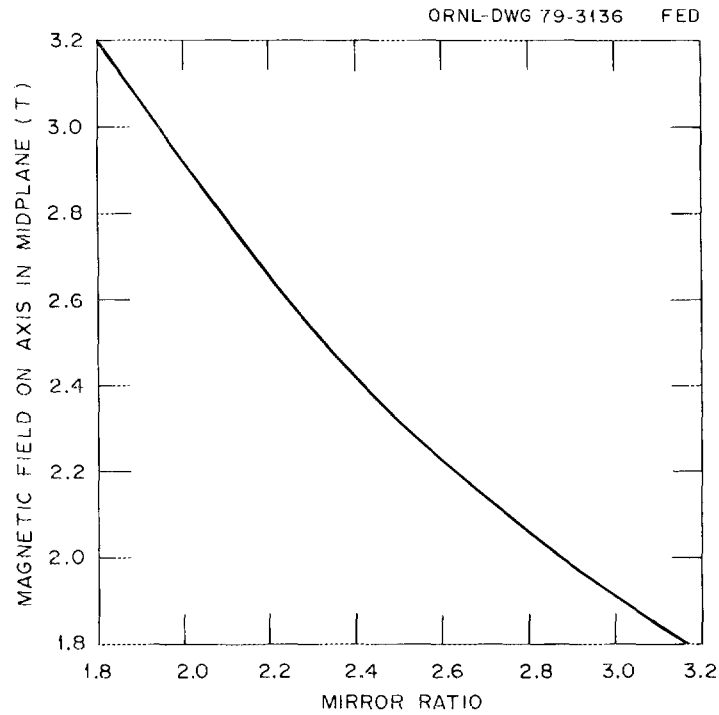


Fig. A.4.1. Maximum magnetic field on axis in the midplane as a function of mirror ratio for NbTi superconducting magnets. An upper limit of 8 T at the windings permits a maximum field on axis in the coil throat of about 6 T.

the coil throat of ~ 6 T; this is held fixed as the mirror ratio is changed. This curve, showing the M^{-1} variation of the field in the midplane, is almost independent of the method by which the mirror ratio is varied.

The flexibility of studying confinement for different mirror ratios in EBT-P is permitted by adding a trim coil just outside of and concentric with each main mirror coil (see Fig. A.7.1 of Sect. A.7.1). The mirror ratio of EBT-P with no current in the trim coils is $M = 2.28$. The trim coil current can aid or oppose that in the main mirror coils, making it possible to span a broad range of mirror ratio (limited only by available microwave frequencies). With EBT-P it will be possible to study annulus formation in high mirror ratio fields. In addition, the effects on particle and energy confinement of varying the magnetic aspect ratio R_T/R_B , where R_T is the major radius and $R_B = (d \log B/dr)^{-1}$, can be studied by changing the mirror ratio and hence R_B .

The toroidal curvature of the magnetic field in EBT results in an inward shift of particle drift orbits from the minor axis toward the major axis of the torus. This shift is largest for the transitional and passing particles, i.e., those having a large component of velocity parallel to the magnetic field. This dispersion of particle drift orbits plays a major role in diffusive and direct particle losses in EBT. The EBT-P magnetics design presented here is based on optimizing single-particle confinement in the vacuum magnetic field subject to the constraints on cost, NbTi superconducting magnet technology, and engineering design considerations. Finite beta and ambipolar electric fields play a major role in particle and energy confinement in EBT, but it is not practical or necessary to include these effects at the machine design level. The role played by these plasma-induced fields in single-particle confinement is well known,² and there is no reason to believe that this will change appreciably in EBT-P.

To carry out a detailed evaluation of particle drift orbits, it is convenient to introduce the longitudinal invariant J

$$J = \oint v_{\parallel} d\ell ,$$

where $1/2 m v_{\parallel}^2 = E - \mu B$ in the absence of electric fields. E is the total energy, μ is the magnetic moment, and $d\ell$ is the arc length along the field line. The integration is over a complete period of the particle motion. Because E , μ , and J are conserved quantities (adiabatically), the particle must lie on a surface of constant J for fixed E and μ . Particle drift surfaces may be determined by calculating J on a grid in the midplane for fixed E and μ and plotting contours of constant J . On the other hand, one can determine just the radial extent of the drift orbit along the line of intersection of the midplane and equatorial plane by plotting J as a function of radius along this line. A typical $J(r)$ curve is illustrated in Fig. A.4.2. The radial extent of particle drift orbits in the equatorial plane as a function of r can be ascertained by superimposing level lines on the $J(r)$ curve. The particular drift orbit having the maximum inward shift for a given E and μ is determined by the position $R(J_{\text{MIN}})$ of the minimum in J . In Fig. A.4.2 this maximum shift is plotted as a function of mirror ratio for passing particles ($v_{\parallel}/V = 1.0$). The mirror ratio is varied by changing the currents in the inner and outer mirror coil windings. Improved centering of the passing particle drift orbits is evident as the mirror ratio is increased; similar improvements obtain for other pitch angles.

A sensitive measure of direct particle losses is afforded by the volumetric efficiency, defined in Fig. A.4.3. The last closed drift orbit is the largest surface of constant J that is contained within the "limiter," taken to be a circle in the midplane centered on the minor axis. The radius of the circle is the minor radius in the midplane of that equatorial plane flux line that just grazes the dewar throat on the inside of the torus. The volumetric efficiency is a sensitive function not only of the inward shift of the last closed drift orbit in the chamber but also of the limiter radius. The $J(r)$

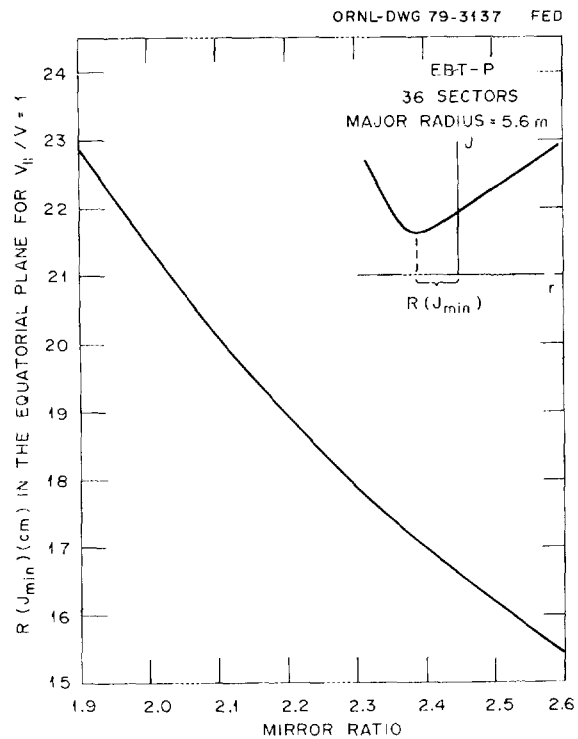


Fig. A.4.2. The maximum inward shift of passing particle ($V_{||}/V = 1.0$) drift orbits from the minor axis of the torus is plotted as a function of mirror ratio, which is varied by changing the currents in the inner and outer mirror coil windings.

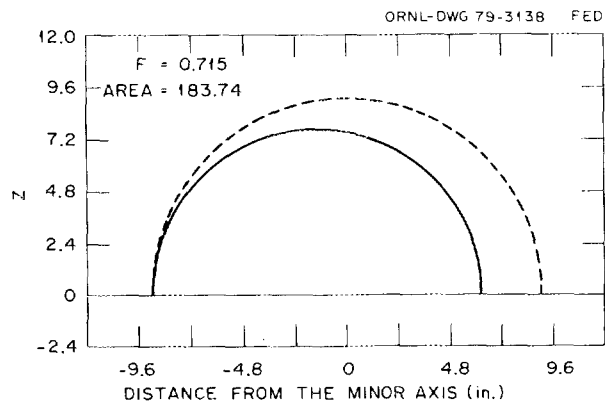


Fig. A.4.3. Last closed drift orbit in the midplane (solid curve) that does not intercept the limiter (dashed curve). The limiter is defined by projecting the inside of the dewar throat along flux lines to the midplane.

curve in Fig. A.4.2 illustrates this point. The toroidal curvature of the magnetic field causes the slope of the $J(r)$ curve to be steeper on the inside of the torus than on the outside; hence, a small change in the clear bore or limiter radius can result in a large change in volumetric efficiency.

In Fig. A.4.4 the volumetric efficiency for the 36-sector EBT-P is plotted as a function of the cosine of the pitch angle for three values of mirror ratio. Two effects lead to the observed improvement in volumetric efficiency as M is increased: better centering of drift orbits and the larger limiter radius that results from increased field line curvature. Note that as the mirror ratio increases, there is a marked improvement in passing particle confinement, a significant decrease in the width of the velocity space loss cone near $V_{\parallel}/V = 0.8$, and a better centering of the mod B surfaces near the midplane ($V_{\parallel}/V = 0$), where the annuli form. The mirror ratio variation in this case is obtained by an aiding current in the outer trim coils. As this current is increased, the current in the inner windings is decreased so as not to exceed the 8-T limit on the field strength at the inner conductor windings.

Volumetric efficiency curves for the 48-sector upgrade of EBT-P are shown in Fig. A.4.5. In this device with no current in the trim coils, the mirror ratio is 2.14. The $M = 1.98$ curve is obtained with the current in the trim coils in the same direction as that in the inner coils, and the $M = 2.42$ curve is obtained with the trim coil current opposing, or in the opposite direction to, that in the main mirror coils.

The EBT-P magnetics design presented here has good single-particle confinement, will satisfy proof-of-principle requirements, has a high degree of flexibility for plasma physics experiments and for later upgrading to a larger device with ARE coils, and will be a significant test of the technology that will be required in the magnetics system of an EBT reactor.

A.4.2 GLOBAL FIELD ERROR CORRECTION COILS

As a result of closed field lines and the lack of rotational transform in EBT, a toroidal current-free plasma equilibrium is possible. However, inevitable magnetic field asymmetries in the system ($\Delta B/B \approx 10^{-4}$) cause the field lines to spiral out and also give rise to a toroidal current along the field lines, which may be given by³

$$I \approx \frac{\pi a^2}{2A} \sigma E_{\perp} \left(\frac{\Delta B}{B} \right),$$

where E_{\perp} is the ambipolar electric field, σ is the Spitzer conductivity, and A is the aspect ratio, R/a . The presence of a toroidal current has a detrimental effect on the plasma, especially on the formation of a negative ambipolar potential well, which is necessary for stable operation.

Externally introduced transverse global correction fields may be used to cancel the toroidal current. It was observed in EBT-I that the plasma was essentially free from toroidal current and instabilities up to some critical value of field error,⁴ given by

$$\left(\frac{\Delta B}{B} \right)_{cr} \approx \rho_j/R \approx 6 \times 10^{-4},$$

where ρ_j is the ion Larmor radius and R is the major radius of the device. Assuming that this critical field estimate also holds for EBT-P, then we find that $\Delta B_{cr} \approx 5$ G. Here we have used $T_j \approx 300$ eV and $R \approx 5.6$ m. The correction coils must be able to provide at least this amount of field. As shown in Fig. A.4.6 there are four correction coils equally spaced around the minor cross section. Opposite coils are operated in pairs to provide a correction field at any angle in the plane. Therefore, the required

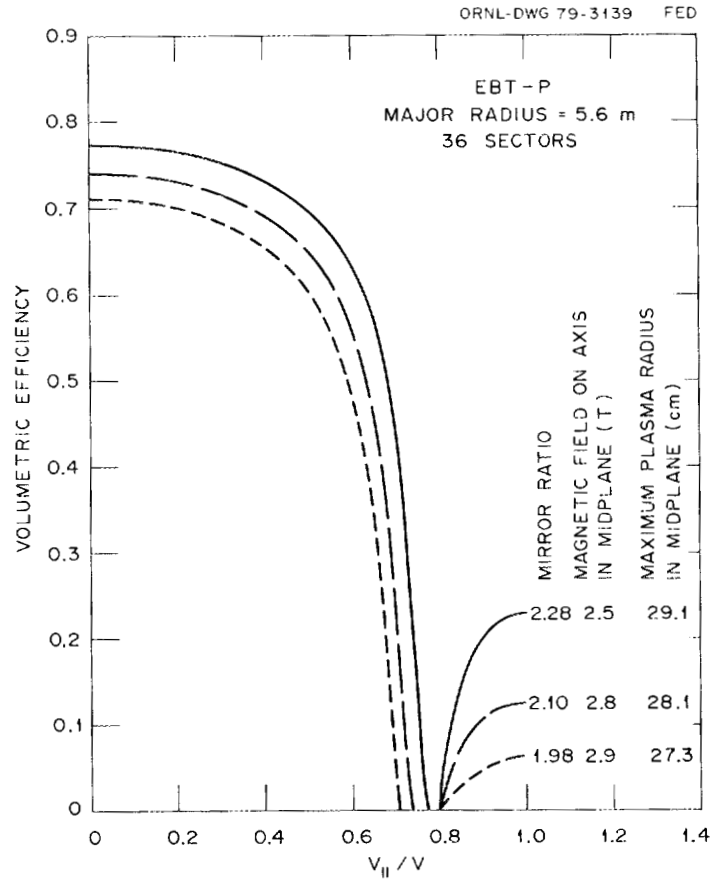


Fig. A.4.4. Effects on confinement of varying the mirror ratio and magnetic field strength in EBT-P. The ratio of the current in the outer trim coil to that in the inner coil is 37.2%, 18.6%, and 0 for mirror ratios of 1.98, 2.10, and 2.28, respectively.

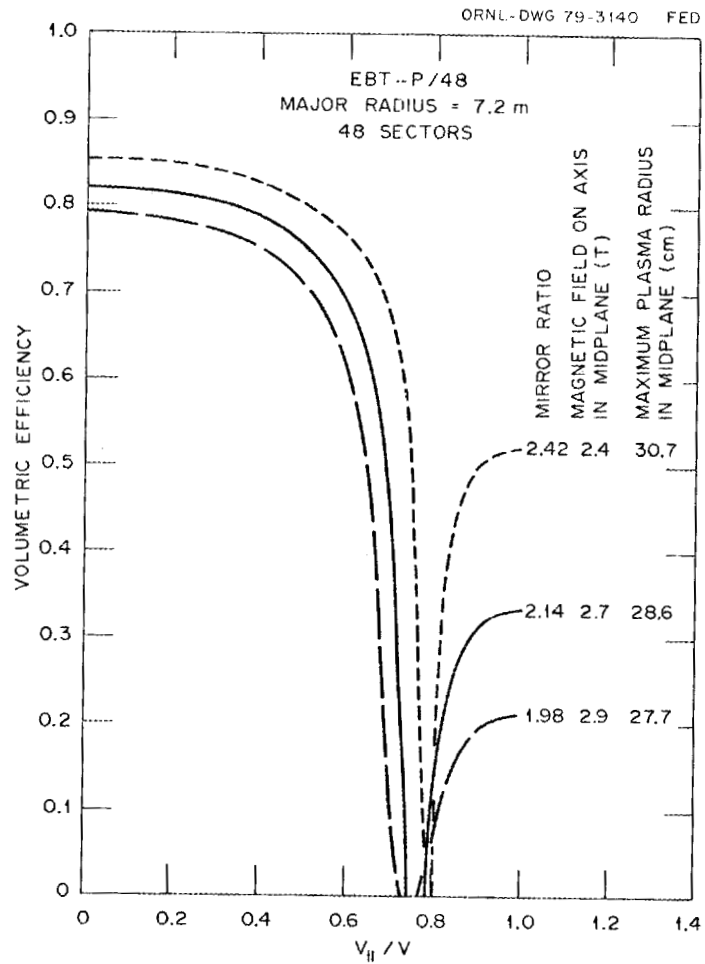


Fig. A.4.5. Effects on confinement of varying the mirror ratio and magnetic field strength for 48 sectors. The ratio of the current in the outer trim coil to that in the inner coil is +18.6%, 0, and -18.6% for mirror ratios of 1.98, 2.14, and 2.42, respectively. (A negative ratio means that the currents in the two coils are in opposite directions.)

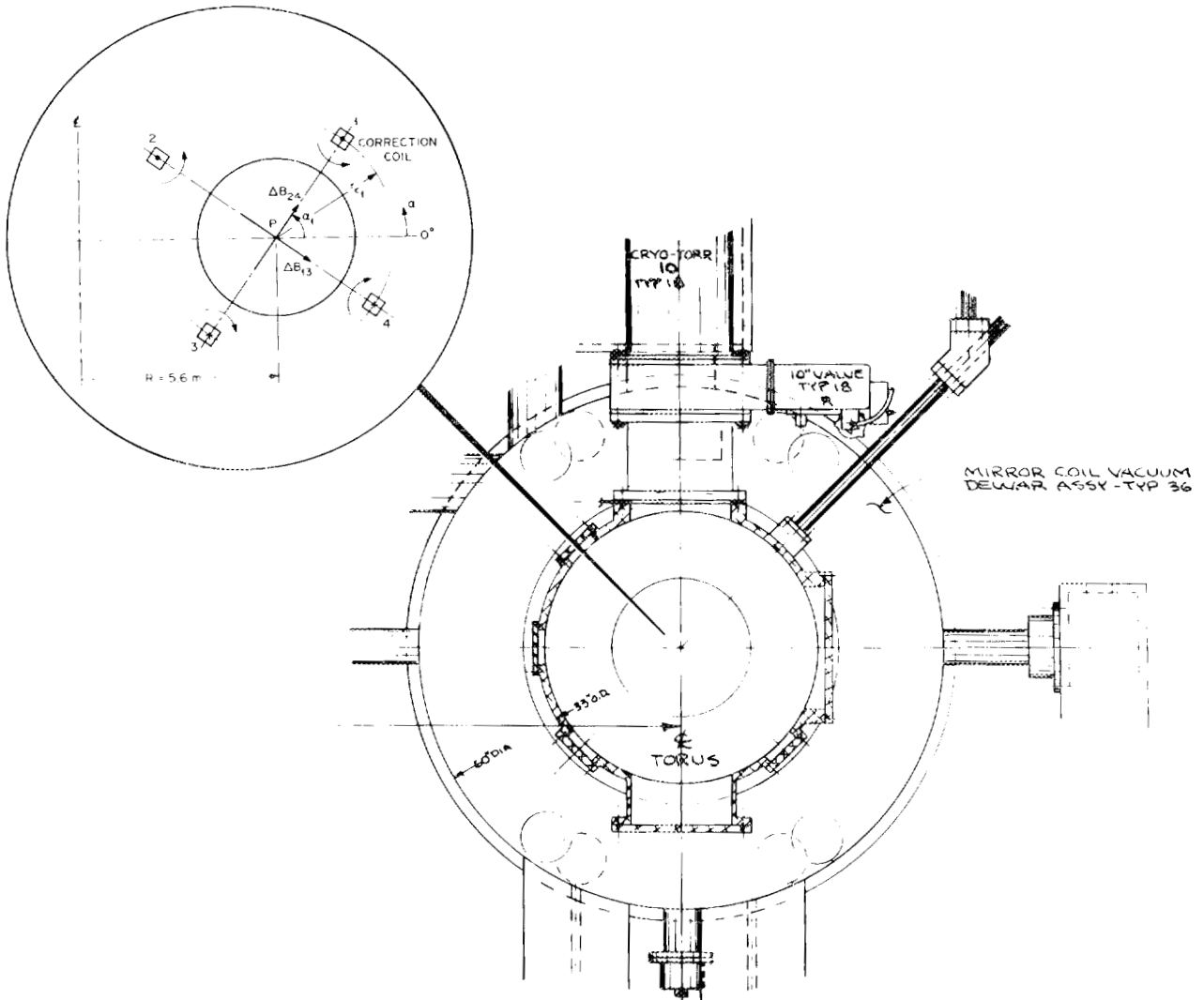


Fig. A.4.6. The locations of the correction coils are shown. The coil positions are determined by the need to leave horizontal and vertical access to the plasma and by the location of future ARE coils.

number of ampere-turns for one correction coil is

$$NI_{cr} = \frac{\pi r_c}{\mu_0} \Delta B_{cr}(T),$$

where r_c is the coil distance from the plasma center (see Table A.4.1) and $\mu_0 = 4\pi \times 10^{-7}$ H/m. Taking $r_c \cong 1$ m, one gets $NI_{cr} \geq 1250$ ampere-turns.

Table A.4.1. Radius and location of the EBT-P global field correction coils (also see Fig. A.4.6)

| Coil | Coil radius R_c (cm) ^a | Coil position radius r_c (cm) | Coil position angle α (degrees) |
|------|-------------------------------------|---------------------------------|--|
| 1 | 602.7 | 78.4 | 57 |
| 2 | 479.5 | 88.8 | 155 |
| 3 | 522.0 | 78.4 | 241 |
| 4 | 631.0 | 78.4 | 335 |

$$^a R_c = R + r_c \cos \alpha.$$

External fields are also utilized, as in EBT-I, to study plasma parameters such as density, density fluctuations, toroidal current, and potential. Therefore, the correction coils must be able to provide more than the 1250 ampere-turns estimated above.

Because of the existence of specialized cavity designs for various diagnostics (e.g., the heavy ion beam probe in EBT-I), the position of the correction coils may have to be adjusted locally in order to accommodate these special cavities. This slight perturbation on the shape of the coil will be of no consequence to the plasma. In Fig. A.4.6 the coil positions are shown.

In developing the design parameters for the correction coils and the dc power supply, the following procedure was used. First, the conductor, shown in Fig. A.4.7, was selected. The effective conduction area is $S_{eff} = 1.142$ cm². If $\ell = 2\pi R_c$ is the length of the outermost correction coil, $\rho = 1.9 \times 10^{-6}$ cm at 50° C, and $R_c = 631$ cm, then $R_\ell = \rho/S_{eff} = 1.9 \times 10^{-6}$ (3964.6/1.142) or $R_\ell \cong 0.67 \times 10^{-2}$ Ω /turn. Initially assuming nine turns per coil (see Fig. A.4.8), then $R_{coil} = 9 \times R_\ell = 9 \times 0.67 \times 10^{-2}$ or $R_{coil} = 0.0603$ Ω /coil. Because two opposite coils will be connected in series in order to produce a perpendicular correction field on the toroidal axis of the torus, $R_{total} = 2 R_{coil} \cong 0.1206$ Ω . Without any cooling, the allowable maximum current for this conductor is $I_{c_{max}} = 500$ A. Thus, $V_{dc} = R_{total} \times I_{c_{max}}$, $V_{dc} = 60.3$ V, $P_{max} = V_{dc} \times I_{c_{max}}$, and $P_{max} \cong 30$ kW. Therefore, two programmable bipolar 30-kW power supplies will be required to power the coils. In Fig. A.4.9 the connections for one set of global field correction coils are shown.

With the use of water cooling, the maximum current in the coil can be increased considerably. The cooling water passages for the nine turns in each coil can be connected in parallel so that the maximum cooling path is the circumference of the coil. The flow rate Q for a circular pipe with smooth walls is given by

$$Q = 6.4 \times 10^3 \left(\frac{\Delta P}{\ell} \right)^{1/2} d^{5/2},$$

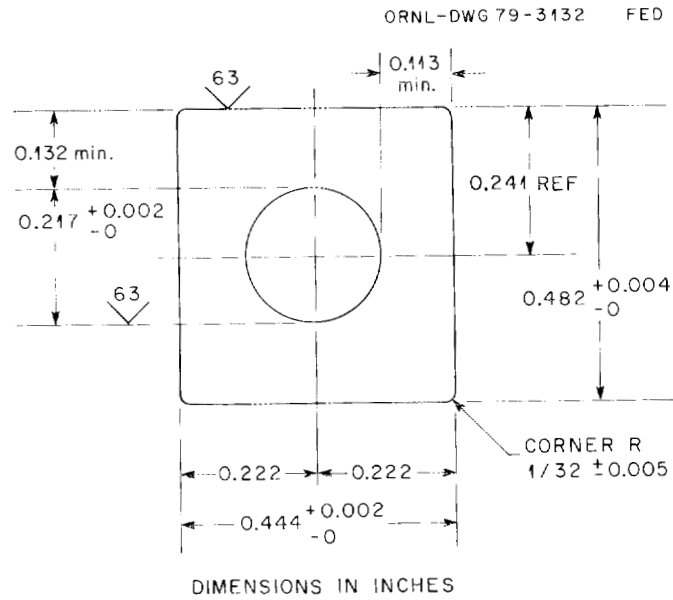


Fig. A.4.7. Selected conductor for this design concept.

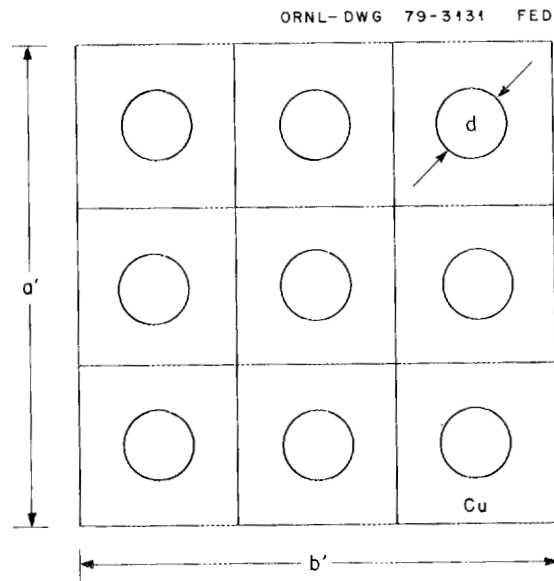


Fig. A.4.8. The cross section of the coil conductor with nine turns is shown. The dimensions are $d = 0.217$ in., $a = 1.446$ in., and $b = 1.332$ in.

ORNL-DWG 79-3130 FED

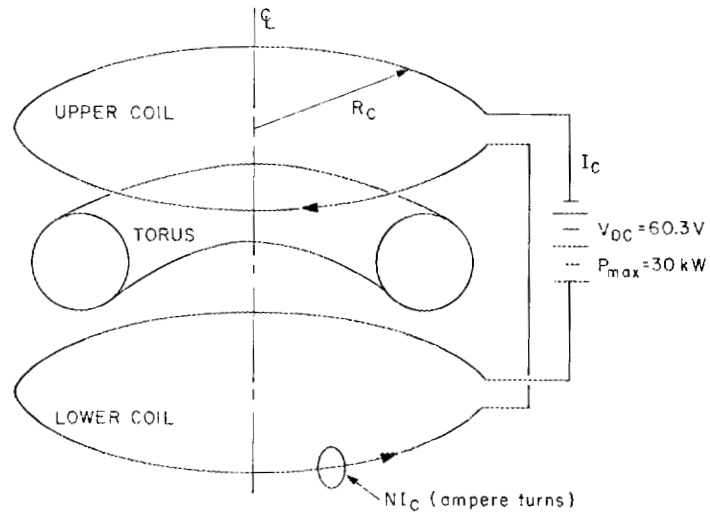


Fig. A.4.9. The coil corrections for one set of field corrections are shown. Note that $N = 9$ turns and $(I_c)_{max} = 500$ A (without water cooling), which gives 3.6 times the estimated critical value of field error and will allow field error effects on the plasma transport to be studied.

where Q = flow rate (cm³/sec), ΔP = pressure drop (atm), ℓ = passage length (cm), and d = diameter of the pipe (cm). For this case $d = 0.551$ cm, $\Delta P = 10.2$ atm, and $\ell = 2\pi R_c = 3966.68$ cm. Thus, $Q = 73.2$ cm³/sec = 1.16 gal/min. The Reynolds number $N_R = 1.18 \times 10^4$, which is greater than the value required for turbulent flow, ensures good heat transfer to the cooling water in the coil. With this flow rate the maximum heat that can be removed is $W_{\max} = 4.186 \times \Delta T \times Q$, where ΔT is the temperature difference due to Joule heating. If one takes $\Delta T_{\max} = 50^\circ$ C, then $W_{\max} = 4.186 \times 50 \times 73.2 = 15.32$ kW, which can be removed with water cooling. Thus,

$$I_{\max} = \sqrt{\frac{W_{\max}}{R_\ell}} = \sqrt{\frac{15,321}{6.7 \times 10^{-3}}}$$

$I_{\max} = 1.512 \times 10^3$ A. Therefore, for the nine-turn coils, 13,500 ampere-turns are available, if needed, to overcome the field errors that may arise during later phases of EBT-P (for example, with ARE coils and divertors, which may introduce some additional field errors into the system).

A.4.3 MIRROR COIL DESIGN CONSIDERATIONS

A.4.3.1 Introduction

At the outset of any magnet design project, the most important things to establish are the real constraints and the significance of small deviations from the desired objectives. Only in this manner can one establish the design parameters with the confidence that unnecessary advances in the state of the art and development have been avoided. Of course, constant communication between the plasma physicists who establish the EBT-P machine goals and parameters and the magnet technologists who must assess what can be accomplished within a realistic time schedule is necessary to establish the constraints. Our understanding of the constraints is a direct result of working on various EBT designs and carrying out this constant dialogue over a number of years.

In other sections the justification and value of the desired magnet field, the minimum working bore (warm bore in the case of superconducting magnets), and the mirror ratio are given. Taken together, these three constraints in effect specify the average current density of the magnet. For a superconducting magnet it can be shown that the maximum field (which is related to the central field by geometry factors and is an important parameter in the selection of conductor and magnet type) is given by the product of winding current density $\langle j \rangle$; inner radius to the windings r ; and F , a factor containing a numerical constant and all the related normalized geometry variables:

$$B_{\max} = \langle j \rangle r F . \tag{A.4.1}$$

Because the magnitude of field, the radius, the mirror ratio, and the quality of field distribution establish the coil geometry within a small range of variables, the current density is not a free choice as it is in most magnet design projects. The final design values chosen in order to meet all of the desired goals for the inner magnet are (1) $B_{\max} = 80$ kG, (2) $2r = 40$ cm, (3) mirror ratio = 2, and (4) $\langle j \rangle = 6600$ A/cm².

With these parameters we established the magnet design without any preconceived preferences for magnet type, conductor, or cooling mode. Our desire is to select the choice that provides the most assurance of success within a reasonable time schedule. Table A.4.2 shows the matrix of possibilities.

Table A.4.2. Type of stabilization and cooling mode

| Material | 1 Pool-boiling, 1-atm, 4.2-K helium | 2 Forced-flow, 4.2-K helium | 3 Forced-flow, pressurized, subcooled helium | 4 Pool-boiling, pressurized, superfluid helium |
|----------------------|---|-----------------------------------|---|---|
| A NbTi | Metastable (cryostability not possible) | Cryostability not possible | Cryostability may be possible | Cryostability may be possible |
| B Nb ₃ Sn | Metastable (cryostability not possible) | Cryostable | Not needed | Cryostable |

Before discussing the possibilities listed in Table A.4.2, we should point out that in the past, ORNL has had extensive experience in testing both superconducting material and magnets. We have made magnets using both NbTi and Nb₃Sn. We have made cryostable, metastable, and adiabatically stabilized magnets. We have not made any forced-flow magnets using the cable-in-conduit conductor, nor have we designed magnets specifically for superfluid operation, although we have some testing experience. Our experience with Nb₃Sn tape conductor is extensive; in fact, the largest and most complicated Nb₃Sn magnet ever built was done by the Magnetics Section at ORNL.

In Table A.4.2 all of the feasible superconducting materials (V₃Ga is too expensive and presents no advantage over Nb₃Sn until fields of 13 T are exceeded) and cooling schemes (subcooled pool-boiling He I is no advantage over 4.2-K helium because cryostability cannot be accomplished unless one uses the superfluid state) for constructing EBT-P superconducting magnets are tabulated. Column 4 may be quickly discounted because cryostability can be achieved by other means and because there is no experience with the use of large amounts of superfluid helium cooling in the U.S. Indeed, one system, the Pion magnet project at Stanford University, had to abandon the superfluid cooling mode after persistently failing to reach the low temperature necessary to establish the He II phase transition. Superfluid temperatures do have great advantages for either extending the operating field range of NbTi and Nb₃Sn or raising the current density of a completely cryostabilized design. With more knowledge of the behavior of superfluid systems, these advantages may be realized sometime in the future. We are watching the French TORE II Project with great interest. Columns 2 and 3 taken together provide one good choice, namely, row B in column 2, a Nb₃Sn forced-flow conductor operated at 4.2 K. We feel this choice of a forced-flow conductor utilizes the high critical temperature of Nb₃Sn while avoiding the extra refrigeration complexity of a pressurized, subcooled, forced-flow system for which no experience exists. Furthermore, the choice attempts to capitalize on the Westinghouse Large Coil Program experience and conductor development. Finally, in column 1 the clear choice is row A because the advantage of working with a ductile alloy, NbTi, outweighs the higher critical temperature T_c and hence higher current-sharing temperature T_s of a brittle material, Nb₃Sn, particularly in the case where cryostability cannot be achieved by the material substitution. Perhaps a further word on the cryostabilization of a conductor in pool-boiling helium is in order here. To a first approximation the type of superconducting material does not influence the overall current density that can be cryostabilized at a particular field. Full cryostability is determined by assuming that a length of conductor in the high field zone has gone normal and that the Joule heating in the copper stabilizer (sometimes aluminum is used) is smaller than the helium heat transfer to the helium at the transition from film boiling back to nucleate boiling. Therefore, to stabilize at a high current density, the controllable variables are a high conductivity matrix and a conductor of small dimension, which result in a large cooling surface. However, a small conductor is not compatible with a high value of current, which is needed for the proper protection of magnets with high stored energy (in the present case $E_s \sim 3$ MJ/coil). In addition, the conductivity of copper decreases as the

field increases (magnetoresistance), making it harder to stabilize a conductor at high fields. Therefore, pool-boiling stabilization at high winding current densities can be achieved only in relatively small magnets at low field. As seen in another section of this report, existing cryostabilized magnets have overall winding current densities much less than the needed 6600 A/cm^2 , with most having values below 2500 A/cm^2 . In summary, we conclude that the best choices for an EBT-P magnet lie in either a metastable, pool-boiling NbTi design or a cryostabilized, forced-flow Nb₃Sn design. Both systems use nominal 4.2-K helium. Considering cost, schedule, minimum development, and simplicity of fabrication and operation, we prefer the pool-boiling NbTi design. There is still too little experience with multi-filamentary Nb₃Sn to select it for the main approach for a major facility, especially because the maximum required field is 80 kG, which is in the acceptable range for NbTi (see Table A.4.3 for practical field limitations on commercial superconducting material). We should also point out that no large magnet has yet been fabricated with a cabled conductor that is the configuration for the forced-cooled Nb₃Sn conductor. Although cables are easier to stabilize than monolithic or built-up conductors because of the large surface areas available for cooling, even cables of NbTi have not been used in any large magnets principally because of their inherent structural deficiencies. Outside of the cable-in-conduit configuration, it is difficult to envision a scheme for containing the movement of cables while simultaneously providing sufficient space for helium cooling.

Table A.4.3. Commercial superconducting material

| | T_c (K) | H_{c2} (kG) | Practical maximum field (kG) at 4.2K |
|---------------------------------------|-----------|---------------|--------------------------------------|
| Alloy (ductile) NbTi | 8-10 | 100-120 | 85 |
| Compound (brittle) Nb ₃ Sn | 18 | 220-250 | 150 |

A.4.3.2 Examples of Metastable Magnets

Although high energy physicists have had great difficulty with low copper-to-superconductor volume ratio (Cu:SC of 1:1-2:1) adiabatic conductor (also incorrectly known as intrinsic), there has been considerable success with metastable magnets wound with an intermediate range of Cu:SC ratio (3-8) conductor. In fact, one could survey the literature and conclude that few cryostabilized magnets have operated as reliably as most metastable magnets. A metastable design is therefore proposed for the EBT-P project, but we reiterate that it is only because the constraints do not permit us to achieve a pool-boiling cryostable design.

It is important to consider the experience to date of all large metastable magnets or magnets wound from conductors with intermediate values of Cu:SC ratio. By intermediate values deliberate avoidance is implied of the low values (Cu:SC < 3) associated with the adiabatically stabilized conductors used in high energy physics experiments and known for their unpredictable behavior (training) and failure to make design values (degradation). Most of the magnets being developed in the high energy labs are pulse coils, which are more difficult to develop. By definition, a large magnet or magnet system is one with stored energy of at least 1 MJ. At this level some means of protection is generally necessary to avoid damage on a quench. Often the intrinsic strength of the composite conductor is not sufficient at stored energies of many megajoules to contain the magnetic forces, and some means of structural reinforcement is required for safe, reliable operation. Generally, magnets in this range are not completely cryostabilized (i.e., a normal zone collapses and the current returns completely to the superconductor). Some magnets in this range can tolerate normal zones if they are sufficiently localized.

All of the magnets in Table A.4.4 operated without training or degradation. Also, in each case the design value was met.⁵ In some of the cases shown, the conductor was cooled by conduction and was not even in intimate contact with helium. Therefore, if such a conductor were also well cooled, one would expect it to perform in a cryostable or partially cryostable mode. Large pool-boiling cryostabilized magnets have average current densities over the windings (excluding structure and bobbin) of between 1.3 and 2.5 kA/cm². One magnet not listed in Table A.4.4 but presently under design is the MHD magnet for Stanford. The project is being managed by MIT and the coil is being designed and fabricated by General Dynamics, Convair Division. It will also be a metastable design and not a cryostable design.

Table A.4.4. Parameters of large metastable magnets
(Cu:SC > 3 and $E_s > 1$ MJ)

| Magnet | E_s (MJ) | Size (m) (bore x length) | B_{max} (kG) | $\langle j \rangle$ (kA/cm ²) | Cu:SC ratio |
|--------------|------------|-----------------------------|----------------|--|-------------|
| Muon channel | 2 | 0.13 x 8 | 50 | 17.6 | 3.5 |
| HYBUC | 1.7 | 0.18 x 0.6 | 123 | 10 | 3 |
| BIM | 10.5 | 1 x 1 | 55 | 5.3 | 8 |
| Rutherford | >1 | ~0.5 x 0.5 | 75 | >5 | 6 |
| W7 | 1.6 | 0.85 x 0.2 | 60 | ~12 | 2.5 |
| CGE | 2 | 0.4 x 0.3 | 78 | 8.4 | ~5 |
| U25 MHD | 34 | 0.68 x 2.6 | 60 | 2.8 | 15 |

Although we cannot achieve cryostability in a pool-boiling design, we should point out that cryostabilization itself does not ensure success for a magnet project. The performance record of magnets made from "conventional" fully cryostabilized conductor is not all that good. Three large ones (two at CERN and one at DESY) suffered internal arcing (with two of these the conductor burned out in a small section), and four others (at BNL, MIT, LLL, and Julich) suffered premature quenches and did not achieve their design point. These latter cases are particularly disturbing. Cryostabilized magnets are not supposed to quench, and their performance is supposed to be predictable. The real difficulty with any magnet design is two-fold. On the one hand, little is known about the disturbance spectrum. What are all the heat inputs, and what are their magnitudes? Even if we postulate various heat inputs to the conductor, we do not know enough about the heat transfer mechanism in restricted spaces. What happens to helium bubbles that are formed, and what part does the hydrodynamics of the helium fluid play? These answers will come only from a well-directed research effort on the performance of various types of superconducting magnets. More discussions on magnet difficulties can be found in Refs. 6 and 7.

The concept of a magnet designed in such a way that it can recover from a normalcy induced over a fairly large region without undergoing a quench is advantageous and important. Our second choice for an EBT-P magnet is a Nb₃Sn cable-in-conduit forced-cooled conductor that can be cryostabilized at 8 T at high current densities (~7 kA/cm² overall is easily obtainable). The conductor is made by putting a cable into a tube that is swaged down and compacted but has a deliberate void fraction of up to 40%. The helium is forced under pressure to flow through the tube where the conductor is placed. Therefore, while the helium circulation is similar to the known and used hollow conductor concept, the conductor itself is not in the walls or on the outside of the tube as in previous examples investigated mainly in Europe; the conductor is in all other respects, however, standard superconducting cable that comes in many varieties. Because of the large cooled surface area and the reasonable heat transfer coefficient of pressurized helium, the conductor is stable and will recover from a normalcy by depositing the Joule

heating into a large-heat-capacity reservoir supplied by the helium. Because the helium is pressurized and is in the single-phase regime, the increase in bath temperature does not result in the formation of bubbles, which in the past has often caused vapor lock leading to thermal runaway. The tube configuration is advantageous in providing a good structural containment for a flexible conductor such as a cable or braid. This is an important factor for scalability to higher currents and to higher fields. With cables or braids a larger conductor can in principle be fabricated from just a larger number of identical strands already used in a smaller device.

The main difficulty in utilizing Nb_3Sn and all the other potential high field compounds is their inherent brittleness. However, the tube configuration may remove this disadvantage because the conductor is not intimately bound to the structure and does not undergo a large strain in order to operate the structure at the maximum permissible stress level.

Forced-cooled conductors offer many advantages such as those listed below:

- (1) low liquid helium inventory,
- (2) mechanical integrity,
- (3) electrical integrity at high discharge voltages,
- (4) easier control of cooldown thermal stress, and
- (5) ease of extrapolation to large size and high fields.

For larger systems the possibility of high discharge voltages will likely prove to be the most important advantage to forced-cooled systems. On the other hand, it is only fair to point out that there are also some disadvantages to forced-cooled systems:

- (1) greater complexity of cryogenic system,
- (2) additional losses due to pumping introduced,
- (3) parallel cooling circuits and complicated plumbing, and
- (4) more difficult protection.

The last two items are of most concern. The complicated hydraulics may prove to be extremely difficult to arrange in small systems where space is not available. A few magnet systems that employ forced-flow cooling of NbTi conductor but without the cable-in-conduit configuration have been built; a complete list of all the large magnets follows:

- (1) Omega, CERN -- compressed helium, hollow conductor;
- (2) Muon channel, SIN -- compressed helium, external tubes;
- (3) Pion Toroids, Stanford -- two-phase helium, external tubes;
- (4) Long Solenoid, Kapitza -- two-phase helium, close-coupled tubes; and
- (5) T-7 Toroid, Kurchatov -- two-phase helium, close-coupled tubes.

With the above considerations, why is the forced-flow Nb_3Sn not our first choice? In addition to the general listing of the disadvantages to forced-cooled schemes, there are specific concerns that we have related to the cable-in-conduit conductor. Basically, they all stem from a lack of experimental experience. What are the hydraulic path lengths that can be tolerated? What is the effect of the external heating? We know that even small temperature differences can produce sudden discontinuous large thermal inputs that can raise the local internal pressure quite high in a very nonuniform manner. These implications must be better understood.

A.4.3.3 Design Considerations for the EBT-P Magnet

In the previous sections we established the conductor material, NbTi, and the stabilization technique, metastable, which are our first choices to satisfy the design parameters because a pool-boiling

cryostable design is precluded. The actual dimensions for the winding are established after consideration of structural requirements. Although no structure is required in the windings to keep within reasonable stress limits, one has to make a careful assessment on whether some structure is required in the form of banding on the outer turns. The bobbin thickness and end flanges must be calculated to take care of not only the winding stresses but also the loads arising under full field and possible fault conditions. At this point in the design we are ready to decide on the conductor and winding details. Is the coil to be potted or ventilated? What is the conductor configuration -- monolithic, built up, or cable? What is the appropriate Cu:SC ratio for maximum stability against perturbations, and what dimensional shape is preferred? This latter point must go along with considerations on the winding mode -- pancake, layer, or hybrid. One must decide the insulation scheme in conjunction with the winding mode. In general, there is no one choice among these alternatives. Each specific application must be analyzed, and as mentioned in the introduction to this summary of magnet design considerations for EBT-P, the constraints must be carefully considered and fully understood. The important aspect in selecting the specifics of the winding is to make the choices compatible and arrive at a self-consistent design.

Cooling design

Our clear preference in magnet designs that are subjected to external heat, in this case radiation, is a ventilated design rather than potted windings in an epoxy. Helium heat capacity is enormous even if only 20% of the winding volume is accessible for helium compared to the metals NbTi and copper, which comprise the superconductor. It is preferable to have heat transfer directly from the surface of the conductor to liquid helium rather than via conduction through a poor thermal conductor as is the case for all potting compounds.

Conductor and filament configuration

In the specification for the purchase of the conductor, the choice of either monolithic or built-up conductor remained open. Only the cable configuration was specifically eliminated from consideration. This is because there are no ac losses anticipated and the need to have accurate field quality translates into the need for close dimensional tolerance, which is difficult to achieve reliably in a Rutherford cable. Whether a straight monolithic conductor is cheaper than a built-up conductor remains for the commercial vendors to decide.

The size of the filaments is not particularly critical in this application. It is necessary to have the filaments much less than about $\ll 200 \mu\text{m}$ to ensure that each filament itself is adiabatically stabilized. It is not necessary to reduce the filaments down to the state-of-the-art limit as is often done for applications in pulse field magnets. A size of $\sim 50 \mu\text{m}$ in diameter is easily obtainable and avoids the problems associated with the defects inherent in much smaller sizes.

Optimum copper to superconductor ratio

When we build a superconducting magnet, we want it to work; that is, we want it to reach design field without quenching. We try to build strong, rigid magnets that do not experience perturbations substantial enough to quench them when they are energized. This task is rendered difficult by our lack of knowledge of the perturbations that quench magnets. The magnets of EBT cannot be cryostable and are in the metastable regime, meaning a large enough perturbation will quench them. In the absence of any clear knowledge about the perturbations they will suffer during operation, we must prefer conductors that require large perturbations to quench them to conductors that can be quenched by small perturbations. Comparison by the size of the perturbation required to quench the conductor gives us the

opportunity to select the best conductor of a class of conductors. For example, we may ask if, all other things being held constant, there is a best Cu:SC ratio that maximizes the perturbation from which the conductor can just recover. Using this best conductor should afford us the greatest chance that the magnet will work.

A straightforward approach to determine the best Cu:SC ratio would be to assume some canonical form of perturbation and calculate the Cu:SC ratio that makes the size of the perturbation greatest. Alternatively, we can say, following Wilson and Iwasa,⁸ that the more stable of two conductors differing only in Cu:SC ratio is the one with the larger minimum propagating zone. Another possibility is to define as the more stable of the two conductors the one with the smaller normal-zone propagation velocity. Implicit in the use of these alternatives is the assumption that the more stable conductor they define will truly have the larger maximum permissible perturbation.

These alternatives can be studied with a minimum of labor if we make the assumption of constant thermophysical properties. First we consider canonical perturbations consisting of an instantaneous deposition of energy E at a point in the conductor. The larger E is, the more stable the conductor is. How does E vary with the Cu:SC ratio?

Shown in Fig. A.4.10 are curves of constant dimensionless energy ϵ_δ in the plane of the Stekly parameter α and the dimensionless current i . Consider a candidate EBT conductor intended for service at 8 T, 4.2 K, and 9000 A cm⁻². We assume that the conductor is a composite of NbTi, whose critical current density is 5.6 x 10⁴ A cm⁻² at 8 T and 4.2 K, and copper, whose residual resistivity ratio is 160. With these data fixed, we find that

$$\alpha = \frac{1.2 \times 10^8}{Ph/A} \cdot \frac{(1-f)^2}{f} \quad (Ph/A \text{ in } W m^{-3} K^{-1}) \quad (A.4.2)$$

$$i = \frac{0.16}{1-f}$$

where f is the volume fraction of copper in the composite.

The quantity Ph/A is not very well known in the early stages of design, but the values occurring in practice range from $\sim 2 \times 10^5$ – $\sim 5 \times 10^6$. As we shall see, the uncertainty in Ph/A will not affect our conclusions about the Cu:SC ratio.

Figure A.4.11 shows curves obtained from Eq. (A.4.2) by fixing Ph/A and letting f vary (f -loci). If we superimpose one of these f -loci on the curves of Fig. A.4.10, the intersections will give ϵ_δ as a function of f . Let us consider the f -locus for which $Ph/A = 1 \times 10^6 W m^{-3} K^{-1}$ (shown dotted in Fig. A.4.10). When $f = 0.84$, the operating current equals the critical current and $\epsilon_\delta = 0$. Near the right-hand side of the graph, the f -locus cuts the curves of constant ϵ_δ at a steep angle so that we start out moving rapidly from curve to curve as f decreases. However, as f continues to decrease, the f -locus becomes nearly parallel to the curves of constant ϵ_δ so that a point is quickly reached at which further reduction of f brings little increase in stability. In the example under discussion, the point of diminishing returns occurs at $i \sim 0.6$, for which $f = 0.73$ and Cu:SC = 2.75. When Cu:SC = 5, $i = 0.96$, and ϵ_δ , which measures stability, is about six times smaller than for Cu:SC = 2.75. Thus, the lower Cu:SC ratio is clearly preferable.

We get the same conclusion no matter which of the f -loci we consider up to values of $Ph/A = 5 \times 10^6 W m^{-3} K^{-1}$. For this value of Ph/A , we see that it is possible to achieve cryostability (both cold-end stability and full stability, depending on the choice of f). Paradoxically, to achieve cryostability when Ph/A is large, we need large Cu:SC ratios. But for EBT, Ph/A will probably be in the range 2–5 x 10⁵ W m⁻³ K⁻¹ so that cryostability is unattainable for any choice of f . This being the case, we must prefer low Cu:SC ratios.

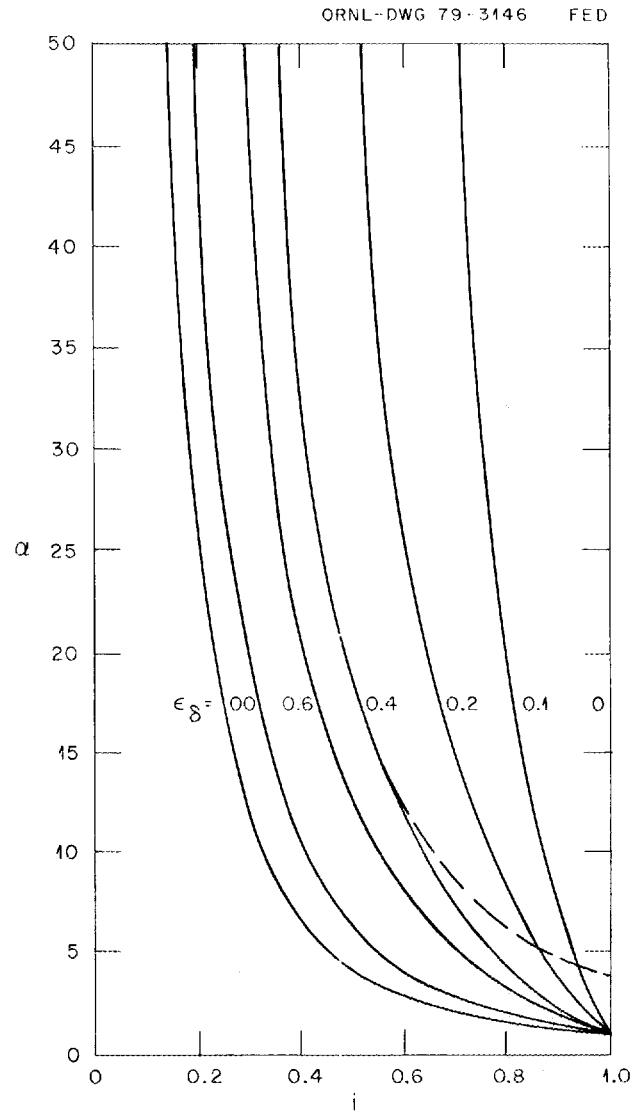


Fig. A.4.10. In the plane of the Stekly parameter α and the dimensionless current i are shown curves of constant dimensionless energy ϵ_δ .

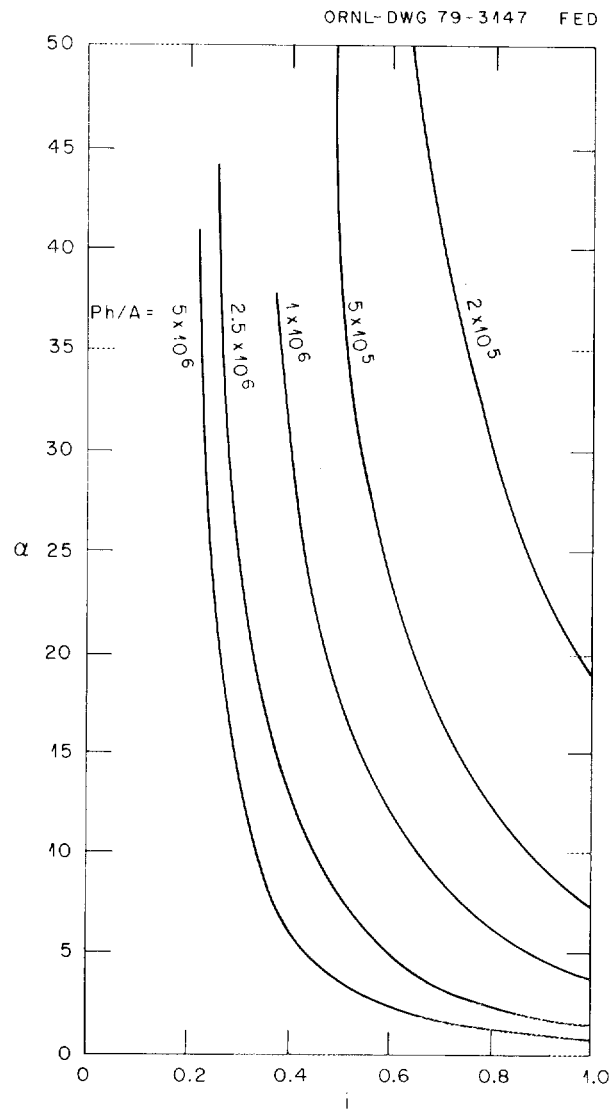


Fig. A.4.11. In the α - i plane the value of f , the volume fraction of copper in the conductor, has been allowed to vary for a specific value of Ph/A .

Figures A.4.12 and A.4.13 show curves of constant dimensionless minimum-propagation-zone energy ϵ_{MPZ} and dimensionless normal-zone propagation velocity n , respectively, in the α - i plane. These families of curves strongly resemble the curves of constant ϵ_g in Fig. A.4.10. If we superimpose the f-loci on them rather than on the curves of Fig. A.4.10, we get the same conclusion as before, namely, that for candidate EBT conductors, a Cu:SC ratio of ~ 3 is preferable to one of ~ 5 .

Winding method

There are advantages and disadvantages to both layer and pancake winding. Below is a tabulation of the principal advantages offered by either scheme:

- (1) Pancake
 - (a) good surface for transmitting large radial compressive forces (easier to prevent conductor motion),
 - (b) solid insulation between pancakes,
 - (c) better packing factor,
 - (d) grading of conductor that can be optimized, and
 - (e) good bubble clearance and helium replenishment between pancakes.
- (2) Layer
 - (a) joints that are kept to a minimum,
 - (b) grading joints that can be kept out of the winding pack,
 - (c) easier layer winding for edge winding of large aspect conductor (no saucer or trapezoid effects), and
 - (d) better winding tightness in axial direction for U-shaped bobbin.

For the EBT-P application the need for minimizing errors introduced by joints and the shorter winding time offered by layer winding both lead to the choice of a layer-wound coil. Actually we should call it a hybrid (or "layercake") because one pancake will be wound on the end and the remainder of the coil will be layer wound. In this manner there is no need to make an entrance through the end flange; furthermore, the input and output leads can be placed in close proximity, making the cancellation of field errors due to the current leads a relatively easy task.

A.4.3.4 Summary

Because the constraints on the magnet design (8.0 T and 6600 A/cm²) preclude the possibility of a cryostabilized pool-boiling magnet, we have selected a NbTi pool-boiling metastable design as our preference over a forced-cooled Nb₃Sn cryostabilized design. A critical review of the existing literature shows that magnets of the type we are proposing have all worked to full operating design value without training. No degradation has been observed in this class of magnet. A stability analysis has shown that the conductor will be more stable against energy perturbations if the Cu:SC ratio is closer to 3:1 rather than 5:1. The conductor will be rectangular and flat wound in a hybrid-type winding that consists of one pancake wound next to the end flange with the remainder of the coil wound in layers.

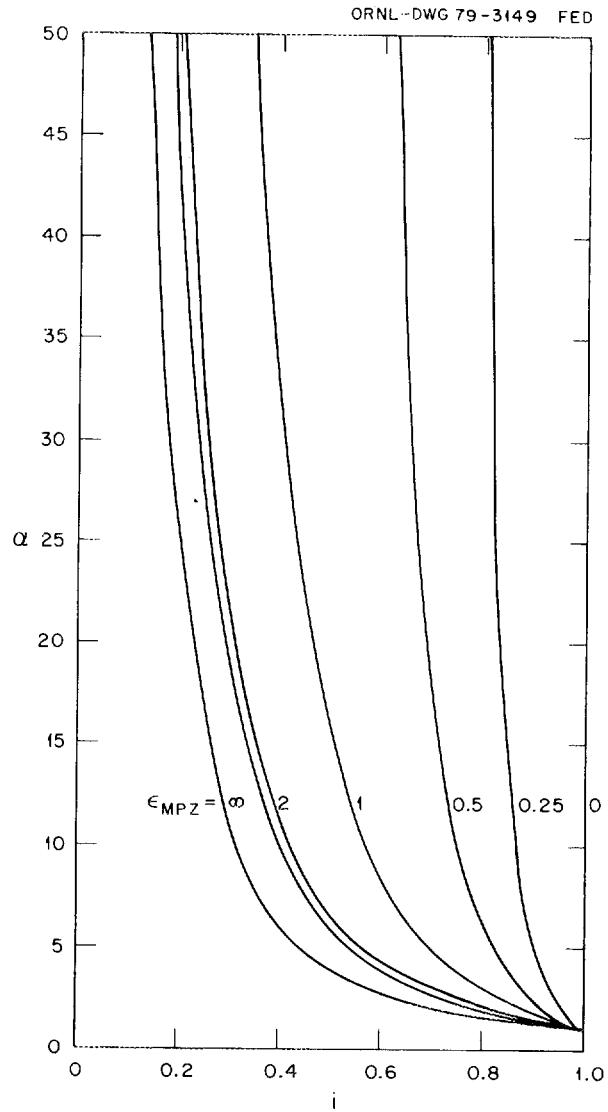


Fig. A.4.12. In the α - i plane the minimum-propagation-zone energy ϵ_{MPZ} has been allowed to vary.

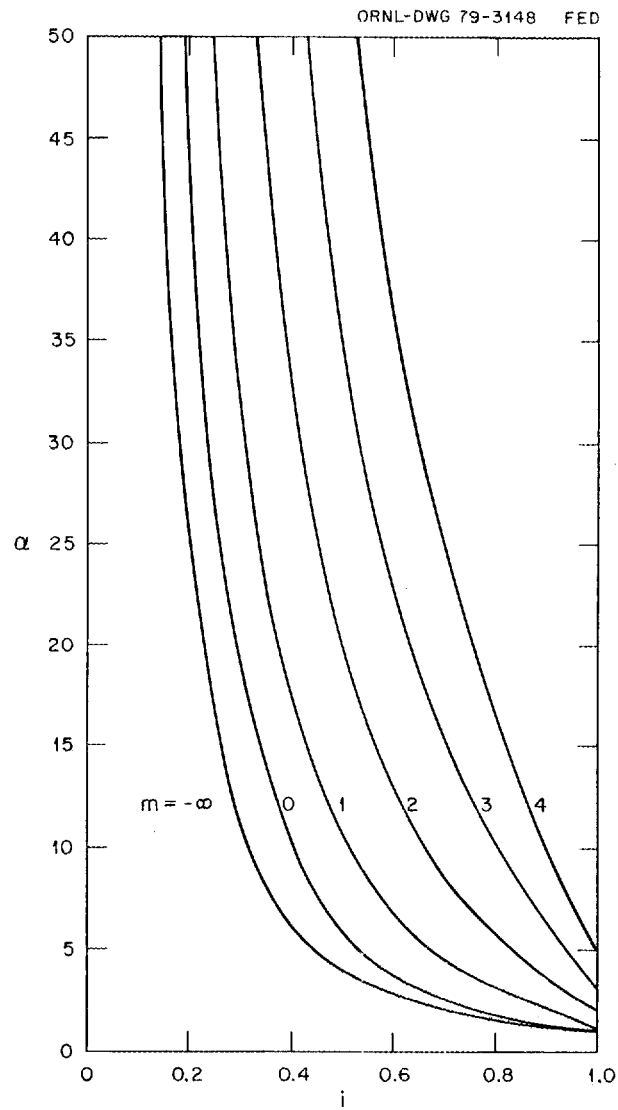


Fig. A.4.13. In the α - i plane the normal-zone propagation velocity m has been allowed to vary.

REFERENCES

1. R. A. Dandl et al., Oak Ridge National Laboratory Report ORNL/TM-5955, Oak Ridge, Tennessee (1978).
2. D. G. McAlees et al., Oak Ridge National Laboratory Report ORNL/TM-5669, Oak Ridge, Tennessee (1976).
3. R. A. Dandl et al., Oak Ridge National Laboratory Report ORNL/TM-6457, Oak Ridge, Tennessee (1978).
4. B. H. Quon et al., Oak Ridge National Laboratory Report ORNL/TM-6704, Oak Ridge, Tennessee (1979).
5. M. S. Lubell, *Cryogenics* 12, 340 (1976).
6. S. Y. Hsieh et al., *IEEE Trans. Magn.* 13, 90 (1977).
7. D. B. Montgomery, *Proc. Symp. on Engineering Problems of Fusion Research*, p. 122 (1976).
8. M. N. Wilson and Y. Iwasa, *Cryogenics* 18, 17 (1978).

A.5 MICROWAVE HEATING

A.5.1 INTRODUCTION

The Microwave Development and Technology Program is an outgrowth of support activities conducted for many years as an integral part of the ORNL High Beta Plasma Program. Its broad purpose is the development of microwave and millimeter wave methods, techniques, components, and systems for plasma heating relevant to the controlled fusion effort. Emphasis upon the development of high power, high frequency (short wavelength) systems is thus implicit. The continuation of this program in close collaboration with the EBT effort is considered essential because of the inherent "applied" nature of technology programs and the resulting aspects of mutual dependence.

Significant past accomplishments of the Microwave Development and Technology Program are exemplified by the microwave power systems presently used on EBT. These systems demonstrate (1) the practicality of the assembly, management, and control of large microwave power sources employing multiple plasma device inputs using both conventional and oversized waveguide transmission lines; (2) the efficient coupling and matching of these transmission lines to plasma devices; (3) compatible design criteria for the utilization of large power microwave inputs in plasma devices; (4) the advance in the state of the art of conventional microwave tubes; and (5) control and monitoring systems integrated into the experimental facility to provide for operational simplicity and flexibility, equipment safety, and personnel safety. These systems therefore model the areas of effort required in the comprehensive future program.

By 1984 the millimeter wave power requirements for EBT-P are expected to be of the order of several megawatts in the general frequency range of 60-110 GHz. This frequency corresponds to electron cyclotron resonances of approximately 20-40 kG and is consistent with existing superconducting magnet development.

High power microwave systems for EBT-P are composed of three basic elements:

- (1) a multiple array of active devices for conversion of dc power to microwave power;
- (2) microwave transmission networks for efficient transfer and coupling of energy to the fusion device;
- (3) supporting electrical and electronic subsystems for overall system control and monitoring, operation of active devices, and safety.

For realization of multimegawatt capability at 110 GHz, an intensive complementary development effort is required in each of these categories. The key element is the development of active devices, whereas the microwave transmission networks and supporting subsystems involve the characteristics of both the active devices and the plasma confinement experiment.

A.5.2 DEVELOPMENT OF MICROWAVE ACTIVE DEVICES

Multimegawatt, continuous wave (cw) electron cyclotron heating (ECH) systems operating at 60-110 GHz are required by the EBT-P program and by subsequent programs. Clearly, this power generation capability is beyond the present state of the art for microwave linear beam tubes. Hence, an intensive development program has been undertaken through subcontract with private industry. This development effort began in 1974 when Varian Associates was commissioned by means of an ORNL subcontract to perform a study for the purpose of determining the best approach for realization of a microwave power device capable of producing 200 kW of cw power at 120 GHz. This study identified the gyrotron, a form of cyclotron resonance maser, as the most promising device for development toward this objective. Then in April 1976 ORNL initiated a development subcontract with Varian with the objective of developing a 200-kW, cw 28-GHz device for use on EBT-S. A further stipulation in the subcontract was that the

device be scalable to 120 GHz. Progress to date on this program has been significant. In May 1978 a gyrotron was operated at 105 kW of cw power, and in September 1978 a 28-GHz gyrotron was operated into the EBT-S device at the 50-kW level with encouraging plasma physics results. At this time it is expected that the 28-GHz, 200-kW, cw development program will be successfully completed by September 1980. Although several challenging design problems remain in this development program, the progress made to date in the 28-GHz program indicates that the gyrotron is the correct choice for this application at higher frequencies.

In view of the encouraging results from the 28-GHz development program and the anticipated need for higher frequency devices at the earliest possible date for EBT-P operation, ORNL awarded two industry subcontracts in mid-1979. Successful completion of these development contracts is expected by 1983. Both subcontractors will pursue the gyrotron as the active device most likely to achieve the goals of 200 kW of cw power at 110 GHz.

The characteristics of these gyrotrons result from the unique plasma heating application for EBT-P, namely, that each gyrotron produce about 200 kW of cw power at millimeter wavelengths. This high power level requires good tube efficiency to keep power supply costs reasonable. The gyrotron realizes high efficiency and high power by (1) having an interaction region many wavelengths long, (2) utilizing the entire electron beam cross section in the interaction region, and (3) keeping the microwave power dissipated in the interaction region low by use of circular electric cavity modes.

The theoretical basis for operation of the gyrotron, or electron cyclotron maser, is well known. This device employs a cloud of monoenergetic electrons in a fast-wave structure. Electron velocity is primarily transverse to the applied axial magnetic field. Phase bunching of the electrons occurs because of the relativistic mass change of the electrons. As these phase-bunched electrons radiate coherently, energy is transferred to the electromagnetic wave. To date, applications of these principles have been limited by the technologies and design detail necessary to incorporate the theory into useful devices. Key elements of the gyrotron include the electron gun, interaction cavity, collector and output system, window, and magnet system. All of these design issues are being addressed by the subcontract developers.

A.5.3 AUXILIARY SYSTEMS

The gyrotron power supply, control systems, and instrumentation currently in operation on EBT-S are considered prototypical for the EBT-P gyrotron system. The operation of multiple gyrotrons on EBT-P will require an extension of this effort in terms of control, suitable operation for the application, overall performance, reliability, and economics. Specifically, it is expected that the operating parameters of these gyrotrons will be nonidentical and will thus require a sophisticated supervisory control system for uniform output control as well as careful monitoring for abnormal conditions. In addition, there is the possibility of locking and/or beating problems associated with oscillator operation. These problems are being addressed in the EBT-P design, and it is expected that multiple gyrotron operation will be demonstrated on EBT-S.

A.5.4 COMPONENTS AND TRANSMISSION

As a direct consequence of using a circular electric cavity mode in the interaction region, the axisymmetric gyrotron produces most of its output power in a few TE_{0n}^0 circular electric waveguide modes. Although these modes have the advantages of very low transmission losses and superior power-handling capability compared to most other waveguide modes, they suffer from the fact that they are not the modes with the lowest cutoff frequency; therefore, they must always be used in a waveguide capable

of propagating a number of modes. To achieve the very low transmission losses and high power-handling capability, the operating frequency must be well above cutoff so that many more modes are in the propagating range.

The practical problems raised by the multimode character are several. First, one must prevent spurious modes from being excited in the waveguide system by irregularities. Spurious mode conversion is caused by either mechanical or electrical imperfections in the waveguide, such as cross-section distortion, departure from axial straightness, surface roughness, and changes in surface conductivity. Once excited, these modes may become cut off somewhere else in the system at other irregularities. These spurious modes can then become trapped between irregularities, and at a particular frequency, one of the spurious modes can absorb a large fraction of power from the main mode, causing localized waveguide heating or even breakdown. This situation can be prevented in two ways. The first is to avoid exciting the spurious modes in the first place by carefully controlling the waveguide shape. Second, if spurious mode excitation cannot be avoided, as in the case of a waveguide bend, then loss must be provided for the trapped (spurious) modes by the use of mode filters in order to reduce the stored energy (Q) of these modes.

In the past, mode filters consisting of waveguide sections of lossy material such as stainless steel have proved to be reliable high power mode filters. They work on the principle that the lower order circular electric modes (TE_{01}^0 , TE_{02}^0 , TE_{03}^0) have lower losses than most other modes in the system so that if a certain amount of loss for the circular electric modes can be tolerated, then the other spurious modes will have even higher fractional power losses in the stainless steel waveguide.

To achieve higher spurious mode losses relative to the circular electric modes, a mode filter consisting of alternating rings of conducting and lossy material sandwiched together in a waveguide section can be utilized. This filter has very low loss for the circular electric modes because the modes produce only circumferential wall currents that travel around the conducting rings. All other modes, however, have axial components to their wall currents that suffer attenuation through the lossy rings. To handle the high average power, these lossy rings must be cooled and made of high temperature material, such as ceramic loaded with carbon. The rings must be less than one-half wavelength thick to prevent mode conversions of their own.

An abrupt quasi-optical bend for the waveguide system consists of two circular waveguides intersecting at 90° with a reflecting, elliptical miter surface at 45° to both waveguides. Such a bend is referred to as a miter bend and to a first approximation behaves as an optical mirror if the waveguide diameter is much greater than a wavelength. Some mode conversion will invariably be present; therefore, mode filters will be required on either side of the bend to absorb spurious modes.

One of the most important measurements in the microwave heating system is the forward and reflected power measured by directional couplers. Two general types of couplers can be used in the oversized waveguide system. The first is a "cross-guide" directional coupler consisting of two 90° miter bends placed back to back on the mitered plane, forming a waveguide cross with a 45° junction. The 45° junction consists of a metal plate perforated with a large number of very small holes in cutoff at the design frequency. The holes transmit an attenuated sample of the incident mode pattern on the high power side of the plate to the forward power arm on the low power side of the plate. The reflected mode pattern on the high power side is similarly coupled to the low power reflected arm of the coupler. Both low power sampling arms are terminated in matched calorimetric loads for total mode power measurements.

Another approach for forward and reflected power monitoring is a coupled mode transducer consisting of a low power dominant mode waveguide that is phase matched to the desired circular electric mode in the high power oversized waveguide. The coupling between waveguides is achieved by an array of small apertures in cutoff spaced by a one-quarter guide wavelength and tapered in size so as to preferentially couple to the desired mode pattern in the oversized waveguide.

A.5.5 MICROWAVE-PLASMA COUPLING

ECH power fed into the plasma chamber undergoes multiple low loss reflections with accompanying changes in polarization and direction. Therefore, the Q of the plasma chamber without the plasma present is very large. However, with magnetic field surfaces at electron cyclotron resonance present in the chamber, the extraordinary wave is heavily damped by absorption during its transit through a resonance region. Because polarization and directional changes accompany successive reflections (resulting in reflected waves comprising both ordinary and extraordinary waves), the total input wave is soon converted to extraordinary waves and is rapidly damped by coupling to the plasma. The resulting loaded Q of the chamber is then very low.

Because the effective loaded Q of the ECH multimode cavity is very low under normal conditions where $\omega > \omega_{pe}$, the impedance presented to the input wave is nearly equal to the impedance of free space. Impedance-matching considerations for the design of the coupling aperture are then similar to those for a radiating antenna. The simplest such aperture suitable for high power use is an oversized waveguide terminating flush with the interior wall of the cavity. The complex electromagnetic field patterns associated with higher mode propagation in such multimode transmission lines obviously do not permit the launching of a linearly polarized wave with high purity.

Because of efficient absorption and plasma shielding effects, microwave power fed into one mirror confinement region of EBT-P does not readily propagate into adjacent regions. Accordingly, it has been necessary to provide a discrete ECH input to each of the 36 mirror confinement regions in order to form and maintain the high beta, hot electron annuli upon which stability depends, as well as to provide uniform heating of the entire volume. The approach is to combine several mirror confinement regions of the bumpy torus into a single multimode cavity by connecting the desired number of confinement regions to a large, external reflecting manifold via identical oversized waveguides entering along the minor radius. No spurious cyclotron resonant regions are involved with this arrangement of entry, and no such regions are likely to interfere with the external reflecting manifold because the magnetic fields everywhere outside the torus are quite small. In this way ECH power fed from the source into the external reflecting manifold via oversized waveguides is coupled into several regions simultaneously. Some degree of balance among power inputs to individual regions is provided by the large Q of the reflecting manifold and by symmetry in the connections. An additional degree of balance and an increase in overall efficiency result because power reflected from one region is available for absorption in another. Additional control of power distribution may be obtained by the use of irises, or "stops," to limit the power fed to a selected region or to remove it entirely.

A.6 DIAGNOSTICS/DATA ACQUISITION

Convenient and reliable measurement of plasma properties as well as of machine parameters is imperative. In addition to standard diagnostic tools, state-of-the art equipment will be necessary to document EBT-P performance. Wherever possible, corroboration of the experimental evidence is highly desirable. Because of the amount of data coming from the experiment, sophisticated computer handling of the data is required both for storage and for preliminary analysis.

Essential measurements include spatial electron and ion densities and temperatures, space potential, fields, plasma lifetimes, and impurity behavior. Table A.6.1 lists available diagnostics and the plasma parameters that can thus be measured. Besides the steady-state plasma, it is important to investigate plasma startup, the effects of plasma fueling and of auxiliary heating, and stability considerations.

The requirements of the data acquisition system can be categorized as data capture and data processing. The system must be capable of the capture of both large and small quantities of data at both high and low rates. Various CAMAC modules that meet these needs are available. Data processing functions include varying amounts of data reduction, calculation, plotting, CTR display, and archiving. A hierarchy of computers logically connected by communications links will meet all requirements. The computational power and mass storage devices will be distributed in such a way as to increase the accessibility of processed data, to minimize data flow over communications lines, and to ensure backup systems for basic data capture. Figure A.6.1 shows a general computer facility of the type required for EBT-P.

Table A.6.1. Planned diagnostics and the related plasma parameters that can be measured

| Diagnostic | Parameters |
|---|---|
| Laser interferometer | $\bar{n}_e \ell, n_e(r), \ell$ (also fluctuations of) |
| Laser Faraday rotation | $B(\text{ring})$ |
| Thomson scattering | $n_e(r), T_e(r), \ell$ |
| Charge exchange analysis | $T_i(r), n_i n_o(r), \text{sputtering}, \ell$ |
| Hard x-ray | $T_e(\text{ring}), n_e(\text{ring})$ |
| Soft x-ray | $T_e(r), n_e(r), \ell, \text{impurities}$ |
| Heavy ion beams (Cs^+, T^+) | $\phi(r), n_e(r), T_e(r), \ell$ |
| Barium beam | $B(r), n_e T_e^{-1/2}(r), \phi(r), \ell$ |
| Spectroscopy | $n_o(r), T_o, \tau_p, n_{\text{impurity}}, T_{\text{impurity}}$ |
| Toroidal current loops | $I_{\text{toroidal}}, \text{field error}$ |
| $d\phi/dt$ coils | W_l |
| Skimmer probe with $d\phi/dt$ coils | Ring position |
| Ionization probes | Ring position, energetic toroidal electron |
| Surface analysis | Sputtering |

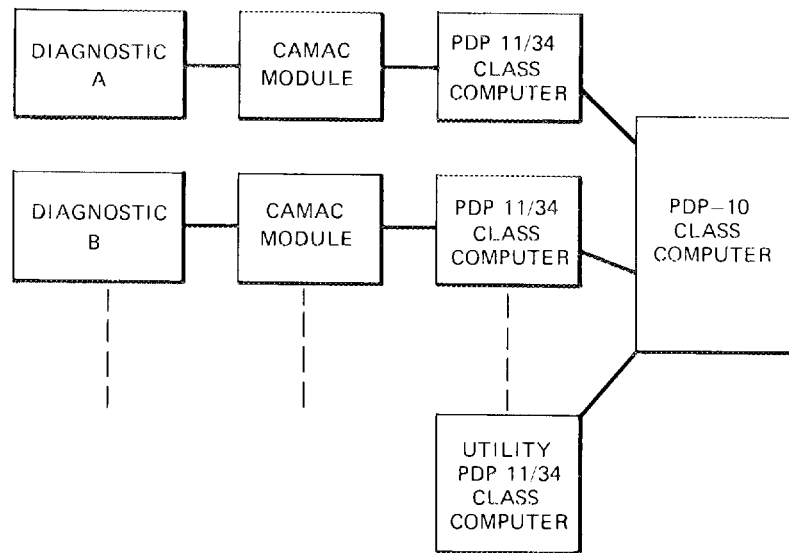


Fig. A.6.1. Generic hierarchy of computers for EBT-P data handling.

A.7 FUTURE OPTIONS

The EBT-P device is designed to allow for future upgrades that will handle experimental verification of theoretical concepts not to be investigated on the first EBT-P. Several of the proposals being considered for future study on an upgraded EBT-P are included here.

A.7.1 ASPECT RATIO ENHANCEMENT COILS

Vacuum field particle confinement in EBT-P can be significantly improved through the addition of low current supplementary toroidal field coils called aspect ratio enhancement (ARE) coils. By varying the current in these coils, the plasma geometry and effective aspect ratio can be changed with the result of either spoiling or enhancing plasma confinement. The ARE coils can be used either independently or with the outer trim coils to investigate confinement in a broad range of field geometry.

Figure A.7.1 shows the position in the equatorial plane of the ARE coils (two per sector). This position is optimum for confinement enhancement and at the same time has the least impact on vacuum chamber access. The coils are D-shaped to minimize their circumference in the canted configuration shown in Fig. A.7.1. The effects of ARE coils on vacuum field geometry are illustrated in Fig. A.7.2, where mod B contours and field lines in the equatorial plane are plotted for I_{ARE} (current in the ARE coils/current in the mirror coils) = 0 and 5%. The current in the outer trim coils is 0, giving a mirror ratio change from 2.28 to 2.55 with an accompanying decrease of about 10% in the geometric mean field. Note that the ARE coils very nearly symmetrize the mod B contours about the minor axis in the midplane, particularly in the region of the hot electron rings. This symmetrization permits an increase of 15% in the radius of the rings and a corresponding increase of about 30% in the volume of plasma confined within the rings. In addition, more efficient utilization of the plasma volume should result in a significant decrease in the amount of microwave power deposited in the cool plasma outside the electron rings. An equally important effect of ARE coils is to lengthen the magnetic field lines on the inside of the torus relative to those on the outside, resulting in significant improvement in the confinement of transitional and passing particles.

One method of defining an ARE factor for ARE coils is afforded by the volumetric efficiency, discussed in Sect. A.4 of this appendix. If, for example, energizing the ARE coils with a given current yields a volumetric efficiency curve that compares favorably with the curve for a torus having twice the major radius and number of sectors, i.e., twice the mechanical aspect ratio, then this definition would give an ARE factor of 2 for that particular ARE coil current.

Volumetric efficiency curves for $I_{ARE} = 0$ (no aspect ratio enhancement) and $I_{ARE} = 5\%$ are presented in Fig. A.7.3 and Fig. A.7.4 for 36 and 48 sectors, respectively. Improved centering of the drift orbits of mirror-trapped particles and a rather dramatic decrease in the width of the velocity space loss cone near $V_{||}/V = 0.8$ are seen in both cases. Based on the passing particle ($V_{||}/V = 1.0$) volumetric efficiency, the ARE factor is at least 2 for $I_{ARE} = 5\%$. It should be noted, however, that much of the observed effect is the result of the larger plasma minor radius in the midplane. The slope of the longitudinal invariant J as a function of radius in the midplane (see Fig. A.4.2 of Sect. A.4.1 of this appendix) is such that a small increase in the radius of the limiting flux line on the inside of the torus can yield a large increase in volumetric efficiency. This effect is more pronounced the closer the limiting flux line is to the ARE coils. This suggests an alternate definition of the ARE factor based on confinement in the interior of the plasma rather than near the edge.

In Fig. A.4.2 of Sect. A.4.1 of this appendix, the maximum inward shift of passing particle drift orbits from the minor axis of the torus (the radial position of the minimum of J) is plotted as a function of mirror ratio. A similar curve for $R(J_{min})$ can be plotted as a function of aspect ratio or

ORNL/DWG/FED 78-454

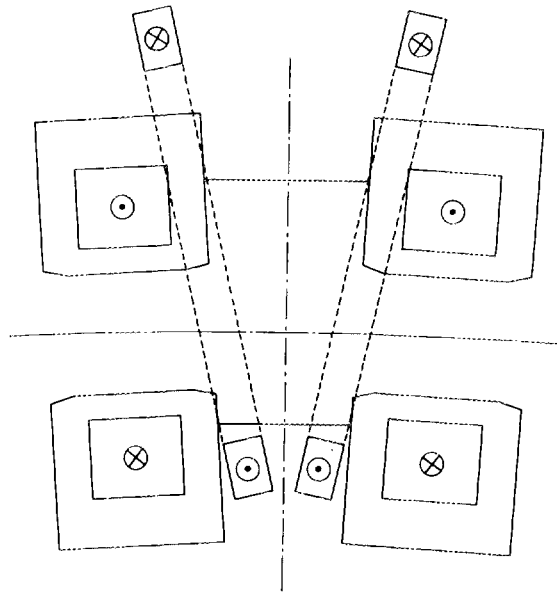


Fig. A.7.1. Sector of EBT-P in the equatorial plane displaying position of the superconducting mirror coils and ARE coils. Dots and crosses indicate polarity of currents when in the enhancement mode.

ORNL/DWG/FED 78-455

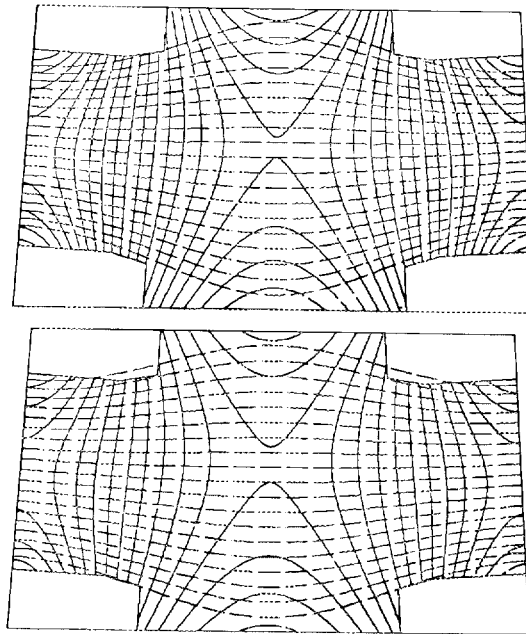


Fig. A.7.2. Effect of ARE coils on field geometry. Mod B contours (solid lines) and field lines (dashed lines) in the equatorial plane are plotted for ARE coil currents I_{ARE} of 0 (top) and 5% (bottom). The current in the outer trim coils is 0.

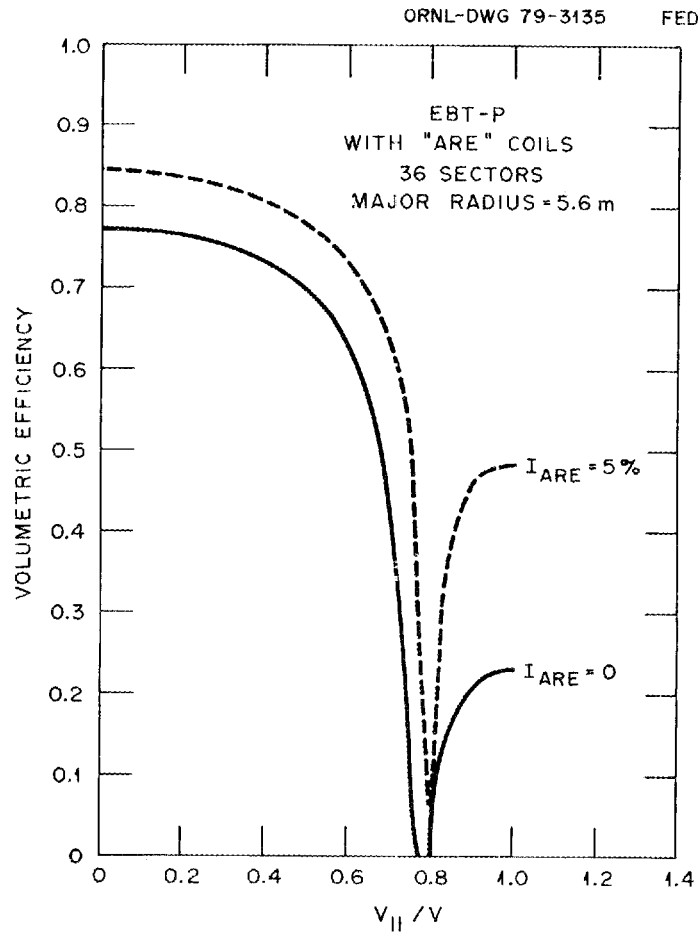


Fig. A.7.3. Effect of ARE coils on particle confinement for 36 sectors. Volumetric efficiency curves are plotted as a function of the cosine of the pitch angle for ARE coil currents I_{ARE} of 0 (solid curve) and 5% (dashed curve).

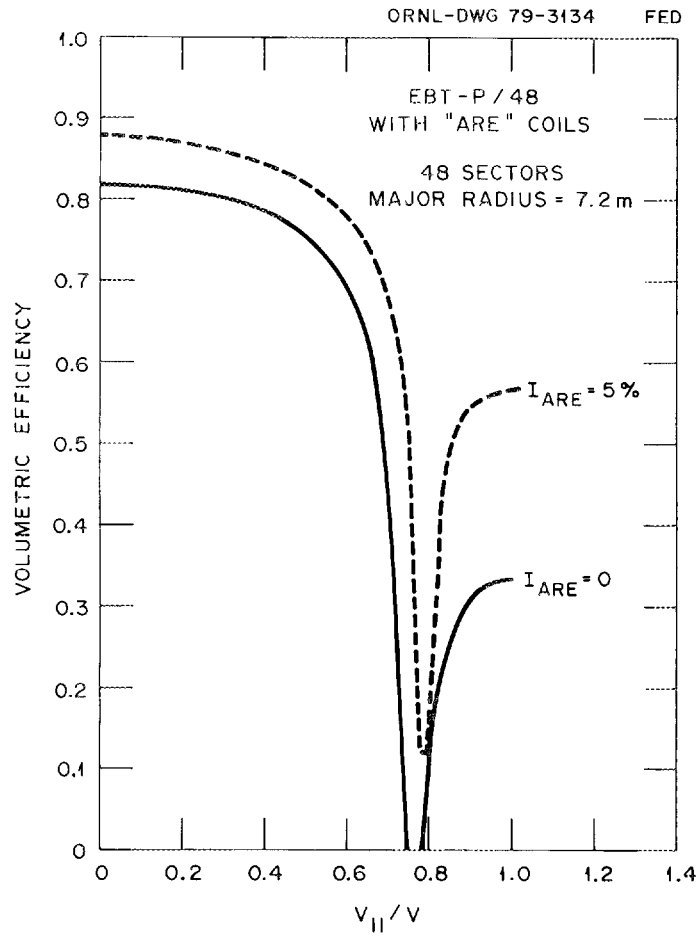


Fig. A.7.4. Effect of ARE coils on particle confinement for 48 sectors. Volumetric efficiency curves are plotted as a function of the cosine of the pitch angle for ARE coil currents I_{ARE} of 0 (solid curve) and 5% (dashed curve).

number of sectors. Using this curve and $R(J_{\min})$ for $V_{\parallel}/V = 1.0$ with different ARE coil currents permits a much more precise definition of aspect ratio enhancement. Figure A.7.5 shows the ARE factor as a function of ARE coil current based on this definition. For ARE coils placed at or near the relative position indicated in Fig. A.7.1, this curve is almost independent of machine size, mechanical aspect ratio, etc. For the ARE coil current of 5% used in Figs. A.7.3 and A.7.4, the enhancement factor is seen to be approximately 1.3. These two definitions of ARE factor probably bracket the effect of ARE coils on the overall confinement properties of the system.

In summary, ARE coils hold the promise of improved particle and energy confinement, increased flexibility for plasma experiments with a broad range of field geometry, and potential impact on reactor size. The addition of ARE coils to EBT-P represents a relatively inexpensive method of testing scaling laws and the effects of changes in the vacuum field confinement characteristics without changing the mechanical aspect ratio.

A.7.2 ION CYCLOTRON HEATING EXPERIMENTS IN EBT-P

A.7.2.1 Introduction

Auxiliary ion heating in an EBT device is essential in order to achieve fusion-relevant ion temperatures. Without auxiliary heating, the only source of energy for plasma ions is collisional transfer from electron cyclotron-heated electrons. The rate of collisional ion heating decreases with plasma temperature, and although it increases with density, the plasma density in EBT devices is limited by the ordinary mode microwave cutoff (for EBT-P with $f = 110$ GHz, $n_e(\max) \cong 2 \times 10^{14}/\text{cm}^3$). Experimental results with ion cyclotron heating in other devices, although perhaps not as definitive as with neutral beam injection, are certainly promising. In addition, for the next generations of EBT devices (EBT-S and EBT-P), ion cyclotron resonance heating (ICRH) appears to have a number of advantages over neutral beam injection.

(1) The technology of rf power sources in the ion cyclotron range of frequencies is well established so that no additional development program is required and long lead times are not required for procurement.

(2) The cost of rf power in this frequency range is low. Realistic estimates of the cost of the entire rf system are 50-75¢/W for a total power in the range of hundreds of kilowatts.

(3) A rf system can be operated in steady state without difficulty and is not in any way limited by the particle removal speed of the vacuum system.

(4) Much of the antenna development and optimization work can be done on EBT-S. In addition, experience with heating strategies, diagnostics, and ECRH/ICRH system compatibility can be obtained on EBT-S using the slow wave.

In view of these considerations we recommend that ICRH be adopted as an auxiliary heating technique in EBT-P and that a vigorous program be carried out on antenna development, preliminary experiments on EBT-S, and theoretical work.

Two types of cold plasma waves propagate in the ion cyclotron range of frequencies: (1) the fast wave (compressional Alfvén wave or magnetosonic wave), which is only weakly cyclotron damped at $\omega = \omega_{ci}$; (2) the slow wave (shear Alfvén wave or ion cyclotron wave), which is resonant and heavily damped at $\omega = \omega_{ci}$. In Sects. A.7.2 and A.7.3 of this appendix, we give a brief overview of the physics involved in the propagation and absorption of these waves, the results of heating experiments on other devices, and the applicability to EBT. In Sect. A.7.4 we discuss some considerations of antenna design and placement, and in Sect. A.7.5 we outline the requirements for an ICRH system for EBT-P.

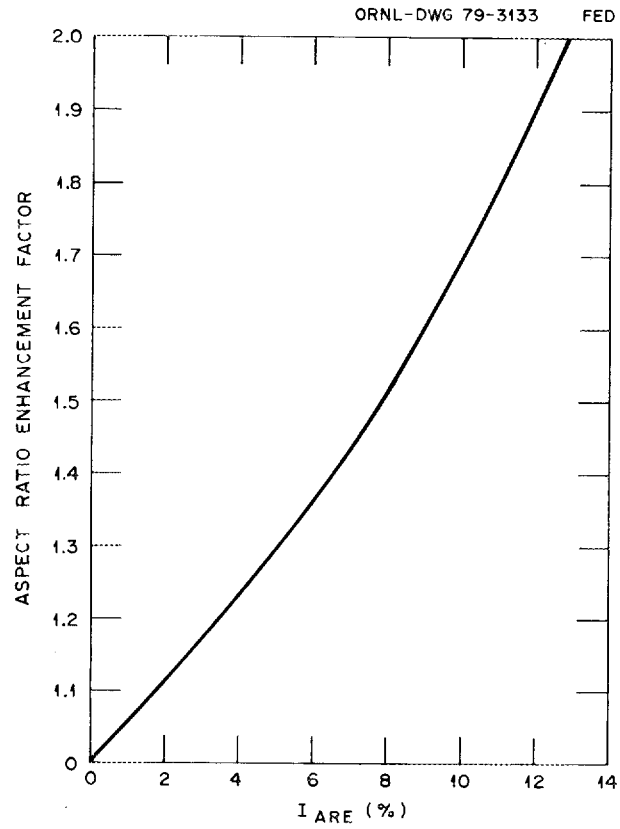


Fig. A.7.5. Aspect ratio enhancement factor for passing particles as a function of ARE coil current.

A.7.2.2 Fast Wave

Most recent experimental and theoretical work has concentrated on the fast, or magnetosonic, wave,¹ including successful heating experiments on ST,² TFR,³ ATC,⁴ and PLT,⁵ all tokamaks.

In a vacuum cavity the slow wave corresponds to the TE mode, with transverse electric fields and a wave magnetic field along the axis. The dispersion relation is¹

$$N = c/V_A(1 + \cos^2 \theta)^{1/2}, \quad (\text{A.7.1})$$

where $N = kc/\omega$ is the index of refraction, V_A is the Alfvén velocity with $c/V_A = f_{pi}/f_{ci}$, and θ is the angle between the wave vector and the static magnetic field. This dispersion relation is valid over the entire frequency range of interest. Because the wavelength increases as the density decreases ($\lambda \cong cf_{ci}/ff_{pi}$), in a cavity of fixed size there exists a minimum density below which the fast wave cannot be excited. The following table shows the index of refraction and wavelength for the range of densities expected in EBT-P. The frequency is taken to be $f = 60$ MHz (the proton cyclotron frequency for $B = 40$ kG), and the angle of propagation is $\theta = 90^\circ$.

| Density (cm^{-3}) | N_1 | $\lambda(\text{cm})$ | $2\pi r_p/\lambda$ |
|------------------------------|-------|----------------------|--------------------|
| $1.0(10)^{13}$ | 10.7 | 46.7 | 3.1 |
| $2.5(10)^{13}$ | 16.9 | 29.0 | 5.0 |
| $7.0(10)^{13}$ | 28.3 | 17.4 | 8.3 |

Here the minor radius of the cavity for EBT-P is taken to be $a = 40$ cm with a plasma radius $r_p = 23$ cm. The expected densities are large enough for excitation of the lower cavity modes. In a cylindrical cavity the modes have the form $B_z \sim J_m(k_\perp r) e^{im\theta + in\phi - i\omega t}$, where we have approximated a torus of major radius R by introducing a toroidal mode number $n = k_z R$ (k_z is the wave vector in the axial direction). In this case the criterion for the existence of cavity modes¹ is

$$J'_m(k_\perp r_p) = J'_m(2\pi r_p/\lambda) = 0. \quad (\text{A.7.2})$$

The first few roots of J'_0 are 3.83, 7.02, and 10.2, and the roots of J'_1 are 1.84, 5.33, 8.54, One sees that the $m = \pm 1$ mode is the only one which will propagate at the lowest density, but at higher densities several modes are possible. This, of course, neglects such features as the toroidal curvature, the segmentation of the cavity, and the magnetic field variation. By including a vacuum layer near the wall, one finds that this rough criterion is modified somewhat,^{1,6} but the conclusion is the same: the excitation of the fast wave depends critically upon the density. However, the use of He⁴ as the majority species with hydrogen as a minority species would increase N by a factor of 1.4 for the same electron density.

Because the electric field of the fast wave is polarized such that it does not effectively accelerate ions, its damping at cyclotron resonance is weak. With the local magnetic field in the z direction, the electric field combination that accelerates ions is $E^+ = E_x + iE_y$ (left-circular polarization). However, because the perpendicular dielectric constant is singular at $\omega = \omega_{ci}$, this component vanishes at resonance.¹ The fast mode does exhibit weak absorption in a single ion species plasma at the fundamental of the ion cyclotron frequency because of the Doppler shift of ions streaming along field lines,

$\Delta\omega = k_{\parallel} v_{\parallel} \approx k_{\parallel} \sqrt{T/M}$. The theoretical heating rate is similar in form to the rate calculated for electrons and is proportional to $RT/\lambda Mc^2$, where $R = B/|B|$ and λ is the free space wavelength. The long wavelength and large ion mass make the heating rate small. The spatial width of the resonance is $\Delta = n\lambda\sqrt{T/Mc^2}$, where n is the toroidal mode number. For $f = 60$ MHz, $T = 100$ eV, and $n = 1$, one finds that $\Delta = 1.63$ mm. There is, however, little experimental evidence for fast-wave heating at the ion cyclotron frequency with a single species plasma.

Heating at the second ion gyroharmonic is also small, although the electric field rotating with the ions is larger. The heating is a finite cyclotron radius effect and is proportional to $k_{\perp}^2 T/M\omega_c^2 = N_{\perp}^2 T/Mc^2$.

Ion mixtures and the ion-ion hybrid resonance

If two ion species are present, the absorption of the fast mode is considerably modified. When the plasma has two ion species, a plasma hybrid resonance occurs between the two cyclotron frequencies. For fixed N_{\parallel} the perpendicular index of refraction is singular for a cold plasma, just as it is for the lower hybrid and upper hybrid resonances. Although heating at this resonance was first reported for the TFR³ experiment, it probably occurred in earlier experiments in which small amounts of other gases were always present.

At the hybrid resonance the component of the electric field perpendicular to the resonant surface becomes very large, but the parallel components do not. The electric field has equal amounts of the components E^+ and E^- and is far more effective for accelerating ions. In addition, the large field amplitude opens the possibility of various nonlinear heating mechanisms.⁴

The presence of two plasma components also tends to modify the linear absorption at the fundamental cyclotron resonance. If the plasma consists of a heavy majority species (such as D^+ or He^3) as well as a light impurity species (such as H^+), the wave polarization is largely determined by the majority so that the left-circular-polarized electric field component remains finite at the fundamental cyclotron frequency of the minority species. In this case heating of the minority species is considerably enhanced.

Recent experiments on PLT⁵ with hydrogen as a minority species in a background of deuterium have shown strong minority heating with some electron heating. The coincidence of the second cyclotron harmonic of deuterium with the fundamental of hydrogen is apparently not important. A minority hydrogen plasma in a background of He^3 is also strongly heated. This heating seems to be the result of cyclotron damping, the simplest of the heating mechanisms. The quasi-linear theory of Stix⁷ has been applied to explain the experiment and seems to fit fairly well.

Toroidal eigenmodes

As a consequence of the weak damping of the fast mode in a single species plasma, it is possible to excite and identify high-Q toroidal eigenmodes. By properly selecting the modes, it may be possible to peak the wave fields in the center of the device, thereby tailoring the heating profile. Toroidal modes have been seen in the ST² and PLT⁵ tokamaks but were not nearly so prominent in ATC⁴ and TFR.³ The probable reason is that the ion-ion hybrid resonance in these tokamaks was present with damping sufficient to wash out the toroidal eigenmodes.

Conclusions

The plasma density in EBT-S is not anticipated to be high enough to permit fast-mode heating whereas in EBT-P the fast mode should propagate. The technique of heating a minority hydrogen species

in a deuterium plasma that has been employed successfully in tokamaks may not be possible in EBT-P because of neutron activation problems in the uranium shielding. However, the cyclotron heating of a moderate fraction of hydrogen in a helium plasma in EBT-P is an attractive possibility.

In addition to the technological and experimental questions to be solved, there are several areas where theoretical work is necessary to assess the potential of fast-wave heating in EBT-P. Calculations should be done to predict the structure of toroidal modes in a segmented cavity with a strong variation in the magnetic field. The quasi-linear calculation of Stix⁷ should be extended to include the mirror field geometry. Also, for finite ion temperature (and a large minority species fraction), a linear turning point occurs on the low magnetic field side of the ion-ion resonance. Linear conversion to hot plasma modes occurs with both ion and electron damping.⁸ At this time the importance of these processes is not understood.

A.7.2.3 The Slow Wave

The slow wave is essentially a shear Alfvén wave at low frequencies that changes into an ion cyclotron wave near the cyclotron frequency. The dispersion relation for a single species cold plasma is¹

$$N_{\parallel}^2 = N^2 \cos^2 \theta = \frac{c^2}{V_A^2} (1 + \cos^2 \theta) \frac{\omega_{ci}^2}{\omega_{ci}^2 - \omega^2} \quad (\text{A.7.3})$$

In contrast to the fast wave, the slow wave has not received much attention recently. It was used more than ten years ago for early experiments on the B-65⁹ stellarator and the B-66¹⁰ mirror. This is the mode for which the concept of ion heating by waves breaking on a magnetic beach was developed.

The slow wave propagates at frequencies below the ion cyclotron frequency and is cut off at higher frequencies. In geometry such as that of EBT, where the magnetic field strength varies along the field lines, the wave propagates on the high field side of resonance (i.e., near the mirror coils) and is cut off on the low field side (i.e., near the midplane). As a slow-mode wave approaches the cyclotron resonant surface from the high field side, N_{\parallel} becomes very large, the group velocity turns parallel to the resonant surface, and the wave is strongly damped. The polarization is given by¹

$$E_x/E_y = i \frac{\omega_{ci}}{\omega} (1 + k_{\perp}^2/k_{\parallel}^2) . \quad (\text{A.7.4})$$

Therefore, the wave is predominantly left-circular polarized.

Because the refractive index of the slow mode is quite large ($N_{\parallel}^2 \sim c^2/V_A^2 = m_i/m_e \Omega_e^2/\omega_{pe}^2$), a high density is not required to "fit" the waves into the EBT cavity. Indeed, the slow mode should be usable on EBT-S as well as on EBT-P.

The boundary conditions for the wave fields can easily be satisfied for short parallel wavelengths (large N_{\parallel}). Several techniques exist for exciting waves with large N_{\parallel} , for example the use of Stix coils as antennas. Although the slow wave is evanescent in the low field region, in one relevant experiment the slow wave has been launched near the edge of a plasma column in a region of low magnetic field. Coupling to the high field region probably occurred in the boundary layer between the plasma and the wall.¹¹ For EBT-P it is difficult to put an antenna in the mirror throat. It may be possible to launch the slow wave with two coils in the midplane of adjacent cavities, adjusting N_{\parallel} by varying the phase of the two coils. This possibility can be tested on EBT-S.

Because of the strong damping, slow-wave toroidal eigenmodes do not exist, and one can expect appreciable ion heating even with weak coupling between the antenna and the region where the slow wave can propagate. Because of strong field gradients and relatively low density, the slow wave can be more efficient than the fast wave for EBT-P.

Multiple ion species

With two ion species the cold plasma dispersion relation is

$$N^2 = 1 - \frac{\omega_{pe}^2}{\omega\omega_{ce}} - \frac{\omega_{p1}^2}{\omega(\omega - \omega_{c1})} - \frac{\omega_{p2}^2}{(\omega - \omega_{c2})}, \quad (\text{A.7.5})$$

where the subscripts 1 and 2 refer to the two ion species.

This dispersion relation is plotted in Fig. A.7.6 for varying magnetic field and constant frequency $f = 60$ GHz. The electron density is $1.0 \times 10^{13} \text{ cm}^{-3}$, and the two species are H and He⁴ in equal concentration. Cyclotron resonance occurs at $B = 40$ kG for hydrogen and at 80 kG for doubly ionized helium. The cutoff region extends over the entire center portion of the plasma. Two antennas in phase with a spacing of 30 cm would excite waves with $N_{||} = 17$ by coupling to the plasma on the surface where $B = 43$ kG.

The second cutoff at $B = 48$ kG is caused by the admixture of helium. The region where the slow mode can propagate becomes narrower with increasing helium concentration. As a consequence, the contribution of the slow wave to ion heating is expected to be negligible when attempting the fundamental resonant heating of a small fraction of a minority species.

Conclusion

The slow wave should be more important for early ICRH experiments than it is for EBT-P. The propagation of this wave and its efficiency for ion heating should be carefully studied as an alternative to fast-wave heating because the density of the plasma is relatively low and the large variation in magnetic field is well suited for damping on a magnetic beach.

A.7.2.4 Antennas

Oscillators in this frequency range are readily available and relatively inexpensive. They may be located some tens of meters away from the machine, with the rf power carried in coaxial cables. A matching network is required for each antenna for a radiation resistance of the order $R \sim 0.1\text{-}0.5 \Omega$ and an inductive reactance $X_L \sim 100\text{-}200 \Omega$.

The fast-wave antennas currently used in tokamaks should be readily adaptable for use in EBT. Because the fast-wave antennas need not be located in the high field region, a simple water-cooled half-turn loop, located close to the wall at a cavity midplane, may suffice. There are a number of design problems associated with the antenna feedthrough insulators. First, the insulators must be shielded from direct exposure to plasma ultraviolet radiation. Second, careful placement will be required so that a cyclotron resonant surface of the 110-GHz microwave power does not come in contact with the insulator material. Finally, leakage of the microwave power through the insulator must be prevented either by a microwave choke structure or by a jacket of deionized water. Although Faraday shields may be necessary, bare antennas should be carefully considered because they are easier to fabricate and much less vulnerable to the plasma environment.

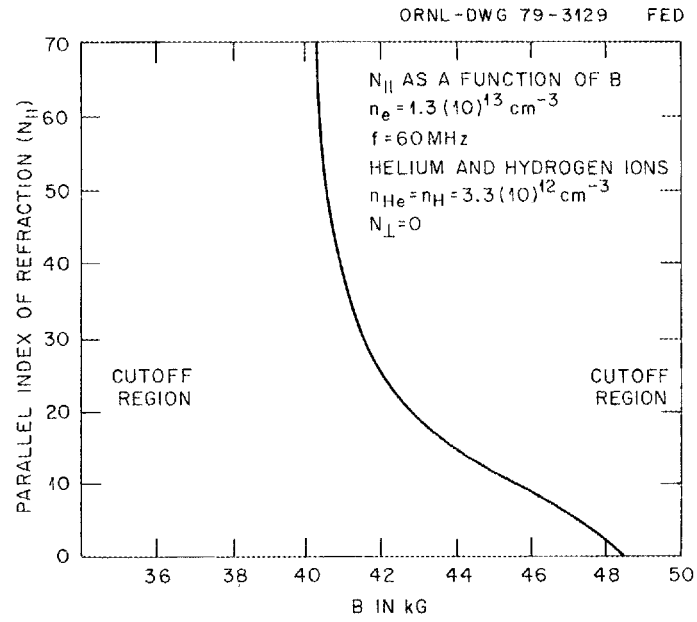


Fig. A.7.6. A plot of the dispersion relation for a varying magnetic field at a frequency of $f = 60 \text{ GHz}$.

In tokamaks these antennas are sometimes used in pairs, with a pair located in the same plane or spaced along the toroidal axis. For EBT-P a pair of antennas in adjacent cavities will provide some control on the spectrum in $N_{||}$. The half-turn loop will launch a wide spectrum of azimuthal modes.

The broad-band antennas for the fast wave may radiate useful amounts of the slow wave in EBT-P, with a strong magnetic field variation and relatively low density. To preferably excite the slow wave, a pair of single-loop antennas may be located in either end of a single cavity, where the magnetic field is large. It is probably not desirable to locate the antennas in the mirror throat but in a location where the metallic wall would shield the antenna from direct exposure to the hot plasma. It seems desirable to use a phased pair of single conductors rather than a Stix coil because extremely high $N_{||}$ is not required. These coils can encircle the plasma because the azimuthal mode number is not critical.

It is very important that antennas be fabricated and tested on EBT-I/S before the final design for EBT-P. More experimental information is critically needed, particularly data on the mode structure and heating mechanisms with relatively low density plasma. This testing can be done at low power levels, with relatively simple antenna structures and arrays of rf probes.

A.7.2.5 ICRH System Specifications

The ICRH system for EBT-P will evolve from the results of preliminary fast-wave experiments performed on EBT-P and from experiments on slow-wave heating on EBT-S. Initial experiments will be aimed at determining the optimum ICRH scheme and antenna design for plasma ion heating. One constraint regarding fast-wave minority species heating is that deuterium may not be usable in EBT-P.

In order to maintain a plasma equilibrium with an $n\tau \sim 10^{14}$ sec/cm⁻³ and a confinement time of ~ 1 sec, 300 kW of heating power is needed. Assuming a heating efficiency of only 20% (fast-wave heating under these conditions would approach 75%, according to ATC results¹²) an ICRH system delivering 1.5 MW and driving six antennas would be required. Because the technology of rf generation is well developed, lead times for procurement of the high power supplies are relatively short; therefore, the actual specification of power can await the initial results of heating efficiency measurements.

Initial experiments on slow-wave heating in a hydrogen plasma will be modeled after similar experiments on EBT-S. Access to the high field region is very limited, but antennas could be placed next to the mirror coil dewar. If experiments on EBT-S show that the slow wave can be launched efficiently in the low field region, then antennas can be placed in the center of cavity sections, where access is plentiful. Should the amount of power coupled to the plasma from one antenna be limited, up to 36 antennas (one per sector) could be used.

Fast-wave minority species heating experiments in a helium plasma with a minority concentration of hydrogen will be considered. Because of the higher density of EBT-P, several toroidal eigenmodes will fit in the machine whereas on EBT-S definitive fast-wave experiments are not possible.

The ICRH control system must be capable of dynamic feedback control because ICRH, ECH, and neutral beam systems may be operated simultaneously in a steady state. In particular, the interplay between ECH and ICRH systems is important. The ECH system will be used for plasma startup, and as the plasma density builds up, the ICRH system can be turned up. As the ion density and confinement time become longer, the ECH system may be turned down or adjusted so as to maintain only the hot electron ring. The relative amounts of the two types of heating will allow control of the plasma potential and, thus, of plasma confinement. Neutral beams and pellets may be used for fueling of the plasma in later phases of the EBT-P program; therefore, the ICRH system should be capable of fairly fast time response in order to maintain a steady-state equilibrium. Neutral beams may also be used for heating ions, so some

combination of ICRH minority species heating and neutral beam majority species heating may be used on gas mixtures.

A.7.3 NEUTRAL BEAMS FOR EBT

A.7.3.1 Introduction

This section of the appendix is a brief progress report of a recently begun, long-term study to determine the compatibility and possible configuration of particle beam heating in a steady-state, microwave-heated (ECH) EBT plasma. This section will include a rationale for the choice of neutral beam heating, a brief review of the accomplishments of a previous study, and the goals and status of the ongoing work. Because this effort is in its infancy, only preliminary results are available.

A.7.3.2 Rationale

The rationale for attempting to use particle beam heating, in particular neutral beam heating, is simple: Neutral beam heating is an effective, modestly efficient method for massive ion heating in tokamaks. The success in PLT is the obvious example.¹³ A cursory comparison of tokamaks and EBT from a geometrical point of view indicates that the EBT beam line energy can be significantly lower than that for a tokamak, and, consequently, technology already exists for pulsed injectors. However, it is not at all clear that such injectors are compatible with the EBT plasma. It must be demonstrated that a neutral beam injection system can effectively deliver the massive heat flux to the plasma in the microwave ECH environment of EBT. Furthermore, a lower beam energy implies a larger particle fluence for the same power. Again, it is not clear that this is compatible with the EBT plasma, particularly when long pulse or steady-state injection is called for.

A.7.3.3 Previous Work

An earlier study, completed for the EBT-II Conceptual Design Study,¹⁴ was an attempt to identify the problem areas. A target plasma conceivably attainable ($5 \times 10^{13} \text{ cm}^{-3}$) and a moderate beam energy (20 keV) were chosen to see what beam power was necessary to bring the plasma to a reactor-relevant regime. It was determined that 1 MW extracted and approximately 300 kW trapped would satisfy the goal. Problems of microwave isolation, particle control, realistic energy deposition and losses, and the steady-state nature of EBT were ignored, however.

A.7.3.4 Goal of the Present Study

The ultimate goal is an operational particle beam injection system on an EBT device compatible with all the nuances of an EBT plasma. The beam sources must either work in a microwave environment or be isolated from the microwave energy. Low energy, high fluence beams can easily swamp the vacuum system; therefore, particle control, possibly through a divertor, must be considered. In the short term, these systems are to be installed on EBT-I/S using ELMO as a test stand. Information learned in the short term should be applicable to later stages of EBT, e.g., EBT-P, although there is a danger in simply extrapolating because the microwave frequency increases dramatically from EBT-S (28 GHz) to EBT-P (110 GHz). A solution at 28 GHz may not work at 110 GHz. In any event, any solution will be reached only with a well-coordinated mix of theory, experiment, and development.

A.7.3.5 Status

Theory

Present theoretical effort is directed toward determining the injection geometry, the beam energy and power, and the beam deposition profile for an EBT-P device. For tokamaks, neutral beam heating has proven to be an effective method for auxiliary heating. It is described well by classical physics processes, and almost all of the deposited neutral beam power is actually absorbed by the plasma. Accordingly, we must consider neutral beam injection as a prime candidate for heating EBT-P.

The physics of an EBT is, of course, different from that of a tokamak, causing the regime of injection parameters to be different. Confinement in an EBT improves with aspect ratio instead of with minor radius as it does in a tokamak. Thus, for a given class of device, the minor radius in an EBT tends to be much smaller than in a tokamak. Furthermore, there is little tangential injection access in a large aspect ratio EBT because of the mirror coils. These two facts make the path length for beam absorption much less in an EBT than in a tokamak.

To alleviate this problem, there are several things that may be done in the design of an optimal injection system.

(1) Lower the beam energy: To increase the beam-trapping cross section, the injection energy can be lowered from the 40 keV typical of PLT and ISX to 20 keV. This is only of limited effectiveness, however, because in this energy range the total cross section for beam trapping goes roughly as $E^{-2/5}$. Lowering the energy also gives a modest gain in the neutralization efficiency of the beam line.

(2) Increase the plasma density: An increased density leads to improved trapping because the beam deposition goes as $\exp(-n_e \sigma_T \ell)$. For Stage I of EBT-P the density will probably be restricted to $\leq 3 \times 10^{13} \text{ cm}^{-3}$, which leads to a relatively thin target, $\bar{n} \leq 10^{15} \text{ cm}^{-2}$.

(3) Decrease the beam radius: Although the access port on EBT-P can be up to 15 cm in radius, a 15-cm beam gives a very flat beam deposition profile. Reducing the radius to 10 cm increases the normalized central fast ion density by 50%. However, this also reduces the power per source. If we assume that (1) $\sim 0.3 \text{ A/cm}^2$ is extracted from the source, (2) the grid transparency is 50%, (3) the beam line transmission efficiency is 70%, and (4) the neutralization efficiency is 80%, then we may also assume that a 20-keV beam will deliver about 530 kW to the plasma, assuming 100% beam absorption. A 15-cm source will deliver about 2.25 times the power of a 10-cm source, thus delivering more power on axis, but it also will deliver much more power to the edge.

To try to resolve these tradeoffs, we developed a new beam deposition code for vertical injection into EBT along the lines of Ref. 15. Because the injection direction is perpendicular to the B field, the fast ion orbits are almost circles characterized by their radius z . The circles are slightly nested inward so that the major radius of the center is a function of ρ , $R_C(\rho)$. Any function $R_C(\rho)$ can be used, but in this case we assumed that the *mod B* contours were subject to a $1/R$ shift so that $R_C(\rho) = \sqrt{R_0^2 - a^2 + \rho^2}$, where R_0 and a are the major and minor radii of the plasma in the midplane. Also, it was assumed that, in good agreement with the EBT-S experimental data, the density and temperature profiles were flat.

For the 36-coil EBT-P configuration, we used $R_0 = 560 \text{ cm}$ and $a = 23.2 \text{ cm}$ and injected the beam vertically down. The fast ion density is represented by a function $H(\rho)$, which is normalized so that the fraction absorbed = $\frac{1}{\text{volume}} \int H(\rho) d(\text{volume})$. Each deposition curve plots both $H(\rho)$ (squares) together with the above integral (circles) taken from the center to $\rho(0)$.

Figures A.7.7.-A.7.10 show $H(\rho)$ for a 10-cm, 20-keV beam for plasma densities of 1.7, 2.4, 3.0, and $5.0 \times 10^{13} \text{ cm}^{-3}$. The $n_e = 3 \times 10^{13} \text{ cm}^{-3}$ density is the highest expected in the first stage of EBT-P and yields only 70% beam absorption. The problem with this case is that 30% of the beam power is

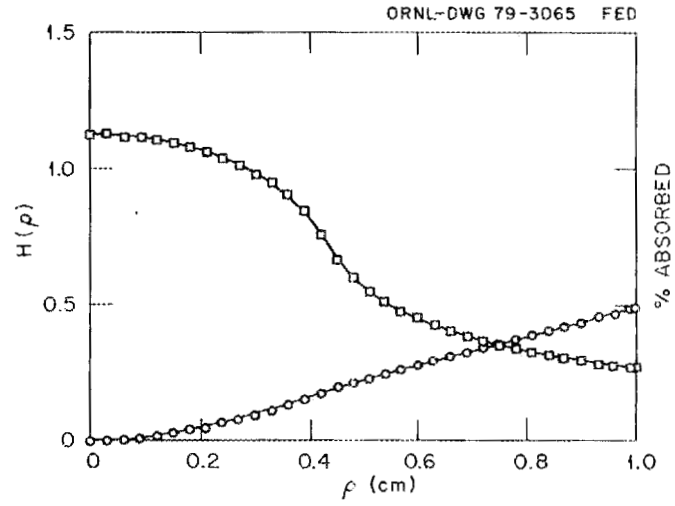


Fig. A.7.7. $H(\rho)$ and volume-integrated efficiency vs ρ for $n_e = 1.7 \times 10^{13} \text{ cm}^{-3}$, $E_B = 20 \text{ keV}$, $r_B = 10 \text{ cm}$, and $T_e = 3.5 \text{ keV}$; total absorbed = 49%.

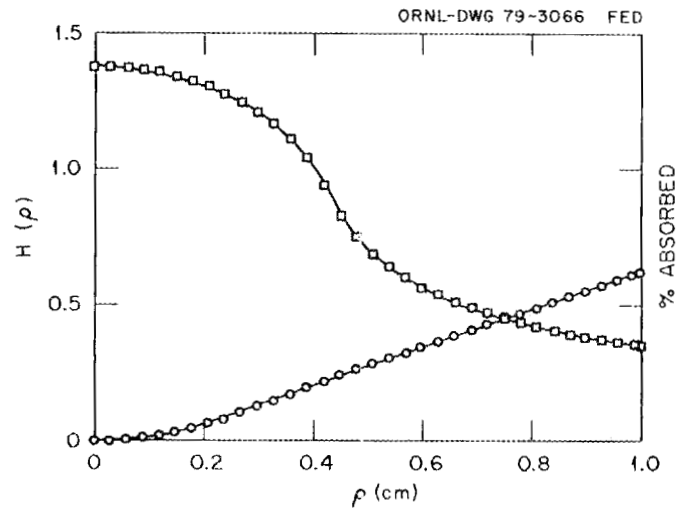


Fig. A.7.8. $H(\rho)$ and volume-integrated efficiency vs ρ for $n_e = 2.4 \times 10^{13} \text{ cm}^{-3}$, $E_B = 20 \text{ keV}$, $r_B = 10 \text{ cm}$, and $T_e = 4.1 \text{ keV}$; total absorbed = 61%.

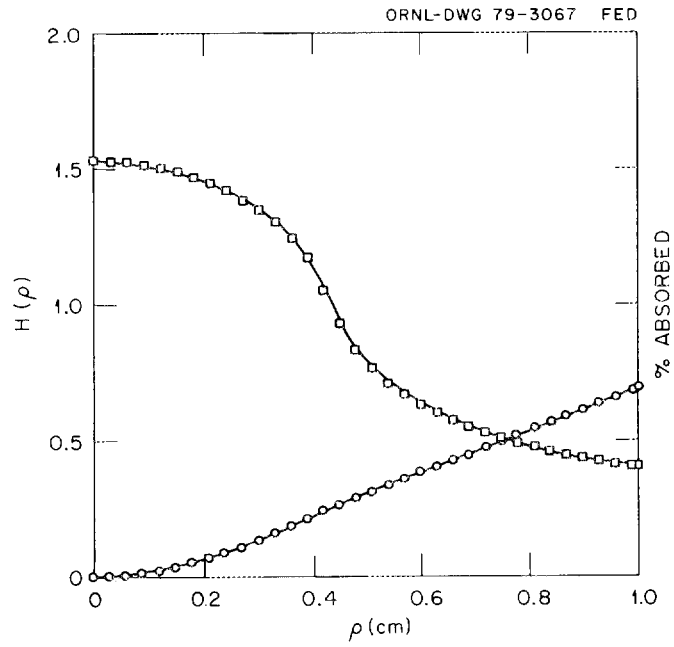


Fig. A.7.9. $H(\rho)$ and volume-integrated efficiency vs ρ for $n_e = 3 \times 10^{13} \text{ cm}^{-3}$, $E_B = 20 \text{ keV}$, $r_B = 10 \text{ cm}$, and $T_e = 4.4 \text{ keV}$; total absorbed = 69%.

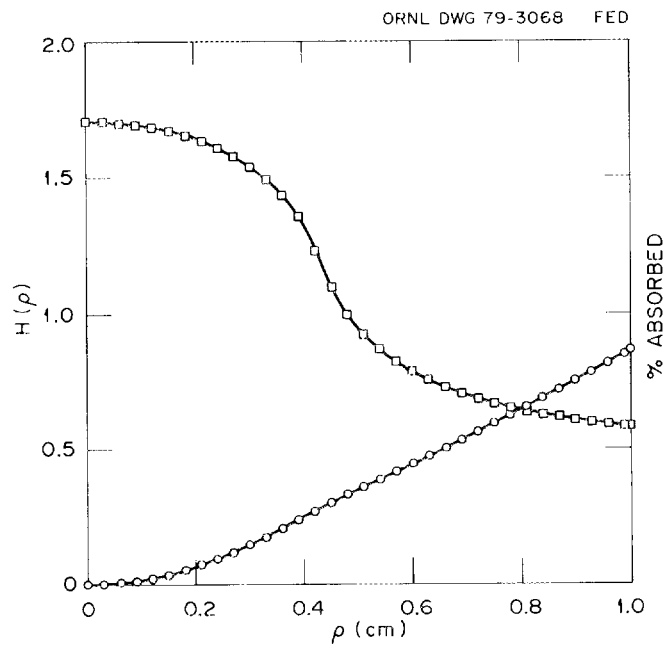


Fig. A.7.10. $H(\rho)$ and volume-integrated efficiency vs ρ for $n_e = 5 \times 10^{13} \text{ cm}^{-3}$, $E_B = 20 \text{ keV}$, $r_B = 10 \text{ cm}$, and $T_e = 4.4 \text{ keV}$; total absorbed = 86%.

wasted and that it must be handled by a beam dump, a severe and possibly costly engineering problem. A density of 10^{14} cm^{-3} is needed to completely absorb the beam.

Figure A.7.11 shows the effect of a larger beam radius (15 cm) on $H(\rho)$ for the $3 \times 10^{13} \text{ cm}^{-3}$ case. As a general rule, the deposition profile is flat from the center out to the beam radius, as can be seen clearly in this plot. The deposition profile is quite broad, and slightly less of the beam is absorbed than for the 10-cm case.

Finally, we examined the effect of lowering the beam energy to 15 keV and 10 keV, as seen in Figs. A.7.12 and A.7.13. Halving the beam energy gives only a 10% increase in beam absorption, as expected, so that this is not a good course to take.

If the low beam absorption problem can be solved, a proper Fokker-Planck calculation for EBT that includes the fast particle loss regions must also be done. Although this can lead to further heating inefficiency, it will probably not be intolerable.

Experiment

Experimental work with microwave compatibility and particle control can presently be done on two machines, ELMO and EBT-I/S. A gas puffing and a gas-flow matching experiment¹⁶ has been done on EBT-I to test the EBT plasma tolerance to massive, pulsed cold gas fluences and the disruptive influence such pulses have on microwave power flow. Flow-matching experiments with and without plasma have given preliminary indications of the particle-handling capabilities of the EBT-I machine ($\sim 100 \text{ mA}$ under typical T-mode conditions). The gas puffing experiment indicated that cold gas pulses up to 7 A equivalent for 0.5 sec are tolerated by the EBT plasma. To be sure, plasma parameters do degrade because the 7-A pulse pushed the plasma into C-mode. However, when the pulse ended, the plasma recovered and there were no massive disruptions during the experiment. The next step will be the installation of a low fluence, 20-keV diagnostic neutral beam with the intention of obtaining spatially resolved ion temperatures. Microwave compatibility will apply only to EBT-I/S, however. Finally, a lower energy ($\sim 5 \text{ keV}$), modest fluence ($\sim 1 \text{ A}$) beam will be installed on ELMO and then on EBT-I/S to test both microwave compatibility and utility of particle control. Again, microwave compatibility can be demonstrated for the highest frequency available, which in this case is 28 GHz. Particle control will be achieved initially through pulse length; however, as the pulse length becomes longer, a divertor will be required.

Development

Massive, pulsed heating beams exist; however, providing steady-state neutral beam heating power in a microwave ECH environment is another question. Initially such beams will have to be developed for EBT-I/S ($\sim 5 \text{ kV}$, 1 A) and scaled up to EBT-P ($\sim 20 \text{ kV}$, 10 A) and beyond. At these power levels and steady-state operation, the question of pumping and particle control arises. It must be remembered that the stable operation of EBT is very sensitive to the particle inventory. Aside from adding massive cryopumps (where compatibility with high power microwave fluence is presently unknown), a conceivable method of particle control is through a divertor. DITE and the Poloidal Divertor Experiment (PDX) are only beginning to examine divertors on tokamaks, and their utility on an EBT device must also be examined. Plans call for this to be done initially on EBT-I/S and later on an upgraded version of EBT-P.

A.7.4 FORCED-FLOW CRYOGENIC SYSTEM

An alternate concept for the mirror coils is to use a forced-flow rather than a pool-boiling-type conductor. This has an impact on the refrigerator design and on the cryogenic distribution system. A schematic that illustrates this system is shown in Fig. A.7.14.

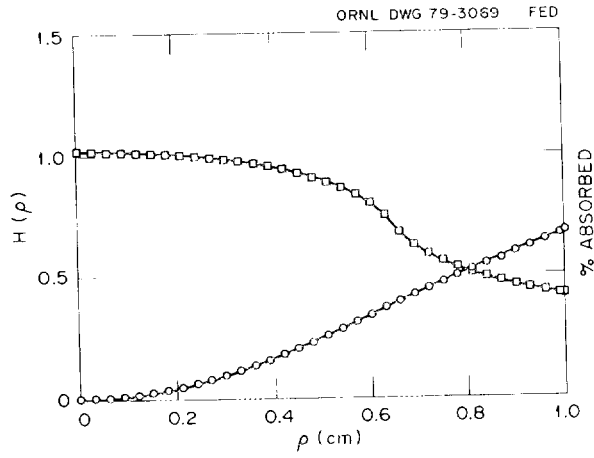


Fig. A.7.11. $H(\rho)$ and volume-integrated efficiency vs ρ for $n_e = 3 \times 10^{13} \text{ cm}^{-3}$, $E_B = 20 \text{ keV}$, $r_B = 15 \text{ cm}$, and $T_e = 4.4 \text{ keV}$; total absorbed = 68%.

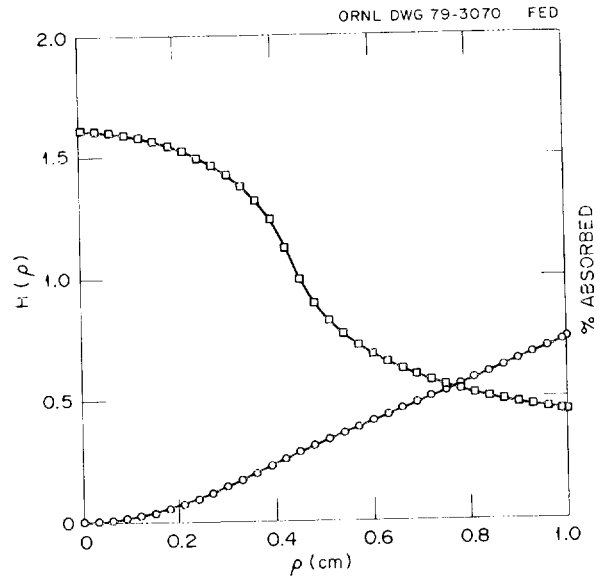


Fig. A.7.12. $H(\rho)$ and volume-integrated efficiency vs ρ for $n_e = 3 \times 10^{13} \text{ cm}^{-3}$, $E_B = 15 \text{ keV}$, $r_B = 10 \text{ cm}$, and $T_e = 4.4 \text{ keV}$; total absorbed = 75%.

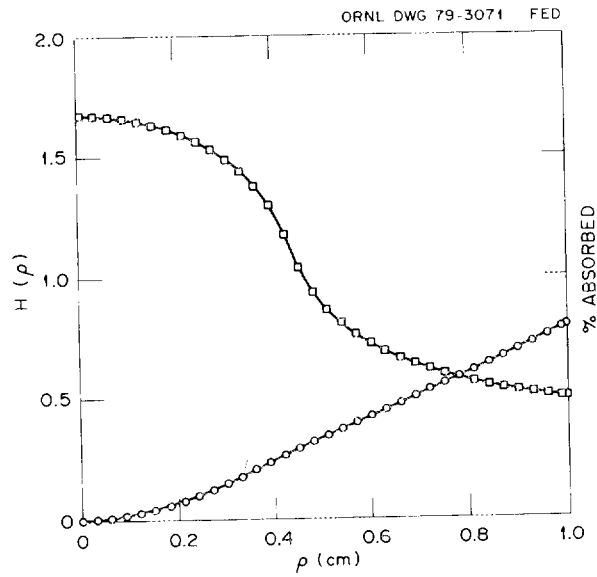


Fig. A.7.13. $H(\rho)$ and volume-integrated efficiency vs ρ for $n_e = 3 \times 10^{13} \text{ cm}^{-3}$, $E_B = 10 \text{ keV}$, $r_B = 10 \text{ cm}$, and $T_e = 4.4 \text{ keV}$; total absorbed = 80%.

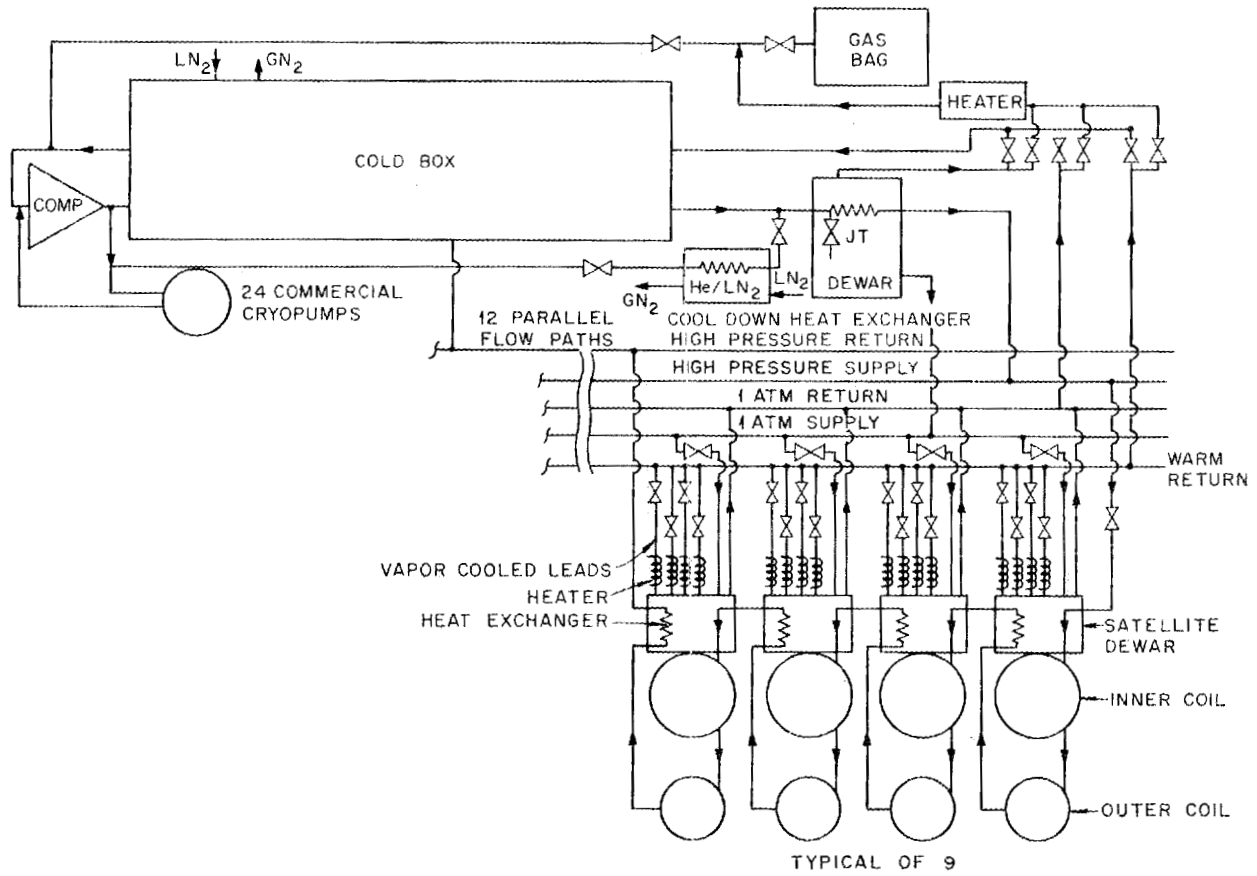


Fig. A.7.14. EBT-P forced-flow helium schematic.

The fundamental difference between a pool-boiling magnet system and a forced-flow magnet system is the addition of high pressure flow lines. The coils are set up to run in 12 parallel paths of 4 coils per path (see schematic) with a flow rate of 5 g/sec in each of the 12 paths. This means that in addition to the high pressure supply (15 atm) and return (9 atm) headers, extra plumbing is required to connect the 4 series coils. Also, a simple heat exchanger is required in each lead dewar to ensure that cold helium is provided to each coil.

All of the components discussed in Sect. 11.4.5.3 are still required in a forced-flow system. One-atm liquid is required to provide cooling for the leads and heat exchanger; structural supports and plasma radiation heating loads are also removed by the 1-atm fluid. The gyrotron magnets still have the same set of requirements as in the pool-boiling design.

The extra plumbing adds an additional 675 W to the required refrigerator capacity. It also complicates the thermodynamic cycle of the refrigerator because the refrigerator must still provide liquid helium at 1 atm as well as providing 15-atm supercritical helium. These additions result in increased capital costs and operating costs as well as increased complexity of operation that reduces the reliability of the cryogenic system.

REFERENCES

1. T. H. Stix, *The Theory of Plasma Waves*, McGraw-Hill, New York, 1962.
2. J. C. Hosea and W. M. Hooke, *Phys. Rev. Lett.* 31, 150 (1973).
3. *Equipe TFR Proc. 3rd Int. Meeting on Theoretical and Experimental Aspects of Heating of Toroidal Plasmas*, Vol. I, p. 87 (1976).
4. H. Takahashi et al., *Phys. Rev. Lett.* 39, 31 (1977).
5. J. Hosea et al., Princeton Plasma Physics Laboratory Report PPPL-1554, Princeton, New Jersey (1979).
6. F. J. Paolini, *Phys. Fluids* 18, 640 (1975).
7. T. H. Stix, *Nucl. Fusion* 15, 737 (1975).
8. R. Perkins, *Nucl. Fusion* 17, 1197 (1977).
9. T. H. Stix and T. W. Palladino, *Phys. Fluids* 3, 641 (1960).
10. J. M. Hooke et al., *Phys. Fluids* 8, 1146 (1965).
11. T. H. White, "High Power Ion Cyclotron Resonance Heating in a Multiple Mirror Machine," dissertation, University of Texas, 1976.
12. H. Takahashi, Princeton Plasma Physics Laboratory Report PPPL-1545, Princeton, New Jersey (1979).
13. H. Eubank et al., *Phys. Rev. Lett.* 43, 270 (1979).
14. R. A. Dandl et al., Oak Ridge National Laboratory Report ORNL/TM-5955, Oak Ridge, Tennessee (1978).
15. J. A. Rome, J. D. Callen, and J. F. Clarke, *Nucl. Fusion* 14, 141 (1974).
16. K. H. Carpenter and J. C. Glowienka, "Gas Injection in EBT-S for Assessment of Particle Loading Effects of Neutral Beam Injection," paper 2S3 presented at the 1979 IEEE Int. Conf. on Plasma Science, Montreal, Canada, June 4-6, 1979.

A.8 TEN-YEAR EBT PROGRAM — FY 1980-89

A.8.1 EBT HIERARCHY

Studies have continued on the long-term EBT program to define more clearly a logical sequence of devices that would provide the information base for a demonstration EBT reactor. At the moment, the program is based upon a sequence of devices operating one at a time with upgrades to enable them to test the critical issues in a systematic fashion. The devices and their basic parameters are given in Table A.8.1. There are, in essence, three devices, each of which is upgraded.

- (1) EBT-1 → EBT-S → EBT-SA1 → EBT-SA2
- (2) EBT-P1 → EBT-PU
- (3) EBT-Q(H) → EBT-Q(DT)

The contributions expected of EBT-S and EBT-P and the time frame are indicated, for the present logic, in Table A.8.2. The vertical arrows indicate when information should be available for a future device. The main features of each upgrade are discussed below.

- (1) EBT-1 → EBT-S (R = 1.5 m)
 - Raise frequency from 18 GHz → 28 GHz
 - Raise power from 60 kW → ≤200 kW
 - Add ion cyclotron heating (ICH)
- (2) EBT-S → EBT-SA1 (R = 1.5 m)
 - Add aspect ratio enhancement (ARE) coils
- (3) EBT-SA1 → EBT-SA2 (R = 1.5 m)
 - Add a divertor
 - Add long pulse neutral injection
 - Add more ECH power, >200 kW
- (4) EBT-SA2 → EBT-P1 (R = 5.6 m)
 - Construct a larger device
 - Raise frequency to 110 GHz
 - Raise power to 1.8 MW
 - Raise ICH power
- (5) EBT-P1 → EBT-PU (various upgrades are possible)
 - Add ARE coils
 - Add a divertor
 - Add long pulse neutral beam
 - Increase number of cavities, 36 → 48 (R = 7.4 m)
- (6) EBT-PU → EBT-Q(H) (R = 16.8 m)
 - Construct a larger device operating in hydrogen
- (7) EBT-Q(H) → EBT-Q(D-T) (R = 16.8 m)
 - Operate in D-T with $Q \sim 4$

EBT-Q(D-T) is a device similar to the Tokamak Fusion Test Reactor (TFTR) operating in D-T with $Q = \frac{\text{fusion power}}{\text{power to plasma}} \sim 4$. This device is, however, closer to an ETF by virtue of its anticipated steady-state operation, with an impurity control system, at an average neutron flux $\sim 20 \text{ W cm}^{-2}$.

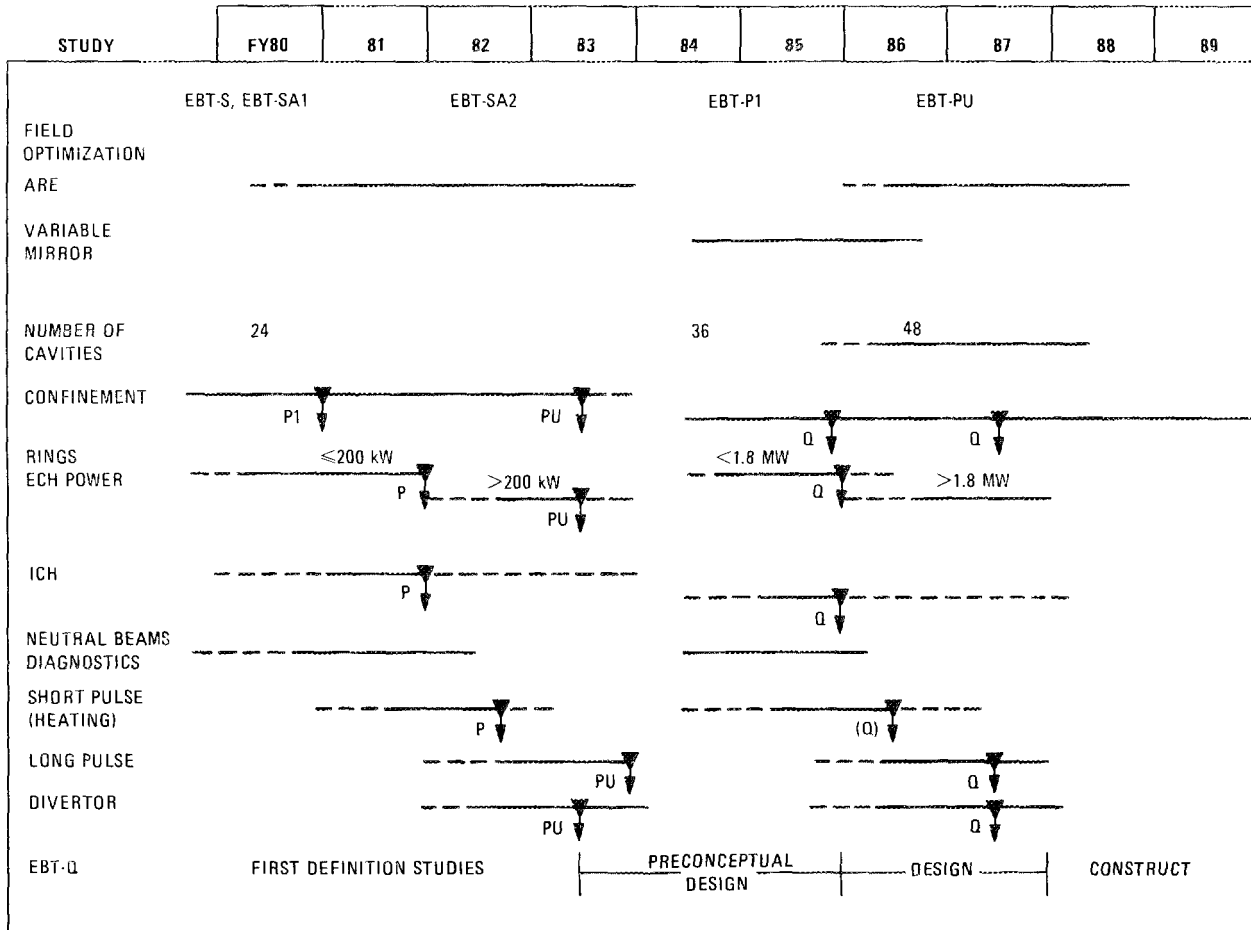
It is intended that each device use in upgrades the advances made in the previous device. This strategy appears possible because of the modular nature of the EBT.

Table A.8.1 Hierarchy of EBT's

| | EBT-1 | EBT-S | EBT-SA | EBT-P1 | EBT-PU | EBT-Q |
|---------------------------|--------------------|--------------------|--------------------|----------------------|----------------------|----------------------|
| B_{res} (kG) | 6.4 | 10.0 | 10.0 | ≤ 39.3 | ≤ 39.3 | 39.3 |
| R (m) | 1.5 | 1.5 | 1.5 | 5.6 | 7.4 | 17.0 |
| f_{ARE} | 1.0 | 1.0 | 1.3 | 1.2 | 2.0 | 3.0 |
| A_{SP} | 8 | 8 | 8 | 16 | 21 | 14 |
| A_{mir} (cm) | 10 | 10 | 10 | 16 | 16 | 45 |
| A_{mid} (cm) | 14 | 14 | 14 | 22 | 22 | 66 |
| N_{coils} | 24 | 24 | 24 | 36 | 48 | 36 |
| n (cm^{-3}) | 2×10^{12} | 6×10^{12} | 6×10^{12} | 1.6×10^{13} | 6.6×10^{13} | 7.8×10^{13} |
| T_e (keV) | 0.3 | 0.6 | 0.8 | 1.9 | 3.3 | 15.3 |
| $n\tau$ (cm^{-3}/sec) | 1×10^{10} | 3×10^{10} | 8×10^{10} | 9×10^{11} | 1×10^{13} | 1×10^{14} |

ORNL-DWG 79-3155 FED

Table A.8.2. EBT schedule - FY 1980/89.



A.8.2 SCHEDULE

The devices discussed above are intended to tackle in a systematic way the critical issues of the EBT program. The schedule indicated in Table A.8.2 is determined to some extent by the time required in each area to complete the research and in part by budget restrictions that will delay the application of possible upgrades.

(1) The confinement studies in EBT-1/S/SA are intended to verify the theoretical models used in establishing the EBT program for EBT-P. This work will be continued in EBT-P, which will demonstrate under proof-of-principle conditions ($n \geq 10^{13} \text{ cm}^{-3}$, $T_i \geq 1 \text{ keV}$) the validity of the theory. In addition, EBT-P will study optimization questions relating to the magnetic configuration, mirror ratio, ARE coils, and number of cavities. By the end of FY 1985, this work should provide the basis for sizing EBT-Q and for making a decision to proceed on detailed design. The upgrades through FY 1987 should provide confirmation of design judgments.

(2) Studies of the production and physics of the hot electron ring using increased power and frequency in EBT-1/S should establish the basis for assessing ring power needs in future devices. By the end of FY 1985, EBT-P will provide confirmation of these assessments for the design of EBT-Q.

(3) Studies of ECH, ICH, and neutral beam heating in EBT-S should lay the groundwork for their application in EBT-P. It should be understood that in the case of neutral beams, long pulse, high power injection is not possible without a divertor because of excessive density buildup. Further, neutral injection has limited application in EBT-S because of its low line density. Information for EBT-Q design in the areas of ECH and ICH can be expected by the end of FY 1985, but definitive information on neutral beam heating should not be expected until at least FY 1986/87.

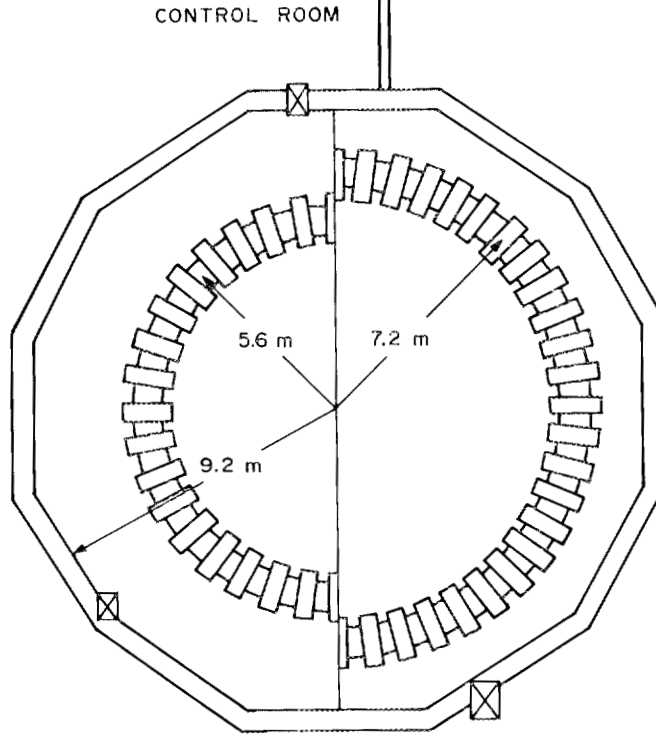
(4) Divertor studies on EBT-S are expected in FY 1982. The design of the divertor for EBT-P could be started earlier; however, confirmation of the effectiveness of the design cannot be expected until FY 1983. Thus, operation of a divertor, given that it could not be installed in EBT-P1, is unlikely before FY 1986.

Thus, the program represents a prudently staged approach to tackling the central issues; only in terms of upgrading EBT-P is there a budgeting problem that could lead to delays of valuable studies.

A.8.3 THE 48 CAVITIES -- EBT-PU

The full upgraded version of EBT-PU is proposed to have 48 cavities, ARE coils, and substantial additional heating. On the basis of the present theoretical models and scaling from EBT-1, it should be capable of achieving $T \geq 3 \text{ keV}$ and $n_e \geq 1 \times 10^{13} \text{ cm}^{-3}$.

The layout of the EBT-P area is planned to accommodate this upgrade, as illustrated in Fig. A.8.1.



BLDG. 9201-2

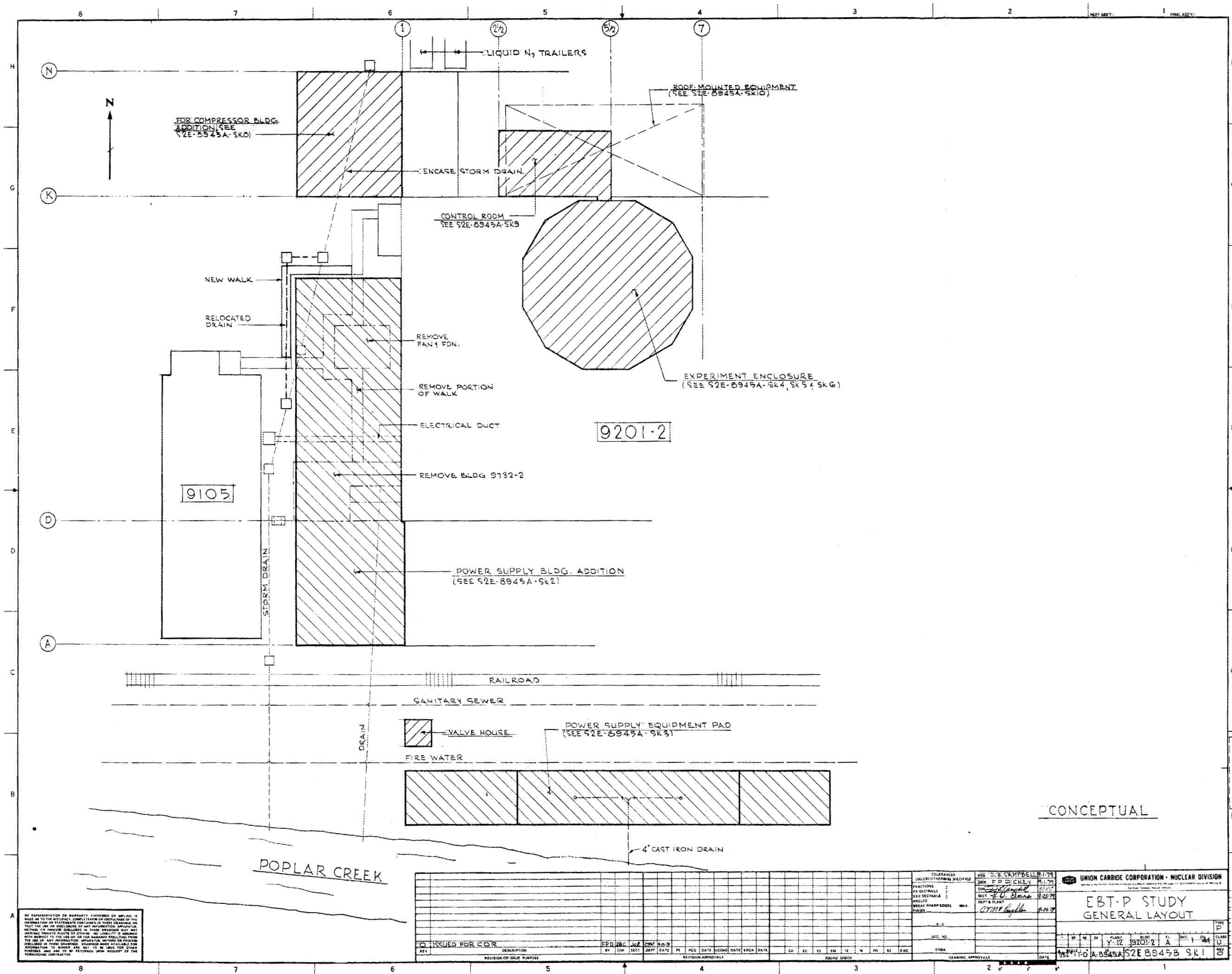
Fig. A.8.1. EBT-P accommodations for expansion.

A.9 DRAWINGS

Engineering drawings prepared for EBT-P are included in this section. A drawing list follows:

| Drawing number | Drawing title | Series number |
|----------------------------|---|---------------|
| Civil | | |
| S2E-8945B-SK1 | EBT-P Study General Layout | 1 |
| S2E-8945A-SK4 | EBT-P Study Experiment Enclosure <u>2nd</u> Fl. | 2 |
| S2E-8945A-SK5 | EBT-P Study Experiment Enclosure Mezz. Fl. | 3 |
| S2E-8945A-SK6 | EBT-P Study Experiment Enclosure <u>1st</u> Fl. | 4 |
| S2E-8945A-SK7 | EBT-P Study Experiment Enclosure Section | 5 |
| S2E-8945A-SK9 | EBT-P Study Control Room | 6 |
| S2E-8945A-SK2 | EBT-P Study Power Supply Bldg. Addition | 7 |
| S2E-8945A-SK3 | EBT-P Study Power Supply Equipment Pad | 8 |
| S2E-8945A-SK8 | EBT-P Study Compressor Bldg. Addition | 9 |
| S2E-8945A-SK10 | EBT-P Study Roof Equipment Plan | 10 |
| Mechanical | | |
| X2E-14270-0003 | EBT-P Device Plan View | 11 |
| X2D-14270-0001 | Vacuum System Schematic | 12 |
| X2E-14270-0004 | Section Elevation through Mirror Cavity | 13 |
| X2E-14270-0005 | Mirror Coil Vacuum System Dewar Assembly | 14 |
| X2E-14270-0006 | Mirror Coil Vacuum Dewar Sections | 15 |
| X2E-14270-0007 | Mirror Coil Vacuum Dewar Sections | 16 |
| X2E-14270-0010 | ARE Coil Option-Location Layout | 17 |
| X2E-14270-0011 (1 of 2) | EBT-P Toroidal Vacuum Vessel Details | 18 |
| X2E-14270-0011 (2 of 2) | EBT-P Toroidal Vacuum Vessel Details | 19 |
| X2D-14270-0002 | Microwave Distribution Manifold | 20 |
| X2E-14270-0009 | Gyrotron Mount | 21 |
| Piping | | |
| X2E-14270-0008 (1 of 2) | EBT-P Equipment Location Layout | 22 |
| X2E-14270-0008 (2 of 2) | EBT-P Equipment Location Layout | 23 |
| P2D-57700-0001 | EBT-P Demineralized Water Flow Sheet | 24 |
| P2D-57681-0001 | EBT-P Cryogenic and Helium Flow Sheet | 25 |
| P2E-95306-0001 | EBT-P Helium Refrigerator Equipment Location | 26 |
| HVAC | | |
| H2E-34110-SK01 | EBT-P Study-HVAC Plan | 27 |
| H2E-34111-SK02 | EBT-P Study-HVAC Plan | 28 |
| H2E-34112-SK03 | EBT-P Study-HVAC Plan | 29 |

| Drawing number | Drawing title | Series number |
|-----------------|--|---------------|
| Electrical | | |
| E2E-34108-SK001 | EBT-P Primary Power System 13.8-kV One-Line Diagram | 30 |
| E2E-34109-SK002 | EBT-P Primary Power System Plan 161-13.8-kV System | 31 |
| E2E-14270-0001 | EBT-P Electrical One-Line Diagram | 32 |
| E2E-14270-0002 | Preliminary Proposal for Locating EBT-P Power Supplies | 33 |
| E2E-14270-0003 | EBT-P Mirror and Trim Coil Power Supply and Energy Dump Schematic Diagram | 34 |
| E2E-14270-0004 | EBT-P Power Supplies Layout Sheet 1 | 35 |
| E2E-14270-0005 | EBT-P Power Supplies Layout Sheet 2 | 36 |
| Instrumentation | | |
| I2E-14270-A006 | EBT-P Control Room Layout | 37 |
| I2E-14270-A010 | EBT-P System Instrumentation Block Diagram | 38 |
| I2E-14270-A007 | EBT-P Cryogenic System Instrumentation Process and Instrumentation Diagram | 39 |
| I2E-14270-A008 | EBT-P Vacuum Process and Instrumentation Diagram | 40 |
| I2E-14270-A005 | EBT-P Typical Instrumentation Flow Diagram | 41 |
| I2E-14270-A009 | EBT-P System Magnet Protection Instrumentation, Voltage Taps | 42 |
| I2E-14270-SK01 | EBT-P Microwave Monitor and Control System | 43 |
| I2E-14270-SK02 | Microwave Alarm and Sensor Plan | 44 |



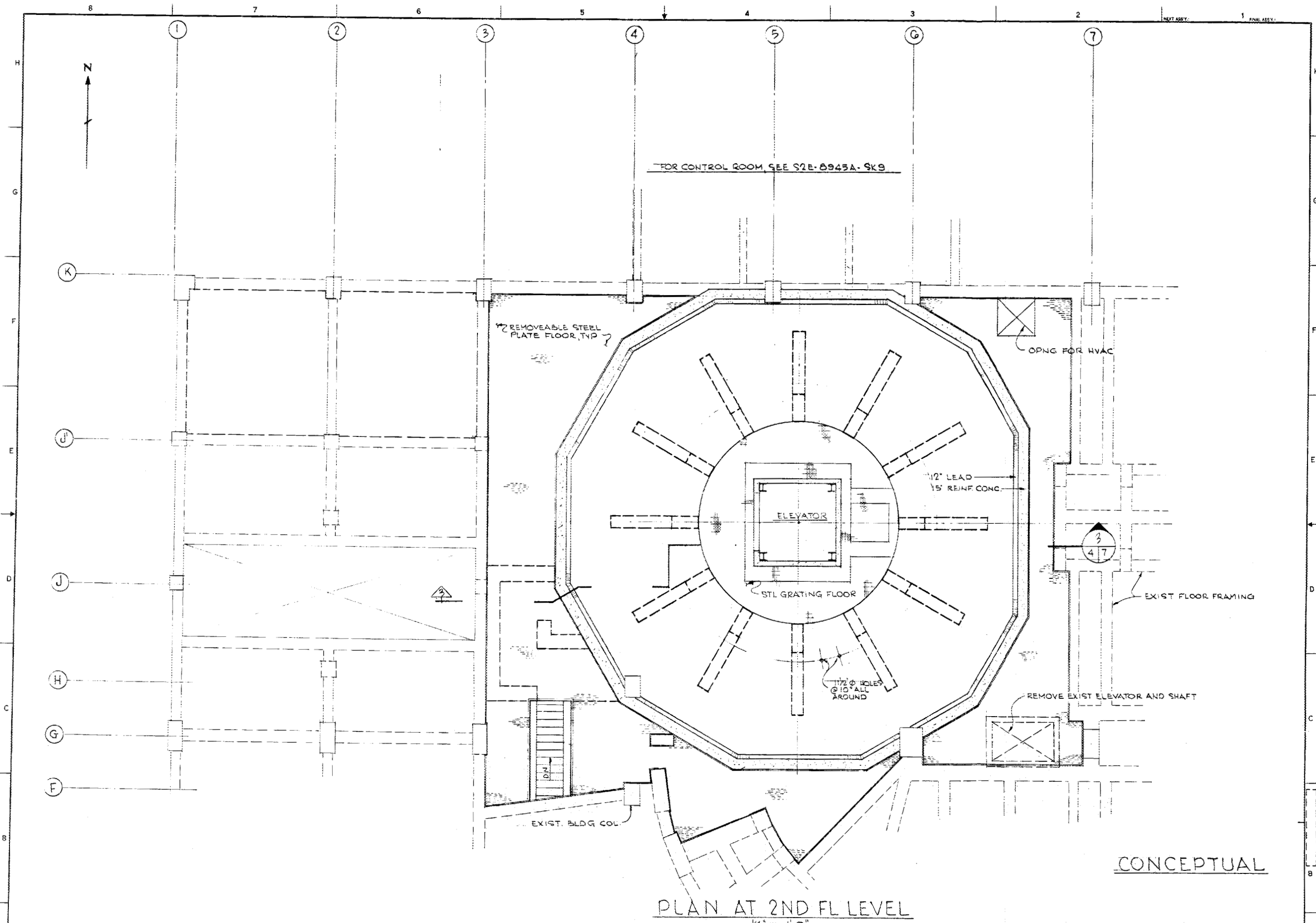
CONCEPTUAL

POPLAR CREEK

NO REPRESENTATION OR WARRANTY EXPRESSED OR IMPLIED IS MADE AS TO THE ACCURACY, COMPLETENESS OR USEFULNESS OF THE INFORMATION OR STATEMENTS CONTAINED IN THESE DRAWINGS OR ANY PART THEREOF. THE USER OF THESE DRAWINGS SHALL BE RESPONSIBLE FOR THE USE OF ANY INFORMATION OBTAINED FROM THESE DRAWINGS IN THE DESIGN, CONSTRUCTION, OPERATION, MAINTENANCE, REPAIR OR REPAIR OF ANY EQUIPMENT OR SYSTEM. THE USER SHALL BE RESPONSIBLE FOR THE USE OF ANY INFORMATION OBTAINED FROM THESE DRAWINGS IN THE DESIGN, CONSTRUCTION, OPERATION, MAINTENANCE, REPAIR OR REPAIR OF ANY EQUIPMENT OR SYSTEM. THE USER SHALL BE RESPONSIBLE FOR THE USE OF ANY INFORMATION OBTAINED FROM THESE DRAWINGS IN THE DESIGN, CONSTRUCTION, OPERATION, MAINTENANCE, REPAIR OR REPAIR OF ANY EQUIPMENT OR SYSTEM.

| REV. | DESCRIPTION | BY | CHK | DATE | REVISED DATE | ISSUED DATE | CA | EC | ES | SM | TE | W | NO | ES | PLAS |
|------|-----------------|----|-----|------|--------------|-------------|----|----|----|----|----|---|----|----|------|
| 0 | ISSUED FOR COR. | | | | | | | | | | | | | | |

| | |
|--|-----------------------|
| UNION CARBIDE CORPORATION - NUCLEAR DIVISION | |
| EBT-P STUDY GENERAL LAYOUT | |
| DATE: 10/12/54 | SCALE: 1/8" = 1'-0" |
| PROJECT: A-8945A | DWG NO: S2E-8945B-SK1 |



NO REPRESENTATION OR WARRANTY EXPRESSED OR IMPLIED IS MADE AS TO THE ACCURACY, COMPLETENESS OR USEFULNESS OF THE INFORMATION OR DATA CONTAINED IN THESE DRAWINGS. THE USER OF THESE DRAWINGS SHALL BE RESPONSIBLE FOR OBTAINING ALL NECESSARY PERMITS AND FOR VERIFYING THE ACCURACY OF ALL INFORMATION AND DATA. THE USER OF THESE DRAWINGS SHALL BE RESPONSIBLE FOR OBTAINING ALL NECESSARY PERMITS AND FOR VERIFYING THE ACCURACY OF ALL INFORMATION AND DATA. THE USER OF THESE DRAWINGS SHALL BE RESPONSIBLE FOR OBTAINING ALL NECESSARY PERMITS AND FOR VERIFYING THE ACCURACY OF ALL INFORMATION AND DATA.

| REV | DESCRIPTION | BY | CHK | DATE |
|-----|-------------|----|-----|------|------|------|------|------|------|------|------|------|------|------|------|------|------|------|------|
| | | | | | | | | | | | | | | | | | | | |

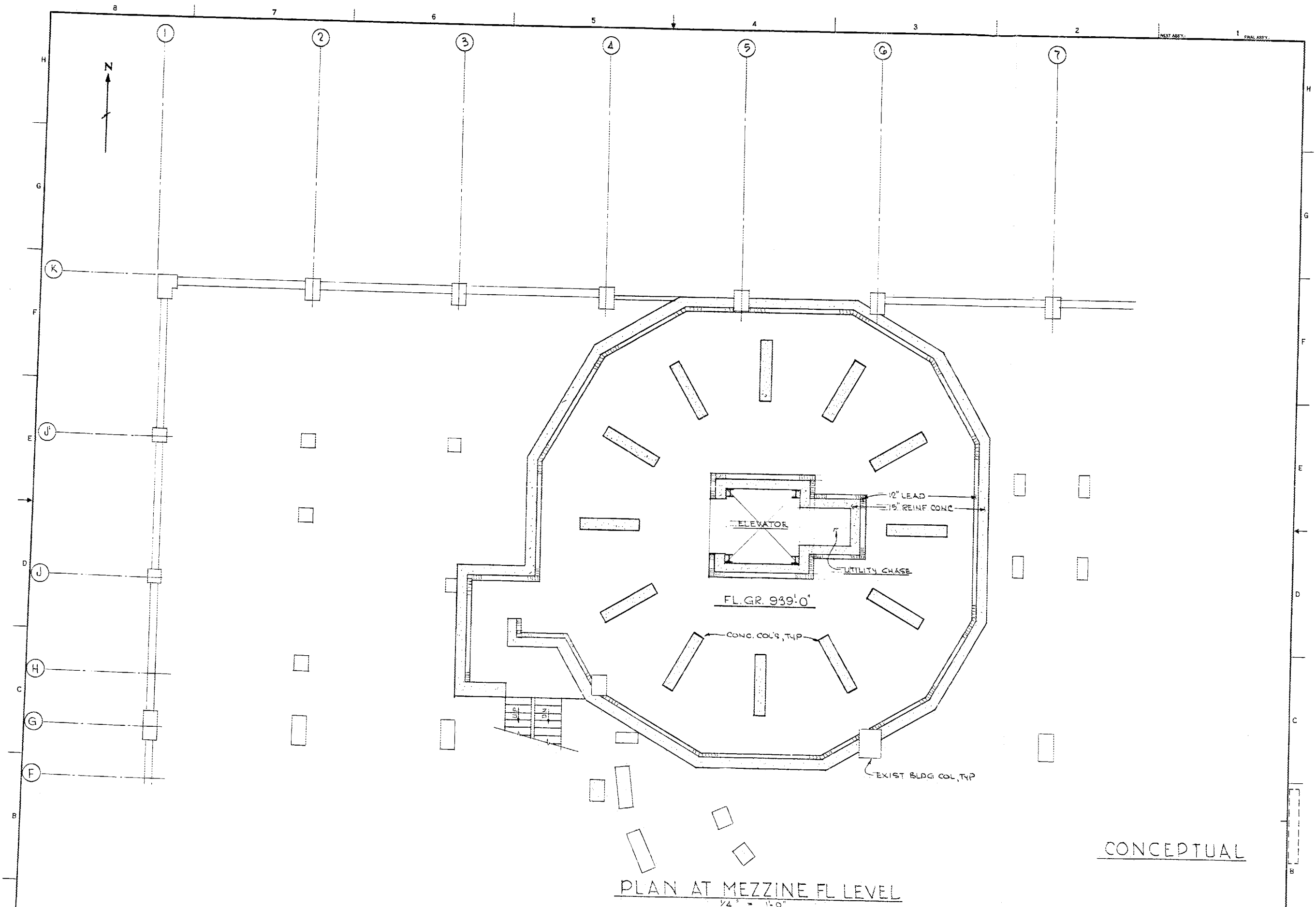
| | | |
|----------------------------|---------------------|------------|
| UNLESS OTHERWISE SPECIFIED | DES. D. B. CAMPBELL | DATE 11-77 |
| FRACCTIONS | DRN. P. DICKEN | DATE 11-77 |
| OF DECIMALS | CHK. J. B. BROWN | DATE 11-77 |
| SAVE DECIMALS | SEC. J. B. BROWN | DATE 11-77 |
| ANGLES | DEPT. & ANT. | DATE 11-77 |
| BREAK SHARP EDGES | MAX. | DATE 11-77 |
| FINISH | DATE 11-77 | DATE 11-77 |
| A. E. | DATE 11-77 | DATE 11-77 |
| UCC NO. | DATE 11-77 | DATE 11-77 |
| IND. | DATE 11-77 | DATE 11-77 |
| DRAWING APPROVALS | DATE 11-77 | DATE 11-77 |

UNION CARBIDE CORPORATION - NUCLEAR DIVISION

EBT-P STUDY

EXPERIMENT ENCLOSURE - 2ND FL.

AS SHOWN A-8945A S2E 8945A SK4



CONCEPTUAL

PLAN AT MEZZINE FL LEVEL
1/4" = 1'-0"

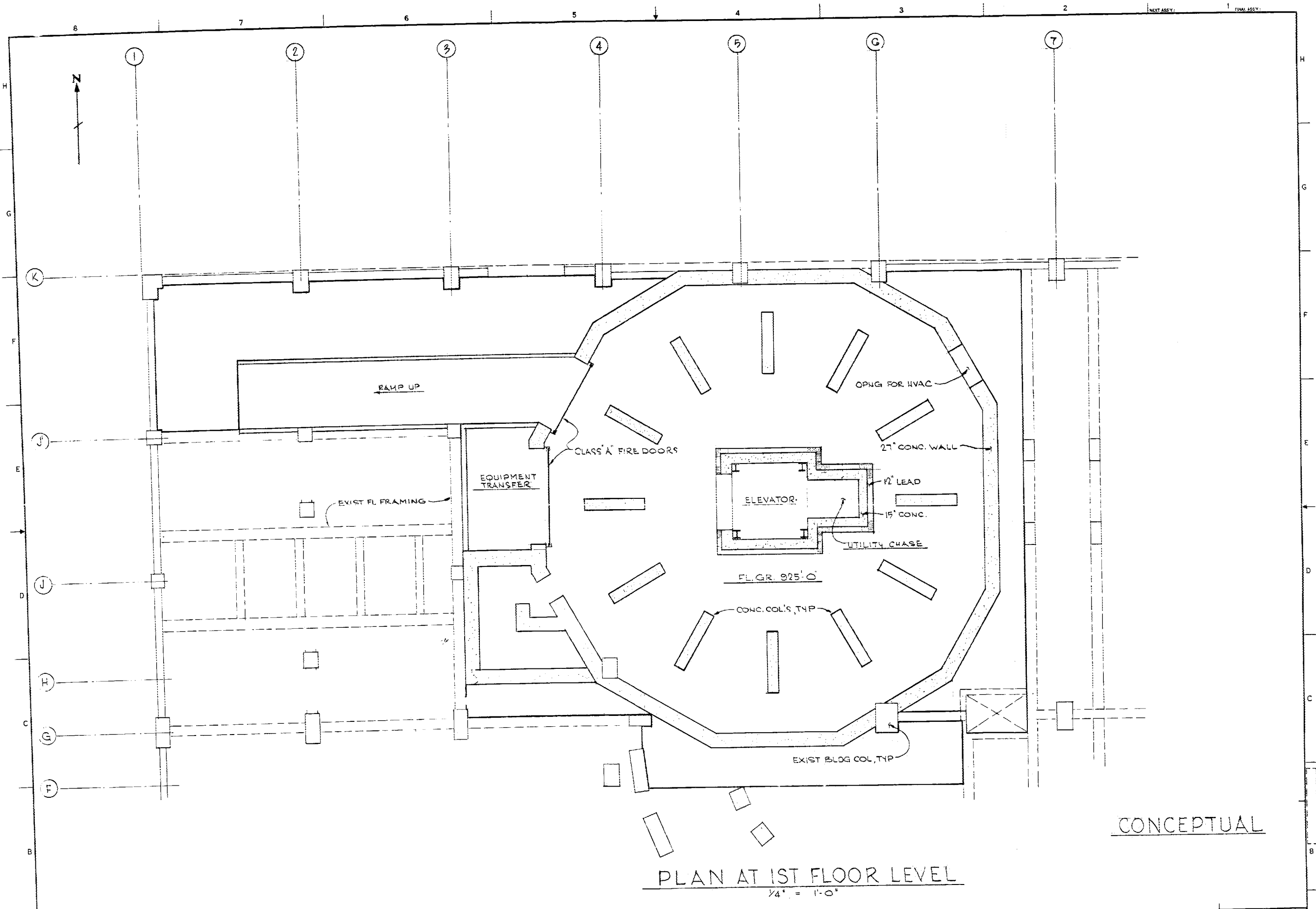
NO REPRESENTATION OR WARRANTY EXPRESSED OR IMPLIED IS MADE AS TO THE ACCURACY, COMPLETENESS OR USEFULNESS OF THE INFORMATION OR STATEMENTS CONTAINED IN THESE DRAWINGS. THE USER OF ANY INFORMATION APPEARING HEREIN SHALL BE RESPONSIBLE FOR OBTAINING NECESSARY PERMITS AND FOR THE PROTECTION OF HIS INTERESTS. THE LIABILITY IS LIMITED TO THE USE OF OR FOR DAMAGES FROM THE PROVISION OF ANY INFORMATION APPEARING HEREIN OR FROM INFORMATION IN THESE DRAWINGS. DRAWINGS NOT AVAILABLE FOR REVISION. NO WORK TO BE RETURNED UPON REQUEST OF THE FORWARDING CONTRACTOR.

| REV | ISSUED FOR | DESCRIPTION | BY | CHK | DATE |
|-----|------------|-------------|----|-----|------|------|------|------|------|------|------|------|------|------|------|------|------|------|------|------|
| | | | | | | | | | | | | | | | | | | | | |

UNION CARBIDE CORPORATION - NUCLEAR DIVISION

EBT-P STUDY
EXPERIMENT ENCLOSURE - MEZZ. FL.

DATE: 10/12/52
SCALE: 1/4" = 1'-0"



PLAN AT 1ST FLOOR LEVEL
 1/4" = 1'-0"

CONCEPTUAL

NO REPRESENTATION OR WARRANTY, EXPRESSED OR IMPLIED, IS MADE BY THE ARCHITECT FOR THE ACCURACY, COMPLETENESS OR UTILITY OF THE INFORMATION OR STATEMENTS CONTAINED IN THESE DRAWINGS OR FOR THE USE OR DISCONTINUANCE OF ANY INFORMATION CONTAINED HEREIN. THE USER OF THESE DRAWINGS SHALL BE RESPONSIBLE FOR THE PROTECTION OF THE INFORMATION CONTAINED HEREIN AND FOR THE PROTECTION OF THE INFORMATION CONTAINED HEREIN FROM THEFT, LOSS, DAMAGE, DESTRUCTION, REPRODUCTION, OR UNAUTHORIZED DISSEMINATION. THE USER OF THESE DRAWINGS SHALL BE RESPONSIBLE FOR THE PROTECTION OF THE INFORMATION CONTAINED HEREIN FROM THEFT, LOSS, DAMAGE, DESTRUCTION, REPRODUCTION, OR UNAUTHORIZED DISSEMINATION. THE USER OF THESE DRAWINGS SHALL BE RESPONSIBLE FOR THE PROTECTION OF THE INFORMATION CONTAINED HEREIN FROM THEFT, LOSS, DAMAGE, DESTRUCTION, REPRODUCTION, OR UNAUTHORIZED DISSEMINATION.

| REV | DESCRIPTION | BY | CHK | DATE | REV | DATE | NO | DATE |
|-----|-------------------------|----|-----|------|-----|------|----|------|----|------|----|------|----|------|----|------|
| 0 | ISSUED FOR CONSTRUCTION | | | | | | | | | | | | | | | |

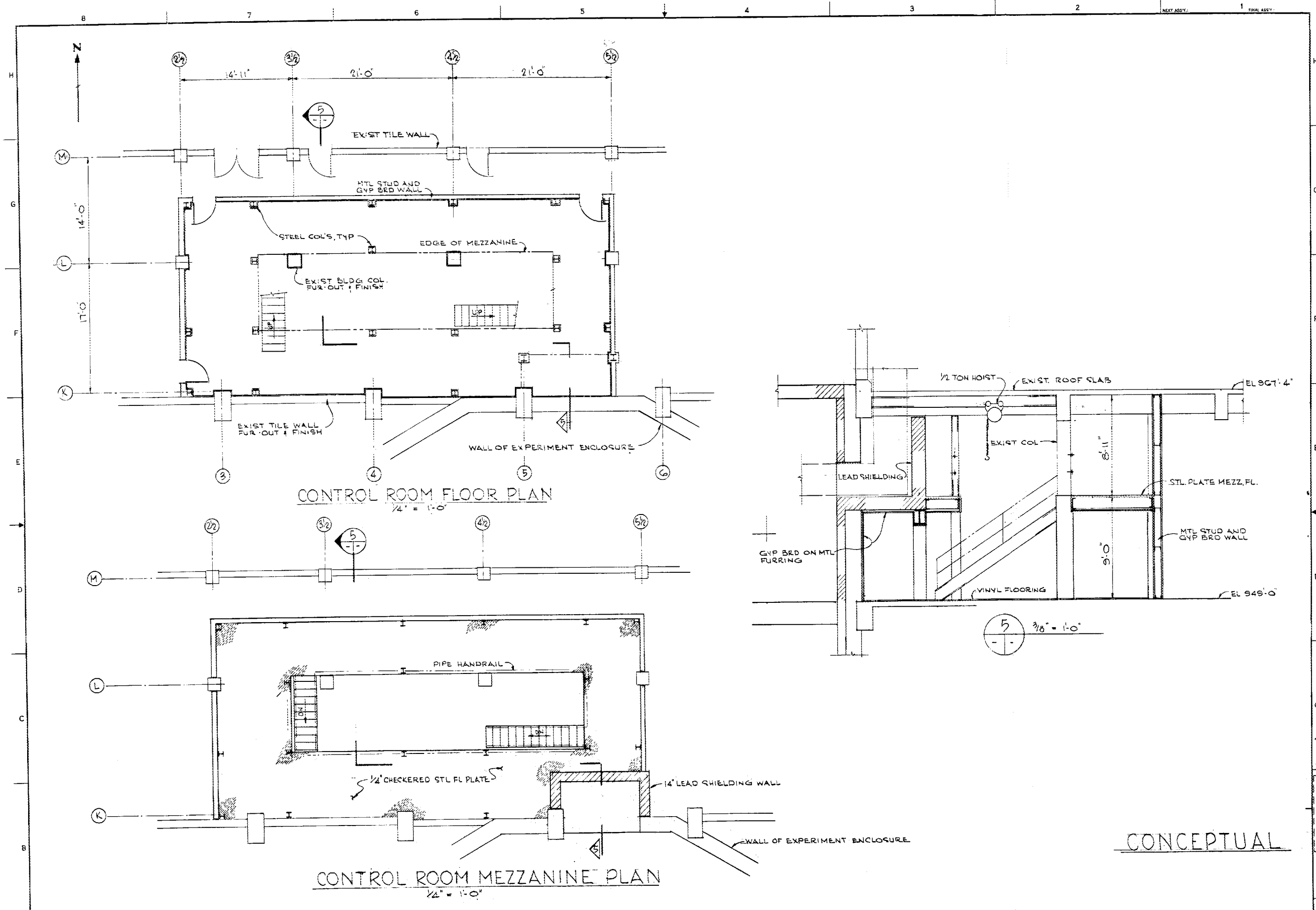
UNION CARBIDE CORPORATION - NUCLEAR DIVISION

E B T - P STUDY
 EXPERIMENT ENCLOSURE - 1ST FL.

SCALE: 1/4" = 1'-0"

DATE: 4/24/54

BY: S2E8945A SKG

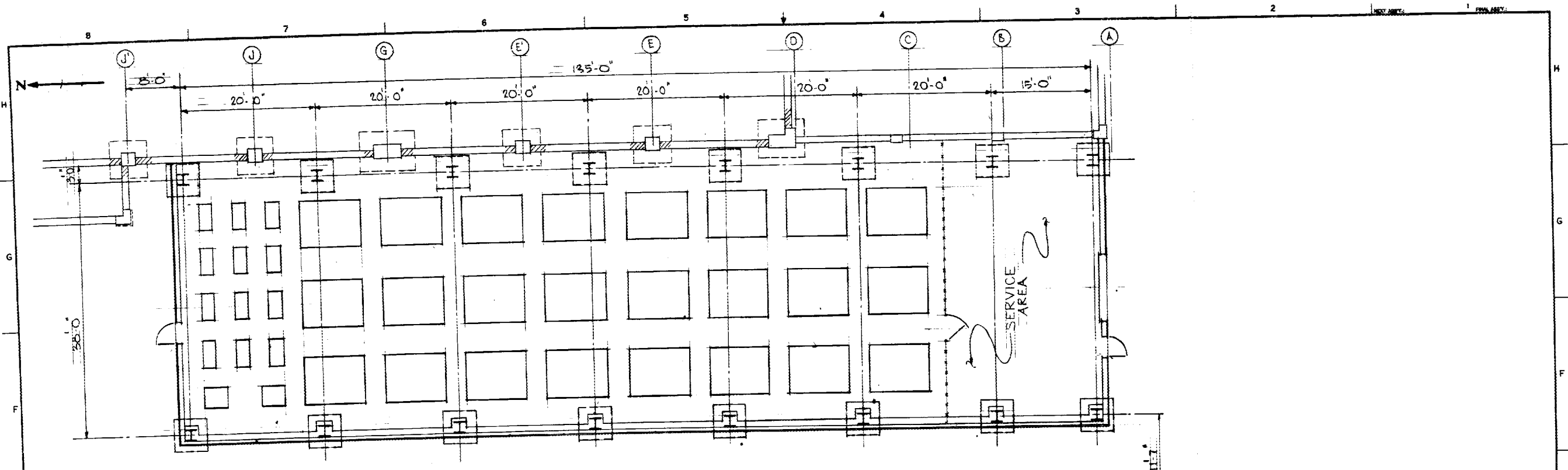


CONCEPTUAL

NO REPRESENTATION OR WARRANTY EXPRESSED OR IMPLIED IS MADE AS TO THE ACCURACY, COMPLETENESS OR USEFULNESS OF THE INFORMATION OR DATA CONTAINED HEREIN OR THE RESULTS THEREOF. THE USER OF THIS DRAWING AGREES TO HOLD UNION CARBIDE CORPORATION HARMLESS FROM AND AGAINST ALL CLAIMS, DAMAGES, LOSSES AND EXPENSES, INCLUDING REASONABLE ATTORNEY'S FEES, THAT MAY BE ASSERTED AGAINST OR INCURRED BY UNION CARBIDE CORPORATION OR ANY OF ITS EMPLOYEES, AGENTS, CONTRACTORS, SUBCONTRACTORS, OR VENDORS, AS A RESULT OF THE USER'S USE OF THIS DRAWING. THIS AGREEMENT SHALL BE APPLICABLE TO ANY REVISIONS, ADDENDUMS, OR SUPPLEMENTS TO THIS DRAWING. THE USER'S USE OF THIS DRAWING SHALL BE LIMITED TO THE PROJECT AND SITE SPECIFICALLY IDENTIFIED HEREIN. ANY OTHER USE OF THIS DRAWING WITHOUT THE WRITTEN CONSENT OF UNION CARBIDE CORPORATION IS STRICTLY PROHIBITED. THIS DRAWING IS THE PROPERTY OF UNION CARBIDE CORPORATION AND IS TO BE RETURNED UPON REQUEST OF THE DRAWING OFFICE.

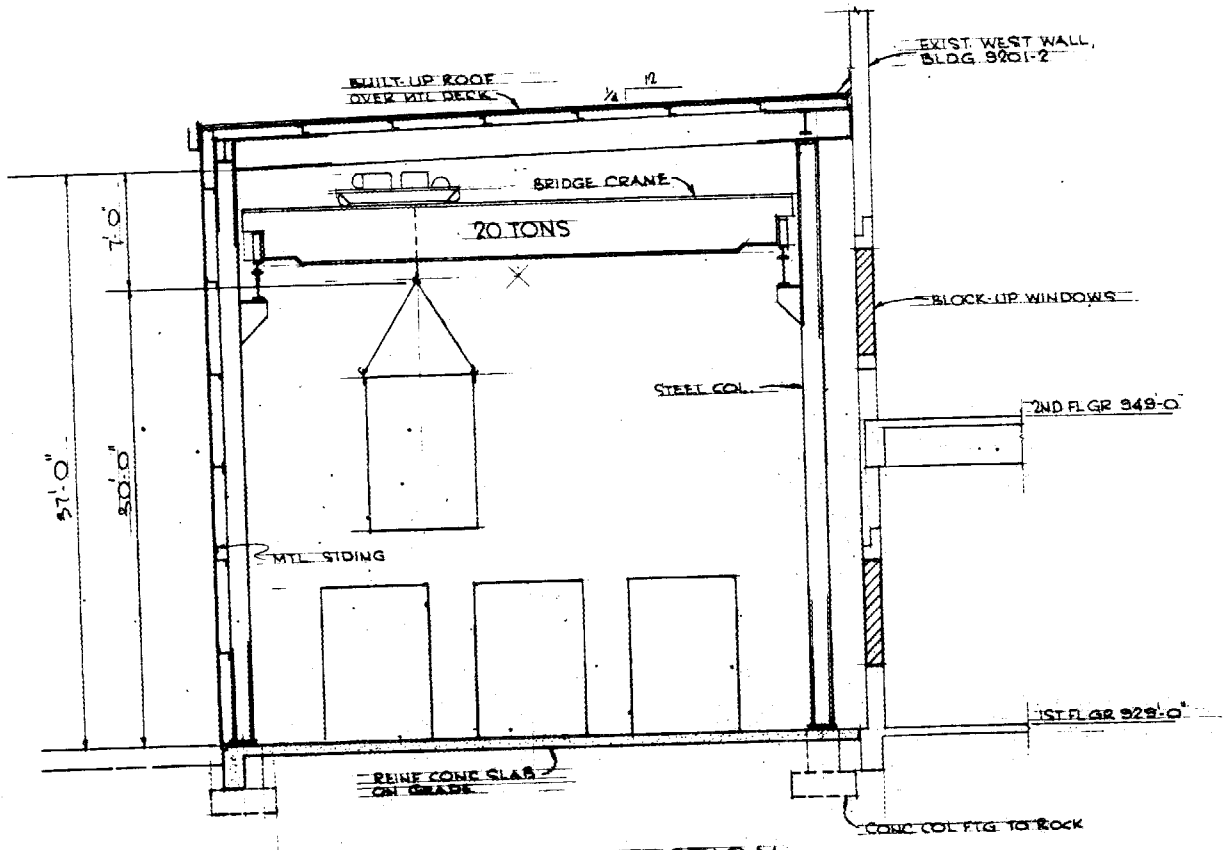
| NO. | DATE | DESCRIPTION | BY | CHK | RECT | DEPT | DATE | REV | DATE | SECOND | DATE | ERD | DATE | CA | EC | ES | EM | IE | IM | PO | SE | XAD | |
|-----|------|----------------|----|-----|------|------|------|-----|------|--------|------|-----|------|----|----|----|----|----|----|----|----|-----|--|
| 1 | | ISSUED FOR CDR | | | | | | | | | | | | | | | | | | | | | |

| | | | |
|--|--|--|---------------|
| TOLERANCES UNLESS OTHERWISE SPECIFIED | FRAC TIONS 1/8 DECIMALS 1/16 ANGLES SHARP EDGES FINISH | DESIGNED BY DRAWN BY CHECKED BY DATE SCALE | DATE SCALE |
| UNION CARBIDE CORPORATION - NUCLEAR DIVISION | DATE | SCALE | DATE |
| E.B.T. - P STUDY CONTROL ROOM | | SCALE | DATE |
| SCALE | | DATE | DATE |



FLOOR PLAN
3/16" = 1'-0"

91.05

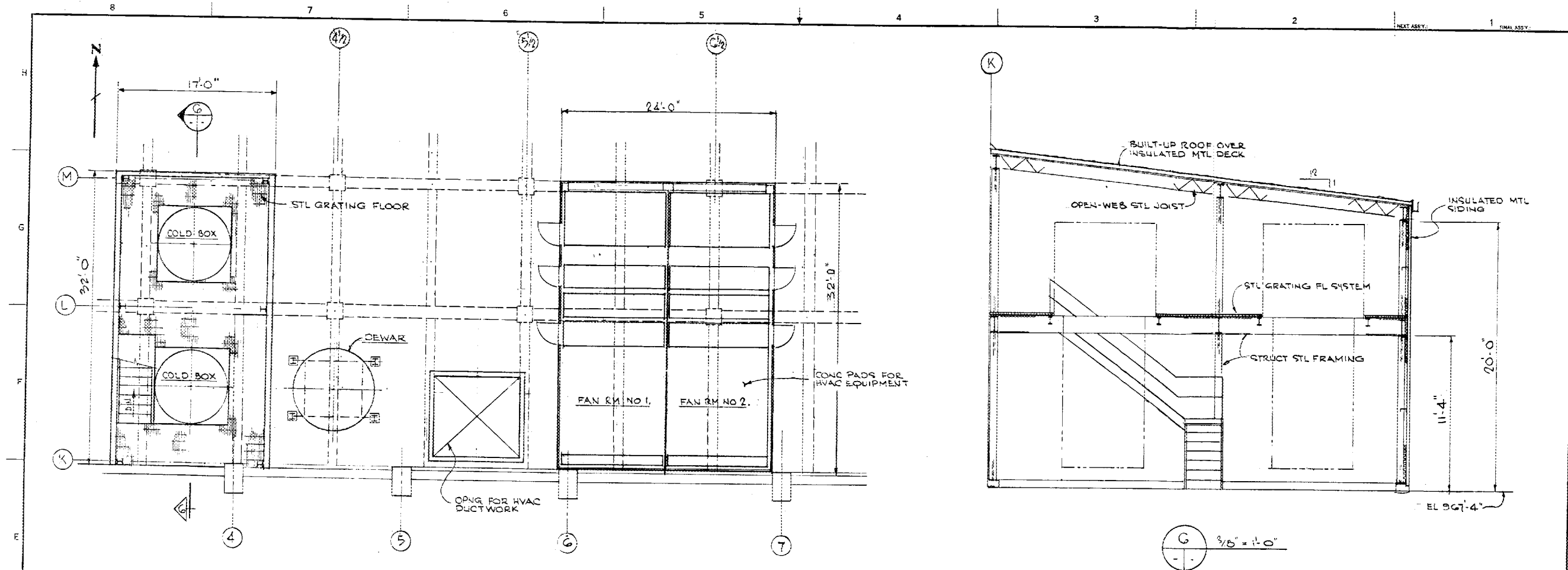


TYP CROSS SECTION
1/4" = 1'-0"

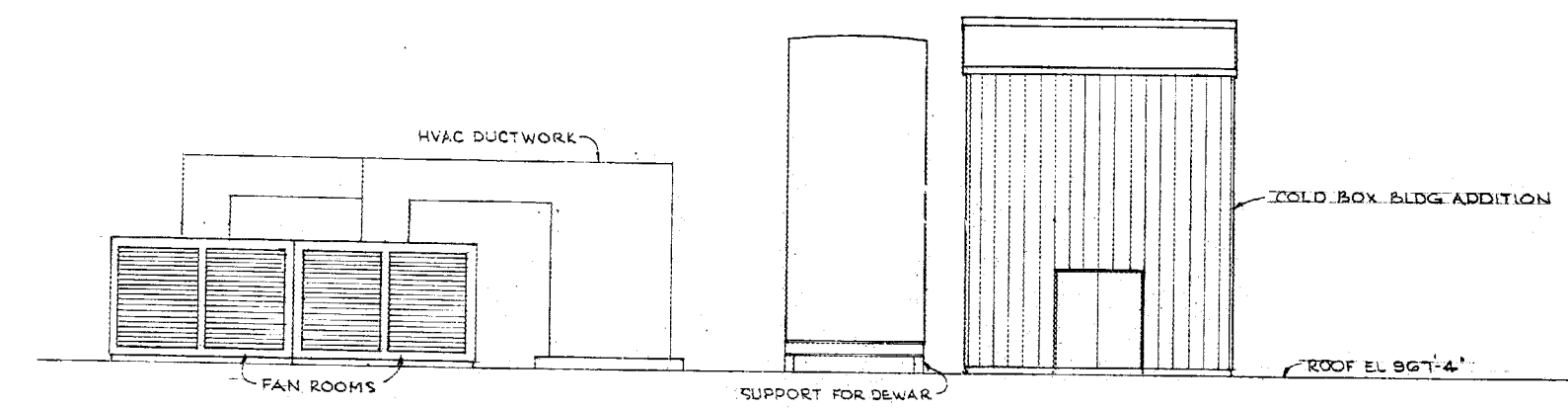
CONCEPTUAL

NOTES

| | | |
|--|--|---|
| REVISIONS NO. DATE BY 1 11/15/54 JTB 2 11/15/54 JTB 3 11/15/54 JTB 4 11/15/54 JTB 5 11/15/54 JTB 6 11/15/54 JTB 7 11/15/54 JTB 8 11/15/54 JTB 9 11/15/54 JTB 10 11/15/54 JTB 11 11/15/54 JTB 12 11/15/54 JTB 13 11/15/54 JTB 14 11/15/54 JTB 15 11/15/54 JTB 16 11/15/54 JTB 17 11/15/54 JTB 18 11/15/54 JTB 19 11/15/54 JTB 20 11/15/54 JTB 21 11/15/54 JTB 22 11/15/54 JTB 23 11/15/54 JTB 24 11/15/54 JTB 25 11/15/54 JTB 26 11/15/54 JTB 27 11/15/54 JTB 28 11/15/54 JTB 29 11/15/54 JTB 30 11/15/54 JTB 31 11/15/54 JTB 32 11/15/54 JTB 33 11/15/54 JTB 34 11/15/54 JTB 35 11/15/54 JTB 36 11/15/54 JTB 37 11/15/54 JTB 38 11/15/54 JTB 39 11/15/54 JTB 40 11/15/54 JTB 41 11/15/54 JTB 42 11/15/54 JTB 43 11/15/54 JTB 44 11/15/54 JTB 45 11/15/54 JTB 46 11/15/54 JTB 47 11/15/54 JTB 48 11/15/54 JTB 49 11/15/54 JTB 50 11/15/54 JTB 51 11/15/54 JTB 52 11/15/54 JTB 53 11/15/54 JTB 54 11/15/54 JTB 55 11/15/54 JTB 56 11/15/54 JTB 57 11/15/54 JTB 58 11/15/54 JTB 59 11/15/54 JTB 60 11/15/54 JTB 61 11/15/54 JTB 62 11/15/54 JTB 63 11/15/54 JTB 64 11/15/54 JTB 65 11/15/54 JTB 66 11/15/54 JTB 67 11/15/54 JTB 68 11/15/54 JTB 69 11/15/54 JTB 70 11/15/54 JTB 71 11/15/54 JTB 72 11/15/54 JTB 73 11/15/54 JTB 74 11/15/54 JTB 75 11/15/54 JTB 76 11/15/54 JTB 77 11/15/54 JTB 78 11/15/54 JTB 79 11/15/54 JTB 80 11/15/54 JTB 81 11/15/54 JTB 82 11/15/54 JTB 83 11/15/54 JTB 84 11/15/54 JTB 85 11/15/54 JTB 86 11/15/54 JTB 87 11/15/54 JTB 88 11/15/54 JTB 89 11/15/54 JTB 90 11/15/54 JTB 91 11/15/54 JTB 92 11/15/54 JTB 93 11/15/54 JTB 94 11/15/54 JTB 95 11/15/54 JTB 96 11/15/54 JTB 97 11/15/54 JTB 98 11/15/54 JTB 99 11/15/54 JTB 100 11/15/54 JTB | | UNION CARBIDE CORPORATION - NUCLEAR DIVISION EBI-P STUDY POWER SUPPLY BLDG. ADDITION 11/15/54 |
|--|--|---|



ROOF EQUIPMENT PLAN
1/4" = 1'-0"



NORTH ELEVATION
1/4" = 1'-0"

CONCEPTUAL

NO REPRESENTATION OR WARRANTY, EXPRESSED OR IMPLIED, IS MADE AS TO THE ACCURACY, COMPLETENESS OR USEFULNESS OF THE INFORMATION OR STATEMENTS CONTAINED IN THESE DRAWINGS OR ANY OTHER DOCUMENTS OF ANY NATURE, INCLUDING ANY INSTRUMENTS OF SERVICE, CONTRACTS, AGREEMENTS, SPECIFICATIONS, AND OTHER DOCUMENTS. THE USER OF THESE DRAWINGS SHALL BE RESPONSIBLE FOR OBTAINING ALL NECESSARY PERMITS AND FOR VERIFYING THE ACCURACY OF ALL INFORMATION AND DATA PROVIDED TO THE ENGINEER. THE ENGINEER SHALL NOT BE RESPONSIBLE FOR ANY ERRORS OR OMISSIONS IN THESE DRAWINGS OR FOR ANY CONSEQUENCES ARISING FROM THE USE OF THESE DRAWINGS. THE USER SHALL BE RESPONSIBLE FOR OBTAINING ALL NECESSARY PERMITS AND FOR VERIFYING THE ACCURACY OF ALL INFORMATION AND DATA PROVIDED TO THE ENGINEER. THE ENGINEER SHALL NOT BE RESPONSIBLE FOR ANY ERRORS OR OMISSIONS IN THESE DRAWINGS OR FOR ANY CONSEQUENCES ARISING FROM THE USE OF THESE DRAWINGS.

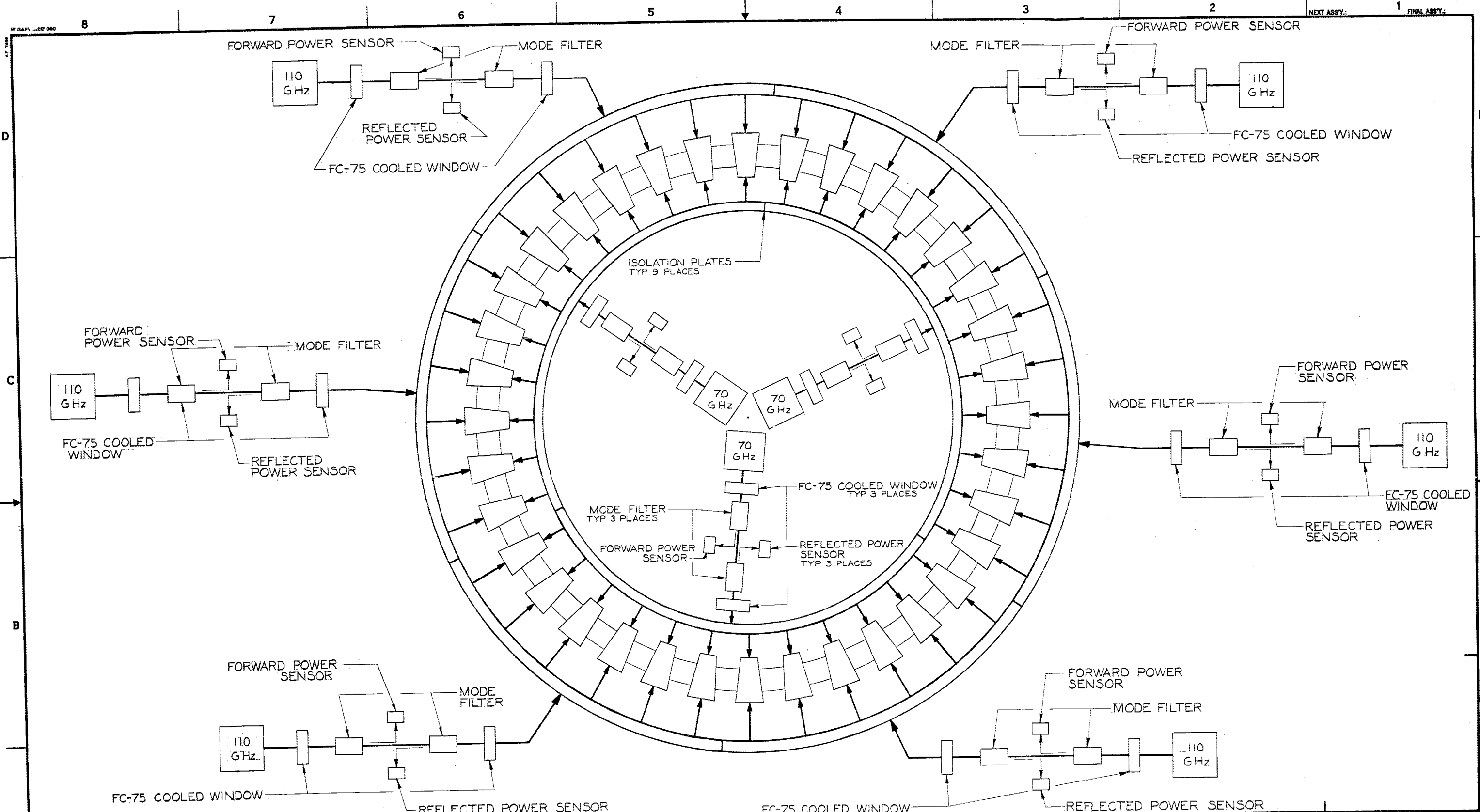
| NO. | DATE | BY | CHK | DEPT | DATE | PK | REV | DATE | REASON | DATE | ENGR | DATE | CA | SC | SE | EM | IL | IN | PO | SE | PAID | |
|-----|------|----|-----|------|------|----|-----|------|--------|------|------|------|----|----|----|----|----|----|----|----|------|--|
| | | | | | | | | | | | | | | | | | | | | | | |

UNION CARBIDE CORPORATION - NUCLEAR DIVISION

EBT-P STUDY
ROOF EQUIPMENT PLAN

SCALE: AS SHOWN

DATE: 10/24/71



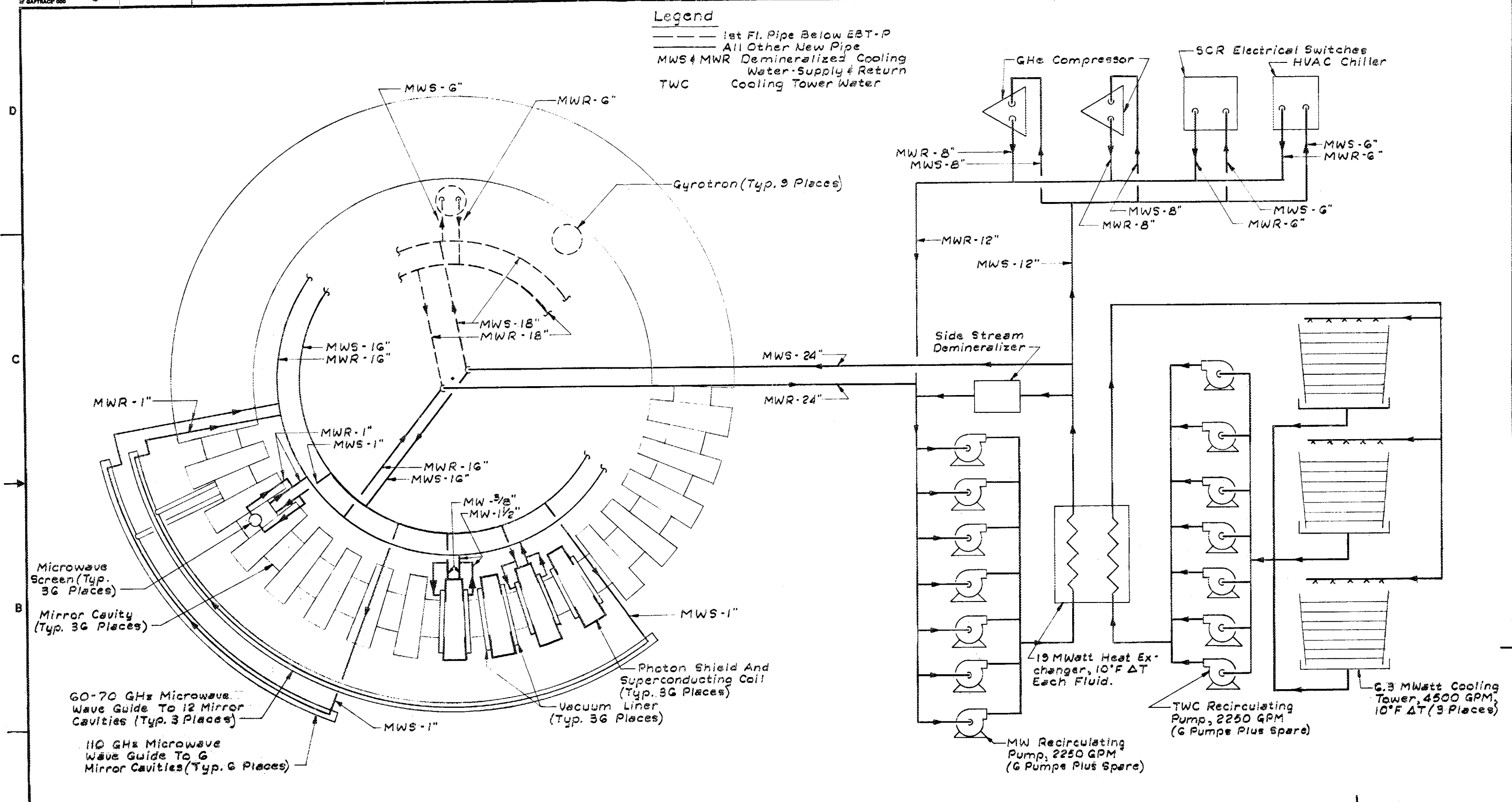
NO REPRESENTATION OR WARRANTY, EXPRESSED OR IMPLIED, IS MADE AS TO THE ACCURACY, COMPLETENESS OR USEFULNESS OF THE INFORMATION OR STATEMENTS CONTAINED IN THESE DRAWINGS, OR THAT THE USE OR DISCLOSURE OF ANY INFORMATION, APPARATUS, METHOD OR PROCESS DISCLOSED IN THESE DRAWINGS MAY NOT INFRINGE PRIVATE RIGHTS OF OTHERS. NO LIABILITY IS ASSUMED WITH RESPECT TO THE USE OF, OR FOR DAMAGES RESULTING FROM THE USE OF, ANY INFORMATION, APPARATUS, METHOD OR PROCESS DISCLOSED IN THESE DRAWINGS. DRAWINGS MADE AVAILABLE FOR INFORMATION TO BIDDER ARE NOT TO BE USED FOR OTHER PURPOSES, AND ARE TO BE RETURNED UPON REQUEST OF THE FORWARDING CONTRACTOR.

| REV | DESCRIPTION | BY | CHK | SECT | DEPT | DATE | PE | REG | DATE | UCCND | DATE | DOE | DATE | CA | EC | EE | EM | IE | M | PD | SE | XAD | |
|-----|-------------|----|-----|------|------|------|----|-----|------|-------|------|-----|------|----|----|----|----|----|---|----|----|-----|--|
| | | | | | | | | | | | | | | | | | | | | | | | |
| | | | | | | | | | | | | | | | | | | | | | | | |

| | | | |
|---------------------------------------|------|---------------|---------|
| TOLERANCES UNLESS OTHERWISE SPECIFIED | | DES R. WRIGHT | 7/16/79 |
| FRACTIONS | ± | DRW E. ZANG | 8/23/79 |
| XX DECIMALS | ± | CHK | |
| XXX DECIMALS | ± | SECT | |
| ANGLES | | DEPT & PLANT | |
| BREAK SHARP EDGES | MAX. | | |
| FINISH | | | |
| A-E | | | |
| UCC-ND | | | |
| DOE | | | |

| | | | |
|--|---------------|--|-------|
| UNION CARBIDE CORPORATION - NUCLEAR DIVISION | | OPERATED FOR THE DEPARTMENT OF ENERGY UNDER U.S. GOVERNMENT CONTRACT W 7405 eng 28 | |
| DAK RIDGE, TENNESSEE • PATOSH, KENTUCKY | | | |
| MICROWAVE DISTRIBUTION MANIFOLD | | | |
| ORNL-EBTP PROJECT DEFINITION STUDY | | | |
| 1 | 48 | 48 | 80 |
| PLANT | BLDG | FL | REV |
| Y-12 | 9204-1 | 2ND | 20 94 |
| CLASS | U | | |
| SCALE | NONE | | |
| ID | X2D14270 0002 | | |
| REV | | | |

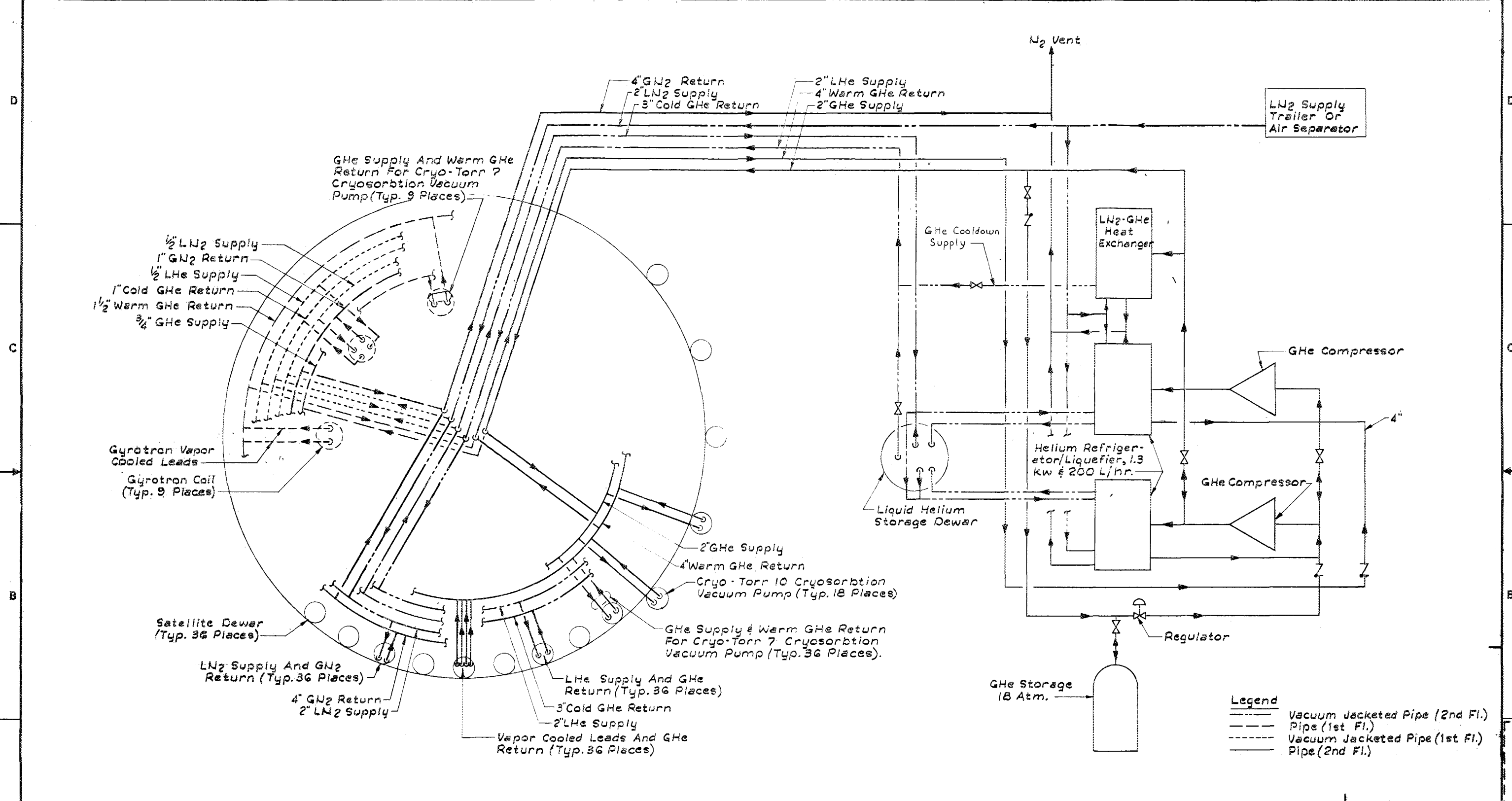
Legend
 - - - 1st Fl. Pipe Below EBT-P
 — All Other New Pipe
 MWS & MWR Demineralized Cooling Water Supply & Return
 TWC Cooling Tower Water



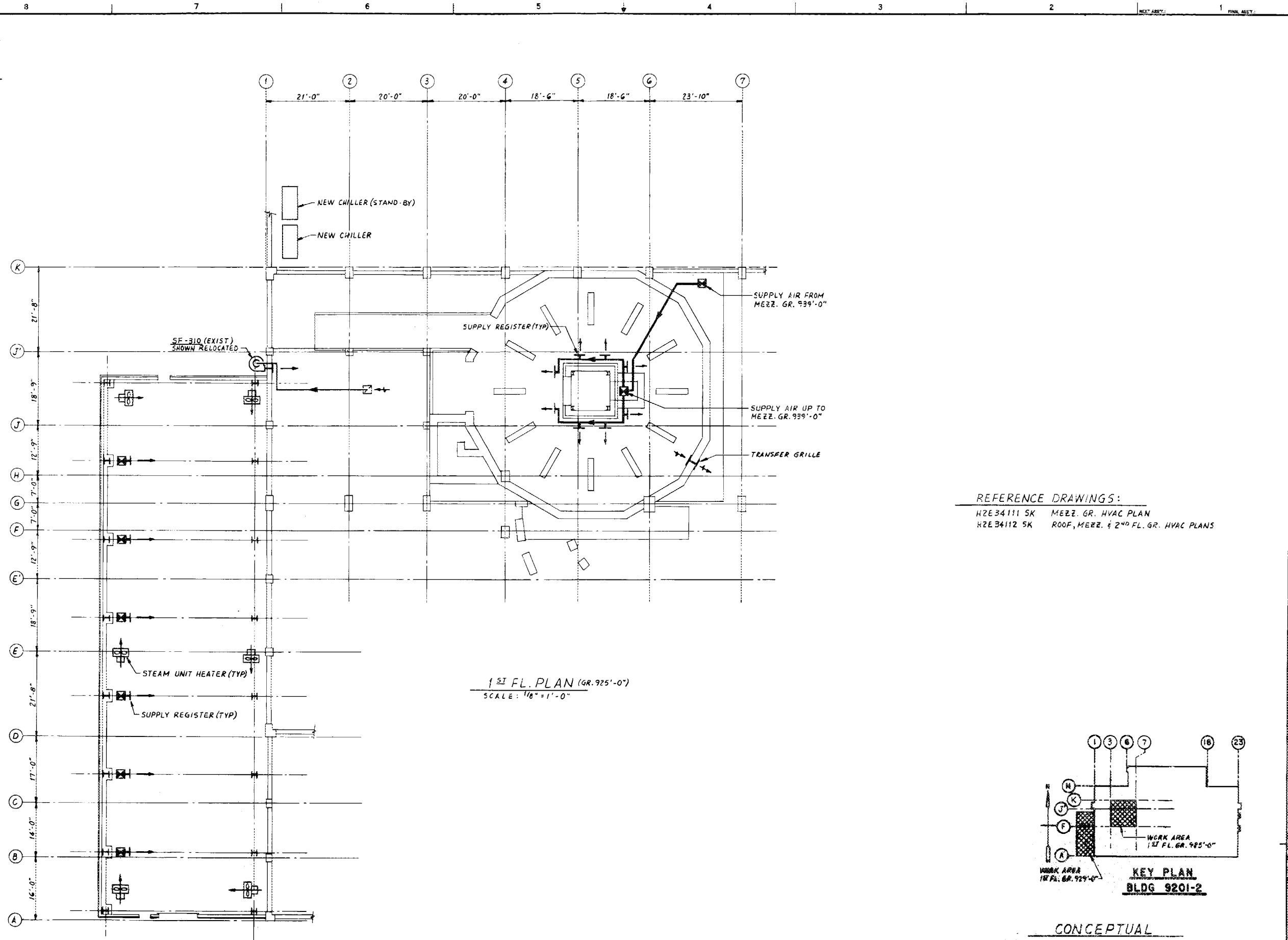
NO REPRESENTATION OR WARRANTY, EXPRESSED OR IMPLIED, IS MADE AS TO THE ACCURACY, COMPLETENESS OR UNBIASEDNESS OF THE INFORMATION OR STATEMENTS CONTAINED IN THESE DRAWINGS, OR THAT THE USE OR DISCLOSURE OF ANY INFORMATION, APPARATUS, METHOD OR PROCESS ENCLOSED IN THESE DRAWINGS MAY NOT INFRINGE PRIVATE RIGHTS OF OTHERS. NO LIABILITY IS ASSUMED WITH RESPECT TO THE USE OF, OR FOR DAMAGES RESULTING FROM THE USE OF, ANY INFORMATION, APPARATUS, METHOD OR PROCESS ENCLOSED IN THESE DRAWINGS. DRAWINGS WHEN AVAILABLE FOR INFORMATION TO BIDDER ARE NOT TO BE USED FOR OTHER PURPOSES, AND ARE TO BE RETURNED UPON REQUEST OF THE FORWARDING CONTRACTOR.

| REV | DESCRIPTION | BY | CHK | SECT | DEPT | DATE | PG | REQ | DATE | ACCND | DATE | ENDA | DATE | CA | SC | EE | EM | IE | M | PD | SE | XAD | ENDA |
|-----|-------------|----|-----|------|------|------|----|-----|------|-------|------|------|------|----|----|----|----|----|---|----|----|-----|------|
| | | | | | | | | | | | | | | | | | | | | | | | |

| | |
|--|--|
| TOLERANCES UNLESS OTHERWISE SPECIFIED: FRACTIONS: 1/16, 1/8, 1/4, 1/2, 3/4, 1, 2, 3, 4, 5, 6, 8, 10, 12, 16, 20, 24, 30, 36, 48, 60, 72, 96, 120, 144, 180, 240, 300, 360, 480, 600, 720, 960, 1200, 1440, 1800, 2400, 3000, 3600, 4800, 6000, 7200, 9600, 12000, 14400, 18000, 24000, 30000, 36000, 48000, 60000, 72000, 96000, 120000, 144000, 180000, 240000, 300000, 360000, 480000, 600000, 720000, 960000, 1200000, 1440000, 1800000, 2400000, 3000000, 3600000, 4800000, 6000000, 7200000, 9600000, 12000000, 14400000, 18000000, 24000000, 30000000, 36000000, 48000000, 60000000, 72000000, 96000000, 120000000, 144000000, 180000000, 240000000, 300000000, 360000000, 480000000, 600000000, 720000000, 960000000, 1200000000, 1440000000, 1800000000, 2400000000, 3000000000, 3600000000, 4800000000, 6000000000, 7200000000, 9600000000, 12000000000, 14400000000, 18000000000, 24000000000, 30000000000, 36000000000, 48000000000, 60000000000, 72000000000, 96000000000, 120000000000, 144000000000, 180000000000, 240000000000, 300000000000, 360000000000, 480000000000, 600000000000, 720000000000, 960000000000, 1200000000000, 1440000000000, 1800000000000, 2400000000000, 3000000000000, 3600000000000, 4800000000000, 6000000000000, 7200000000000, 9600000000000, 12000000000000, 14400000000000, 18000000000000, 24000000000000, 30000000000000, 36000000000000, 48000000000000, 60000000000000, 72000000000000, 96000000000000, 120000000000000, 144000000000000, 180000000000000, 240000000000000, 300000000000000, 360000000000000, 480000000000000, 600000000000000, 720000000000000, 960000000000000, 1200000000000000, 1440000000000000, 1800000000000000, 2400000000000000, 3000000000000000, 3600000000000000, 4800000000000000, 6000000000000000, 7200000000000000, 9600000000000000, 12000000000000000, 14400000000000000, 18000000000000000, 24000000000000000, 30000000000000000, 36000000000000000, 48000000000000000, 60000000000000000, 72000000000000000, 96000000000000000, 120000000000000000, 144000000000000000, 180000000000000000, 240000000000000000, 300000000000000000, 360000000000000000, 480000000000000000, 600000000000000000, 720000000000000000, 960000000000000000, 1200000000000000000, 1440000000000000000, 1800000000000000000, 2400000000000000000, 3000000000000000000, 3600000000000000000, 4800000000000000000, 6000000000000000000, 7200000000000000000, 9600000000000000000, 12000000000000000000, 14400000000000000000, 18000000000000000000, 24000000000000000000, 30000000000000000000, 36000000000000000000, 48000000000000000000, 60000000000000000000, 72000000000000000000, 96000000000000000000, 120000000000000000000, 144000000000000000000, 180000000000000000000, 240000000000000000000, 300000000000000000000, 360000000000000000000, 480000000000000000000, 600000000000000000000, 720000000000000000000, 960000000000000000000, 1200000000000000000000, 1440000000000000000000, 1800000000000000000000, 2400000000000000000000, 3000000000000000000000, 3600000000000000000000, 4800000000000000000000, 6000000000000000000000, 7200000000000000000000, 9600000000000000000000, 12000000000000000000000, 14400000000000000000000, 18000000000000000000000, 24000000000000000000000, 30000000000000000000000, 36000000000000000000000, 48000000000000000000000, 60000000000000000000000, 72000000000000000000000, 96000000000000000000000, 120000000000000000000000, 144000000000000000000000, 180000000000000000000000, 240000000000000000000000, 300000000000000000000000, 360000000000000000000000, 480000000000000000000000, 600000000000000000000000, 720000000000000000000000, 960000000000000000000000, 1200000000000000000000000, 1440000000000000000000000, 1800000000000000000000000, 2400000000000000000000000, 3000000000000000000000000, 3600000000000000000000000, 4800000000000000000000000, 6000000000000000000000000, 7200000000000000000000000, 9600000000000000000000000, 12000000000000000000000000, 14400000000000000000000000, 18000000000000000000000000, 24000000000000000000000000, 30000000000000000000000000, 36000000000000000000000000, 48000000000000000000000000, 60000000000000000000000000, 72000000000000000000000000, 96000000000000000000000000, 120000000000000000000000000, 144000000000000000000000000, 180000000000000000000000000, 240000000000000000000000000, 300000000000000000000000000, 360000000000000000000000000, 480000000000000000000000000, 600000000000000000000000000, 720000000000000000000000000, 960000000000000000000000000, 1200000000000000000000000000, 1440000000000000000000000000, 1800000000000000000000000000, 2400000000000000000000000000, 3000000000000000000000000000, 3600000000000000000000000000, 4800000000000000000000000000, 6000000000000000000000000000, 7200000000000000000000000000, 9600000000000000000000000000, 12000000000000000000000000000, 14400000000000000000000000000, 18000000000000000000000000000, 24000000000000000000000000000, 30000000000000000000000000000, 36000000000000000000000000000, 48000000000000000000000000000, 60000000000000000000000000000, 72000000000000000000000000000, 96000000000000000000000000000, 120000000000000000000000000000, 144000000000000000000000000000, 180000000000000000000000000000, 240000000000000000000000000000, 300000000000000000000000000000, 360000000000000000000000000000, 480000000000000000000000000000, 600000000000000000000000000000, 720000000000000000000000000000, 960000000000000000000000000000, 1200000000000000000000000000000, 1440000000000000000000000000000, 1800000000000000000000000000000, 2400000000000000000000000000000, 3000000000000000000000000000000, 3600000000000000000000000000000, 4800000000000000000000000000000, 6000000000000000000000000000000, 7200000000000000000000000000000, 9600000000000000000000000000000, 12000000000000000000000000000000, 14400000000000000000000000000000, 18000000000000000000000000000000, 24000000000000000000000000000000, 30000000000000000000000000000000, 36000000000000000000000000000000, 48000000000000000000000000000000, 60000000000000000000000000000000, 72000000000000000000000000000000, 96000000000000000000000000000000, 120000000000000000000000000000000, 144000000000000000000000000000000, 180000000000000000000000000000000, 240000000000000000000000000000000, 300000000000000000000000000000000, 360000000000000000000000000000000, 480000000000000000000000000000000, 600000000000000000000000000000000, 720000000000000000000000000000000, 960000000000000000000000000000000, 1200000000000000000000000000000000, 1440000000000000000000000000000000, 1800000000000000000000000000000000, 2400000000000000000000000000000000, 3000000000000000000000000000000000, 3600000000000000000000000000000000, 4800000000000000000000000000000000, 6000000000000000000000000000000000, 7200000000000000000000000000000000, 9600000000000000000000000000000000, 12000000000000000000000000000000000, 14400000000000000000000000000000000, 18000000000000000000000000000000000, 24000000000000000000000000000000000, 30000000000000000000000000000000000, 36000000000000000000000000000000000, 48000000000000000000000000000000000, 60000000000000000000000000000000000, 72000000000000000000000000000000000, 96000000000000000000000000000000000, 120000000000000000000000000000000000, 144000000000000000000000000000000000, 180000000000000000000000000000000000, 240000000000000000000000000000000000, 300000000000000000000000000000000000, 360000000000000000000000000000000000, 480000000000000000000000000000000000, 600000000000000000000000000000000000, 720000000000000000000000000000000000, 960000000000000000000000000000000000, 1200000000000000000000000000000000000, 1440000000000000000000000000000000000, 1800000000000000000000000000000000000, 2400000000000000000000000000000000000, 3000000000000000000000000000000000000, 3600000000000000000000000000000000000, 4800000000000000000000000000000000000, 6000000000000000000000000000000000000, 7200000000000000000000000000000000000, 9600000000000000000000000000000000000, 12000000000000000000000000000000000000, 14400000000000000000000000000000000000, 18000000000000000000000000000000000000, 24000000000000000000000000000000000000, 30000000000000000000000000000000000000, 36000000000000000000000000000000000000, 48000000000000000000000000000000000000, 60000000000000000000000000000000000000, 72000000000000000000000000000000000000, 96000000000000000000000000000000000000, 120000000000000000000000000000000000000, 144000000000000000000000000000000000000, 180000000000000000000000000000000000000, 240000000000000000000000000000000000000, 300000000000000000000000000000000000000, 360000000000000000000000000000000000000, 480000000000000000000000000000000000000, 600000000000000000000000000000000000000, 720000000000000000000000000000000000000, 960000000000000000000000000000000000000, 1200000000000000000000000000000000000000, 1440000000000000000000000000000000000000, 1800000000000000000000000000000000000000, 2400000000000000000000000000000000000000, 3000000000000000000000000000000000000000, 3600000000000000000000000000000000000000, 4800000000000000000000000000000000000000, 6000000000000000000000000000000000000000, 7200000000000000000000000000000000000000, 9600000000000000000000000000000000000000, 12000000000000000000000000000000000000000, 14400000000000000000000000000000000000000, 18000000000000000000000000000000000000000, 24000000000000000000000000000000000000000, 300, 36000000000000000000000000000000000000000, 48000000000000000000000000000000000000000, 600, 72000000000000000000000000000000000000000, 96000000000000000000000000000000000000000, 1200, 144000000000000000000000000000000000000000, 1800, 2400, 3000, 3600, 4800, 6000, 7200, 9600, 12000, 14400, 18000, 24000, 300, 36000, 48000, 600, 72000, 96000, 1200, 144000, 1800, 2400, 3000, 3600, 4800, 6000, 7200, 9600, 12000, 14400, 18000, 24000, 300, 36000, 48000, 600, 72000, 96000, 1200, 1440000000 | |
|--|--|

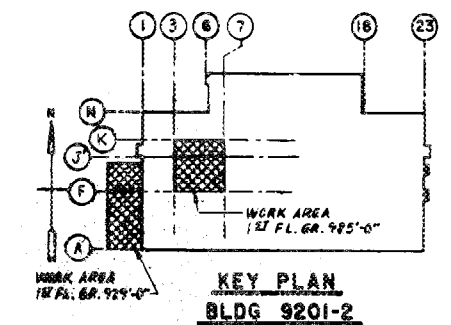


| | | | | | | | | | | | | | | | | | | | | |
|--|--|--|--|--|--|--|--|--|--|--|--|--|--|--|---|--|---|--|---|--|
| NO REPRESENTATION OR WARRANTY, EXPRESSED OR IMPLIED, IS MADE AS TO THE ACCURACY, COMPLETENESS OR USEFULNESS OF THE INFORMATION OR STATEMENTS CONTAINED IN THESE DRAWINGS, OR THAT THE USE OR DISCLOSURE OF ANY INFORMATION, APPARATUS, METHOD OR PROCESS DISCLOSED IN THESE DRAWINGS MAY NOT INFRINGE PRIVATE RIGHTS OF OTHERS. NO LIABILITY IS ASSUMED WITH RESPECT TO THE USE OF, OR FOR DAMAGES RESULTING FROM THE USE OF, ANY INFORMATION, APPARATUS, METHOD OR PROCESS DISCLOSED IN THESE DRAWINGS. DRAWINGS MADE AVAILABLE FOR INFORMATION TO ENDOR ARE NOT TO BE USED FOR OTHER PURPOSES, AND ARE TO BE RETURNED UPON REQUEST OF THE FORWARDING CONTRACTOR. | | | | | | | | | | | | | | | TOLERANCES UNLESS OTHERWISE SPECIFIED FRACTIONS ± XX DECIMALS ± XXX DECIMALS ± ANGLES ± BREAK SHARP EDGES MAX. FINISH A-E UCC-ND ENDA | | DES KINSEY 9-79 DRW STEPHENS 9-79 CHK Steve Kinsey 9-79 SECT DEPT & PLANT | | UNION CARBIDE CORPORATION - NUCLEAR DIVISION EBT-P CRYOGENIC & HELIUM FLOW SHEET | |
| REV DESCRIPTION BY CHK SECT DEPT DATE PE REQ DATE UCCND DATE ENDA DATE CA EC EE EM IE M PD SE XAD | | | | | | | | | | | | | | | EBT-P CRYOGENIC FLOW SHT 3 P U N 7-72 9201-2 2 25 84 SCALE NONE A-8845 P20576810001 | | | | | |



1ST FL. PLAN (GR. 925'-0")
SCALE: 1/8" = 1'-0"

REFERENCE DRAWINGS:
HZE34111 SK MEZZ. GR. HVAC PLAN
HZE34112 SK ROOF, MEZZ. & 2ND FL. GR. HVAC PLANS

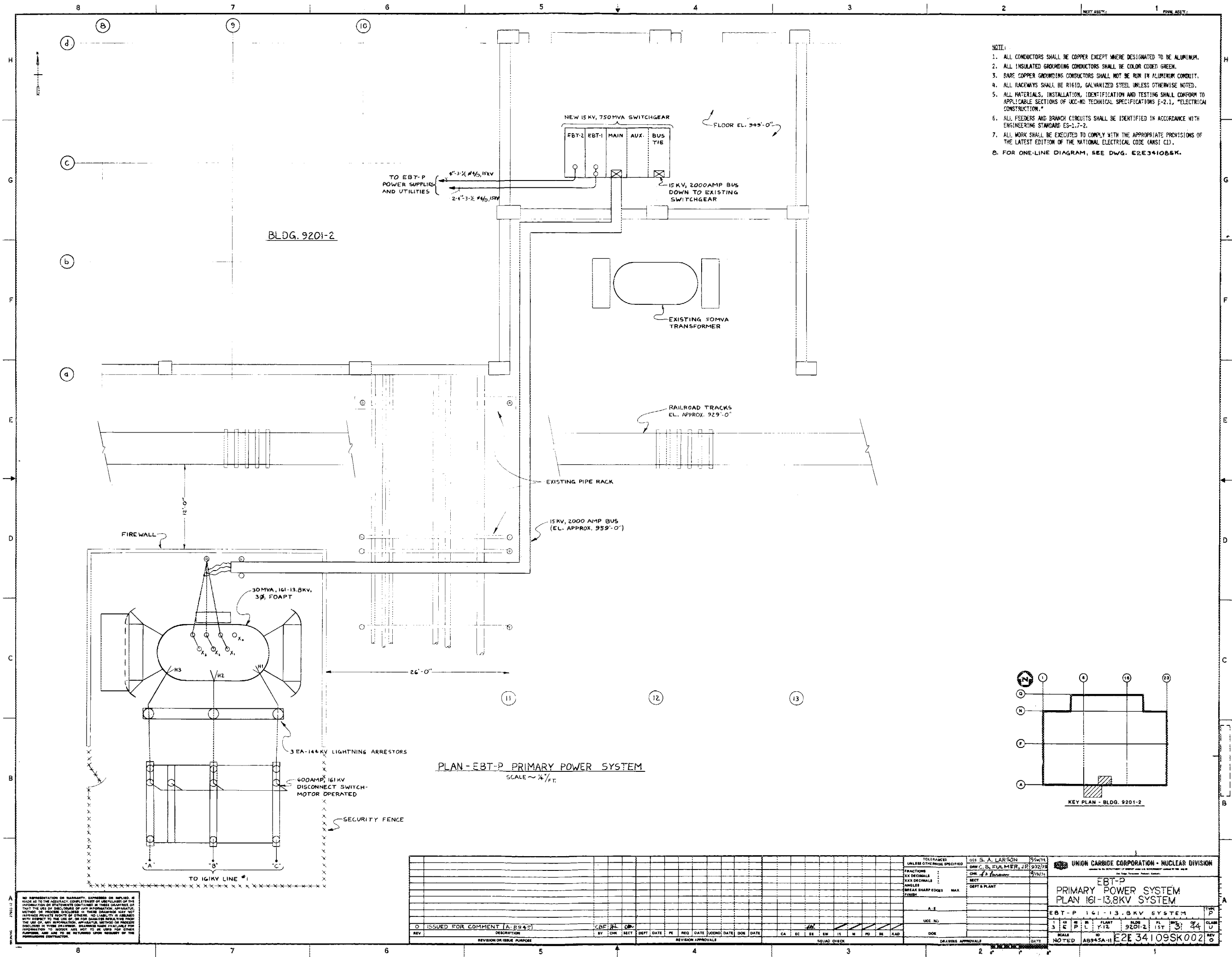


KEY PLAN
BLDG 9201-2

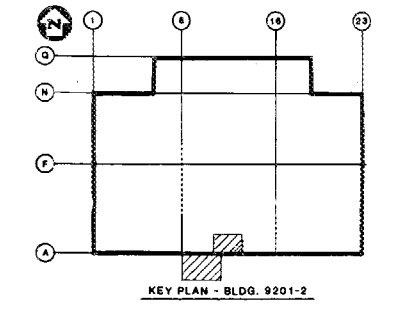
CONCEPTUAL

THIS REPRESENTATION IS A PRELIMINARY SKETCH OF WORK OR IS SUBJECT TO THE NECESSARY CHECKS AND REVISIONS OF THE CONTRACTOR OR ARCHITECT. IT IS NOT TO BE USED FOR CONSTRUCTION OR FOR ANY OTHER PURPOSE WITHOUT THE WRITTEN APPROVAL OF THE ARCHITECT. THE CONTRACTOR SHALL BE RESPONSIBLE FOR OBTAINING ALL NECESSARY PERMITS AND APPROVALS. THE CONTRACTOR SHALL BE RESPONSIBLE FOR OBTAINING ALL NECESSARY PERMITS AND APPROVALS. THE CONTRACTOR SHALL BE RESPONSIBLE FOR OBTAINING ALL NECESSARY PERMITS AND APPROVALS.

| | |
|--|--|
| UNION CARBIDE CORPORATION - NUCLEAR DIVISION | |
| EBT-P STUDY HVAC PLAN | |
| 4/8/81 7-72 9201-2 7 27 89 11 | |
| HET/LS 4-8-81 HZE 34110 SKO/17 | |



- NOTE:
1. ALL CONDUCTORS SHALL BE COPPER EXCEPT WHERE DESIGNATED TO BE ALUMINUM.
 2. ALL INSULATED GROUNDING CONDUCTORS SHALL BE COLOR CODED GREEN.
 3. BARE COPPER GROUNDING CONDUCTORS SHALL NOT BE RUN IN ALUMINUM CONDUIT.
 4. ALL RACEWAYS SHALL BE RIGID, GALVANIZED STEEL UNLESS OTHERWISE NOTED.
 5. ALL MATERIALS, INSTALLATION, IDENTIFICATION AND TESTING SHALL CONFORM TO APPLICABLE SECTIONS OF UOC-ND TECHNICAL SPECIFICATIONS E-2.1, "ELECTRICAL CONSTRUCTION."
 6. ALL FEEDERS AND BRANCH CIRCUITS SHALL BE IDENTIFIED IN ACCORDANCE WITH ENGINEERING STANDARD ES-1.7-2.
 7. ALL WORK SHALL BE EXECUTED TO COMPLY WITH THE APPROPRIATE PROVISIONS OF THE LATEST EDITION OF THE NATIONAL ELECTRICAL CODE (ANSI C).
 8. FOR ONE-LINE DIAGRAM, SEE DWG. E2E341085K.

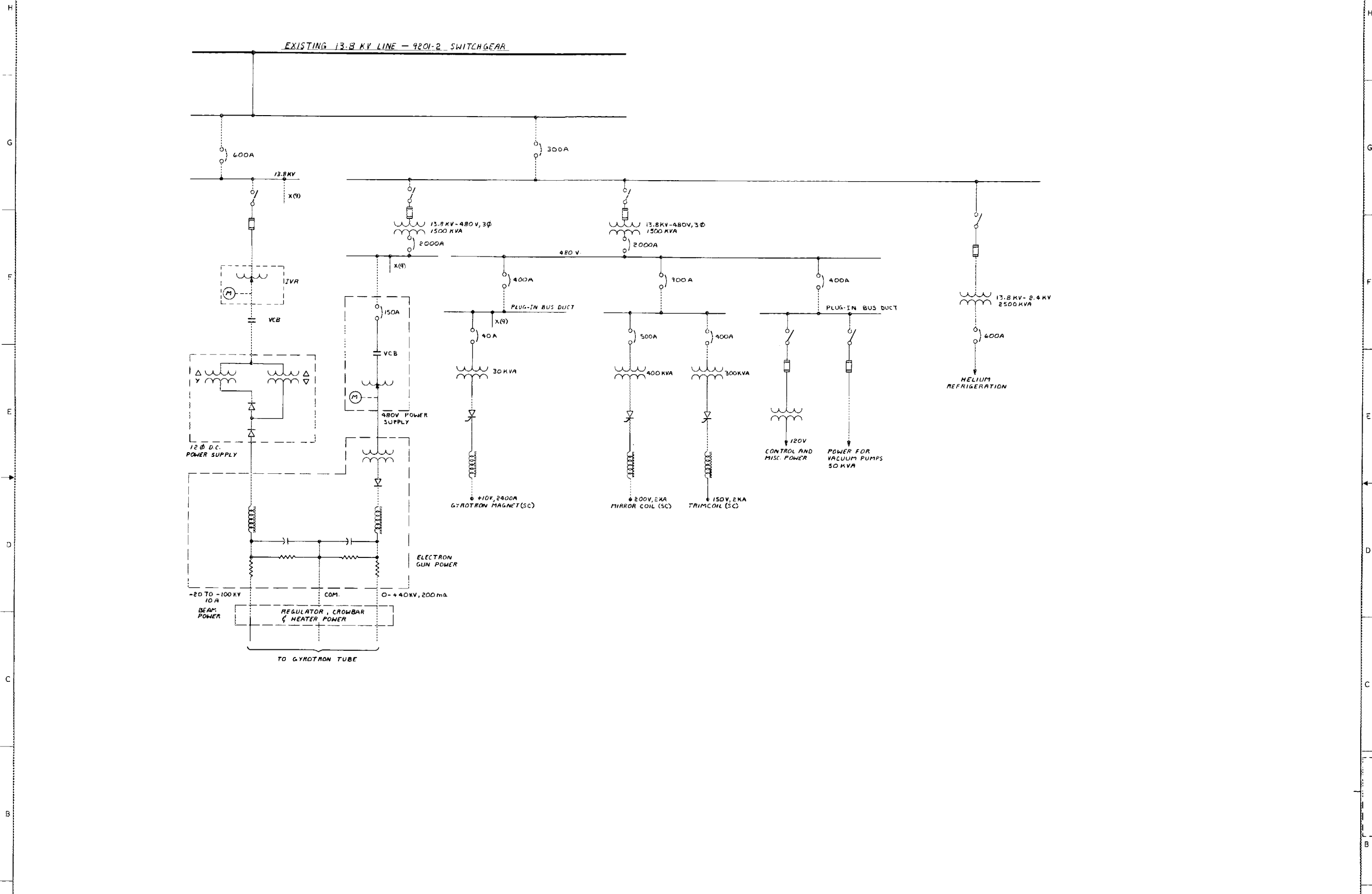


PLAN-EBT-P PRIMARY POWER SYSTEM
SCALE ~ 1/4" = 1'-0"

NO REPRESENTATION OR WARRANTY, EXPRESSED OR IMPLIED, IS MADE AS TO THE ACCURACY, COMPLETENESS OR RELIABILITY OF THE INFORMATION OR STATEMENTS CONTAINED IN THESE DRAWINGS OR THAT THE USE OF SUCH INFORMATION OR STATEMENTS WILL BE LIMITED TO THE USE OF ANY INFORMATION, APPLICABLE METHOD OR PROCEDURE TO BE DETERMINED BY THE USER. THE USER SHALL BE RESPONSIBLE FOR OBTAINING ALL NECESSARY PERMITS AND FOR OBTAINING ALL NECESSARY INFORMATION TO BE USED FOR OTHER PURPOSES AND FOR BEING HELD HARMLESS BY THE CONTRACTOR.

| REV | DESCRIPTION | BY | CHK | SECT | DEPT | DATE | PE | REQ | DATE | APPROV | DATE | DOE | DATE | CA | EC | EE | EM | IS | IN | PD | RE | SE | TEAD |
|-----|------------------------------|----|-----|------|------|------|----|-----|------|--------|------|-----|------|----|----|----|----|----|----|----|----|----|------|
| 0 | ISSUED FOR COMMENT (A. 8942) | | | | | | | | | | | | | | | | | | | | | | |

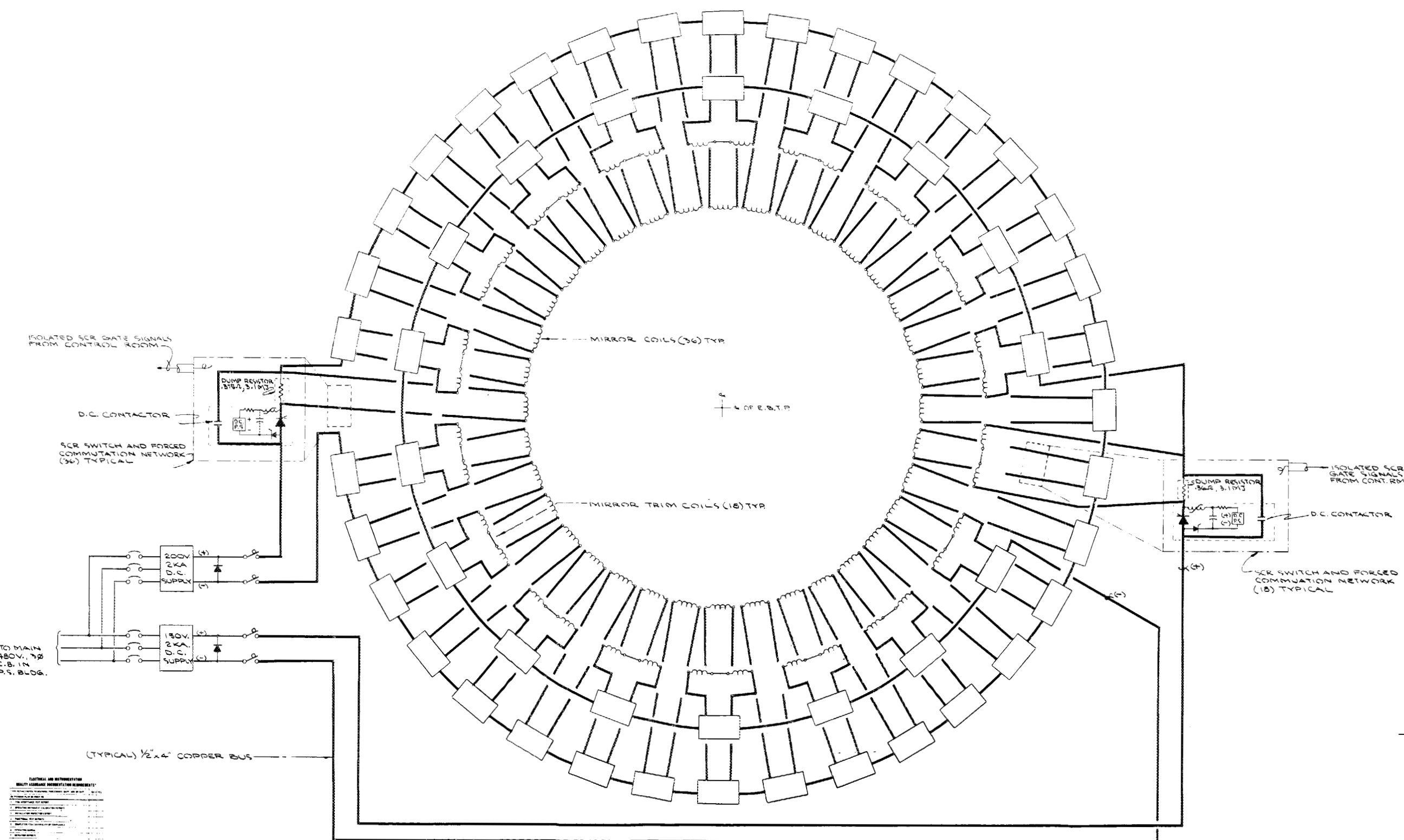
| | | |
|---------------------------------------|--------------------------------|--|
| TOLERANCES UNLESS OTHERWISE SPECIFIED | DES. S. A. LARSON 9/24/71 | UNION CARBIDE CORPORATION - NUCLEAR DIVISION |
| FRACTIONS 1/16 DECIMALS | CHK. C. S. EULMER, JR. 9/22/72 | |
| ANGLES BREAK SHARP EDGES FINISH | CHK. J. S. ... 9/21/71 | |
| | | |
| A. E. | | |
| U.C.E. NO. | | |
| DRAWING APPROVALS | | |
| DATE | | |
| NOTED AB945A-11 E2E 34109SK002 | | |



NO REPRESENTATION OF WARRANTY EXPRESSED OR IMPLIED IS MADE AS TO THE ACCURACY, COMPLETENESS OR USEFULNESS OF THE INFORMATION OR STATEMENTS CONTAINED IN THESE DRAWINGS OR THAT THE USE OF THESE DRAWINGS OF ANY INSTRUMENT, APPARATUS OR PROCESS DESCRIBED IN THESE DRAWINGS MAY NOT IMPROVE PRIVATE RIGHTS OF TITLE, NO LIABILITY IS ASSUMED BY THE USE OF ANY INFORMATION APPARATUS OR PROCESS DESCRIBED IN THESE DRAWINGS. DRAWINGS MADE AVAILABLE FOR INFORMATION TO BIDDERS ARE NOT TO BE USED FOR OTHER PURPOSES, AND ARE TO BE RETURNED UPON REQUEST OF THE CONTRACTING CONTRACTOR.

| | |
|--|--|
| TOLERANCES UNLESS OTHERWISE SPECIFIED: DIMENSIONS: FRACTIONS: 1/16, 1/8, 1/4, 3/8, 1/2, 5/8, 3/4, 7/8, 1, 1 1/4, 1 1/2, 1 3/4, 2, 2 1/4, 2 1/2, 3, 3 1/4, 3 1/2, 4, 4 1/4, 4 1/2, 5, 5 1/4, 5 1/2, 6, 6 1/4, 6 1/2, 7, 7 1/4, 7 1/2, 8, 8 1/4, 8 1/2, 9, 9 1/4, 9 1/2, 10, 10 1/4, 10 1/2, 11, 11 1/4, 11 1/2, 12, 12 1/4, 12 1/2, 13, 13 1/4, 13 1/2, 14, 14 1/4, 14 1/2, 15, 15 1/4, 15 1/2, 16, 16 1/4, 16 1/2, 17, 17 1/4, 17 1/2, 18, 18 1/4, 18 1/2, 19, 19 1/4, 19 1/2, 20, 20 1/4, 20 1/2, 21, 21 1/4, 21 1/2, 22, 22 1/4, 22 1/2, 23, 23 1/4, 23 1/2, 24, 24 1/4, 24 1/2, 25, 25 1/4, 25 1/2, 26, 26 1/4, 26 1/2, 27, 27 1/4, 27 1/2, 28, 28 1/4, 28 1/2, 29, 29 1/4, 29 1/2, 30, 30 1/4, 30 1/2, 31, 31 1/4, 31 1/2, 32, 32 1/4, 32 1/2, 33, 33 1/4, 33 1/2, 34, 34 1/4, 34 1/2, 35, 35 1/4, 35 1/2, 36, 36 1/4, 36 1/2, 37, 37 1/4, 37 1/2, 38, 38 1/4, 38 1/2, 39, 39 1/4, 39 1/2, 40, 40 1/4, 40 1/2, 41, 41 1/4, 41 1/2, 42, 42 1/4, 42 1/2, 43, 43 1/4, 43 1/2, 44, 44 1/4, 44 1/2, 45, 45 1/4, 45 1/2, 46, 46 1/4, 46 1/2, 47, 47 1/4, 47 1/2, 48, 48 1/4, 48 1/2, 49, 49 1/4, 49 1/2, 50, 50 1/4, 50 1/2, 51, 51 1/4, 51 1/2, 52, 52 1/4, 52 1/2, 53, 53 1/4, 53 1/2, 54, 54 1/4, 54 1/2, 55, 55 1/4, 55 1/2, 56, 56 1/4, 56 1/2, 57, 57 1/4, 57 1/2, 58, 58 1/4, 58 1/2, 59, 59 1/4, 59 1/2, 60, 60 1/4, 60 1/2, 61, 61 1/4, 61 1/2, 62, 62 1/4, 62 1/2, 63, 63 1/4, 63 1/2, 64, 64 1/4, 64 1/2, 65, 65 1/4, 65 1/2, 66, 66 1/4, 66 1/2, 67, 67 1/4, 67 1/2, 68, 68 1/4, 68 1/2, 69, 69 1/4, 69 1/2, 70, 70 1/4, 70 1/2, 71, 71 1/4, 71 1/2, 72, 72 1/4, 72 1/2, 73, 73 1/4, 73 1/2, 74, 74 1/4, 74 1/2, 75, 75 1/4, 75 1/2, 76, 76 1/4, 76 1/2, 77, 77 1/4, 77 1/2, 78, 78 1/4, 78 1/2, 79, 79 1/4, 79 1/2, 80, 80 1/4, 80 1/2, 81, 81 1/4, 81 1/2, 82, 82 1/4, 82 1/2, 83, 83 1/4, 83 1/2, 84, 84 1/4, 84 1/2, 85, 85 1/4, 85 1/2, 86, 86 1/4, 86 1/2, 87, 87 1/4, 87 1/2, 88, 88 1/4, 88 1/2, 89, 89 1/4, 89 1/2, 90, 90 1/4, 90 1/2, 91, 91 1/4, 91 1/2, 92, 92 1/4, 92 1/2, 93, 93 1/4, 93 1/2, 94, 94 1/4, 94 1/2, 95, 95 1/4, 95 1/2, 96, 96 1/4, 96 1/2, 97, 97 1/4, 97 1/2, 98, 98 1/4, 98 1/2, 99, 99 1/4, 99 1/2, 100, 100 1/4, 100 1/2, 101, 101 1/4, 101 1/2, 102, 102 1/4, 102 1/2, 103, 103 1/4, 103 1/2, 104, 104 1/4, 104 1/2, 105, 105 1/4, 105 1/2, 106, 106 1/4, 106 1/2, 107, 107 1/4, 107 1/2, 108, 108 1/4, 108 1/2, 109, 109 1/4, 109 1/2, 110, 110 1/4, 110 1/2, 111, 111 1/4, 111 1/2, 112, 112 1/4, 112 1/2, 113, 113 1/4, 113 1/2, 114, 114 1/4, 114 1/2, 115, 115 1/4, 115 1/2, 116, 116 1/4, 116 1/2, 117, 117 1/4, 117 1/2, 118, 118 1/4, 118 1/2, 119, 119 1/4, 119 1/2, 120, 120 1/4, 120 1/2, 121, 121 1/4, 121 1/2, 122, 122 1/4, 122 1/2, 123, 123 1/4, 123 1/2, 124, 124 1/4, 124 1/2, 125, 125 1/4, 125 1/2, 126, 126 1/4, 126 1/2, 127, 127 1/4, 127 1/2, 128, 128 1/4, 128 1/2, 129, 129 1/4, 129 1/2, 130, 130 1/4, 130 1/2, 131, 131 1/4, 131 1/2, 132, 132 1/4, 132 1/2, 133, 133 1/4, 133 1/2, 134, 134 1/4, 134 1/2, 135, 135 1/4, 135 1/2, 136, 136 1/4, 136 1/2, 137, 137 1/4, 137 1/2, 138, 138 1/4, 138 1/2, 139, 139 1/4, 139 1/2, 140, 140 1/4, 140 1/2, 141, 141 1/4, 141 1/2, 142, 142 1/4, 142 1/2, 143, 143 1/4, 143 1/2, 144, 144 1/4, 144 1/2, 145, 145 1/4, 145 1/2, 146, 146 1/4, 146 1/2, 147, 147 1/4, 147 1/2, 148, 148 1/4, 148 1/2, 149, 149 1/4, 149 1/2, 150, 150 1/4, 150 1/2, 151, 151 1/4, 151 1/2, 152, 152 1/4, 152 1/2, 153, 153 1/4, 153 1/2, 154, 154 1/4, 154 1/2, 155, 155 1/4, 155 1/2, 156, 156 1/4, 156 1/2, 157, 157 1/4, 157 1/2, 158, 158 1/4, 158 1/2, 159, 159 1/4, 159 1/2, 160, 160 1/4, 160 1/2, 161, 161 1/4, 161 1/2, 162, 162 1/4, 162 1/2, 163, 163 1/4, 163 1/2, 164, 164 1/4, 164 1/2, 165, 165 1/4, 165 1/2, 166, 166 1/4, 166 1/2, 167, 167 1/4, 167 1/2, 168, 168 1/4, 168 1/2, 169, 169 1/4, 169 1/2, 170, 170 1/4, 170 1/2, 171, 171 1/4, 171 1/2, 172, 172 1/4, 172 1/2, 173, 173 1/4, 173 1/2, 174, 174 1/4, 174 1/2, 175, 175 1/4, 175 1/2, 176, 176 1/4, 176 1/2, 177, 177 1/4, 177 1/2, 178, 178 1/4, 178 1/2, 179, 179 1/4, 179 1/2, 180, 180 1/4, 180 1/2, 181, 181 1/4, 181 1/2, 182, 182 1/4, 182 1/2, 183, 183 1/4, 183 1/2, 184, 184 1/4, 184 1/2, 185, 185 1/4, 185 1/2, 186, 186 1/4, 186 1/2, 187, 187 1/4, 187 1/2, 188, 188 1/4, 188 1/2, 189, 189 1/4, 189 1/2, 190, 190 1/4, 190 1/2, 191, 191 1/4, 191 1/2, 192, 192 1/4, 192 1/2, 193, 193 1/4, 193 1/2, 194, 194 1/4, 194 1/2, 195, 195 1/4, 195 1/2, 196, 196 1/4, 196 1/2, 197, 197 1/4, 197 1/2, 198, 198 1/4, 198 1/2, 199, 199 1/4, 199 1/2, 200, 200 1/4, 200 1/2, 201, 201 1/4, 201 1/2, 202, 202 1/4, 202 1/2, 203, 203 1/4, 203 1/2, 204, 204 1/4, 204 1/2, 205, 205 1/4, 205 1/2, 206, 206 1/4, 206 1/2, 207, 207 1/4, 207 1/2, 208, 208 1/4, 208 1/2, 209, 209 1/4, 209 1/2, 210, 210 1/4, 210 1/2, 211, 211 1/4, 211 1/2, 212, 212 1/4, 212 1/2, 213, 213 1/4, 213 1/2, 214, 214 1/4, 214 1/2, 215, 215 1/4, 215 1/2, 216, 216 1/4, 216 1/2, 217, 217 1/4, 217 1/2, 218, 218 1/4, 218 1/2, 219, 219 1/4, 219 1/2, 220, 220 1/4, 220 1/2, 221, 221 1/4, 221 1/2, 222, 222 1/4, 222 1/2, 223, 223 1/4, 223 1/2, 224, 224 1/4, 224 1/2, 225, 225 1/4, 225 1/2, 226, 226 1/4, 226 1/2, 227, 227 1/4, 227 1/2, 228, 228 1/4, 228 1/2, 229, 229 1/4, 229 1/2, 230, 230 1/4, 230 1/2, 231, 231 1/4, 231 1/2, 232, 232 1/4, 232 1/2, 233, 233 1/4, 233 1/2, 234, 234 1/4, 234 1/2, 235, 235 1/4, 235 1/2, 236, 236 1/4, 236 1/2, 237, 237 1/4, 237 1/2, 238, 238 1/4, 238 1/2, 239, 239 1/4, 239 1/2, 240, 240 1/4, 240 1/2, 241, 241 1/4, 241 1/2, 242, 242 1/4, 242 1/2, 243, 243 1/4, 243 1/2, 244, 244 1/4, 244 1/2, 245, 245 1/4, 245 1/2, 246, 246 1/4, 246 1/2, 247, 247 1/4, 247 1/2, 248, 248 1/4, 248 1/2, 249, 249 1/4, 249 1/2, 250, 250 1/4, 250 1/2, 251, 251 1/4, 251 1/2, 252, 252 1/4, 252 1/2, 253, 253 1/4, 253 1/2, 254, 254 1/4, 254 1/2, 255, 255 1/4, 255 1/2, 256, 256 1/4, 256 1/2, 257, 257 1/4, 257 1/2, 258, 258 1/4, 258 1/2, 259, 259 1/4, 259 1/2, 260, 260 1/4, 260 1/2, 261, 261 1/4, 261 1/2, 262, 262 1/4, 262 1/2, 263, 263 1/4, 263 1/2, 264, 264 1/4, 264 1/2, 265, 265 1/4, 265 1/2, 266, 266 1/4, 266 1/2, 267, 267 1/4, 267 1/2, 268, 268 1/4, 268 1/2, 269, 269 1/4, 269 1/2, 270, 270 1/4, 270 1/2, 271, 271 1/4, 271 1/2, 272, 272 1/4, 272 1/2, 273, 273 1/4, 273 1/2, 274, 274 1/4, 274 1/2, 275, 275 1/4, 275 1/2, 276, 276 1/4, 276 1/2, 277, 277 1/4, 277 1/2, 278, 278 1/4, 278 1/2, 279, 279 1/4, 279 1/2, 280, 280 1/4, 280 1/2, 281, 281 1/4, 281 1/2, 282, 282 1/4, 282 1/2, 283, 283 1/4, 283 1/2, 284, 284 1/4, 284 1/2, 285, 285 1/4, 285 1/2, 286, 286 1/4, 286 1/2, 287, 287 1/4, 287 1/2, 288, 288 1/4, 288 1/2, 289, 289 1/4, 289 1/2, 290, 290 1/4, 290 1/2, 291, 291 1/4, 291 1/2, 292, 292 1/4, 292 1/2, 293, 293 1/4, 293 1/2, 294, 294 1/4, 294 1/2, 295, 295 1/4, 295 1/2, 296, 296 1/4, 296 1/2, 297, 297 1/4, 297 1/2, 298, 298 1/4, 298 1/2, 299, 299 1/4, 299 1/2, 300, 300 1/4, 300 1/2, 301, 301 1/4, 301 1/2, 302, 302 1/4, 302 1/2, 303, 303 1/4, 303 1/2, 304, 304 1/4, 304 1/2, 305, 305 1/4, 305 1/2, 306, 306 1/4, 306 1/2, 307, 307 1/4, 307 1/2, 308, 308 1/4, 308 1/2, 309, 309 1/4, 309 1/2, 310, 310 1/4, 310 1/2, 311, 311 1/4, 311 1/2, 312, 312 1/4, 312 1/2, 313, 313 1/4, 313 1/2, 314, 314 1/4, 314 1/2, 315, 315 1/4, 315 1/2, 316, 316 1/4, 316 1/2, 317, 317 1/4, 317 1/2, 318, 318 1/4, 318 1/2, 319, 319 1/4, 319 1/2, 320, 320 1/4, 320 1/2, 321, 321 1/4, 321 1/2, 322, 322 1/4, 322 1/2, 323, 323 1/4, 323 1/2, 324, 324 1/4, 324 1/2, 325, 325 1/4, 325 1/2, 326, 326 1/4, 326 1/2, 327, 327 1/4, 327 1/2, 328, 328 1/4, 328 1/2, 329, 329 1/4, 329 1/2, 330, 330 1/4, 330 1/2, 331, 331 1/4, 331 1/2, 332, 332 1/4, 332 1/2, 333, 333 1/4, 333 1/2, 334, 334 1/4, 334 1/2, 335, 335 1/4, 335 1/2, 336, 336 1/4, 336 1/2, 337, 337 1/4, 337 1/2, 338, 338 1/4, 338 1/2, 339, 339 1/4, 339 1/2, 340, 340 1/4, 340 1/2, 341, 341 1/4, 341 1/2, 342, 342 1/4, 342 1/2, 343, 343 1/4, 343 1/2, 344, 344 1/4, 344 1/2, 345, 345 1/4, 345 1/2, 346, 346 1/4, 346 1/2, 347, 347 1/4, 347 1/2, 348, 348 1/4, 348 1/2, 349, 349 1/4, 349 1/2, 350, 350 1/4, 350 1/2, 351, 351 1/4, 351 1/2, 352, 352 1/4, 352 1/2, 353, 353 1/4, 353 1/2, 354, 354 1/4, 354 1/2, 355, 355 1/4, 355 1/2, 356, 356 1/4, 356 1/2, 357, 357 1/4, 357 1/2, 358, 358 1/4, 358 1/2, 359, 359 1/4, 359 1/2, 360, 360 1/4, 360 1/2, 361, 361 1/4, 361 1/2, 362, 362 1/4, 362 1/2, 363, 363 1/4, 363 1/2, 364, 364 1/4, 364 1/2, 365, 365 1/4, 365 1/2, 366, 366 1/4, 366 1/2, 367, 367 1/4, 367 1/2, 368, 368 1/4, 368 1/2, 369, 369 1/4, 369 1/2, 370, 370 1/4, 370 1/2, 371, 371 1/4, 371 1/2, 372, 372 1/4, 372 1/2, 373, 373 1/4, 373 1/2, 374, 374 1/4, 374 1/2, 375, 375 1/4, 375 1/2, 376, 376 1/4, 376 1/2, 377, 377 1/4, 377 1/2, 378, 378 1/4, 378 1/2, 379, 379 1/4, 379 1/2, 380, 380 1/4, 380 1/2, 381, 381 1/4, 381 1/2, 382, 382 1/4, 382 1/2, 383, 383 1/4, 383 1/2, 384, 384 1/4, 384 1/2, 385, 385 1/4, 385 1/2, 386, 386 1/4, 386 1/2, 387, 387 1/4, 387 1/2, 388, 388 1/4, 388 1/2, 389, 389 1/4, 389 1/2, 390, 390 1/4, 390 1/2, 391, 391 1/4, 391 1/2, 392, 392 1/4, 392 1/2, 393, 393 1/4, 393 1/2, 394, 394 1/4, 394 1/2, 395, 395 1/4, 395 1/2, 396, 396 1/4, 396 1/2, 397, 397 1/4, 397 1/2, 398, 398 1/4, 398 1/2, 399, 399 1/4, 399 1/2, 400, 400 1/4, 400 1/2, 401, 401 1/4, 401 1/2, 402, 402 1/4, 402 1/2, 403, 403 1/4, 403 1/2, 404, 404 1/4, 404 1/2, 405, 405 1/4, 405 1/2, 406, 406 1/4, 406 1/2, 407, 407 1/4, 407 1/2, 408, 408 1/4, 408 1/2, 409, 409 1/4, 409 1/2, 410, 410 1/4, 410 1/2, 411, 411 1/4, 411 1/2, 412, 412 1/4, 412 1/2, 413, 413 1/4, 413 1/2, 414, 414 1/4, 414 1/2, 415, 415 1/4, 415 1/2, 416, 416 1/4, 416 1/2, 417, 417 1/4, 417 1/2, 418, 418 1/4, 418 1/2, 419, 419 1/4, 419 1/2, 420, 420 1/4, 420 1/2, 421, 421 1/4, 421 1/2, 422, 422 1/4, 422 1/2, 423, 423 1/4, 423 1/2, 424, 424 1/4, 424 1/2, 425, 425 1/4, 425 1/2, 426, 426 1/4, 426 1/2, 427, 427 1/4, 427 1/2, 428, 428 1/4, 428 1/2, 429, 429 1/4, 429 1/2, 430, 430 1/4, 430 1/2, 431, 431 1/4, 431 1/2, 432, 432 1/4, 432 1/2, 433, 433 1/4, 433 1/2, 434, 434 1/4, 434 1/2, 435, 435 1/4, 435 1/2, 436, 436 1/4, 436 1/2, 437, 437 1/4, 437 1/2, 438, 438 1/4, 438 1/2, 439, 439 1/4, 439 1/2, 440, 440 1/4, 440 1/2, 441, 441 1/4, 441 1/2, 442, 442 1/4, 442 1/2, 443, 443 1/4, 443 1/2, 444, 444 1/4, 444 1/2, 445, 445 1/4, 445 1/2, 446, 446 1/4, 446 1/2, 447, 447 1/4, 447 1/2, 448, 448 1/4, 448 1/2, 449, 449 1/4, 449 1/2, 450, 450 1/4, 450 1/2, 451, 451 1/4, 451 1/2, 452, 452 1/4, 452 1/2, 453, 453 1/4, 453 1/2, 454, 454 1/4, 454 1/2, 455, 455 1/4, 455 1/2, 456, 456 1/4, 456 1/2, 457, 457 1/4, 457 1/2, 458, 458 1/4, 458 1/2, 459, 459 1/4, 459 1/2, 460, 460 1/4, 460 1/2, 461, 461 1/4, 461 1/2, 462, 462 1/4, 462 1/2, 463, 463 1/4, 463 1/2, 464, 464 1/4, 464 1/2, 465, 465 1/4, 465 1/2, 466, 466 1/4, 466 1/2, 467, 467 1/4, 467 1/2, 468, 468 1/4, 468 1/2, 469, 469 1/4, 469 1/2, 470, 470 1/4, 470 1/2, 471, 471 1/4, 471 1/2, 472, 472 1/4, 472 1/2, 473, 473 1/4, 473 1/2, 474, 474 1/4, 474 1/2, 475, 475 1/4, 475 1/2, 476, 476 1/4, 476 1/2, 477, 477 1/4, 477 1/2, 478, 478 1/4, 478 1/2, 479, 479 1/4, 479 1/2, 480, 480 1/4, 480 1/2, 481, 481 1/4, 481 1/2, 482, 482 1/4, 482 1/2, 483, 483 1/4, 483 1/2, 484, 484 1/4, 484 1/2, 485, 485 1/4, 485 1/2, 486, 486 1/4, 486 1/2, 487, 487 1/4, 487 1/2, 488, 488 1/4, 488 1/2, 489, 489 1/4, 489 1/2, 490, 490 1/4, 490 1/2, 491, 491 1/4, 491 1/2, 492, 492 1/4, 492 1/2, 493, 493 1/4, 493 1/2, 494, 494 1/4, 494 1/2, 495, 495 1/4, 495 1/2, 496, 496 1/4, 496 1/2, 497, 497 1/4, 497 1/2, 498, 498 1/4, 498 1/2, 499, 499 1/4, 499 1/2, 500, 500 1/4, 500 1/2, 501, 501 1/4, 501 1/2, 502, 502 1/4, 502 1/2, 503, 503 1/4, 503 1/2, 504, 504 1/4, 504 1/2, 505, 505 1/4, 505 1/2, 506, 506 1/4, 506 1/2, 507, 507 1/4, 507 1/2, 508, 508 1/4, 508 1/2, 509, 509 1/4, 509 1/2, 510, 510 1/4, 510 1/2, 511, 511 1/4, 511 1/2, 512, 512 1/4, 512 1/2, 513, 513 1/4, 513 1/2, 514, 514 1/4, 514 1/2, 515, 515 1/4, 515 1/2, 516, 516 1/4, 51 | |
|--|--|

SCHEMATIC DIAGRAM
MIRROR COILS



FACTORY AND INSTRUMENT

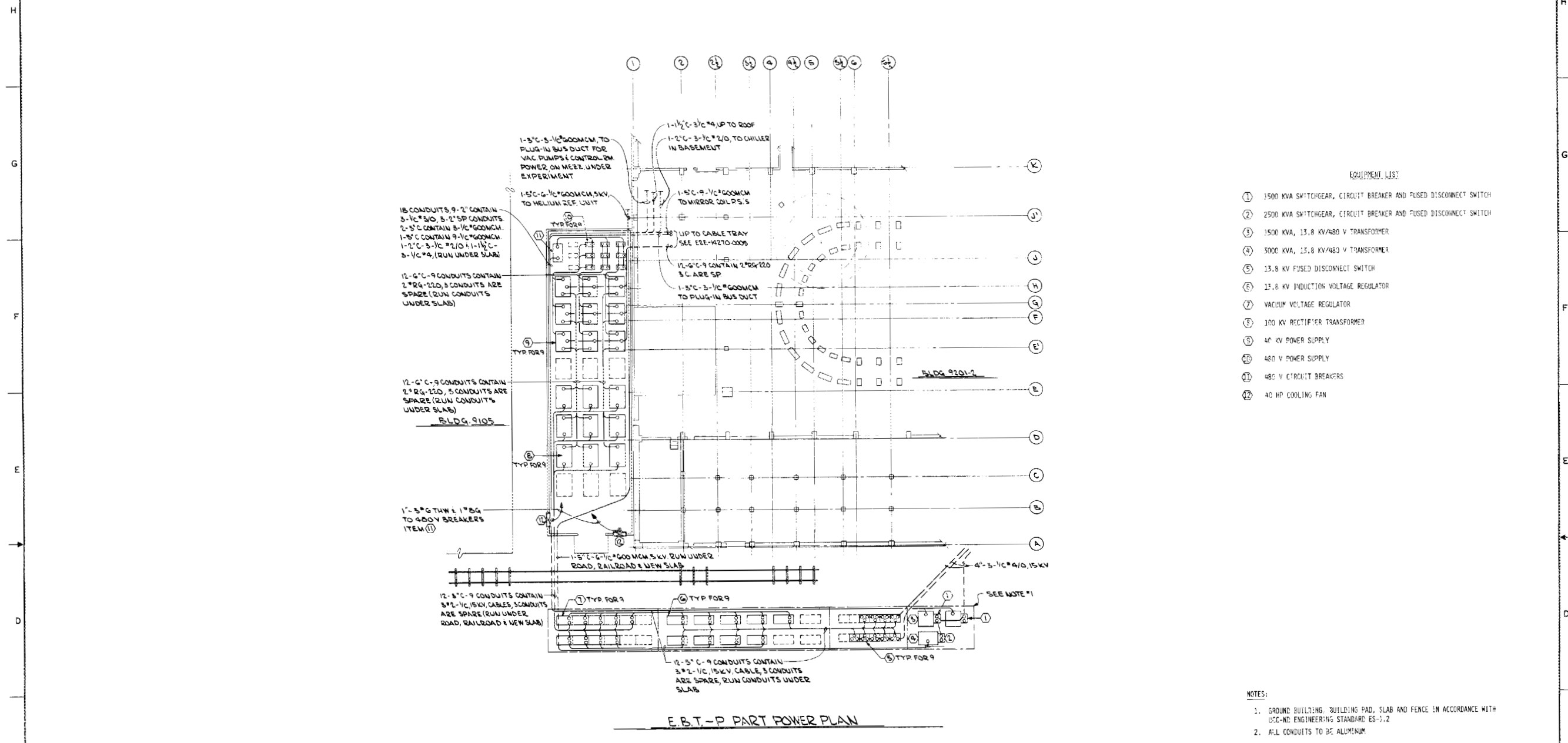
| NO. | DESCRIPTION | QTY | REMARKS |
|-----|-------------|-----|---------|
| 1 | ... | ... | ... |
| 2 | ... | ... | ... |
| 3 | ... | ... | ... |
| 4 | ... | ... | ... |
| 5 | ... | ... | ... |
| 6 | ... | ... | ... |
| 7 | ... | ... | ... |
| 8 | ... | ... | ... |
| 9 | ... | ... | ... |
| 10 | ... | ... | ... |

NO REPRESENTATION OR WARRANTY, EXPRESS OR IMPLIED, IS MADE AS TO THE ACCURACY, COMPLETENESS OR USABILITY OF THE INFORMATION OR STATEMENTS CONTAINED IN THESE DRAWINGS OR THAT THE USE OF SUCH INFORMATION OR STATEMENTS WILL BE WITHOUT LIABILITY TO THE DRAWING ENGINEER OR THE COMPANY. THE USER OF ANY INFORMATION, APPLICABLE TO THESE DRAWINGS, SHALL BE RESPONSIBLE FOR OBTAINING ALL NECESSARY PERMITS AND APPROVALS FROM THE APPROPRIATE AGENCIES AND FOR THE PROTECTION OF THE INFORMATION CONTAINED HEREIN FROM UNAUTHORIZED DISCLOSURE. THE USER SHALL BE RESPONSIBLE FOR THE PROTECTION OF THE INFORMATION CONTAINED HEREIN FROM UNAUTHORIZED DISCLOSURE.

| REV | DESCRIPTION | BY | CHK | SECT | DEPT | DATE | PR | REQ | DATE | ISSUED | DATE | DOE | DATE |
|-----|--------------------|----|-----|------|------|------|----|-----|------|--------|------|-----|------|
| 0 | ISSUED FOR COMMENT | | | | | | | | | | | | |

| | | | |
|---------------------------------------|------------------------|---|-------------------|
| TOLERANCES UNLESS OTHERWISE SPECIFIED | | DESIGNED BY: EVANS | DATE: 8/19 |
| FRACTIONS: 1/16 | DECIMALS: 0.001 | CHK'D BY: EVANS | DATE: 8/19 |
| ANGLES: 30° | MAX. DIMENSIONS: 0.001 | SECT: 7A | DATE: 8/29 |
| UNLESS SHOWN OTHERWISE | | DEPT'S PLANT: | |
| UNLESS SHOWN OTHERWISE | | SCALE: NONE | DATE: 8/29 |
| UNLESS SHOWN OTHERWISE | | PROJECT: E.B.T.P. MIRROR & TRIM COIL PWR SUPPLY & ENERGY DUMP SCH. DIAG. | REV: 10 |
| UNLESS SHOWN OTHERWISE | | PLANT: 2E | CLAS: U |
| UNLESS SHOWN OTHERWISE | | BLDG: 14270 | CLAS: U |
| UNLESS SHOWN OTHERWISE | | REV: 10003 | REV: 10 |

UNION CARBIDE CORPORATION - NUCLEAR DIVISION



EQUIPMENT LIST:

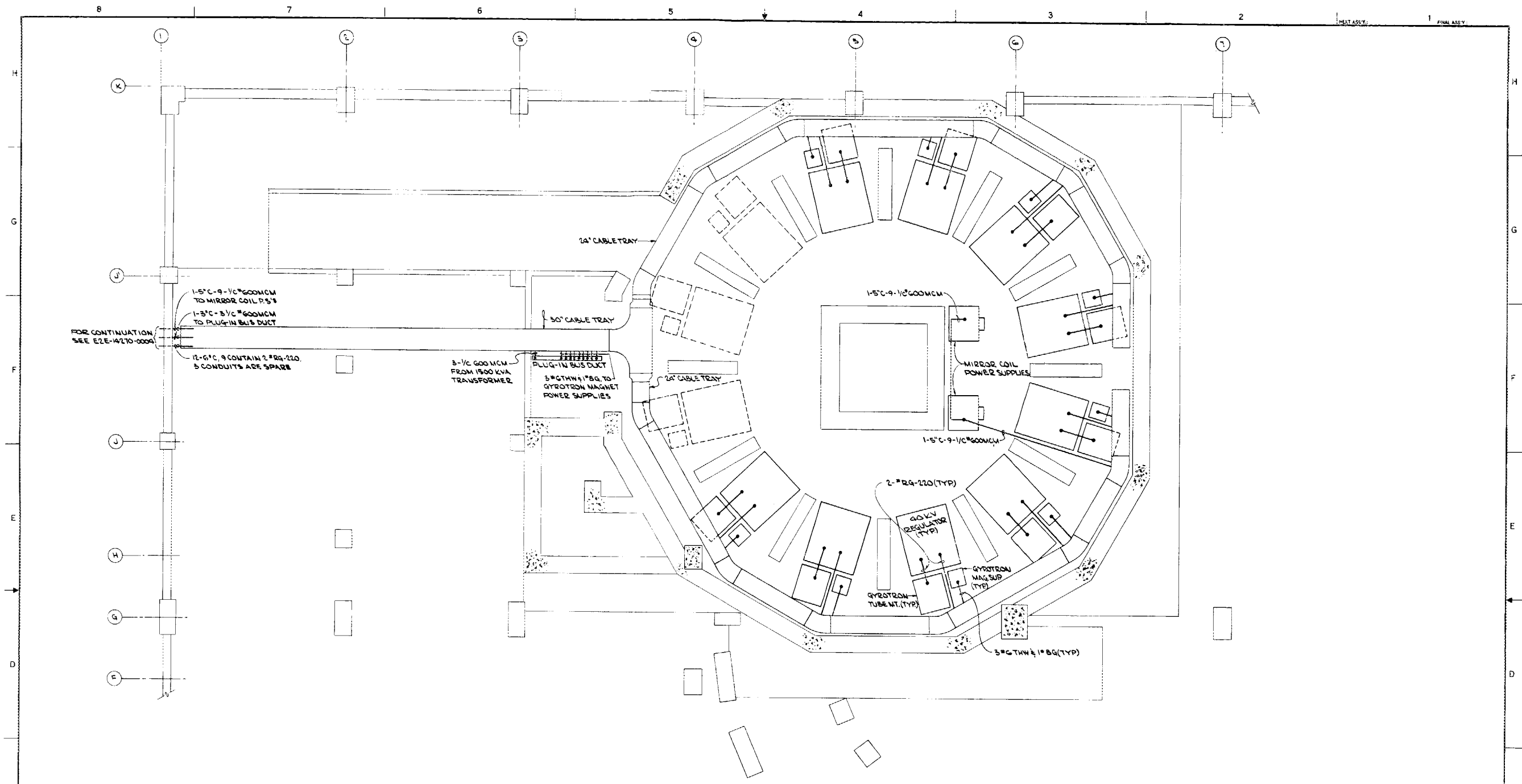
- ① 1500 KVA SWITCHGEAR, CIRCUIT BREAKER AND FUSED DISCONNECT SWITCH
- ② 2500 KVA SWITCHGEAR, CIRCUIT BREAKER AND FUSED DISCONNECT SWITCH
- ③ 1500 KVA, 13.8 KV/480 V TRANSFORMER
- ④ 3000 KVA, 13.8 KV/480 V TRANSFORMER
- ⑤ 13.8 KV FUSED DISCONNECT SWITCH
- ⑥ 13.8 KV INDUCTION VOLTAGE REGULATOR
- ⑦ VACUUM VOLTAGE REGULATOR
- ⑧ 100 KV RECTIFIER TRANSFORMER
- ⑨ 40 KV POWER SUPPLY
- ⑩ 480 V POWER SUPPLY
- ⑪ 480 V CIRCUIT BREAKERS
- ⑫ 40 HP COOLING FAN

- NOTES:
1. GROUND BUILDING, BUILDING PAD, SLAB AND FENCE IN ACCORDANCE WITH USC-ND ENGINEERING STANDARD ES-1.2
 2. ALL CONDUITS TO BE ALUMINUM

E.B.T.-P PART POWER PLAN

NO REPRESENTATION OR WARRANTY EXPRESSED OR IMPLIED IS MADE AS TO THE ACCURACY, COMPLETENESS OR USEFULNESS OF THE INFORMATION OR FEATURES CONTAINED IN THESE DRAWINGS, OR THAT THE USE OR MISUSE OF ANY INFORMATION APPEARING HEREON OR THEREON SHALL BE THE RESPONSIBILITY OF THE USER. THE USER SHALL BE RESPONSIBLE FOR OBTAINING ALL NECESSARY PERMITS AND APPROVALS FROM THE APPROPRIATE AGENCIES AND FOR OBTAINING ALL NECESSARY INFORMATION FROM THE USER OF ANY INFORMATION APPEARING HEREON OR THEREON. THE USER SHALL BE RESPONSIBLE FOR OBTAINING ALL NECESSARY INFORMATION FROM THE USER OF ANY INFORMATION APPEARING HEREON OR THEREON. THE USER SHALL BE RESPONSIBLE FOR OBTAINING ALL NECESSARY INFORMATION FROM THE USER OF ANY INFORMATION APPEARING HEREON OR THEREON.

| | | | | |
|--|--|-------------------------------|--|--|
| UNLESS OTHERWISE SPECIFIED | | DESIGNED BY: R.S. BASTER 8-78 | UNION CARBIDE CORPORATION - NUCLEAR DIVISION | |
| DRAWN BY: D. DELAND JT 9-79 | | CHECKED BY: R.S. BASTER | E.B.T.-P POWER SUPPLIES LAYOUT SHEET #1 OF 2 | |
| TOLERANCES: FRACTIONS: 1/16 DECIMALS: .005 | | DATE: 9-79 | PWR SUP LAYOUT SH 1 | |
| SAMPLES: BREAK SHARP EDGES: MAX FINISH: | | SCALE: 1/8" = 1'-0" | REV 0 | |
| REVISION APPROVALS: | | DATE: 9-79 | E.E.L. 14270 0004 | |



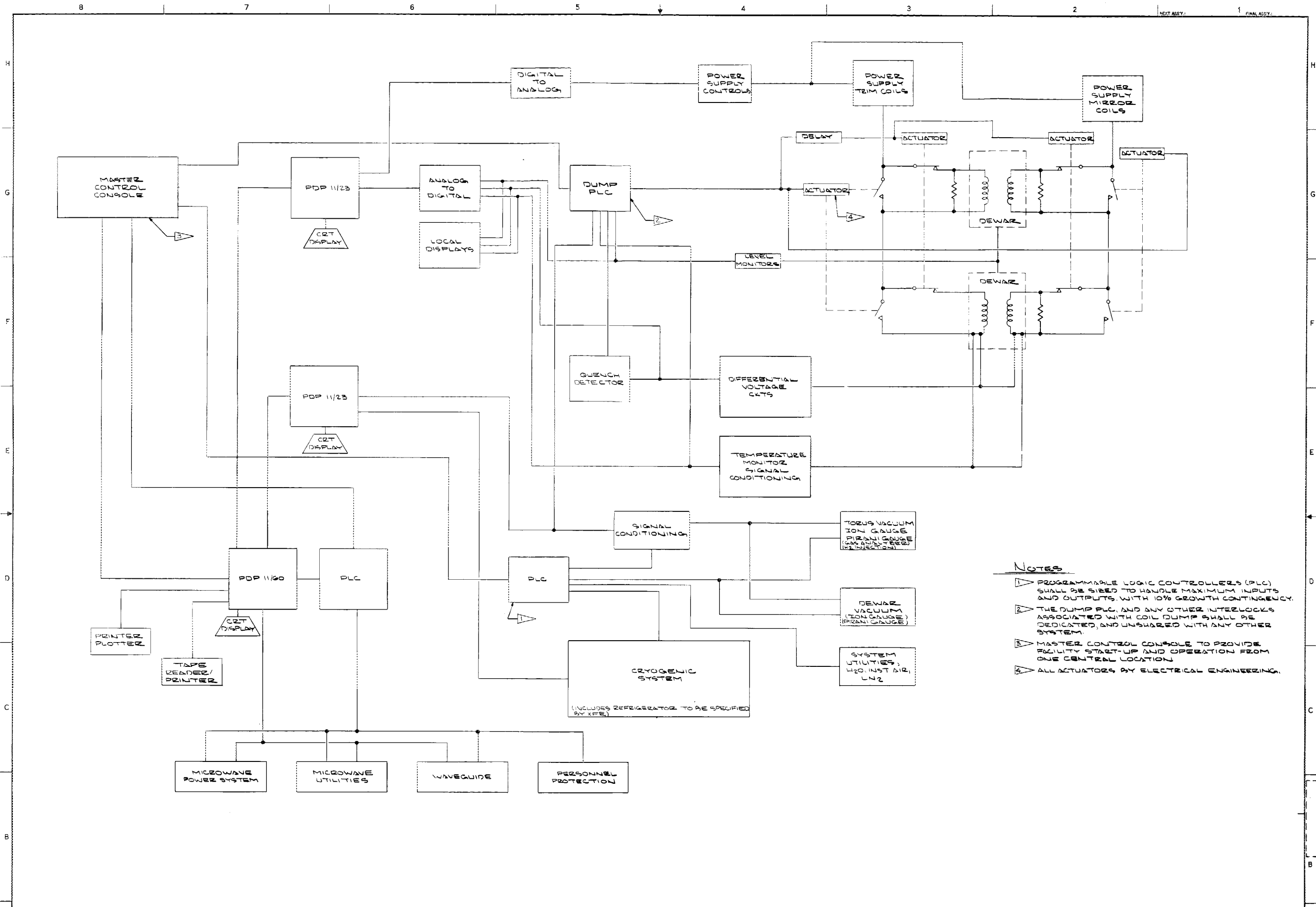
E.B.T.-P PART PLAN-1ST FL.
SCALE: 1/4"=1'-0"

ALL INFORMATION IS UNCLASSIFIED EXCEPT WHERE SHOWN OTHERWISE. THIS DOCUMENT IS UNCLASSIFIED EXCEPT WHERE SHOWN OTHERWISE. UNCLASSIFIED INFORMATION IS UNCLASSIFIED EXCEPT WHERE SHOWN OTHERWISE. UNCLASSIFIED INFORMATION IS UNCLASSIFIED EXCEPT WHERE SHOWN OTHERWISE.

| NO. | REVISION OR REUSE PURPOSE | BY | CHK | DEPT | DATE | REV | DATE | REV | DATE | REV | DATE | REV | DATE | REV | DATE |
|-----|---------------------------|----|-----|------|---------|-----|------|-----|------|-----|------|-----|------|-----|------|
| 0 | FOR COMMENT | RP | | | 5/22/77 | | | | | | | | | | |

| | |
|------------------------------|------------------|
| UNCLASSIFIED | DATE: 5-22-77 |
| EXCEPT WHERE SHOWN OTHERWISE | BY: RP |
| EXCEPT WHERE SHOWN OTHERWISE | CHK: [Signature] |
| EXCEPT WHERE SHOWN OTHERWISE | DATE: 5-22-77 |
| EXCEPT WHERE SHOWN OTHERWISE | REV: 1 |

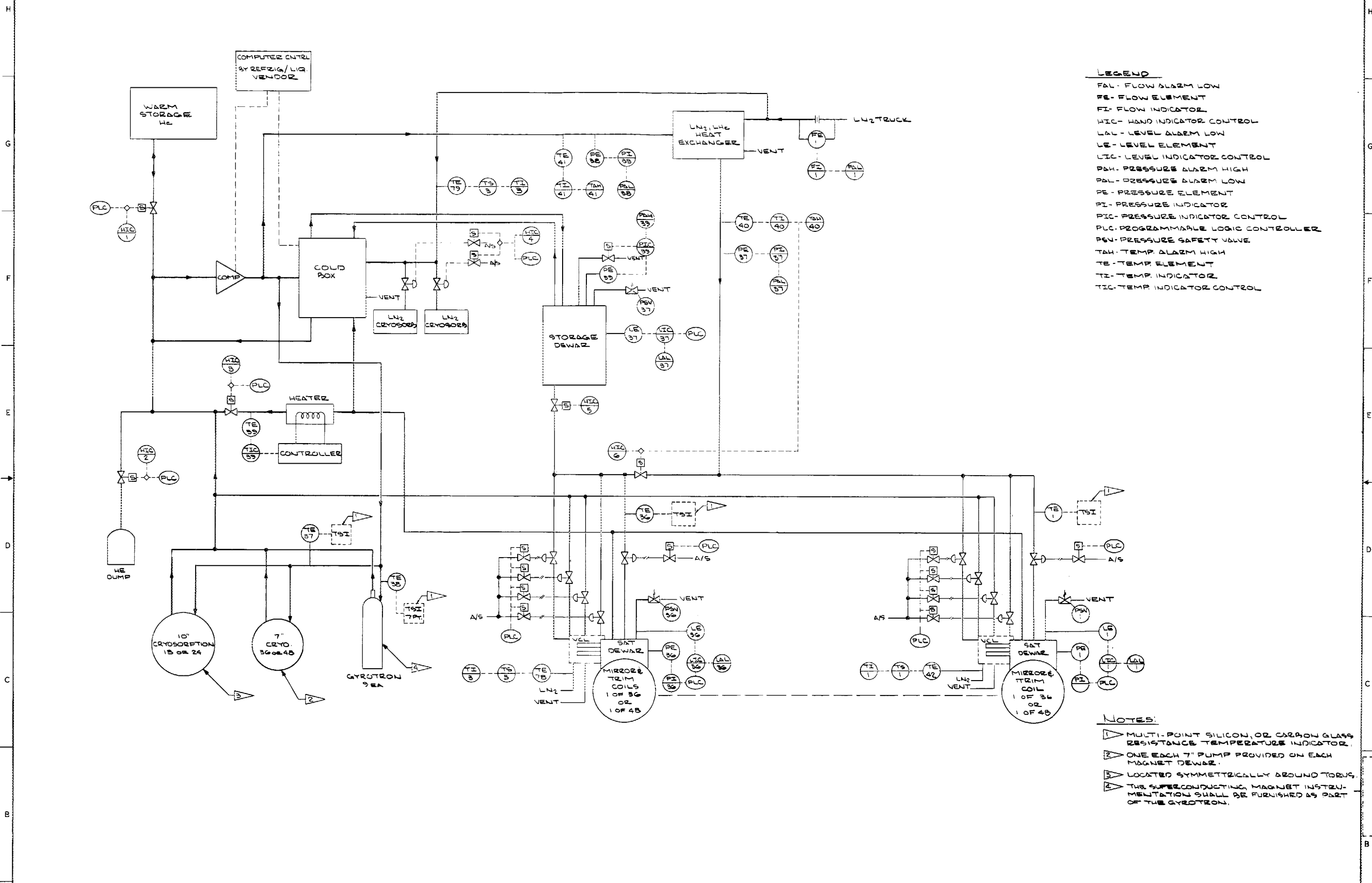
UNION CARBIDE CORPORATION - NUCLEAR DIVISION
 E.B.T.-P
 POWER SUPPLIES
 LAYOUT SHEET 2
 PWR SUP LAYOUT SH 2
 DATE: 5/22/77
 DRAWN BY: RP
 CHECKED BY: [Signature]
 E.L.E. 14210-0005



- NOTES**
- 1 PROGRAMMABLE LOGIC CONTROLLERS (PLC) SHALL BE SIZED TO HANDLE MAXIMUM INPUTS AND OUTPUTS WITH 10% GROWTH CONTINGENCY.
 - 2 THE DUMP PLC, AND ANY OTHER INTERLOCKS ASSOCIATED WITH COIL DUMP SHALL BE DEDICATED, AND UNSHARED WITH ANY OTHER SYSTEM.
 - 3 MASTER CONTROL CONSOLE TO PROVIDE FACILITY START-UP AND OPERATION FROM ONE CENTRAL LOCATION.
 - 4 ALL ACTUATORS BY ELECTRICAL ENGINEERING.

NO REPRESENTATION OR WARRANTY, EXPRESSED OR IMPLIED, IS MADE AS TO THE ACCURACY, COMPLETENESS OR USEFULNESS OF THE INFORMATION OR STATEMENTS CONTAINED IN THESE DRAWINGS OR THAT THE USE OR DISCLOSURE OF ANY INFORMATION CONTAINED HEREIN OR PROVIDED HEREON IN THESE DRAWINGS SHALL NOT BE HELD RESPONSIBLE BY THE DRAWING ENGINEER OR ANY OTHER PERSONS WHOSE SERVICES ARE USED IN THE PREPARATION OF THESE DRAWINGS. THE USER OF ANY INFORMATION CONTAINED HEREIN SHALL BE RESPONSIBLE FOR THE PROTECTION OF THIS INFORMATION. INFORMATION CONTAINED HEREIN IS UNCLASSIFIED AND IS TO BE RELEASED UPON REQUEST OF THE INFORMATION CONTROLLER.

| | | | | | | | | | | | | | |
|---|--|--|--|--|--|--|--|--|--|---|--|---|--|
| TOLERANCES UNLESS OTHERWISE SPECIFIED FRACTIONS: XX DECIMALS XX DECIMALS ANGLES: DEPT & PLANT BREAK SHARP EDGES MAX. LENGTH | | | | | | | | | | DESIGNED BY: J. J. WILSON DRAWN BY: M. J. WILSON CHECKED BY: M. J. WILSON DATE: 12/12/84 | | UNION CARBIDE CORPORATION - NUCLEAR DIVISION 1000 UNIVERSITY AVENUE, SUITE 1000 BOSTON, MASSACHUSETTS 02116 | |
| PROJECT: EPT-10 SYSTEM INSTRUMENTATION BLOCK DIAGRAM SYS INSTRU BLK DIAG | | | | | | | | | | SCALE: 1" = 10'-0" DATE: 12/12/84 | | DRAWING NO: 12E14270A010B | |
| REVISIONS: REV. NO. DESCRIPTION BY CHK. DATE 1. INITIAL ISSUE | | | | | | | | | | APPROVED: [Signature] DATE: 12/12/84 | | DRAWING APPROVALS: [Signature] DATE: 12/12/84 | |



- LEGEND**
- FAL - FLOW ALARM LOW
 - FE - FLOW ELEMENT
 - FI - FLOW INDICATOR
 - HIC - HAND INDICATOR CONTROL
 - LAL - LEVEL ALARM LOW
 - LE - LEVEL ELEMENT
 - LIC - LEVEL INDICATOR CONTROL
 - PAH - PRESSURE ALARM HIGH
 - PAL - PRESSURE ALARM LOW
 - PE - PRESSURE ELEMENT
 - PI - PRESSURE INDICATOR
 - PIC - PRESSURE INDICATOR CONTROL
 - PLC - PROGRAMMABLE LOGIC CONTROLLER
 - PSV - PRESSURE SAFETY VALVE
 - TAH - TEMP ALARM HIGH
 - TE - TEMP ELEMENT
 - TI - TEMP INDICATOR
 - TIC - TEMP INDICATOR CONTROL

- NOTES:**
- ▷ MULTI-POINT SILICON, OR CARBON GLASS RESISTANCE TEMPERATURE INDICATOR.
 - ▷ ONE EACH 7" PUMP PROVIDED ON EACH MAGNET DEWAR.
 - ▷ LOCATED SYMMETRICALLY AROUND TORUS.
 - ▷ THE SUPERCONDUCTING MAGNET INSTRUMENTATION SHALL BE FURNISHED AS PART OF THE GYROTRON.

NO REPRESENTATION OR WARRANTY, EXPRESSED OR IMPLIED, IS MADE AS TO THE ACCURACY, COMPLETENESS OR USEFULNESS OF THE INFORMATION OR STATEMENTS CONTAINED IN THESE DRAWINGS OR THAT THE USE OR MISUSE OF ANY INSTRUMENTATION, APPARATUS, EQUIPMENT OR PROCEDURE DESCRIBED IN THESE DRAWINGS MAY BE THE SUBJECT OF PATENT RIGHTS OF OTHERS. NO LIABILITY IS ASSUMED BY THE DRAWING ENGINEER OR ARCHITECT FOR ANY DAMAGE TO PERSONS OR PROPERTY OR FOR ANY CONSEQUENCES ARISING FROM THE USE OF ANY INSTRUMENTATION, APPARATUS, EQUIPMENT OR PROCEDURE DESCRIBED IN THESE DRAWINGS. REVISIONS SHALL BE AVAILABLE FOR INFORMATION TO USERS AND NOT TO BE USED FOR OTHER PURPOSES. THIS DRAWING IS TO BE RETURNED UPON REQUEST OF THE PURCHASING CONTRACTOR.

| REV | FOR COMMENT | DESCRIPTION | BY | CHK | DEPT | DATE | PR | REQ | DATE | SUBCD | DATE | DOE | DATE | CA | EC | EE | EN | IE | IF | IS | IT | JE | KA | KB | KC | KE | KF | KG | KH | KI | KL | KN | CO | DATE | SCALE | DATE |
|-----|-------------|-------------|----|-----|------|------|----|-----|------|-------|------|-----|------|----|----|----|----|----|----|----|----|----|----|----|----|----|----|----|----|----|----|----|----|------|-------|------|
| | | | | | | | | | | | | | | | | | | | | | | | | | | | | | | | | | | | | |

UNION CARBIDE CORPORATION - NUCLEAR DIVISION

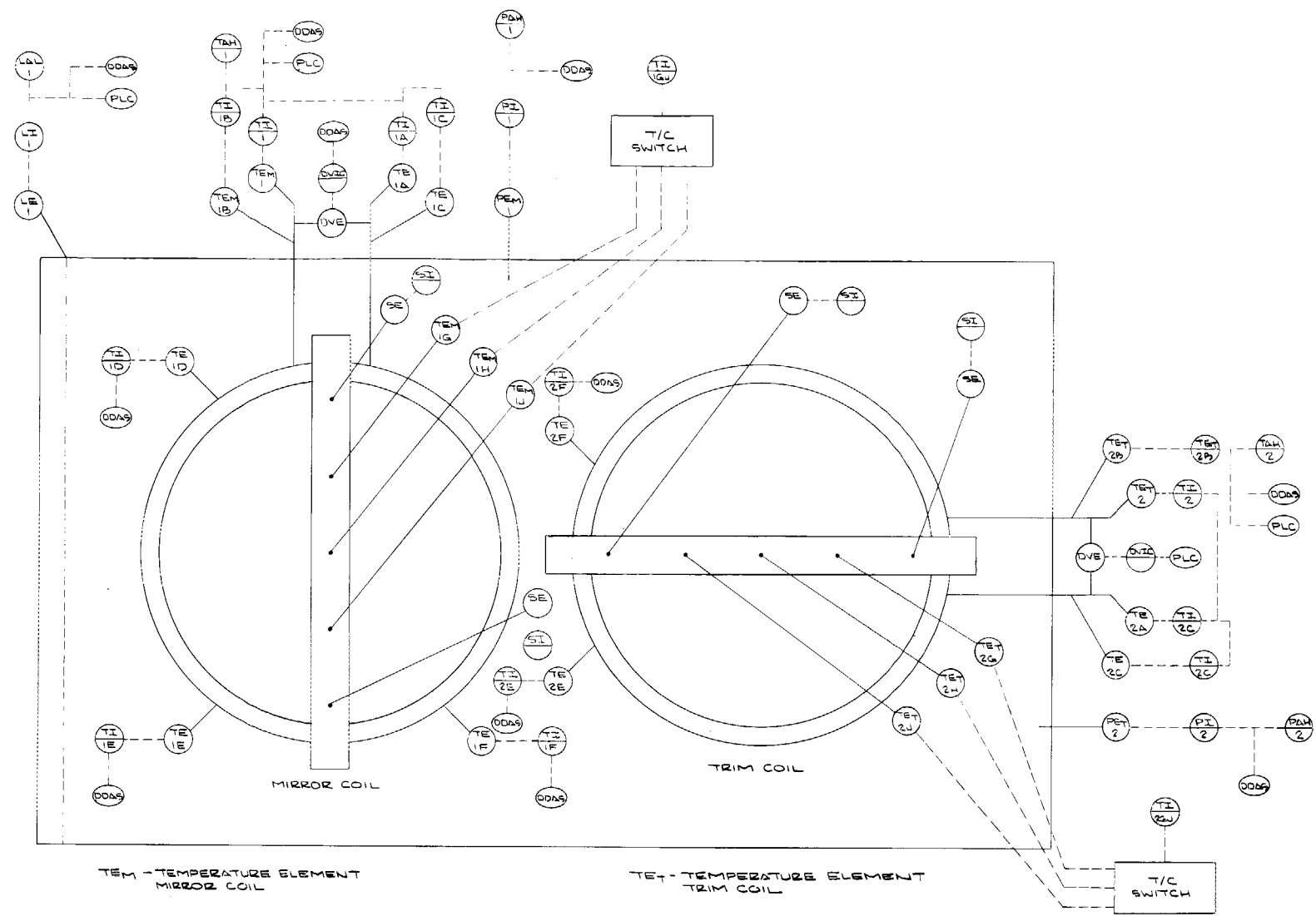
EDT-P CRYOGENIC SYSTEM
INSTRUMENTATION PROCESS AND
INSTRUMENT DIAGRAM

UNSTR. PROCESS & INSTR. DIAG. 78

DATE: 12/15/78

SCALE: 1/2" = 1'-0"

PROJECT: 4270/10078



TEM - TEMPERATURE ELEMENT MIRROR COIL
 TE - TEMPERATURE ELEMENT TRIM COIL

TYPICAL MAGNET INSTRUMENTATION

- LEGEND**
- DVE - DIFFERENTIAL VOLTAGE ELEMENT
 - DVI - DIFFERENTIAL VOLTAGE INDICATOR
 - PLC - PROGRAMMABLE LOGIC CONTROLLER
 - TE - TEMPERATURE ELEMENT
 - TI - TEMPERATURE INDICATOR
 - DDAS - DIGITAL DATA ACQUISITION SYSTEM
 - SE - STRAIN GAUGE ELEMENT
 - SI - STRAIN INDICATOR
 - LE - LEVEL ELEMENT
 - LI - LEVEL INDICATOR
 - PE - PRESSURE ELEMENT
 - PI - PRESSURE INDICATION

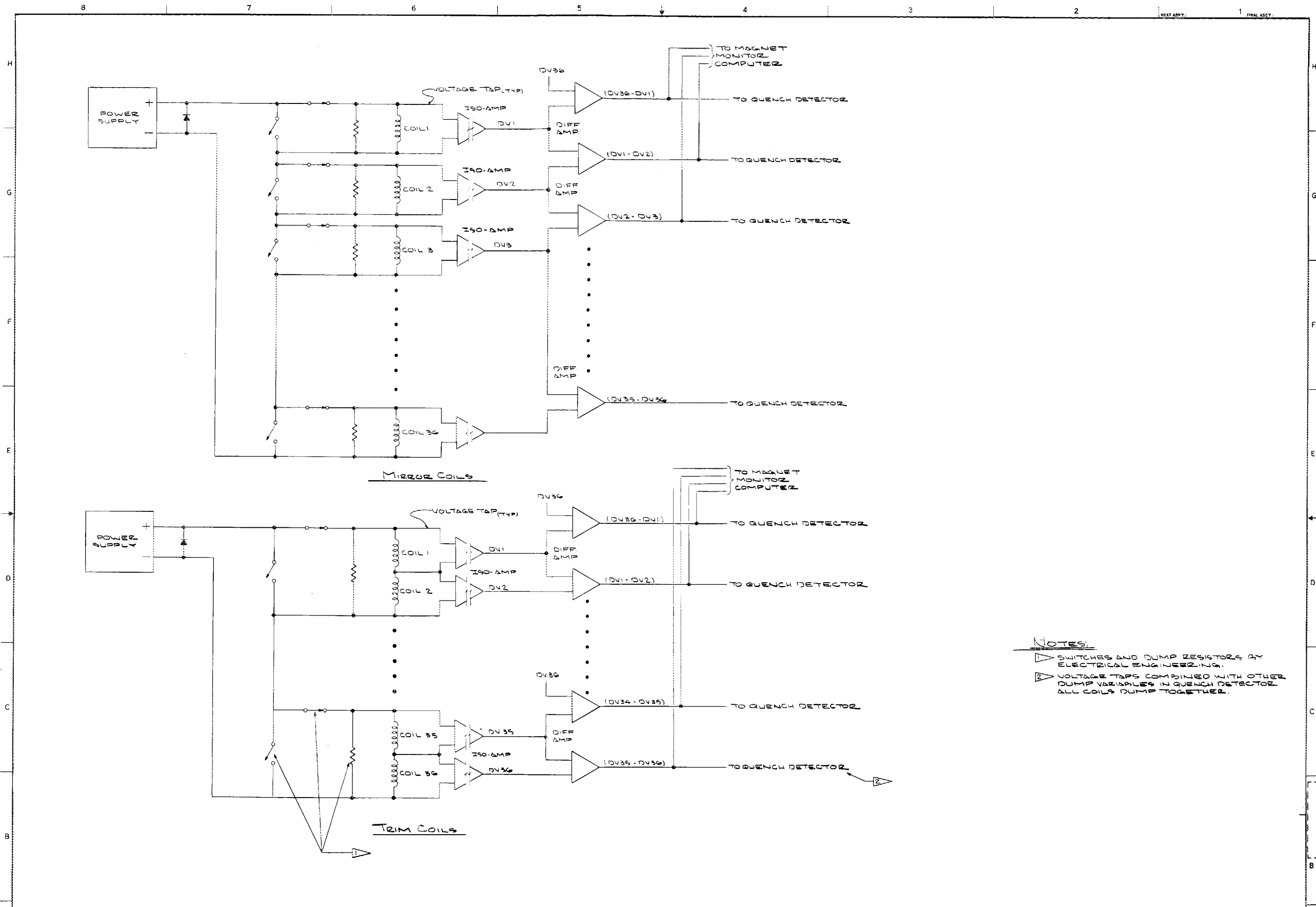
NO REPRESENTATION OR WARRANTY, EXPRESSED OR IMPLIED, IS MADE BY THE COMPANY OR ITS AGENTS OR EMPLOYEES IN CONNECTION WITH THE USE OF ANY OF THE INFORMATION CONTAINED HEREIN. THE USER OF THIS INFORMATION SHALL BE RESPONSIBLE FOR THE PROPER USE OF THE INFORMATION AND FOR THE RESULTS THEREOF. THE COMPANY SHALL NOT BE RESPONSIBLE FOR ANY DAMAGE, LOSS, OR INJURY TO PERSONS OR PROPERTY, INCLUDING THE USER'S BUSINESS, ARISING FROM THE USE OF THIS INFORMATION. THE USER SHALL BE RESPONSIBLE FOR OBTAINING NECESSARY PERMITS AND APPROVALS FROM THE APPROPRIATE AUTHORITIES BEFORE USING THIS INFORMATION. THE USER SHALL BE RESPONSIBLE FOR OBTAINING NECESSARY PERMITS AND APPROVALS FROM THE APPROPRIATE AUTHORITIES BEFORE USING THIS INFORMATION.

| REV | DATE | DESCRIPTION |
|-----|------|-------------|
| | | |
| | | |
| | | |

| REV | DATE | DESCRIPTION | BY | CHK | DEPT | DATE | REV | DATE | DESCRIPTION | DATE |
|-----|------|-------------|----|-----|------|------|-----|------|-------------|------|
| | | | | | | | | | | |
| | | | | | | | | | | |

| | |
|--------------------------------------|----------------------------|
| TOLERANCE UNLESS OTHERWISE SPECIFIED | DESIGNER: M. PLETCHER 6-75 |
| FRACTIONS | DRAWN: W. MAXFIELD 6-75 |
| XX DECIMALS | CHK |
| XX DECIMALS | SECT |
| ANGLES | DRFT & PLANT |
| BREAK SHAW EDGES | MAX |
| FINISH | |

UNION CARBIDE CORPORATION - NUCLEAR DIVISION
 EBT-10
 TYPICAL MAGNET INSTRUMENTATION
 FLOW DIAGRAM
 TYP. MISC. INSTR. FLOW DIAG.
 3 1/2" x 5 1/2" 380-2 2/28 84
 IZE 14270 A005

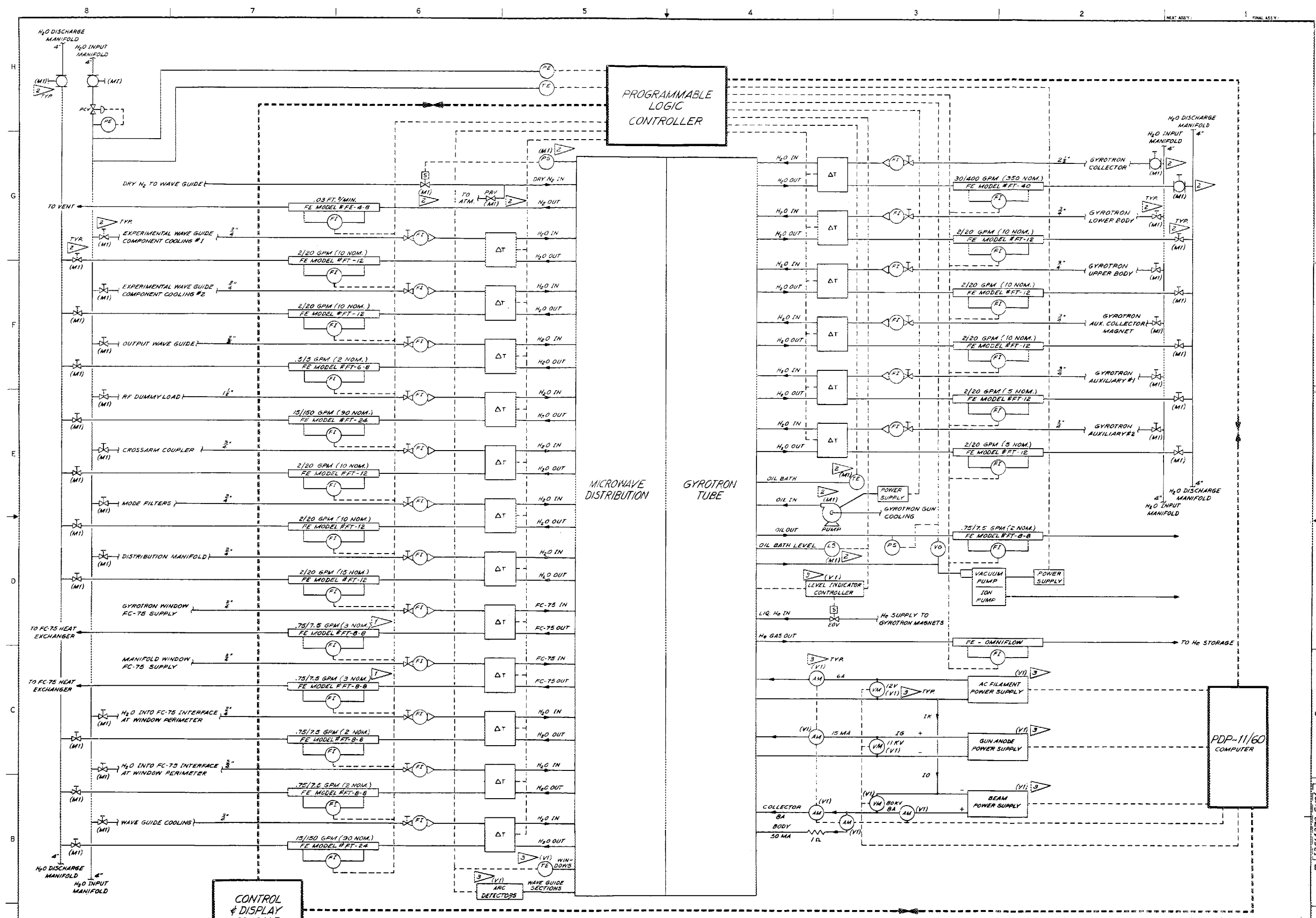


- NOTES:**
- 1 SWITCHES AND DUMP RESISTORS BY ELECTRICAL ENGINEERING.
 - 2 VOLTAGE TAPS COMBINED WITH OTHER DUMP VARIABLES IN QUENCH DETECTOR. ALL COILS DUMP TOGETHER.

NO REPRESENTATION OF WARRANTY, EXPRESS OR IMPLIED, IS MADE AS TO THE ACCURACY, COMPLETENESS OR USEFULNESS OF THE INFORMATION OR ELEMENTS CONTAINED IN THESE DRAWINGS, OR THAT THE USE OF ANY PORTION OF ANY INFORMATION APPEARING HEREON OR INCORPORATED IN THESE DRAWINGS WILL NOT IN ANY MANNER INFRINGE ON THE RIGHTS OF ANY PATENT OR OTHER INTELLECTUAL PROPERTY RIGHTS OF ANY OTHER PARTY. THE USER OF THIS INFORMATION SHALL BE RESPONSIBLE FOR OBTAINING ALL NECESSARY PERMITS AND APPROVALS FOR THE USE OF ANY INFORMATION APPEARING HEREON OR INCORPORATED IN THESE DRAWINGS. UNLESS OTHERWISE SPECIFIED, ALL DIMENSIONS ARE IN INCHES. DIMENSIONS ARE TO BE TAKEN UNLESS OTHERWISE SPECIFIED. DIMENSIONS ARE TO BE TAKEN UNLESS OTHERWISE SPECIFIED. DIMENSIONS ARE TO BE TAKEN UNLESS OTHERWISE SPECIFIED.

| UNLESS TOLERANCES UNLESS OTHERWISE SPECIFIED | | | | | | | | | | DEV: [] | | UNION CARBIDE CORPORATION - NUCLEAR DIVISION | | | | | | | | | | | |
|---|-------------|----|-----|------|------|------|----|-----|------|--------------|------|--|------|----|----|----|----|----|----|----|----|-----|------|
| FRAXIONS: 1/16 DECIMALS: .001 | | | | | | | | | | DRAWN: [] | | PROJECT: [] | | | | | | | | | | | |
| FIVE DECIMALS: .00001 | | | | | | | | | | CHECKED: [] | | DEPT & PLANT: [] | | | | | | | | | | | |
| ANGLES: ALL | | | | | | | | | | DATE: [] | | SCALE: [] | | | | | | | | | | | |
| SHARP EDGES: MAX. 1/32" | | | | | | | | | | DATE: [] | | DATE: [] | | | | | | | | | | | |
| ALL DIMENSIONS ARE TO BE TAKEN UNLESS OTHERWISE SPECIFIED | | | | | | | | | | DATE: [] | | DATE: [] | | | | | | | | | | | |
| REVISION OR ISSUE PURPOSE | | | | | | | | | | DATE | | DATE | | | | | | | | | | | |
| REV | DESCRIPTION | BY | CHK | FEET | DEPT | DATE | FE | REQ | DATE | ACQ | DATE | NOE | DATE | CA | EC | EF | EM | IE | IN | PD | SE | SLD | DATE |
| FOR COMMENT | | | | | | | | | | DATE | | DATE | | | | | | | | | | | |
| REVISION OR ISSUE PURPOSE | | | | | | | | | | DATE | | DATE | | | | | | | | | | | |

UNION CARBIDE CORPORATION - NUCLEAR DIVISION
 EAST-D SYSTEM MAGNET
 PROTECTION INSTRUMENTATION
 VOLTAGE TAPS
 DRAWN: []
 CHECKED: []
 DATE: []
 SCALE: []
 ITC 4270 (A009) B



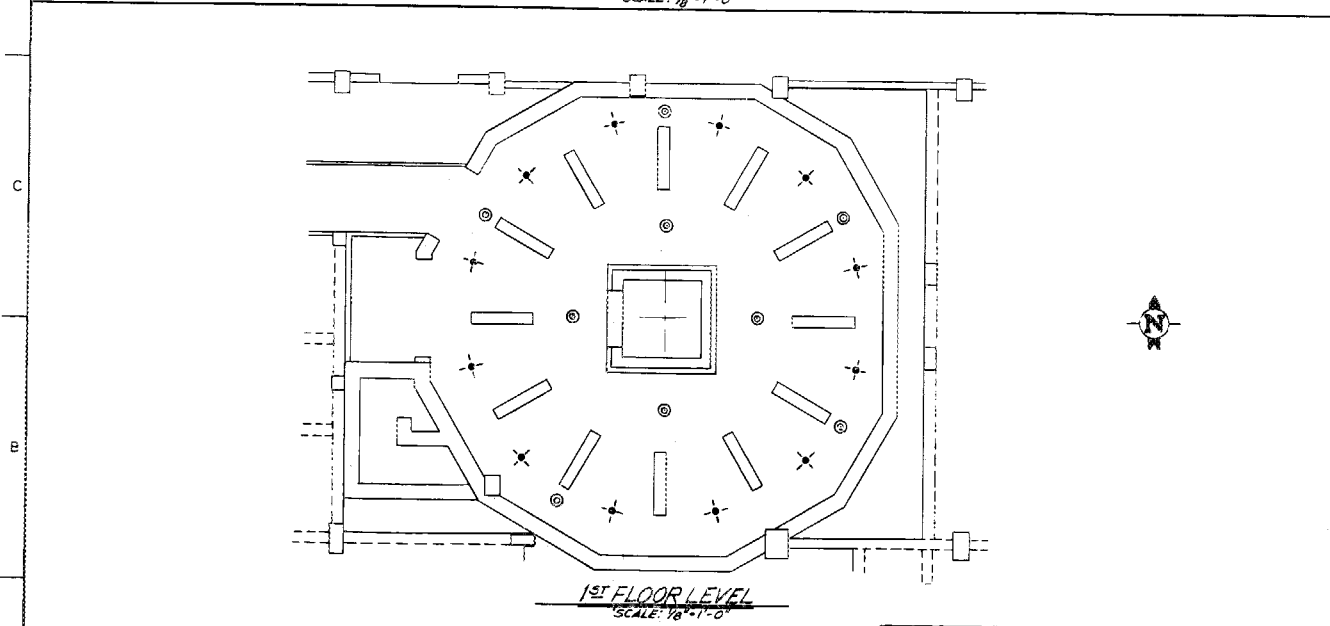
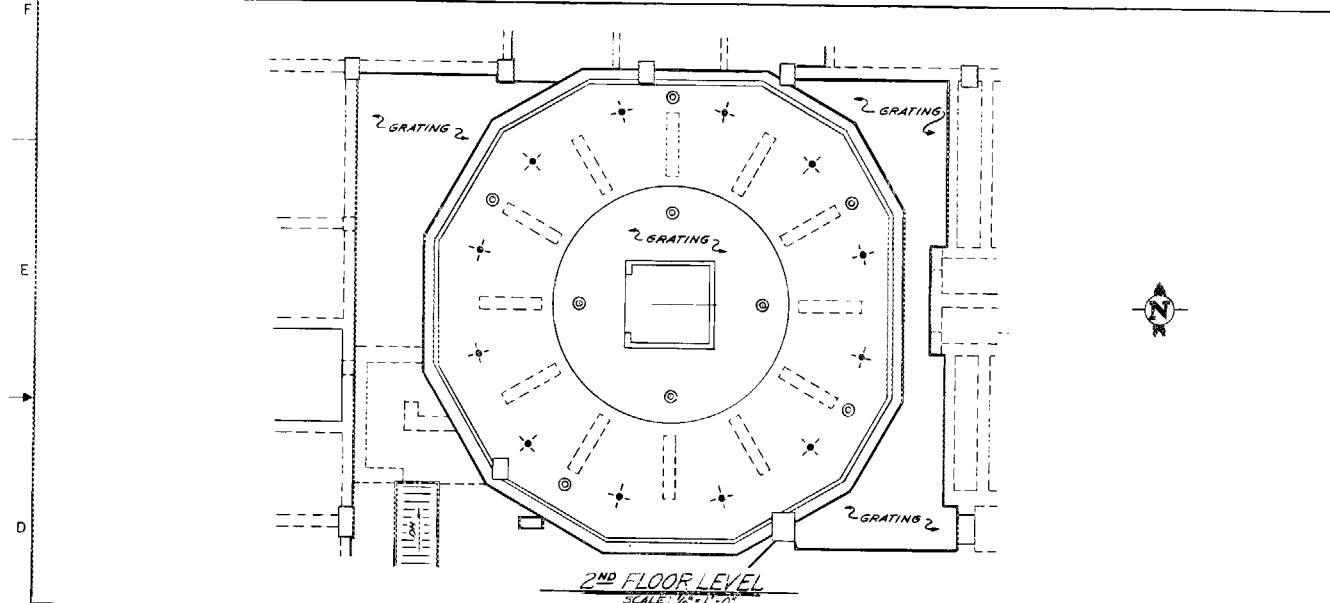
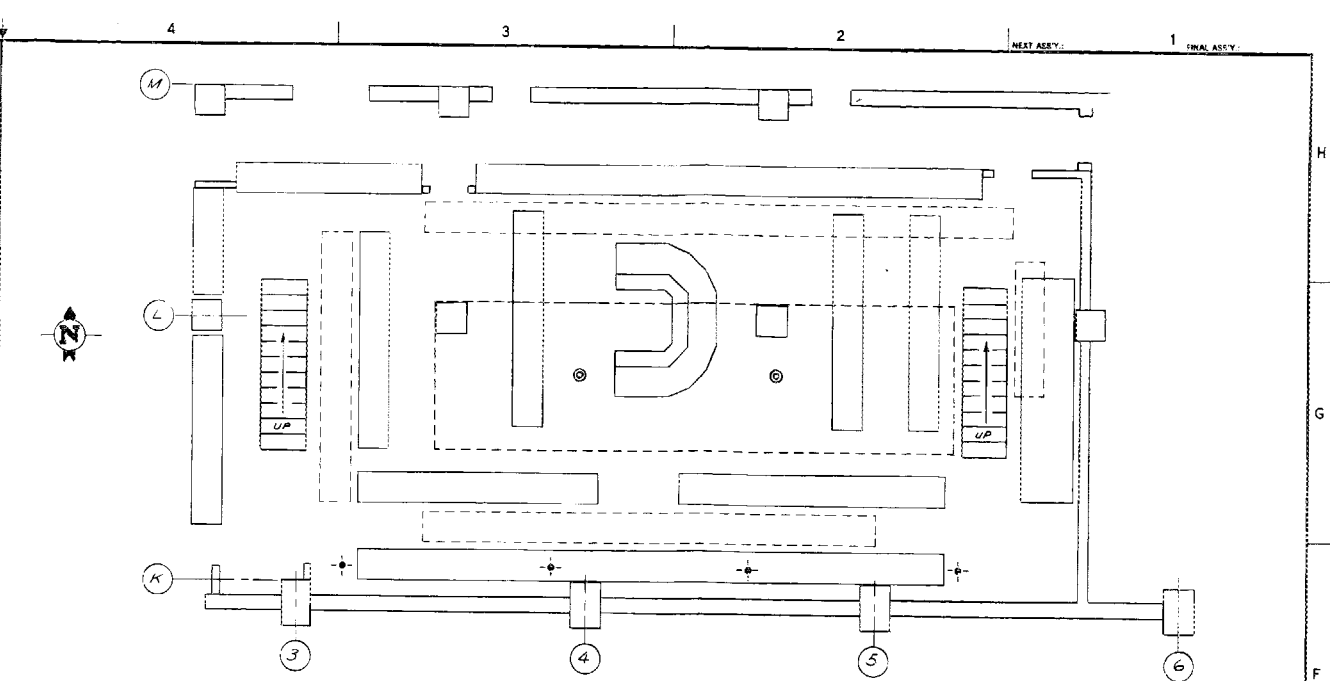
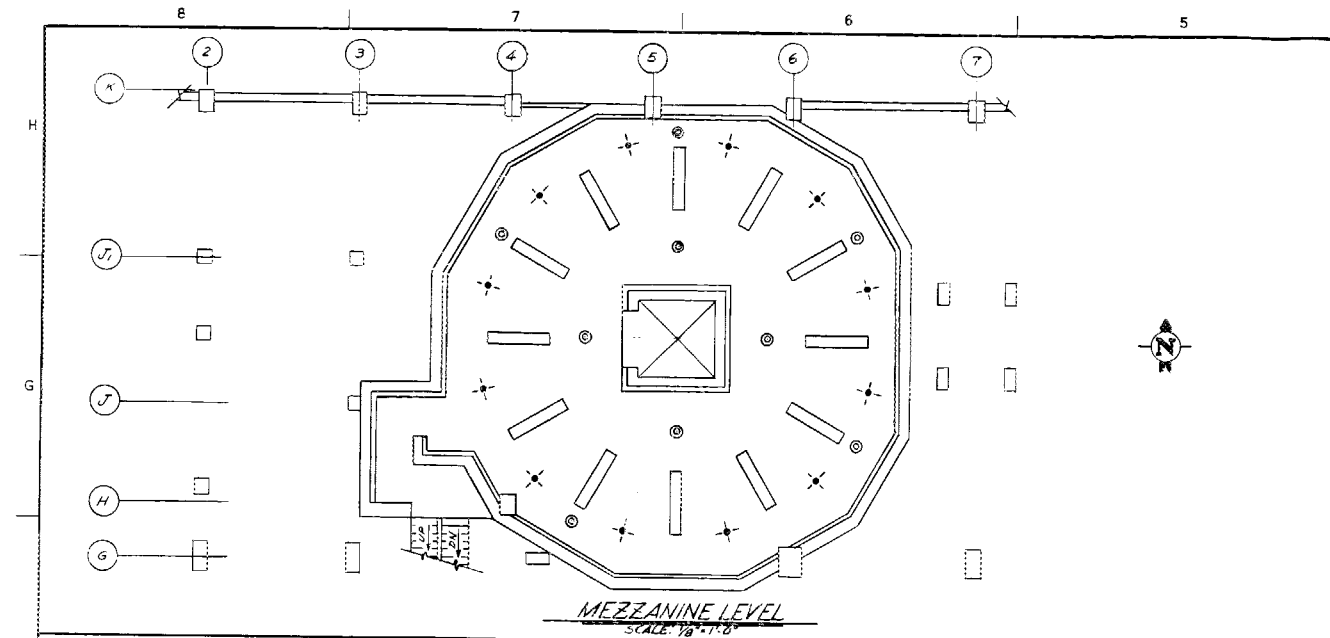
- NOTES**
- 1 SPECIAL FC-75 (3 M COMPANY) FLUID WITH CHARACTERISTICS DIFFERENT FROM H₂O.
 - 2 (M1) - PROVIDED BY MECHANICAL ENGINEERING
 - 3 (V1) - PROVIDED BY GYROTRON SYSTEM VENDOR

| REV | DESCRIPTION | BY | CHK | SECT | DEPT | DATE | FE | REQ | DATE | ISSUED | DATE | CHK | DATE | CA | CE | EE | EP | IE | II | IO | IS | ISD | |
|-----|-------------|----|-----|------|------|------|----|-----|------|--------|------|-----|------|----|----|----|----|----|----|----|----|-----|--|
| 0 | FOR COMMENT | | | | | | | | | | | | | | | | | | | | | | |

| | | |
|---------------------------------------|-------------------|--------------------------|
| TOLERANCES UNLESS OTHERWISE SPECIFIED | | DES H.L. MITCHELL 6/75 |
| 1X FRACTIONS | DECIMALS | DRW C.A. MARKHAM/CA 6/75 |
| 2X DECIMALS | INCHES | |
| 3X DECIMALS | ANGLES | |
| 4X DECIMALS | BREAK SHARP EDGES | |
| 5X DECIMALS | FINISH | |
| USE IN | | |
| DATE | | |
| DRAWING APPROVALS | | |
| DESIGNER | | |
| CHECKER | | |
| DATE | | |

| | |
|--|----------|
| UNION CARBIDE CORPORATION - NUCLEAR DIVISION | |
| E8T-P | |
| MICROWAVE MONITOR & CONTROL SYSTEM | |
| REV | DATE |
| 1 | 12/12/82 |
| 2 | 12/13/82 |
| 3 | 12/13/82 |
| 4 | 12/13/82 |
| 5 | 12/13/82 |
| 6 | 12/13/82 |
| 7 | 12/13/82 |
| 8 | 12/13/82 |
| 9 | 12/13/82 |
| 10 | 12/13/82 |

1. All dimensions are in inches unless otherwise specified. 2. All tolerances are in inches unless otherwise specified. 3. All dimensions are in inches unless otherwise specified. 4. All dimensions are in inches unless otherwise specified. 5. All dimensions are in inches unless otherwise specified. 6. All dimensions are in inches unless otherwise specified. 7. All dimensions are in inches unless otherwise specified. 8. All dimensions are in inches unless otherwise specified. 9. All dimensions are in inches unless otherwise specified. 10. All dimensions are in inches unless otherwise specified.



LEGEND
 + MICROWAVE SENSOR
 ⊙ AUDIO/VISUAL ALARM

NO REPRESENTATION OR WARRANTY, EXPRESSED OR IMPLIED, IS MADE AS TO THE ACCURACY, COMPLETENESS OR USEFULNESS OF THE INFORMATION OR DATA CONTAINED IN THESE DRAWINGS, OR ANY PART THEREOF, OR THE RESULTS OF ANY OPERATION, ANALYSIS, DESIGN OR PROCESS CONDUCTED IN RELIANCE THEREON. THE USER SHALL BE RESPONSIBLE FOR THE PROTECTION OF HIS INTERESTS AND FOR THE PROTECTION OF HIS PERSON AND PROPERTY. THE USER SHALL BE RESPONSIBLE FOR THE PROTECTION OF HIS INTERESTS AND FOR THE PROTECTION OF HIS PERSON AND PROPERTY. THE USER SHALL BE RESPONSIBLE FOR THE PROTECTION OF HIS INTERESTS AND FOR THE PROTECTION OF HIS PERSON AND PROPERTY.

| REV | DESCRIPTION | BY | CHE | SECT | DEPT | DATE | PI | REQ. DATE | ISSUE DATE | DOE DATE | CA | SC | ES | EM | IS | M | PL | BE | XAD |
|-----|-------------|----|-----|------|------|------|----|-----------|------------|----------|----|----|----|----|----|---|----|----|-----|
| 0 | FOR COMMENT | | | | | | | | | | | | | | | | | | |

UNION CARBIDE CORPORATION - NUCLEAR DIVISION

DRG. NO. **EBT-P**
MICROWAVE ALARM & SENSOR PLAN

DATE: 8/79
 DRAWN BY: C.A. KIRKPATRICK
 CHECKED BY: N.L. MITCHELL

SCALE: AS NOTED
 NO. 12E14270 SK02

12E14270-SK02

LIST OF ABBREVIATIONS

| | |
|--------|--|
| ARE | aspect ratio enhancement |
| ATC | Adiabatic Toroidal Compressor |
| CRT | cathode ray tube |
| cw | continuous wave |
| dc | direct current |
| DITE | Diverted Injected Tokamak Experiment |
| DOE | Department of Energy |
| D-T | deuterium-tritium |
| EBT | ELMO Bumpy Torus |
| EBT-P | ELMO Bumpy Torus Proof-of-Principle |
| EBTR | ELMO Bumpy Torus Reactor |
| EBT-S | ELMO Bumpy Torus Scale Experiment |
| ECH | electron cyclotron heating |
| ECRH | electron cyclotron resonance heating |
| ETF | Engineering Test Facility |
| FED | Fusion Energy Division |
| ICRH | ion cyclotron resonance heating |
| IP | industrial participant |
| ISX | Impurity Study Experiment |
| LED | light-emitting diode |
| MCC | master control console |
| MHD | magnetohydrodynamic |
| MOA | Memorandum of Agreement |
| ORNL | Oak Ridge National Laboratory |
| ORO | Oak Ridge Operations |
| PDX | Poloidal Divertor Experiment |
| PLC | programmable logic controller |
| PLT | Princeton Large Torus |
| PMP | Project Management Plan |
| PQAA | Project Quality Assurance Assessment |
| PQAP | Project Quality Assurance Plan |
| rf | radio frequency |
| RGA | residual gas analyzer |
| SCR | silicon-controlled rectifier |
| ST | Symmetric Tokamak |
| TFTR | Tokamak Fusion Test Reactor |
| TFR | Tokamak Fontenay-aux-Roses |
| UCC-ND | Union Carbide Corporation Nuclear Division |
| WBS | work breakdown structure |
| 1-D | one-dimensional |
| 2-D | two-dimensional |
| 3-D | three-dimensional |

INTERNAL DISTRIBUTION

1. R. G. Alsmiller, Jr.
2. S. I. Auerbach
3. F. W. Baity, Jr.
4. V. C. Baker
5. J. K. Ballou
6. D. B. Batchelor
7. M. C. Becker
8. M. Bender
9. L. A. Berry
10. F. Bieniosek
11. W. B. Bigney
12. B. L. Bishop
- 13-162. A. L. Boch
163. S. K. Borowski
164. D. E. Brashears
165. R. A. Brown
166. R. L. Brown
167. E. H. Bryant
168. D. B. Campbell
169. J. A. Cobble
170. R. J. Colchin
171. R. J. Copeland
172. J. A. Cox
173. R. H. Dilworth
174. R. A. Dory
175. L. Dresner
176. R. B. Easter
177. H. O. Eason, Jr.
178. O. C. Eldridge
179. D. E. Ferguson
180. W. A. Fietz
181. W. M. Fletcher
182. W. Fulkerson
183. T. A. Gabriel
184. J. C. Glowienka
185. W. R. Hamilton
186. C. E. Hammons
187. H. H. Haselton
188. G. R. Haste
189. P. N. Haubenreich
190. C. L. Hedrick, Jr.
191. H. N. Hill
192. R. M. Hill, Jr.
193. J. T. Hogan
194. C. C. Hopkins
195. E. F. Jaeger
196. G. R. Jasny
197. S. P. Kinsey
198. S. A. Larson
199. R. A. Lillie
200. R. L. Livesey
201. M. S. Lubell
202. J. N. Luton, Jr.
203. J. W. McCormick
204. H. C. McCurdy
205. M. W. McGuffin
206. T. J. McManamy
207. F. C. Maienschein
208. J. W. Melton
209. R. A. Michelotti
210. R. V. Miskell
211. H. L. Mitchell
212. O. B. Morgan, Jr.
213. J. R. Moore
214. D. R. Norris
215. L. W. Owen
216. G. F. Pierce
217. H. Postma
218. W. H. Power
219. R. K. Richards
220. C. R. Richmond
221. J. A. Rome
222. M. W. Rosenthal
223. C. R. Schaich
224. J. Sheffield
225. D. J. Sigmar
226. J. P. Smith
227. D. A. Spong
228. D. Steiner
229. P. H. Stelson
230. L. A. Stephens, Jr.
231. W. L. Stirling
232. J. D. Stout
233. P. B. Thompson

- | | |
|-----------------------|--|
| 234. P. A. Tabor | 244. R. A. Wright |
| 235. H. E. Trammel | 245. J. W. Yarbrough |
| 236. D. B. Trauger | 246. H. T. Yeh |
| 237. N. A. Uckan | 247. A. Zucker |
| 238. T. Uckan | 248-249. Laboratory Records, ORNL-RC |
| 239. J. R. Weir, Jr. | 250. Fusion Energy Division Library |
| 240. W. M. Wells | 251-252. Fusion Energy Division Communications Center |
| 241. T. L. White | 253. ORNL Patent Office |
| 242. M. K. Wilkinson | |
| 243. R. E. Wintenberg | |

EXTERNAL DISTRIBUTION

254. D. S. Beard, Office of Fusion Energy, Department of Energy, Mail Stop G-234, Washington, DC 20545
- 255-259. J. R. Bilton, Ebasco Services, Inc., Two Rector Street, New York, NY 10006
260. J. F. Clarke, Office of Fusion Energy, Department of Energy, Mail Stop G-234, Washington, DC 20545
261. F. E. Coffman, Office of Fusion Energy, Department of Energy, Mail Stop G-234, Washington, DC 20545
262. N. A. Davies, Office of Fusion Energy, Department of Energy, Mail Stop G-234, Washington, DC 20545
- 263-267. R. J. DeBellis, McDonnell Douglas Astronautics Company, P.O. Box 516, St. Louis, MO 63166
268. J. F. Decker, Office of Fusion Energy, Department of Energy, Mail Stop G-234, Washington, DC 20545
- 269-278. W. R. Ellis, Office of Fusion Energy, Department of Energy, Mail Stop G-234, Washington, DC 20545
279. G. M. Haas, Office of Fusion Energy, Department of Energy, Mail Stop G-234, Washington, DC 20545
280. C. C. Hawkins, Department of Energy, Oak Ridge Operations, P.O. Box E, Oak Ridge, TN 37830
281. E. E. Kintner, Office of Fusion Energy, Department of Energy, Mail Stop G-234, Washington, DC 20545
282. J. A. Lenhard, Department of Energy, Oak Ridge Operations, P.O. Box E, Oak Ridge, TN 37830
283. W. A. Marton, Office of Fusion Energy, Department of Energy, Mail Stop G-234, Washington, DC 20545
284. M. R. Murphy, Office of Fusion Energy, Department of Energy, Mail Stop G-234, Washington, DC 20545
- 285-289. R. E. Papsco, Grumman Aerospace Corporation, P.O. Box 31, Bethpage, NY 11714
- 290-294. L. K. Price, Department of Energy, Oak Ridge Operations, P.O. Box E, Oak Ridge, TN 37830
295. M. Roberts, Office of Fusion Energy, Department of Energy, Mail Stop G-234, Washington, DC 20545
296. J. M. Turner, Office of Fusion Energy, Department of Energy, Mail Stop G-234, Washington, DC 20545
- 297-302. T. C. Varljen, Westinghouse Electric Corporation, Fusion Power Systems Department, P.O. Box 10864, Pittsburgh, PA 15236

303. S. S. Waddle, Department of Energy, Oak Ridge Operations, P.O. Box E, Oak Ridge, TN 37830
304. R. J. Willard, Department of Energy, Oak Ridge Operations, P.O. Box E, Oak Ridge, TN 37830
305. R. A. Zich, Office of Fusion Energy, Department of Energy, Mail Stop G-234, Washington,
DC 20545